
# UNIVERSITA' DEGLI STUDI DI TRIESTE

**XXIV CICLO DEL DOTTORATO DI RICERCA IN SCIENZE E TECNOLOGIE CHIMICHE E FARMACEUTICHE**

This thesis was financed by the Mexican Government:

CONACYT FELLOWSHIP

## TOWARDS SELF-ASSEMBLED DEVICES, A CARBON NANOTUBE APPROACH

Settore scientifico-disciplinare: CHIM/06

PhD Student

Antonio Esaú Del Río Castillo

Coordinator

Prof. Enzo Alessio

Advisor

Prof. Maurizio Prato

Co-advisor:

Francesco Bonaccorso

Academic year: 2010/2011

*To my family and Edith.*

# Acknowledgements

I am extremely grateful to my supervisors, Prof. Maurizio Prato for his continuous support during my research activity and Dr. Francesco Bonaccorso who has been an inspiration and support in the last part of my work.

I would like to thank Professor Andrea Ferrari for inviting me to develop an important part of my work at Nanomaterials and Spectroscopy group in the University of Cambridge.

I am grateful whit the Prof. Davide Bonifazi, Prof. Giacinto Scoles, Prof. Lucia Pasquato, Dr. Tatiana da Ros and Dr. Stefan Mezzasalma for their critiques, support and advice on my research work.

Thanks to the Pos-Docs at Trieste University, Valeria Ferraro, Riccardo, Francesca Toma, Marek Grzelczak, Caroline Hadad, Daniel Romero, Luigi Feruglio, Francesco Giacalone, William Dobbs, Susana Bosi and Zois Syrgiannis and the Pos-Docs at Nanomaterials and Spectroscopy group Tawfique Hassan, Zhipei Sun, Weiping Wu, Ravi Shankar, Andrea Fasoli, Shakil Arwan, (from Nokia), Vincenzo Armendola (Univ. of Padova) and Oksana Trushkevich, for their help, patience, lessons, discussions, jokes and some beers.

Special thanks to those that besides sharing their knowledge, they offer me their friendship Laura Soriano, Victoria Valdivia and Mildred Quintana.

I would like to thank for their special talks, lessons and meals in the TEM facilities to Claudio Gamboz.

I would like to thank all my PhD partners to help me and teach me some of organic chemistry… i muli Alessia Battigelli, Tomas Marangoni, Alejando Montellano, Alessandra Micoli, Antonio Turco, Chiara Fabbro, Nicola da Zordi, Valeria Zamolo, Marco Carini and Sara Cipolone, also I wish to thank the italian comunity in Cambridge Giulia Privitera, Antonio Lombardo, Felice Torrisi, Silvia Milana and Daniel Popa, the mexican comunnity of Cambridge Oscar Tenoria and Ivonne Medina, all of them make my stay in Italy and UK “stresslly” pleasant ☺

Special thanks to non-academic friends that supported and helped me; I am deeply in debt with you guys, Luigi Persia and Jessica Garduza, Marco Bura and Flavia Crasso.

This work has been supported by the National Council of Science and Technology, a dependence of the Mexican Government. Also thank to Gonzalo Mendoza Felix Rocio Alvarado Cruz and the Senator Guillermo Tamborrel Suárez for their guidance to get economical support from Secretary of Education through Lic. Juan Angel.

Quiero agradecer a mis papás Antonio Del Rio y Martha Patricia Castillo y a mi hermano Ulises que sin su apoyo, paciencia y amor este trabajo no hubiera sido terminado.

A mis abuelitos Guillermo Castillo y Eva Becerril que siempre me han apoyado y aconsejado. Gracias abuelita, siempre recordaré *tus recomendaciones*.

I am especially grateful with my best friend and love Edith Torres, she has been a strong support in this adventure, thanks for everything.

I thank to the families Castillo Izaguirre, Sanchez Del Río, Del Río Contreras and Del Angel Servín for their help, advice and support in my entire personal and professional career.

Last but not least, I thank to all my friends, in hard moments I always have their advice, and unconditional friendship.

Thanks to all.

# List of acronyms

| | |
|---|---|
| AFM | Atomic Force Microscopy |
| ALD | Atomic Layer Deposition |
| AP-SWNT | As Produced SWNTs |
| APTES | 3-Aminopropyltriethoxysilane |
| AuNP | Gold Nanoparticles |
| AuNP/NT/AuNP | Complex SWNT With AuNPs in ihe ends. |
| Boc | Di-Tert-Butyl Dicarbamate |
| Boc-PDA | N-Boc-1,3-Propanediamine |
| Boc-PDA-SWNT | SWNT Functionalized with N-Boc-1,3-Propanediamine |
| BWF | Breit Wigner Fano |
| CNT | Carbon Nanotube |
| CNT-FET | Carbon Nanotube Field-Effect Transistor |
| CO | Carbon Monoxide |
| CoMoCat | Cobalt-Molybdenum Catalyst (Swnts) |
| CTAB | Cetyl Trimethylammonium Bromide |
| CVD | Chemical Vapour Deposition |
| Cys-SWNT | Cystamine Functionalized Swnts |
| DGU | Density Gradient Ultracentrifugation |
| DI | Distilled Water |
| DNA | Deoxyribonucleic Acid |
| DOS | Density of States |
| DR | Double Resonance |
| ds-DNA | Double strand DNA |
| DTAB | Dodecyl Trimethyl Ammonium Bromide |
| EDC | 1-Ethyl-3-(3-Dimethylamino Propyl) Carbodiimide |
| EDIPA | N, N-Diisopropylathylamine |
| ENIAC | Electronic Numerical Integrator And Computer |
| EtOH | Ethanol |
| FET | Field-Effect Transistor |
| fin FET | Fin Gate-Field Effect Transistor |
| FLG | Few Layer Graphene |
| GAA | Gate All-Around |
| GAA-FET | Gate All-Around Field-Effect Transistor |
| GPE | Gas Phase Epitaxy |

| | |
|---|---|
| HAADF | High Angle Annular Dark Field |
| HATU | O-(7-Azabenzotriazol-1-Yl)-N, N, N', N'-Tetramethyluronium Hexafluorophosphate |
| $HfO_2$ | Hafnium Dioxide |
| HiPco | High-Pressure Carbon Monoxide (SWNT) |
| HOPG | High Ordered Pyrolithic Graphite |
| IBM | International Business Machine |
| IFM | Intermediate Frequency Mode |
| IPA | Isopropyl Alcohol |
| IR | Infrared |
| ITO | Indium-Tin Oxide |
| ITRS | International Technology Roadmap for Semiconductors |
| MBE | Molecular Beam Epitaxy |
| MOSFET | Metal-Oxide-Semiconductor Field-Effect Transistor |
| m-SWNT | Metallic SWNT |
| MWNT | Multi-Walled Carbon Nanotube |
| NEC | Nippon Electric Company |
| $NH_4OH$ | Ammonium Hydroxide |
| NIST | National Institute of Standards and Technology |
| $NO_2$ | Nitrogen Dioxide |
| NT | Nanotube |
| OAS | Optical Absorption Spectra |
| OD | Optical Density |
| PAA | Pyrene Acetic Acid |
| PBA | Pyrene Butyric Acid |
| PBA-SWNTs | Single Wall Carbon Nanotube functionalized with Pyrene Butyric Acid |
| PDA | 1, 3-Propanediamine |
| PEG | Polyethylene Glycol |
| PL | Photoluminescence |
| PLE | Photoluminescence Excitation |
| PMMA | Poly(Methyl Methacrylate) |
| PVP | Polyvinyl Pyrrolidon |
| RBM | Radial Breathing Mode |
| RNA | Ribonucleic Acid |
| SA | Self-Assembly |
| SAM | Self-Assembled Monolayer |
| SAMFET | Self-Assembled Monolayer Field-Effect Transistor |
| SC | Sodium Cholate |
| SDBS | Sodium Dodecyl Benzene Sulphonate |
| SDS | Sodium Dodecyl Sulphate |

| | |
|---|---|
| SE | Secondary Electrons |
| Si | Silicon |
| SiO2 | Silicon Dioxide |
| SiOX-SWNT | SWNT Coated With Silicon Oxide(X) |
| SLG | Single Layer Graphene |
| s-NHS | Sulpha-N-Hydroxysuccinimide |
| $SOCl_2$ | Thionil Chloride |
| SPR | Surface Plasmon Resonance |
| s-SWNT | Semiconducting SWNTs |
| S-SWNT-S | Selective SWNT Ends Functionalized with Sulphur Atoms |
| STEM | Scanning-Transmission Electron Microscopy |
| STM | Scanning Tunnelling Microscope |
| strep-SWNT | Streptavidin Functionalized SWNT |
| SWNT | Single-Walled Carbon Nanotube |
| TB | Tris Buffer |
| TEM | Transmission Electron Microscopy |
| TEOS | Tetraethyl Orthosilane |
| TFT | Thin-Film Transistor |
| TGA | Thermogravimetric Analysis |
| THF | Tetrahydrofuran |
| TMOS | Tetramethoxysilane |
| UHV | Ultra High Vacuum |
| UV-vis | Ultraviolet-Visible |
| VHS | Van Hove Singularities |

# Contents

## Chapter 3: The gate dielectric.

## Chapter 4: Contact resistance between SWNT and electrodes



## Chapter 5: Future work, assembling the device

# Riassunto

Nell'ultimo decennio i materiali nanostrutturati di carbonio, in particolare i nanotubi di carbonio a singola parete (single walled carbon nanotubes, SWNTs), sono stati considerati promettenti sostituti del silicio per la costruzione di dispositivi elettronici di nuova generazione. Questo è dovuto alle loro uniche proprietà fisiche e chimiche. Gli scienziati di tutto il mondo hanno compiuto un enorme sforzo per introdurre i materiali a base di carbonio nel mercato. Nonostante questi tentativi, non sono ancora state ottenute delle applicazioni commerciali per i dispositivi elettronici a base di nanotubi di carbonio. Gli ostacoli sono legati principalmente a due ragioni: la prima riguarda le proprietà chimico-fisiche dei nanotubi, infatti le forti interazioni π-π tra i nanotubi portano alla formazione di grossi aggregati; inoltre i CNTs, nella loro forma iniziale, sono molto difficili da disperdere nei comuni solventi organici , sono chimicamente inerti; e soprattutto sono costituiti da una miscela di nanotubi semiconduttori e metallici. Il secondo ostacolo è correlato alla costruzione e alle caratteristiche del dispositivo, bisogna infatti considerare l'alta resistenza di contatto tra i SWNTs e gli elettrodi, la scelta dei materiali dell'elettrodo dei gate, la struttura e il materiale dielettrico dei gate, ed infine il modo in cui i SWNTs sono in contatto con gli elettrodi.

Secondo me, se si desidera usare un nuovo materiale nelle applicazioni di alta tecnologia, sarà necessario utilizzare nuove metodologie e superare i paradigmi. In questo lavoro di tesi ho provato a mimare la natura, assemblando gli oggetti dal basso verso l'alto (bottom up approach). Per la costruzione bottom up del dispositivo ho unito le proprietà di legame della chimica organica e le proprietà fisiche dei materiali inorganici. Quindi, per affrontare la sfida della costruzione e del miglioramento di dispositivi di nuova generazione, ho utilizzato procedure non-convenzionali nella produzione di dispositivi elettronici: processi sol-gel per la sintesi del dielettrico dei gate; legami chimici per

migliorare la resistenza tra gli elettrodi e il nanotubo; ed avanzato l'idea di utilizzare origami di DNA come processo generale dispositivo per l'assemblamento del dispositivo. Per classificare i nanotubi è stato applicato un approccio top down, in quanto le attuali tecnologie nella sintesi dei SWNTs non sono ancora capaci di ottenere un materiale con una singola caratteristica elettronica.

Lo scopo di questa tesi è dimostrare che è possibile utilizzare le tecniche bottom up per la costruzione di dispositivi, sostituendo l'uso dei processi top down che sono attualmente in uso nell'industria del silicio.

La tesi è organizzata come segue:

• Nel Capitolo 1 vengono introdotte le proprietà dei materiali a base di carbonio e il modo in cui possono cambiare e migliorare le attuali tecnologie del silicio. Inoltre viene presentata una breve rassegna delle proprietà elettroniche e ottiche dei SWNTs, includendo le tecniche spettroscopiche e ottiche per la loro caratterizzazione: spettroscopia di assorbimento e Raman.

• Nel Capitolo 2 vengono discusse le metodologie di crescita dei SWNTs, le proprietà dei nanotubi di partenza, le tecniche di purificazione e la classificazione per caratteristiche elettroniche. Viene anche descritta l'esfoliazione del grafene.

• Il Capitolo 3 tratta della progettazione e della sintesi del materiale dielettrico sui SWNTs e sul grafene. Viene brevemente spiegato il processo sol-gel.

• Nel Capitolo 4 viene spiegata la sintesi di nanoparticelle metalliche ed il legame selettivo con i SWNTs.

• Il Capitolo 5 è dedicato alle prospettive del progetto, riguardanti principalmente l'assemblaggio del dispositivo, focalizzando il lavoro nella manipolazione del DNA e dei SWNTs.

Questo lavoro è stato sostenuto dal Consiglio Nazionale per la Scienza e le Tecnologie CONACyT (Governo Messicano).

# Abstract

In the last decade the nanostructured carbon materials, especially single walled carbon nanotubes (SWNTs), had emerged as probable substitutes for Silicon in the next generation of electronic devices. This is due to their unique physic and chemical properties. Likewise, scientists all around the world have made a huge effort to introduce carbon materials into the market. Despite this effort, commercial application for carbon nanotubes in electronic devices has not yet been achieved. The hindrances are due to two reasons mainly: the first one is for the physico-chemical properties of carbon nanotubes; for example, the strong π-π interactions between nanotube creates thick bundles; in the pristine form CNTs are almost indispersible in any solvent; nanotubes are practically inert chemically; and finally the synthesis of SWNTs produces a mixture of semiconducting and metallic nanotubes. The second hindrance is related to the device construction and characteristics, *e. g.* the high contact resistance between SWNT and electrodes, the selection of electrode materials, the gate dielectric structure and material are also importants, and finally how the SWNT is contacted with electrodes.

In my opinion, if it is desired to use a new material in high technology applications, will be necessary to use new methodologies and break paradigms. In this work I try to mimic what nature does, assemble objects from the bottom up. So, for the bottom up construction of the device I combine the assembly qualities of organic chemistry and the physical properties of inorganic materials. In this way, to deal with the challenges of construction and improvement of the “next device generation” I used non-conventional procedures in electronic devices: sol-gel process for the synthesis of the gate dielectric; organic chemistry for improvement on the electrodes-nanotube resistance; and propose the use of DNA origami as general assembly process for the device. For the sorting of nanotubes it is applied a top-down approach, the current technologies in the synthesis of SWNTs are not able to render a single electric behaviour yet.

The scope of this work is to demonstrate that it is feasible to use bottom up techniques in the construction of devices, replacing the use of “top down” processes that are currently in use in the silicon industry.

The thesis is organized as follows:

- In the **chapter 1** the carbon materials characteristics are introduced and how they can change the actual Silicon technologies. Additionally a brief review the electronic and optical properties of SWNTs, including the optical spectroscopy techniques used for their characterization: absorption and Raman.
- **Chapter 2** discuses briefly the grow methodologies of SWNTs, the as-produced characteristics, purification techniques and sorting by electronic behaviour. Graphene exfoliation is reviewed.
- **Chapter 3** deals with the design and synthesis of the dielectric material on SWNTs and over graphene. Sol gel process is briefly explained.
- In **chapter 4** is explained the synthesis of metallic nanoparticles and the selective linking with SWNTs.
- **Chapter 5** is dedicated to perspectives and further work, concerning mainly to device assembly, focusing in the manipulation of DNA and SWNTs.

This work has been supported by the National Council for Science and Technologies, CONACyT (Mexican Government).

# Chapter 1

# Nanostructured carbon materials, a short review.

## 1.1 Introduction.

### 1.1.1. The onset.

The transistor is one of the more revolutionary and sophisticated inventions made by mankind and its applications can be seen everywhere. The revolution over the world made by the transistor are more than obvious, from the watches in our wrists, passing through pacemakers, portable computers, to space shuttle and communication satellites. However, despite its simple function, the transistor is a very complex device. Modifications on the transistor structure and change of materials have not ceased since its invention. Nowadays, many different configurations, materials and structures had been proposed to continue the technological revolution started in 1947.

The first device able to amplify and/or switch *on* and *off* an electric signal was the thermionic valve invented by Lee de Forest in 1906, and named triode. At that time, not many applications were foreseen, but in reality and year by year , this invention changed

the world and the way we look at it with endless applications ranging from wireless communications, radar detection, television to computers, etc.. ENIAC was the first machine able to make complex mathematical operations. It was made entirely by thermionic valves and able to perform 5 000 operations per second with "only" 18 000 valves, a consumption of 200 kW and a total weight of 28 tons. By 1945 Bell Labs felt the necessity to develop new alternatives, and in 1947, John Bardeen and Walter Brattain succeed in the construction of an amplifier circuit using a "point contact **trans**fer res**istor**" that was called transistor (1), figure 1.1. The two inventors observed that simply placing 2 metallic contacts (called source and drain) separated just from a small gap occupied by a semiconductor material (Germanium), the channel, it was possible to control electric signals. Five years later, Geoffrey W. A. Dummer, from the British minister of defence, presented at the Symposium of Progress in Quality Electronic Components his idea of integrates an entire circuit using a single semiconductor chip. However, this bright idea remained a dream until 1958, when Texas Instruments accomplished the construction of the first integrated circuit (figure 1.2) taking all the credit. The realization of this revolutionary concept device was honoured by the Nobel Prize in 2000 to Jack Kilby for manufacture the device (2). These events triggered the unstoppable growth of the actual electronic era.

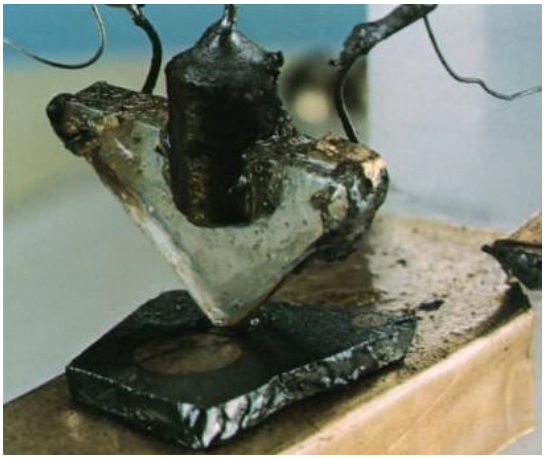

**Figure 1.1.** First transistor based on Germanium and Gold electrodes, made in 1947 at Bell Laboratories.(1)

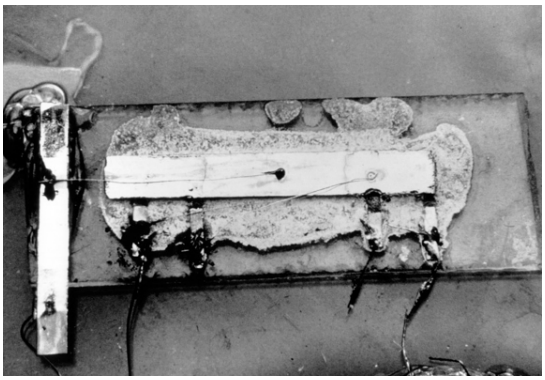

**Figure 1.2.** Jack Kilby created the first integrated circuit at Texas Instruments to prove that resistors and capacitors could exist on the same piece of semiconductor material. His circuit consisted of a sliver of germanium with five components linked by wires.

### 1.1.2 Moore's low and its implications.

By the mid 60's the rise of integration had been triggered, exploiting new configurations and technologies. The use of Silicon displaced Germanium and the old fashioned valves. In the 1962 it was possible to incorporate $2^3$ (8) transistors in the same circuit chip, in 1963 this number increases to $2^4$ (16), in 1964 $2^5$ (32), and so on following the same tendency for the next years. Gordon Moore (3) observed and studied this trend and predicts that in *ten years time* (from 1965) *the number of transistors on a single chip were raised to 65 000 units* ($2^{16}$)*!!!* This prediction was very close to the reality. Indeed, in 1979 Motorola launched his microprocessor 68 000. The number corresponds to the number of transistors integrated in it, with each transistor having a channel length (distance between emitter and collector, or source and drain) of 4 µm.

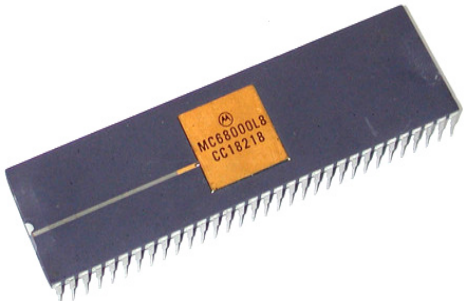


**Figure 1.3** 1979 Motorola MC68000 microprocessor.

Until now this tendency has been followed very closely, by now (2012) the number of transistors on a single silicon chip microprocessor raises the $2^{31}$ ($2.6 \times 10^9$) units in an area of 512 $mm^2$ (10 core Xeon westmere-EX from Intel®), using transistors with a channel length of 0.032 µm!

In the 80's scientists thought that size reduction of the channel length could hit the barrier of 100 nm due to technological limits. However, nowadays scientists have overpass the 100 nm barrier, and the newest technologies works on the nano regime. The International Technology roadmap for semiconductors (ITRS) identified 7.4 nm the node to be reached in 2021. This tendency to shrink the dimensions makes necessary to take into account quantum phenomena. Indeed, with size reduction, the thickness of the gate dielectric and the distance between electrodes becomes too short producing electron tunnelling effects and phenomena known as short channel effects. For instance, as the channel area is

reduced, doping elements, like potassium, aluminium or sulphur, becomes inhomogeneous distributed producing malfunctions that can ultimately bring to change in the transistor performances. Moreover, these phenomena increase the power consumption and at the same time reduce the device lifetime.

However, the dimension shrinking is not the only possible solution for continuing with more Moore. Nowadays, transistor with sub 50 nm channel lengths are produced thank to the exploitation of new materials. For instance, the $HfO_2$ insulator layer on the gate replaced the previous one made of $SiO_2$. In addition new configurations were and are nowadays investigated. To mention a few:

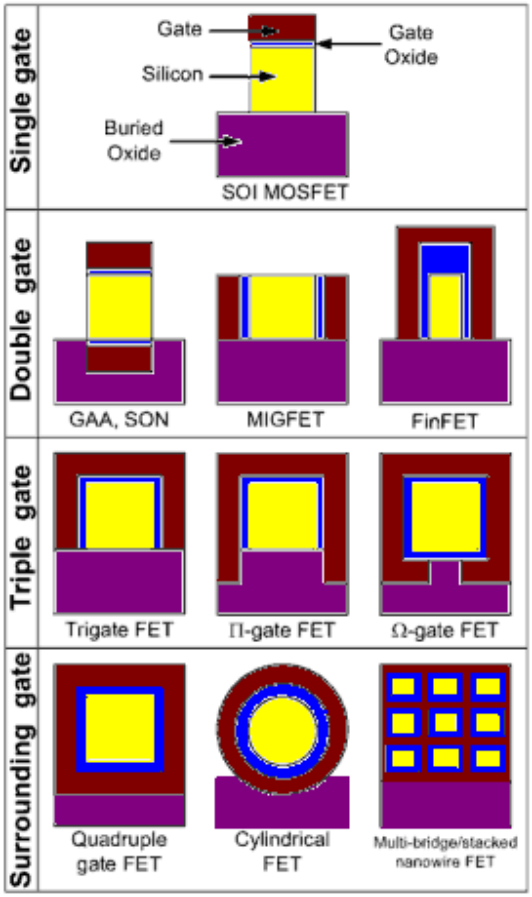


**Figure 1.4.** Schematic representation of diverse configurations of silicon transistors. Taken from (188)

- Fin field- effect transistors (finFETs) where the channel is a Silicon thin fin and the gates are located on both sides of the fin (4–7).
- Dual-gate FET. In this configuration, the channel is sandwiched between the gate dielectrics.
- Ω shape-gate FET, where the gate electrode and dielectric material surrounds the channel, taking a Ω shape (8).
- Gate-all-around- FET (GAA-FET), where the dielectric metallic contact surrounds the semiconductor channel. In theory this configuration permit a better control over the gate with respect to the configuration enlisted previously (8–10).

The actual configuration used in microprocessors is based on the metal oxide semiconductor field effect transistor (MOSFET), consisting basically of source and drain, , and the third electrode, the gate that controls the electric current flows between source and drain. A number of materials had been studied as alternative to the channel body such, graphene, carbon nanotubes (CNTs), molybdenum disulfide (11), indium arsenide (12), only to mention a few. CNTs and graphene will be widely discussed in the next section, being the main topic of this thesis.

### 1.1.3. Carbon-based materials for electronics.

Carbon is the sixth element of the periodic table and the sixth most abundant element over the planet. Carbon is the second constituent of the human body. Carbon presents a great chemical affinity with a wide number of elements. This is the reason of the almost ten million of different compounds existing in nature. Moreover, many materials, like polymers, are mainly constituted by carbon atoms.

The only carbon allotropes known before 1985 were graphite and diamond. Sir H. Kroto, Richard Smalley, Robert Curl, James Heath and Sean O'Brien in 1985 discovered by accident a new allotrope of carbon: *the fullerene*. It has a soccer ball shape and is composed by 60 carbon atoms (13) in a pentagonal-hexagonal arrangement. Additionally, they reported the existence of other fullerene molecules like $C_{70}$ (13). Krätchmer and Huffman in 1990 reported the synthesis of bigger fullerene molecules $C_{76}$, $C_{78}$ and $C_{84}$ (14). In 1999 Piskoti published the discovery of $C_{36}$, a small fullerene-like molecule (15). Another breakthrough in the “carbon wold” was done by Ijima in 1991. The Japanese microscopist published the first characterization of carbon nanotubes, which can be considered like elongated fullerenes (16). After these discoveries other nanostructures were proposed and synthesized, like nano-onions (17), nanoribbons (18), nanocones (19), peapods (20, 21), etc. giving rise to a number of applications in many field of science and stimulating the interest of many researchers all around the world.

7 years ago, the ground-breaking experiments on graphene in Manchester added the two-dimensional allotrope at the carbon family and initiated a field of research moving at an ever faster rate, and gained the 2010 Physics Nobel prize to Andre Geim and Kostya Novoselov.

The possibility to engineer on demand nanostructures opened the doors to the availability of new properties that are not present in bulk materials. This is due essentially to the surface to volume ratio that is larger in nanostructures with respect to bulk materials. Thus, the availability of new materials with new properties is reflected in the opportunity to develop new applications, new science, new technologies and new experimental procedures.

Table 1.1 Carbon allotropes made of carbon. Information taken from (22).

| **Dimensions** | **0-D** | **1-D** | **2-D** | **3-D** |
|---|---|---|---|---|
| **Allotropes** | $C_{60,}$ fullerenes | Nanotube, carbynes | Graphene Fiber | Diamond, amorphous |
| **Hybridization** | $sp^2$ | $sp^2$ ($sp$) | $sp^2$ | $Sp^3$ |
| **Density (g/cm$^3$)** | 1.72 | 1.2-2<br>2.68-3.13 | 2.26<br>~ 2 | 3.515<br>2-3 |
| **Bond length (Å)** | 1.4 (C=C)<br>1.46 (C-C) | 1.44 (C=C) | 1.42 (C=C)<br>1.44 (C=C) | 1.54 (C-C) |
| **Electronic Properties** | Semiconductor<br>$E_g$=1.9eV | Metal or semiconductor | Conductor | Insulating<br>$E_g$=5.47eV |
| | 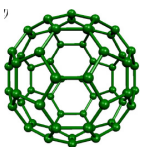 | 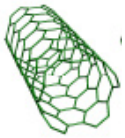 | 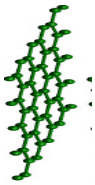 | 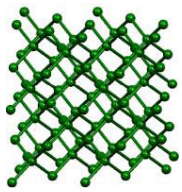 |

Thanks to these discoveries we can make a list from zero dimensional to 3-dimensional carbon allotropes, as shown in table 1.1, carbon is the only element that has all the three dimensional allotropes. This is explained by the fact that a carbon atom has six electrons

($1s^2$ $2s^2$ $2p^2$), which can be hybridized in sp, $sp^2$ or $sp^3$. For instance the newest carbon allotropes (fullerenes, nanotubes and graphene) have $sp^2$ hybridization while for example diamond is a $sp^3$ carbon material.

The electrical properties of these carbon materials are determined by the π bonds that originate from the $p_z$ orbitals that extend orthogonal to the honeycomb surface. This gives rise to delocalized electrons with energy bands close to the Fermi level (23–31). The most interesting carbonaceous material for electronic applications are graphene and nanotubes both from the morphologic and electronic point of view.

#### 1.1.3.1 Graphene.

Graphene is a flat monolayer of carbon atoms arranged in a 2D lattice. It consists of carbon atoms arranged in a 2-dimensional honeycomb crystal lattice with a bond length of 1.42 Å (32, 33) A schematic of a single layer graphene (SLG) is shown in Fig. 1.5, including “armchair” and “zig-zag” edges, named after their characteristic appearance on the atomic scale. The carbon atoms are $sp^2$ hybridized and three of the four valence electrons participate in the bonds to their next neighbours (σ–bonds). The fourth π electron orbital is oriented perpendicular to the sheet, forming with the neighbouring ones a highly delocalized network of π bonds.

The electronic properties of graphene are well known since 1947 with the study conducted by P. R. Wallace (34). The study of graphene was delayed due to the difficulty of isolate the single atomic layer.

Mechanical exfoliation of graphene was proposed by Geim and Novoselov in 2004 (24), they demonstrate the predicted properties of this peculiar one-atom thick material. The synthesis of graphene monolayer by heating SiC was first reported in 1896 (35) but characterized in 2004 (36), both procedures open new avenues in material sciences.

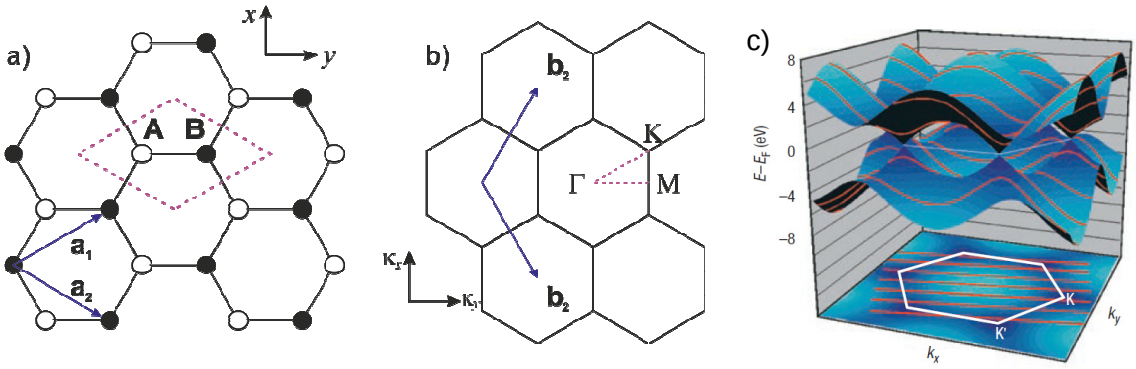


**Figure 1.5. a)** Representation of a small graphene crystal, each dot represent a carbon atom, the dotted red line is the unit cell. **b)** Primitive graphene cell un reciprocal space and **c)** Conduction and valence band, touching in six high symmetry points in the Fermi level, in this case is a sea representation of a semiconductor nanotube. Adapted from (62) and (189)

The graphene lattice consists of two sub-lattices A and B (fig. 1.5 a), which lead to crystal symmetry (34, 37). As a consequence, the charge carriers (*n*) can be described by the Dirac equation (38) *i.e.* the band structure of graphene exhibits a linear dispersion relation for *n*, with momentum *k* proportional to energy *E* (38). The energy bands associated with the sub-lattices intersect at zero energy. For this configuration graphene is "commonly" called a semimetal.

Charge carriers in graphene have a very small effective mass (39), hence graphene shows exceptional properties relevant to electronic devices. These include carrier mobilities up to 15 000 $cm^2/Vs$ for graphene on $SiO_2$ (40) and hundreds of thousands of $cm^2/Vs$ for suspended graphene (41–43), for typical charge density (*n*) ~$10^{12}$ $cm^{-2}$. Very recently, mobilities up to $10^6$ $cm^2/Vs$ with *n* of $10^{11}cm^{-2}$ were reported for suspended graphene at helium liquid temperature (44). These mobility values are at least 40 times higher than typical Si mobility. In addition, high current carrying capability exceeding $1x10^8$ $A/cm^2$ (45), high thermal conductivity (46, 47), high transparency (48) and mechanical stability (49, 50) have been reported.

### 1.1.3.2 Carbon Nanotubes.

Graphene has been used as a model for the calculations of the electronic and vibrational properties of carbon nanotubes. The differences between graphene and SWNTs can be explained in terms of curvature and confinement (51). Curvature effects arise because in a non-planar geometry the C–C bonds in SWNTs assume a mixed σ–π character. Confinement effects arise because the electronic wave-functions in a SWNT have to be commensurate to the tube circumference, resulting in the quantization of the electronic momentum component perpendicular to the tube axis. In figure 1.5 are shown both the direct and the reciprocal lattice of the graphene. $a_i$ define the direct lattice unit vectors in the real space, while $b_j$ are those of the reciprocal space related from the follow expression:

$$a_i \cdot b_j = 2\pi\delta_{ij} \begin{cases} 2\pi & if \;\; i = j \\ 0 & if \;\; i \neq j \end{cases}$$

The dashed rhombuses, in figure 1.5 (a), represent the unit cell in the direct lattice. In the sites A and B are located the carbon atoms, while $a_1$ and $a_2$ are given by

$$a_1 = \left( \frac{\sqrt{3}a}{2}, \frac{a}{2} \right)$$
$$a_2 = \left( \frac{\sqrt{3}a}{2}, -\frac{a}{2} \right)$$

where $a=|a_1|=|a_2|=1.42\sqrt{3}=2.46$ Å represent the lattice constant of graphene. In figure 1.5(c) the grey hexagon represents the first Brillouin zone of the graphene. $b_1$ and $b_2$ are the reciprocal lattice vectors defined as:

$$b_1 = \left( \frac{2\pi}{\sqrt{3}a}, \frac{2\pi}{a} \right)$$
$$b_2 = \left( \frac{2\pi}{\sqrt{3}a}, -\frac{2\pi}{a} \right)$$

The reciprocal lattice constant σ is 3 $a$ 4π . The high symmetry points are indicated with Γ, K and M. In graphene the valence band and the conduction band cross at the K point of the Brillouin zone (see figure 1.5 c).

The unique Fermi surface of graphene consists of the corner points of the hexagonal Brillouin zone, labeled as the *K* points (and the *K'* points related to *K* points by time-reversal symmetry). This peculiarity in the Fermi surface is responsible for the metallic or semiconducting nature of SWNTs. Figure 2.3 shows the *ab-initio* calculations of the electronic bands of graphene along the high-symmetry *M–Γ–K* directions (52). The valence band, $\pi$ and the conduction band, $\pi^*$ meet at the Fermi level at the *K* point of the Brillouin zone (53).

There are two basic approaches to calculate the energy bands of a material, the free electron approximation and the tight-binding approximation. In the latter, the electrons are considered to be part of the atoms forming the solid. Due to small atomic distances, the valence electrons of different atoms interact with each other (54) .

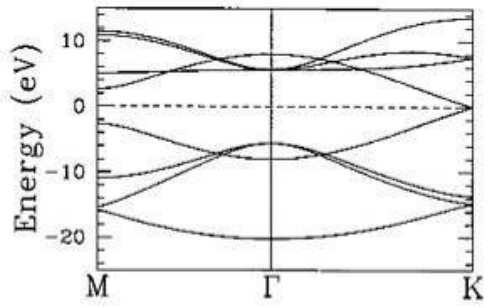


**Figure 1.6.** Electronic band structures of graphene. The Fermi level is set to zero. Reproduced from (57)

The tight-binding approximation works very well for the empirical calculation for graphene band structures (54). For the SWNTs, the zone-folding scheme within the tight-binding approximation is used (55, 56).

When forming a nanotube, due to periodic boundary conditions imposed along the circumferential direction, only a certain set of *k* states of the planar graphene sheet is permitted (57). Plotting the allowed wave vectors of a SWNT onto the Brillouin zone of graphene they result in a series of parallel lines (see figure 1.7) (54). These are determined by the chiral indices of SWNTs (57–59). Following the basis of the zone-folding scheme (54), the electronic band structure of a SWNT is given by the graphene

electronic energies along these allowed *k* lines (53, 55, 56). If $C_h$ is the chiral vector of the tube defining its circumference, the allowed values of *k* should satisfy the relationship:

$$k \cdot C_h = 2\pi \ p$$

where *p* is an integer which defines the lines perpendicular to $C_h$ (57). Whenever the allowed *k* values include one of the *K* points, the SWNT is a metal with a non-vanishing density of states (DOSs) at the Fermi level (57, 59). When the point *K* is not included, the SWNT is a semiconductor with a defined band gap. The states near the Fermi energy in SWNTs are all dependant on the states near the *K* point. Therefore, their transport and electronic/optical properties are directly related to the properties of the states on the allowed lines (57, 59). For example, the conduction band and valence bands of a s-SWNT come from states along the line closest to the *K* point (57, 59).

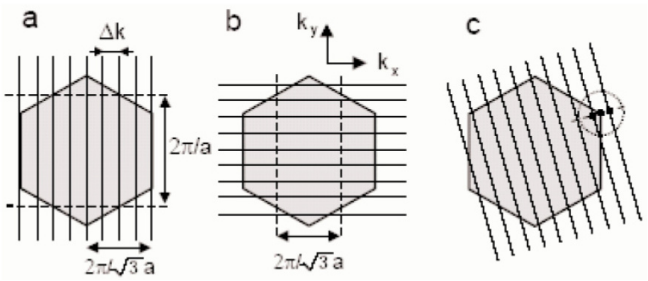


**Figure 1.7.** Graphene zone-folding for armchair (a), zig-zag (b) and chiral (c) SWNTs. Reproduced from (57)

Semiconducting SWNTs, furthermore, can be divided into two families (60): the ν = 1 family, for which (*n* - *m*) mod(3) = 1 and the ν = -1 family, for which (*n* -*m*) mod(3) = -1. For each family of SWNTs the quantity 2*n* + *m* is constant and the chiral indexes of the next neighbours are given by (*n* + 1, *m* - 2). Tubes (8,1), (7,3) and (6,5) belong to the same ν = 1 family (see vertical black arrow in Figure 1.8), while, tubes (9,1), (8.3) and (7,5) belong to the same ν = -1 family (vertical red arrow in Figure 1.8). Going from

"zig-zag" to armchair tubes within the same family both diameter and chiral angle increase. Tubes belonging to different families have different optical properties.

The zone-folding approximation ignores the effects of deviation from pure $sp^2$ hybridization due to tube curvature (61, 62). This deviation leads to mixing of *s* and *p* bands, which is significant for small diameter tubes (61). A small band gap, of the order of 10meV, opens up in non-armchair metallic tubes, which are thus known as quasi-metallic. In contrast, armchair tubes remain unaffected because of their symmetry (52)(54). To a first approximation, irrespective of the chirality, the band gaps of the large-gap and tiny-gap SWNTs decrease with ~1 *dt* and ~1 2 *t d* respectively (52, 64) . For most experimentally observed SWNTs, the band gap in the tiny-gap variety which arises from the curvature effects are so small that the (*n* −*m*) 3 = *i* tubes can be considered as metallic at room temperature (57, 58). Thus, a (7,1) SWNT, for example, would be metallic, whereas an (8,0) SWNT would be semiconducting in nature (57).

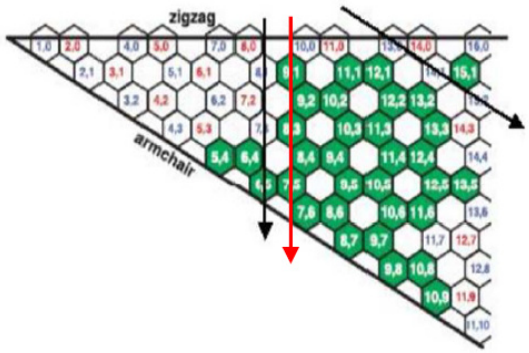


**Figure 1.8.** Graphene sheet showing indexed lattice points. Tubes belonging to the ν = 1 family and to the ν = -1 family are traced respectively by vertical black and red arrows. Adapted from (60)(53).

The one-dimension (1D) nature of SWNTs strongly influences their optical properties (62). Indeed, for this particular structure, their electronic density of states (DOS) is characterized by the presence of the so-called Van Hove Singularities (VHSs), where the DOS diverge (65). Figure 1.9 shows how the VHSs are equally distributed above and below the Fermi energy and their distribution are expected to determine the optical absorption and emission properties of SWNTs (62).

The presence of VHSs in SWNTs was first theoretically predicted in 1992 (62) and then experimentally proved by means of Scanning Tunnelling Microscopy STM (66, 67).

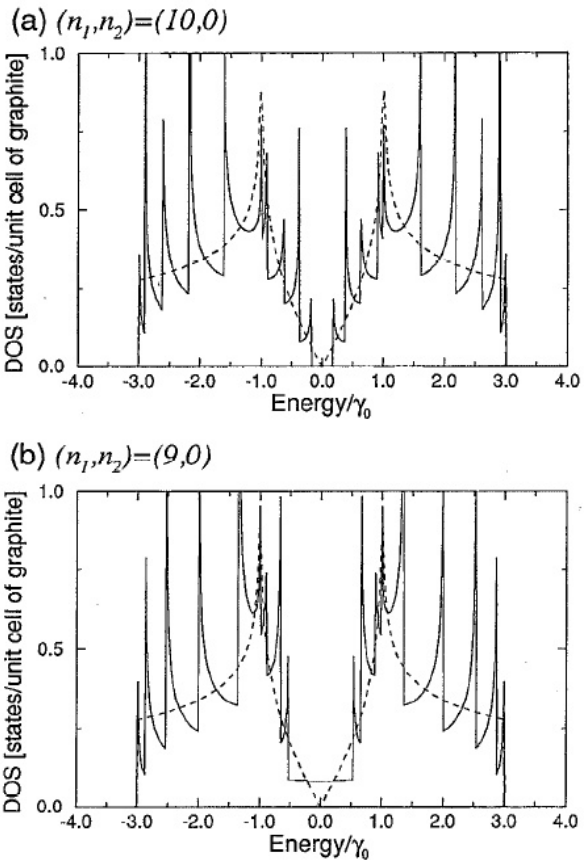


**Figure 1.9.** Theoretical DOS of a (10,0) (a) and a (9,0) (b) SWNT. Taken from (62)

The optical properties of SWNTs are dominated by the transitions between these VHSs (58, 68). For example, the optical absorption peaks from SWNTs strongly correspond to the energy gaps (60, 69–71). The optical absorption spectra of SWNTs calculated for polarized light (72) show that the selection rules for optical absorption between the valence and conduction $\pi$ subbands with subband index $n$ are $\Delta_n$ =1and $\Delta_n$ = 0 for light polarization perpendicular and parallel to the SWNT axis, respectively (73). The optical absorption for the polarization perpendicular to the nanotube axis is suppressed almost completely when the depolarization effect is taken into consideration (72, 74). Thus in SWNTs, the optical absorption occurs only when the polarization is parallel to the SWNT axis for inter-subband transitions, with $\Delta n$ = 0 (73). The polarization effect is important for the optimization of SWNT-polymer composites for optical applications (75–77). However, it has not been widely studied. The approximate inverse relationship between the transition energies $E_{ii}$ and diameter $d_t$ irrespective of the chiral angle was first explained by White and Mintmire in 1998 (64).

In the following year, extension of this idea led to the widely used 'Kataura plot' (Fig. 1.10) with well-defined and well-separated optical transition energy $E_{ii}$ ($i$ = 1, 2, 3...) positions against $d_t$ from different SWNT species (53, 78). Hence, $d_t$ could be inferred from the optical absorption peaks or the resonance energies in Raman spectra, thereby complementing the data obtained from the radial breathing modes (RBMs) (68, 79). This relationship between $d_t$ and $E_{ii}$ works surprisingly well at low excitation energies (71). The initial form of the Kataura plot was very useful in interpretation of the Raman spectra for SWNT diameters ranging from ~1.2-1.5nm and for laser energies between 1.9-2.5eV (57). However, strong deviations are observed in high energy $E_{ii}$ lines as they broaden up (52, 62, 79–81). This broadening originates in deviations from the linear dispersion of the energy bands away from the Fermi level, an effect termed as the 'trigonal warping' (62). Because s-SWNTs have direct bandgap, photoluminescence (PL) from s-SWNTs due to carrier recombination can be observed (Fig. 1.11). The mechanism leading to PL from isolated s-SWNTs involves carrier excitation into the second subband ($c_2$ in Fig. 1.12(a)), non-radiative relaxation into the first subband ($c_1$ in Fig. 1.12(a)) and recombination with the emission of a photon ($c_1$ to $v_1$ or $E_{11}$ in Fig. 1.12(a)) (60).

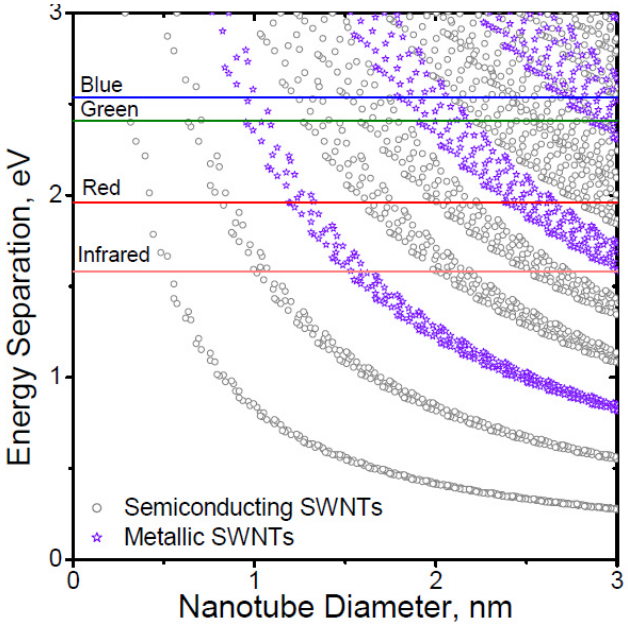


**Figure 1.10:** (color) The original 'Kataura plot' of SWNTs showing relationships between the transition energies and diameters of different SWNTs. The horizontal lines show some of the commonly used laser excitation energies in Raman spectroscopy; from top: Blue (2.54eV; 488nm), Green (2.41eV; 514.5nm), Red (1.96eV; 633nm) and Infrared (1.58eV; 785nm). Based ion data from (190) (53)

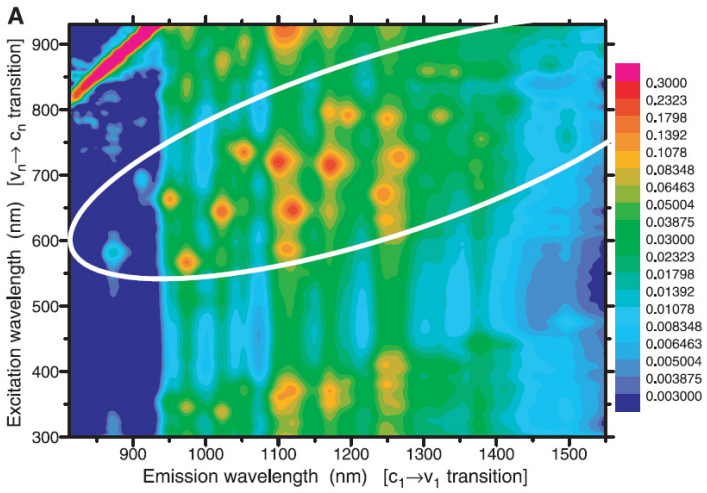


**Figure 1.11:** Contour plot of PL intensity versus excitation and emission wavelengths from SDS micelle encapsulated SWNTs. The resonance spots inside the white ellipse represent different species of SWNTs with absorption (excitation) and emission wavelength/energies. Reproduced from (60)

Relaxation channels offered by m-SWNTs in close proximity (*e.g.* in bundles) prevent PL from s-SWNTs. PL from SWNTs can only be observed when the s-SWNTs are isolated through micelle encapsulation, or in small bundles (typically less than 10) (69), enabling direct studies of their optical properties. PL excitation (PLE) spectroscopy is a crucial step forwards the determination of SWNT species (chiralities) in an ensemble of isolated SWNTs. The transition energies of SWNTs can be probed by PLE spectroscopy by scanning the excitation wavelength through the $E_{ii}$ ($i$=2, 3, 4…) range and measuring the emission from $E_{11}$ transitions. Therefore, each and every s-SWNT species can be identified by its distinct set of $E_{excitation}$, $E_{emission}$ resonance spots; as shown by the encircled region in Figure 1.11. However, systematic deviations from the original Kataura plot were observed in the spectral data from the micelle encapsulated isolated SWNTs (60, 79, 82). In addition to the stronger than expected deviation of $E_{ii}$ from the $d_t$ dependence, the $E_{11}$ $E_{22}$ ratios were found to approach values much smaller than 2 (60) in contrast to the original theoretical predictions by White and Mintmire (64, 65). Also, decrease in the PL intensity for SWNTs with small chiral angles (*i.e.* zigzag SWNTs) was observed, an effect which could not be explained using the singleparticle model (Figs. 1.12(a) and (b))(58).

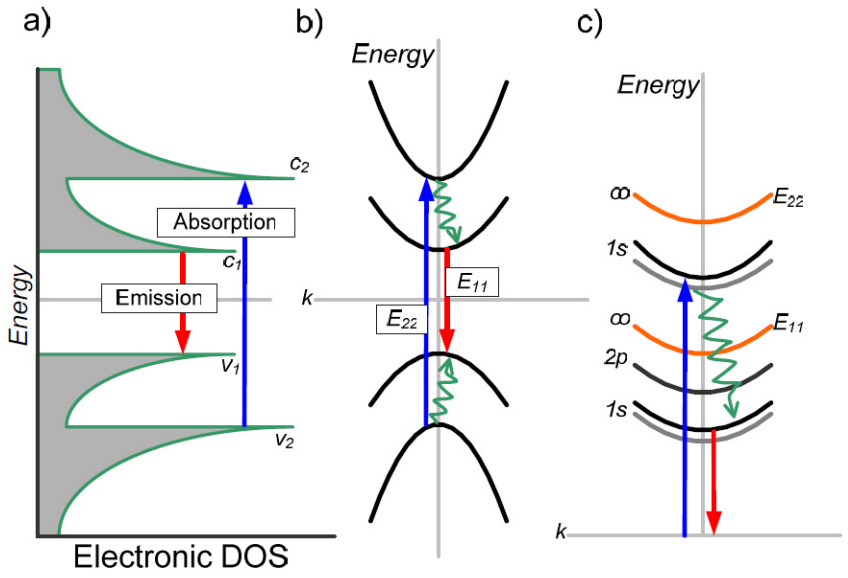


**Figure 1.12.**: (a) and (b) The band structure and optical transitions in a simplified single-particle picture and its corresponding DOSs. Optical absorption at $E_{22}$ and emission at $E_{11}$ are shown by an upward and a downward pointing arrow. The jagged arrows represent relaxation from $E_{22}$ to $E_{11}$. (c) A simplified picture of the exciton band structure and optical transition. The one-photon process can only produce excitons at *s* level. The ground state represents a vacuum state, *i.e.* with no excitons. Adapted from (83) (53)

Optical techniques to probe SWNTs are very advantageous from the experimental point of view. The measurements are non-destructive and can usually be carried out at room temperature under ambient pressure with minimal sample preparation. Also, due to the one dimensional confinement of electronic structures, a strong optical response from SWNTs can be obtained (83). The changes in the surrounding dielectric environment due to solvents, dispersants or bundling of nanotubes cause the electronic properties of SWNTs to deviate from their isolated counterparts. Such changes in the SWNT transition energies can be probed by optical absorption (OAS) (84–86), Raman (87, 88), PLE spectroscopy (89, 90). OAS and PLE are particularly useful in estimating the quality and stability of SWNT dispersions (82, 91). Raman spectroscopy is widely used to determine the composition of SWNTs in a sample. Systematic chirality assignment through the RBM region (71, 79, 85, 87, 88, 92) may be used as a complementary technique to OAS

(60, 93) and PLE spectroscopy (60, 88). Also, disorder and defects in SWNTs can be probed using Raman spectroscopy (94). PLE may also be used to monitor subtle changes in SWNT dispersions due to bundling or other external perturbations (85, 95) in addition to the identification of different SWNT species (60, 96).

#### 1.1.3.3 Raman spectroscopy

The Raman effect consists of the inelastic scattering of light on crystals or molecules, where the incoming photons either lose or gain quanta of vibrational energy (97, 98). During a scattering event, (1) an electron is excited from the valence energy band to the conduction energy band by absorbing a photon, (2) the excited electron is scattered by emitting (or absorbing) phonons, and (3) the electron relaxes to the valence band by emitting a photon.

The two processes are called respectively Stokes and anti-stokes. In the Raman scattering, both energy and momentum must be conserved (97, 98). Only the optical phonon with q ~ 0 can satisfy momentum conservation (97, 98). Raman spectroscopy is a fast, powerful and non-destructive method for characterization of carbon materials (99). A number of important informations, such as diameter, chirality, metallic or semiconducting character and orientation can be obtained from Raman characterization of SWNTs

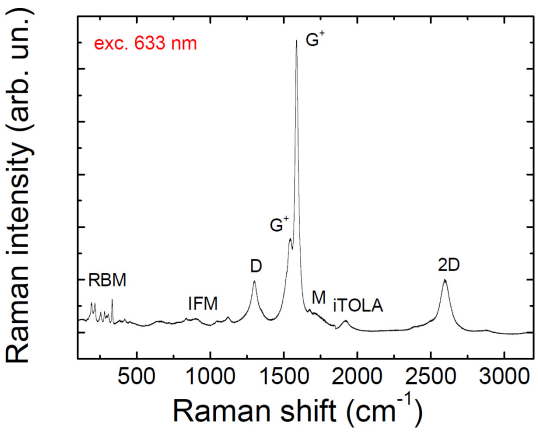


**Figure 1.13**: (color) A typical Raman spectrum of purified CoMoCAT SWNT powders acquired with excitation energy of 1.96eV. Other than the first-order single-resonance RBM and G band features, many other harmonics and combination modes (i.e. iTOLA, M, 2D) are observed, as well as disorderinduced bands (e.g. D band) and intermediate frequency mode (IFM). Taken from (53)

The Raman spectra of carbon nanotubes consist of a rich set of features. In fig 1.13 is shown the typical Raman spectrum of CoMoCAT SWNTs with

excitation wavelength fixed at 633nm. Other than the first-order single-resonance RBM and G band features and the disorder induced bands (e.g. D band), many other modes such as: iTOLA, M, 2D are observed, as well as the intermediate frequency mode (IFM) (99). The feature-rich Raman spectra from SWNTs can be used to characterize several aspects of isolated, bundled, as-grown, purified, doped, functionalized or even single SWNTs (68, 83, 87, 91, 100). The Raman intensity depends on the polarization of the light. This can be used to characterize the orientation of SWNTs (101). According to the resonance Raman scattering RRS process for SWNTs, a strong Raman intensity is observed from only the SWNTs whose optical transition energies are within the resonance window of $E_{Laser}$ (102). This is why resonance Raman spectroscopy is a dominant optical characterization technique for SWNTs. The next sections describe the important Raman signatures from SWNTs.

#### 1.1.3.3.1 Radial Birthing Modes

The low frequency feature observed in fig. 1.13 in the 120 to 350 $cm^{-1}$ region for the usual SWNT diameter range (~0.7-2 nm) are the so called radial breathing modes (RBM) (28). The RBM mode is unique in SWNTs and is not observed in other carbonaceous materials. It is used to determine the diameter and chirality of SWNT samples. In the RBM mode, all the carbon atoms move in phase in the radial direction, creating a breathing-like vibration of the entire SWNT, see figure 1.14 (a). The force required for such radial deformation of SWNTs increases as the diameter decreases (54).

The RBM frequency ($\omega_{RBM}$) is inversely proportional to the SWNT diameter $d_t$ (71, 91) and can be expressed as:

$$\omega_{RBM} = \frac{C_1}{d_t^{\kappa}} + C_2(d_t)$$

where, $C_1$ is a constant and $C_2$ is likely to depend on diameter $d_t$ and an exponent κ (54). A variety of $C_1$ and $C_2$ values have been proposed. However, their precise values are only critical for chirality assignment. The $\omega_{RBM}$ of bundled SWNTs is different from their

isolated counterparts by as much as 10% (103). For $d_t$ < 1 nm, this equation is not expected to hold due to nanotube lattice distortions, leading to a chirality dependence of $\omega_{RBM}$ (104). For SWNTs with $d_t$ > 2nm, the intensity of the RBM feature is weak and is hardly observable (83).

In general, the RBM mode may be used to estimate the $d_t$ distribution and electronic type of SWNTs. The latter is possible due to the 'grouping' of semiconducting-SWNTs and metallic-SWNTs by $d_t$ in the Kataura plot (71, 79). Fig. 1.14 (b) shows an example of SWNTs characterization by electronic types. In this particular case, the figure shows the RBMs from commercially available CoMoCAT SWNTs (93) at λ=633 nm (1.96 eV) laser excitation. Correlation between the Kataura plot (71, 79, 105) and fig. 1.14 (b) confirms that both metallic-SWNTs and semiconducting-SWNTs in the sample contributes to the RBMs. It should be noted that, Raman is a strongly resonant process and hence, does not provide a reasonable characterization of the diameter and type distribution unless a range of laser excitation is used (71, 79).

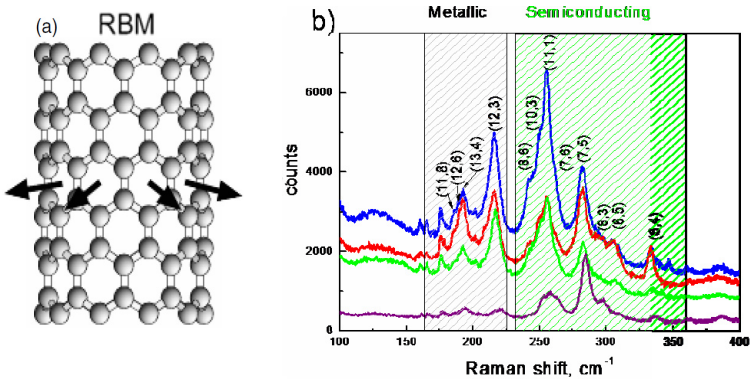


**Figure 1.14:** (a) Schematic of the origin of the RBM in SWNTs. RBMs from (b) purified CoMoCAT SWNTs. Reproduced from (191)(53).

1.1.3.3.2 D-mode

The D peak is a Raman feature that appears in materials in the presence of structural disorder (106–109). It originates by a breathing mode of hexagonal rings and it is observed in the frequency region between 1200 and 1400 $cm^{-1}$. The D mode originates from phonons close to **K** and should be thus forbidden, because it does not satisfy the **q** ~ 0 selection rule. The reason because it is observed can be explained only taking in account a double resonance (DR) process. In this process the momentum conservation is guaranteed by the elastic scattering of electrons with defects. This process consists in the excitation of an electron-hole pair, followed by electron-phonon scattering with exchanged momentum **q ~ k,** where **K** represents the momentum at the **K** point of the Brillouin zone. The electron is then elastically scattered by a defect, with exchanged momentum –q thus guarantying the total momentum conservation law and at the end recombines radiatively with the hole (109). The D peak can be activated only in presence of defects (106, 107). The process is schematized in figure 1.15.

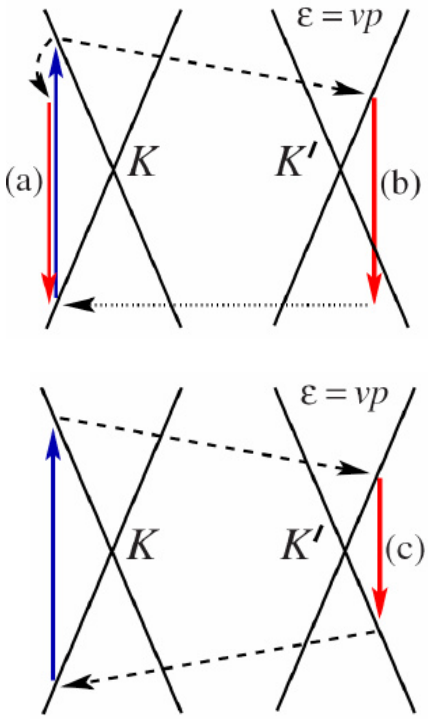


**Figure 1.15:** Schematic representation of the role of electron dispersion (Dirac cones, shown by solid lines) in the one-phonon (a, b) and two-phonon Raman scattering (c). Vertical solid arrows represent interband electronic transitions accompanied by photon absorption or emission (photon wave vector is neglected), dashed arrows represent phonon emission, the horizontal dotted arrow represents the impurity scattering. Taken from (53)

Looking at the intermediate electronic states involved in the Raman scattering, it is possible to note that for one phonon scattering (processes (a), (b)) at least one intermediate state must be virtual, since energy and momentum conservation cannot be satisfied simultaneously in all processes. For the two-phonon scattering (process (c)) all intermediate states can be real (53). It is important to emphasize the qualitative difference

between the fully resonant process (c) and the double-resonant (109) process (b), where one intermediate state is still virtual. In the case of the D peak, the electron-phonon scattering takes place at the same **K** point (110–113). The 2*D* peak is a two-photon process, thus the electron is not scattered back by a defect but by a second phonon(53).

The D peak is dispersive because its position depends on the excitation energy. Due to the presence of a KA, the phonon dispersion of the highest optical branch at K is also strongly dispersive with slope α. Therefore, an excitation energy $\hbar\omega_L$ selects a phonon with energy $\hbar\omega_K + \alpha\,\hbar\omega_L/\beta$, resulting in a linear relation between the excitation energy and the D peak position (53).

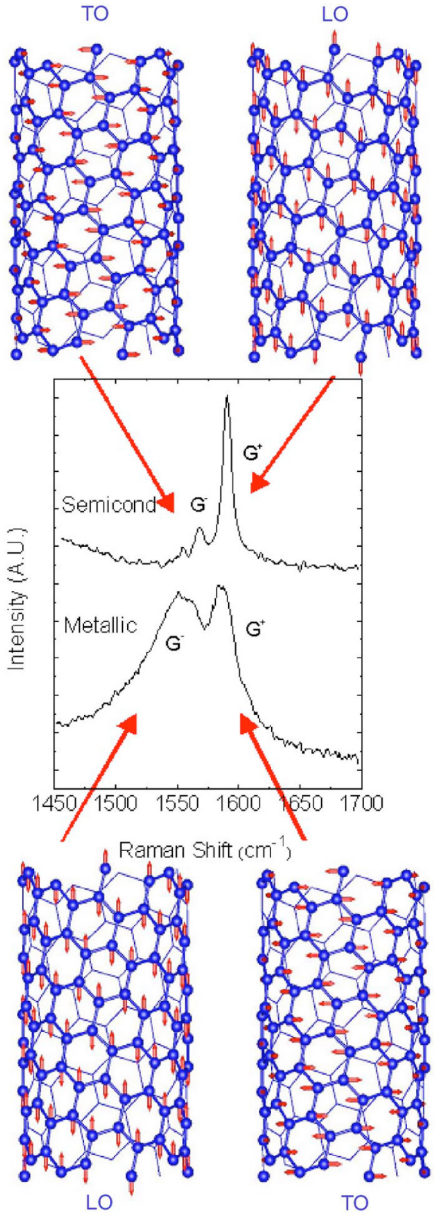


**Figure 1.16.** Raman $G^+$ and $G^-$ peaks for semiconducting and metallic SWNTs. In semiconducting tubes the two peaks have a Lorentzian shape and a FWHM of ~12 $cm^{-1}$. In metallic tubes the $G^-$ peak is downshifted and much broader. The assignment of the spectral features is also indicated. Adapted from (51, 53)

1.1.3.3.3 G-band

The Raman spectrum of SWNTs, in the range 1500-1600 $cm^{-1}$, is characterized by the presence of two distinct features so-called $G^+$ and $G^-$ modes. The origin of these two peaks arises by the splitting of the double degenerate, Raman-active $E_{2g}$ mode of graphene. The $G^+$ peak position ($\omega_G^+$ ~ 1591 $cm^{-1}$) is almost independent from the diameter, while on the contrary, the G- peak position decreases with the diameter. The latter can be expressed by $\omega_G^- = \omega_G^+ - c/(d_t)^2$, with $c$ being different for m-SWNTs and s-SWNTs ($c_{Metallic} > c_{Semiconducting}$) (114). Hence, the position of the $G^-$ peaks can be used to correlate the $d_t$

distribution of SWNTs obtained from the RBM (71, 79, 115). From the diameter dependence of the $G^-$ band, it can be concluded that the *G* band for large diameter CNTs is similar to the *G* band of graphite. Indeed, for large diameter MWNTs, only a single peak at ~1582cm$^{-1}$ is observed, just like in graphite (28). Both the $G^+$ and $G^-$ peak positions are independent of the SWNT chiral angle (83). In semiconducting SWNTs the shape of both these two features appears as Lorentians, while in metallic SWNTs the shape is very broad and its position is downshifted respect the semiconducting counterpart.

The $G^+$ and $G^-$ peaks originates from the LO and TO modes, which are polarized along the tube axis and along the circumference, respectively (fig. 1.16) (51). In semiconducting SWNTs, the $G^+$ peak is assigned to the LO mode while the G- is assigned to the TO mode. In metallic SWNTs the assignment is the opposite: the LO mode is affected by KA causing a downshift of its frequency. Thus the $G^+$ peak originates from the TO mode, while the $G^-$ originates from the LO mode. The LO mode in m-SWNTs has a notably lower frequency than the $G^-$ peak (TO) from the s-SWNTs. In addition, it exhibits a broad and asymmetric Breit-Wigner-Fano (BWF) line-shape due to phonon-plasmon coupling and softening of the LO phonon (116), peaking at ~1540 cm$^{-1}$ (54). The splitting and conformation of the G band together with the simultaneous detection of the RBM make possible the distinction between metallic and semiconducting SWNTs. The frequency shift in $G^-$ band for the m-SWNTs can also be used to identify doping effects (117). The full width at half maximum (FWHM) of the *G* band is ~5cm$^{-1}$, smaller than in graphene (~12cm$^{-1}$), except for the broad BWF features (118)

### 1.1.2.4 Optical absorption spectroscopy

OAS is the simplest among the optical probing technique used for SWNTs characterization from both an experimental and theoretical point of view. OAS is usually based on the observation of the absorption peaks related to the $eh_{11}$ and $eh_{22}$ transitions from the s-SWNTs and $eh_{11}$ from the m-SWNTs (69, 71). Therefore, typical optical absorption measurements for SWNTs range from 400 to 2000 nm (3 eV-620 meV).

Despite the fact that SWNTs have sharply peaked DOSs, the absorption peaks are usually broad. Several factors are responsible for this broadening. SWNT sample usually contain many different species, each with a different set of absorption peaks, adding up to produce a broad peak (69). In addition, even if the sample consists of only a single nanotubes species, interaction with the environment or bundling can broaden the spectral features (83). OAS from isolated SWNTs exhibit a series of sharp absorption peaks (25 meV), in contrast to the broad peaks typically observed from the SWNTs bundles (69, 71). The background at the lower energy regions in SWNTs absorption spectra stems from the higher-lying Plasmon excitation in SWNTs and is observed in both isolated and bundles SWNTs (54).

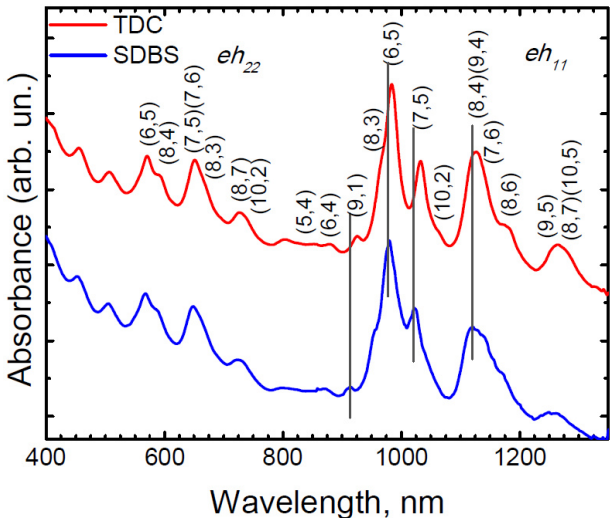


**Figure 1.17**: Optical absorption spectrum of CoMoCAT SWNTs dispersed in DI water using sodium Taurodeoxycholate (TDC, red line) and sodium dodecylbenzene sulfonate (SDBS, blue line) as surfactant. The absorption peaks from different SWNT species are assigned according to Refs. (60, 79). The shift in the peak positions and widths are due to different surfactants *i.e.* dielectric environments. (53)

It is not easy to unambiguously identify the SWNTs chirality from OAS; especially if the transition energies of more than one SWNTs species overlap. However, the assignment of SWNTs through OAS alone may be possible by correlating the $eh_{11}$ and

$eh_{22}$ for single SWNTs species in the absorption spectra from mostly isolated SWNTs, as done in figure 1.17. During assignment, environmental effects, which induce shifts in the transition energies, must be considered. Enrichment of s-SWNTs and m-SWNTs in a sample can be easily demonstrated by OAS since the $eh_{ii}$ transition energies for s-SWNTs and m-SWNTs are grouped separately (71, 119). Population analysis from OAS can also be qualitatively performed. This is very useful during the enrichment of a particular SWNT species (119). Concentration of SWNTs in dispersion may also be estimated using OAS. For example, the optical density (OD) of a SWNTs species in solution, can be defined as OD= $-\log_{10}(I/I_0)$, where $I$ represents the intensity of light at a specified wavelength $\lambda$ that has passed through a sample (transmitted light intensity) and $I_0$ is the incident light intensity. If $A_\lambda$ is absorbance of material at wavelength $\lambda$, $\alpha_\lambda$ is the absorption coefficient at wavelength $\lambda$, $l$ is the length of optical path and $c$ is the concentration of material, then according to Beer-Lambert law,

$$A_\lambda = \alpha_\lambda lc$$

## 1.2 Carbon nanotube field effect transistor

The basic difference between a silicon transistor and nanotube transistor relies in the dimensionality. As was explained before, the morphology of SWNT prevents or highly reduces the electron scattering, as result, the transistor can work in the ballistic regime. Another notable difference between silicon and nanotube transistor is the switching mechanism.

Indeed, in a silicon-based FET the flow control of electrons or holes from source to drain is achieved via a change in size and shape of the “conductive channel” created and influenced by the voltage, or lack of voltage, applied on the gate terminal. This voltage creates a depletion region or an insulating zone within a doped semiconductor channel. This insulating zone expands and encroach the “conductive channel” between electrodes. In this way, if a voltage is applied to the gate terminal, the depletion region expands closing the channel. In this condition, the resistance between source and drain becomes large, and the FET is turned off like a switch. Contrary if the gate voltage is zero, the

depletion region is reduced. In this configuration, the channel is and the electrons can flow through the channel, so the FET is turned on (120).

On the other hand, in a nanotube transistor the switching capability is controlled by the Shottky barrier in the metal-nanotube junction (26, 70, 121). Indeed, some studies indicates that charge carriers can change the electric behaviour from *p*-type to *n*-type or vice versa (122). These characteristics make nanotube-transistor an unique and interesting device for fundamental study.

In this introductory chapter, the 3 main points for the construction of a nanotube transistor will be discussed: the dielectric gate material, the nanotube-electrode junction and the determinist placement in a desired position of the nanotube.

### 1.2.1 The dielectric material

CNT-based transistors are usually fabricated over a $Si/SiO_2$ substrate. Diverse processes have been developed for the placement of nanotubes over the substrate followed by the deposition of metallic electrodes. The latter can be carried out with different strategies such as lithography and metal evaporation, atomic layer deposition (ALD), gas phase epitaxy (GPE) or molecular beam epitaxy (MBE).

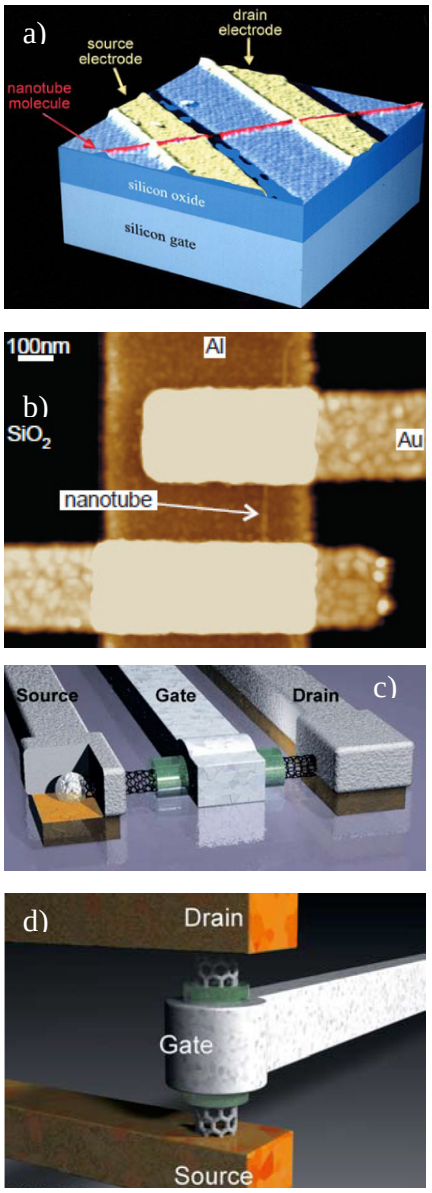


**Figure 1.18.** a) and b) are non-true coloured AFM and SEM images respectively of a back-gate nanotube FET (125)(127). c) representation of a common top-gate CNT-FET and d) an idealization of a gate-all-around CNT FET., both taken from (192)

The nanotubes can be directly grown (by chemical vapour deposition (CVD)) on the sample using metallic seeds (123) such as iron or nickel particles and a carbon gas as precursor (this process will be discussed in the next chapter). An alternative relies on the deposition from a dispersion (123, 124) to form a nanotube network. The substrate is highly doped making it conductive and act as gate in which a voltage is applied to control the electron flow through the nanotube. This configuration was first published in 1998 (125, 126). However, this arrangement suffers very large contact resistance, poor voltage gain, a big subthreshold slope, among others. However, this structure (figure 1.18 a) was rapidly improved changing the metal composition, and depositing an individual nanotube over an alumina electrode acting as a gate electrode This structure enabled the creation of different logic gates configurations (127). In 2002, Avouris group at IBM proposed to use a top gate configuration figure 1.18 b), controlling the doping and increasing the electronic properties of previous back-gate devices (128), they achieved a subthreshold slope of 130 mV / decade, the subthreshold slope is related with the device swiftness response to change between off (low current) and on (high current) states, e. g., the average subthreshold for a silicon transistor is 60 mV / dec (129). The top-gate configuration of Avouris resembles, for some aspects, the one of silicon transistors.

Dai and co-workers published the first gate all around (GAA) nanotube transistor, with 60 mV / decade (130), figure 1.18 c and d. They used DNA as linker between the nanotube and the $HfO_2$ dielectric deposited by ALD. In 2009 Avouris demonstrates the possibility to build a GAA transistor using a thin coating layer of $NO_2$ (131), improving the control over the electron flow, and opening the possibility to engineering doping over the naked nanotube between the coating and the electrodes. However, the building process using ALD makes this procedure quite complicated. A different approach for a GAA transistor is a vertical scaling (132). In this configuration, nanotubes are grown directly on the substrate and orthogonally at it. The nanotubes are coated via dielectric/metal deposition (a top-down approach). Unfortunately the GAA device is the most difficult configuration to achieve, even for silicon technologies (9, 10, 133). It is notable that the most used techniques to build GAA device is ALD. This strategy has some drawbacks. First of all, it suffers high production cost. Moreover, ALD hinders the

scaling up of the production. Thus, it is fundamental the development of new strategies, both for the discovery of new materials and devices. In table 1.2 the start of the art results from diverse references is reported. In this thesis I will show my approach to overcome this challenge: a bottom up synthesis of a GAA dielectric, see chapter 3.

### 1.2.2 The nanotube-electrode junction

A key issue for nanotube transistors is the nanotube-electrode contact (134–136). It is known that the surface of nanotubes is inert (137, 138), However, despite this problematic, nanotubes-based transistor are fabricated placing the tube on the top (or bottom) of metal electrodes just being attracted by van deer Waals forces, (139, 140). Recently the National Institute of Standards and Technology (NIST) reported the self-destruction of nanotube devices due to the high resistance in the metal-nanotube junction (141, 142). To overcome this huge problem, different strategies have been proposed to improve the contact resistance. Ref (143) proposed the use of ultrasound for melting the electrodes so that nanotube can be embedded in the melted electrodes. A better approach relies in the change of the electrode material. This permits to tailor the work function of the electrodes themselves, modulating the electronic behaviour of the final device. For instance Calcium, Hafnium or Chromium electrodes produce a *n*-type behaviour (134, 144, 145), while on the other hand Titanium or Palladium give origin to *p*-type behavior. In contrast Magnesium produce ambipolar devices (146, 147). Similar devices are reported for some conductive polymers (148).

Additionally the electronic behaviour can change in the presence of atmospheric oxygen (145) or exotic materials (149–153), making even more complicated and challenging the construction of a device. Indeed, the fabrication must be very accurate, avoiding chemical doping to prevent non desired and uncontrollable behaviours/performances.

The most reactive parts of the nanotube are the tips. It is possible to selectively oxidize the nanotube tips and use this reactive oxygen groups to get a covalent bonding with metal electrodes, it is expected to improve the electron transfer, reduce the work function, and thus increase the device lifetime. This subject will be discussed in chapter 3.

**Table 1.2.** Chronological review of CNT-FETs reported in diverse references.

| Year | FET Configuration | Electrode material | Gate characteristics | Channel characteristics | On/off ratio | Transcon-ductance (μS) | Sub-threshold slope (mV/dec) | Ref. |
|---|---|---|---|---|---|---|---|---|
| 2001 | Back-gate | Au | $Al_2O_3$ | SWNT | $10^5$ | 0.3 | ~110 | (127) |
| 2002 | Top-gate | Ti | TiC-SiO2 | SWNT | $10^4$ | 0.125 | 130 | (154) |
| 2004 | Local top-gate | Pd | ALD $HfO_2$/Al | SWNT | $10^5$ | 20 | 80 | (155) |
| 2004 | Local top-gate | Pd | ITO-W | HSQ functionalized SWNT | $10^6$ | | 200 | (150) |
| 2005 | Back-gate | Cr/Au | $SiO_2$ | APTES-SAM SWNT | $10^4$ | 0.5 | 2000 | (156) |
| 2005 | Back-gate | Pd | $SiO_2$ 10 nm | SWNT 5μm length | $10^6$ | - | 85 | (157) |
| 2005 | Local back-gate | Pd | $SiO_2$-$Al_2O_3$ | SWNT | $10^5$ | 12.5 | 140 | (158) |
| 2005 | Back-gate | Al - Pd | $SiO_2$ 900 nm | SWNT | $10^3$ | - | - | (159) |
| 2006 | Back-gate | Pd | $SiO_2$-$Al_2O_3$ | functionalized-SWNT | $10^6$ | - | 115 | (160) |
| 2006 | Ω-shape | Ti/Au | ALD $HfO_2$ | DNA wrapped SWNT | - | - | 60 | (130) |
| 2006 | Back-gate | Au | Dielectrop. | DNA wrapped SWNT | $10^3$ | - | - | (161) |
| 2007 | Back-gate | Ti-Au/Pd | $SiO_2$-Organic SAM | SAM SWNT | $10^5$ | 0.5 | 300 | (162) |
| 2008 | All-around-gate | | WN/$Al_2O_3$ | ALD coated SWNT | - | - | 250 | (131) |
| 2008 | Back-gate | Mo/Co | $SiO_2$ | *In situ* growth SWNT | $10^6$ | | 200 | (163) |
| 2008 | Back-gate | Pd | ALD-$HfO_2$ 20nm | coated SWNT | $10^3$ | - | 120 | (164) |
| 2009 | Back-gate | Au | $SiO_2$ 200 nm | SWNT network | $10^2$ | - | ~2000 | (165) |
| 2009 | Top-gate | Ti/Au | CVD-Al2O3 | SWNT network | $10^5$ | - | - | (166) |
| 2009 | Top-gate | Cr/Au | ALD-$HfO_2$ 100 nm | coated SWNT | <10 | | - | (167) |
| 2009 | Back-gate | Au/Cr | PEI-$SiO_2$ | SWNT network | <10 | - | - | (149) |
| 2010 | Top-gate | Ti/Pd | ALD-$HfO_2$ 12 nm | 4 nm diam. SWNT | 2 | 14 | - | (168) |
| 2010 | Local bottom-gate | Pd | $HfO_2$ 10 nm | 15 nm chann. SWNT | $10^5$ | 40 | 85 | (169) |
| 2010 | Top-gate | Sc | ALD $Y_2O_3$ | *In situ* growth SWNT | $10^5$ | 5 | 60 | (170) |
| 2012 | Back-gate | Pd/Au | W/$HfO_2$ | 9 nm channel length SWNT | $10^4$ | 40 | 94 | (171) |

### 1.2.3 The Self-assembly of the device

The last point to discuss is the deterministic placement of the nanotube in a desired location. CNT is a non conventional material as silicon, with CNTs it is not possible to grow a nanotube layer using GPE, molecular beam epitaxy (MBE) or ALD to growth a perfect and crystalline surface. Traditional methodologies for the production of electronic devices are not applicable for the case of nanotubes. Moreover, the reduced dimensionality hinders the use of some (macro) mechanical tweezers to locate the tubes in an electric circuit, exploiting a naïve pick-up procedure, *i.e.* using atomic force microscopy (AFM) or nanotweezers. For the placement of nanotubes in the desired location was proposed the use of electric fields. This process is based on a controlled placement of CNTs on metal electrodes using an alternating-current electric field. A drop of SWNTs dispersion is dripped over the contacts. The ac electric field mainly attracts the metallic nanotubes in dispersion towards electrodes .This technique is useless for our objective. A simpler way for CNTs placement is to use chemical selectivity. For this purpose some groups reported the functionalization of the substrate with amino groups and the successful location of functionalized-nanotubes between electrodes (156, 172). For this purpose, DNA is a powerful tool that has been exploited.

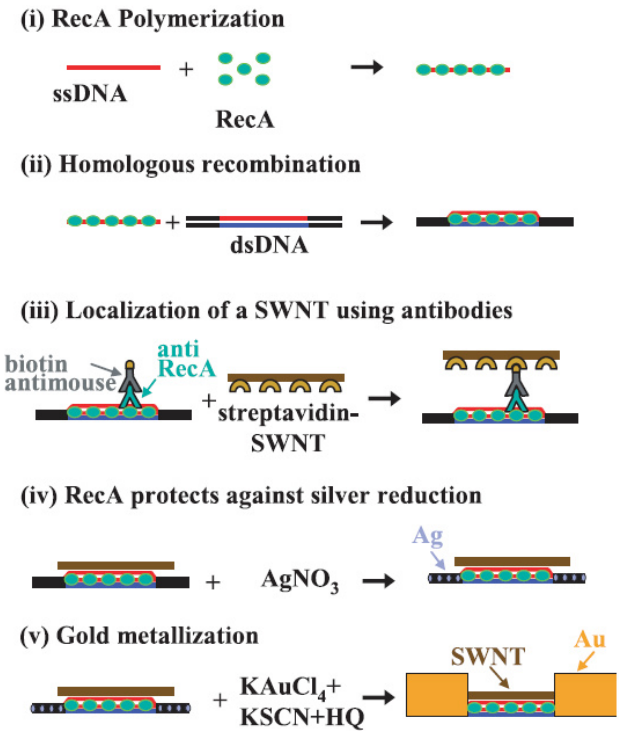


**Figure 1.19.** Assembly of a DNA-templated FET and wires contacting it. Steps are as follows: (i) RecA monomers polymerize on a ssDNA molecule to form a nucleoprotein filament. (ii) Homologous recombination reaction leads to binding of the nucleoprotein filament at the desired address on an aldehydederivatized scaffold dsDNA molecule. (iii) The DNA-bound RecA is used to localize a streptavidin-functionalized SWNT, utilizing a primary antibody to RecA and a biotin-conjugated secondary antibody. (iv) Incubation in an AgNO3 solution leads to the formation of silver clusters on the segments that are unprotected by RecA. (v) Electroless gold deposition, using the silver clusters as nucleation centers, results in the formation of two DNA-templated gold wires contacting the SWNT bound at the gap. Taken from (179)

Indeed, it is possible to functionalize the DNA with small molecules or proteins, like streptavidine or biotin (173–175), or growth metal particles over non functionalized DNA strands (176–178). Sivan and co-workers succeed in the fabrication of a self-assembled CNT-FET using a DNA template (179), figure 1.19. They use a streptavidin functionalized single-strand DNA to attach and deterministically place a biotin functionalized SWNT. Additionally silver and gold metals were grown on un-functionalized DNA, acting as electrodes.

In the last years the fabrication of complex DNA structures had evolved, Gothelf and Dwyer groups creates repetitive geometrical patterns with DNA using pre-designed sequences (180–183). In 2006 the invention of DNA-origami opened new perspectives in this field (184). Some groups had exploited the electric properties of nanotubes and the assembly characteristics of DNA-origami and successfully achieved templates and interconnections (185, 186). These studies establish the foundations of electronic design based in programmed DNA patterns (182, 187). Unfortunately, this methodology is still probabilistic and essentially, more structural stability studies need to be performed. To date, at the best of my knowledge, there are no reports on the successfully realization of a full functional DNA-CNT circuit, although strong efforts are being done in many laboratories worldwide.

The issues related to the assembly of electronic nanotube devices indicate that the best option is to try to imitate what nature does. A bottom-up machinery to locate, move, ensemble and test the device, this is what our cells does in our bodies all the time! e. g. ribosome is able to ensemble complex structures as enzymes and proteins. For instance, some enzymes, like tRNA synthetase, are able to ensemble RNA and correct mistakes (polymerase enzymes) on the DNA strand itself. Specialized proteins, like Tubulin and Kinesin, are able to transport and locate other proteins and nutrients inside the cell.
The ensemble of the nanotube-transistor is a quite complex subject. In this thesis work I exposed it as further work and will be discussed briefly in chapter 5.

CNTs stimulated the imagination of many scientists, offering opportunities for hundreds of applications. The discovery of CNTs was thought to be a breakthrough that could potentially revolutionize many areas ranging from electronic to optoelectronic. Now, 20 years after their discovery, these applications can be counted on the fingers of one hand. These applications are limited to the use of bulk CNTs, and mainly explore the mechanical properties of CNTs. The CNTs in commercial applications are used as composite fibers in polymers, and are commercialized by 3 companies Easten-Bell Sports, in bicycle components, Zyvex Technologies, in maritime vessels, and Amroy Europe Oy, in epoxy resins. The latter are 30 % stronger than other composite materials and are used in wind turbines, marine paints and sport gear.

The target of this work is to demonstrate the feasibility to fabricate a CNT-FET using a bottom up approach. The thesis deals essentially with two challenges: the fabrication of a gate dielectric material and the improvement of the contact between the nanotube and metallic electrodes. We demonstrate that using different approaches in the fabrication of nano-devices it is possible to overcome the limitations imposed by current technologies and thus be able to exploit the electrical properties of individual SWNTs. With this work I propose a new option that might be a viable option for the full exploitation of, CNTs for electronic devices.

## 1.3 References.


(1) Bardeen, J.; Brattain, W. . . *Physical Review*. **1948**, *74*, 230-231.
(2) Kilby, J. S. *United States Patent Office*. **1964**, *3,138,743*, 1-5.
(3) Moore, G. E. *Electronics*. **1965**, *38*, 114-117.
(4) Ahmed, S.; Bell, S.; Tabery, C.; Bokor, J.; Kyser, D. *Digest. International Electron Devices Meeting,*. 251-254.
(5) Tang, C.-S.; Chou, H.-M.; Lee, J.-W.; Li, Y. *4th IEEE Conference on Nanotechnology*. **2004**, 281-283.
(6) Yu, B.; Chang, L.; Ahmed, S.; Wang, H.; Bell, S.; Yang, C.-yuh; Tabery, C.; Ho, C.; Xiang, Q.; King, T.-jae; Bokor, J.; Hu, C.; Lin, M.-ren; Kyser, D. *IEEE Electron Device Meeting*. **2002**, 251-254.
(7) Kuo, C.; Hisamoto, D.; Kedzierski, J.; Anderson, E.; Takeuchi, H.; Asano, K.; Subramanian, V.; Bokor, J. *IEEE Transactions on Electron Devices*. **2001**, *48*, 880-886.
(8) Tang, C.-shao; Chou, H.-mu; Lee, J.-wem; Yu, S.-M.; Li, Y. In *IEEE Conference on Nanotechnology*; 2004; pp. 281-283.
(9) Colinge, J. P.; Gao, M. H.; Romano-Rodriguez, A.; Maes, H.; Claeys, C. *IEDM Technical Digest. IEEE International Electron Devices Meeting, 1990*. **1990**, 595-598.
(10) Liang, G. *IEEE Conference on electron devices and solid state circuits*. **2007**, 129-132.
(11) Radisavljevic, B.; Radenovic, a.; Brivio, J.; Giacometti, V.; Kis, a. *Nature Nanotechnology*. **2011**, *6*.
(12) Bryllert, T.; Samuelson, L.; Jensen, L. E.; Wernersson, L. *63rd Device Research Conference Digest, 2005. DRC '05*. **2004**, *1*, 157-158.
(13) Kroto, H. W.; Heath, J. R.; O'Brien, S. C.; Curl, R. F.; Smalley, R. E. *Nature*. **1985**, *318*, 162-163.
(14) Krätschmer, W.; Lamb Lowell, D.; Fostiropolous, K.; Huffman, D. R. *Nature*. **1990**, *347*, 1-2.
(15) Piskoti, C.; Yarger, J.; Zettl, A. *Nature*. **1998**, *393*, 771-774.
(16) Iijima, S. *Nature*. **1991**, *354*, 56-58.
(17) Ugarte, D. *Nature*. **1992**, *359*, 707-709.
(18) Igami, M.; Fujita, M.; Mizuno, S. *Applied Physics Letters*. **1998**, *870*, 130-132.
(19) Ge, M.; Sattler, K. *Chemical Physics Letters*. **1994**, *221*, 192-196.
(20) Tabin, C. J.; Speed, M. P.; Smith, B. W.; Monthioux, M.; Luzzi, D. E. *Nature*. **1998**, *396*, 323-324.
(21) Lee, J.; Kim, H.; Kahng, S.-J.; Kim, G.; Son, Y.-W.; Ihm, J.; Kato, H.; Wang, Z. W.; Okazaki, T.; Shinohara, H.; Kuk, Y. *Nature*. **2002**, *415*, 1005-8.
(22) Lepro, X. N. Insitúto Potosino de Investigación Científica y Tecnológica,, México, 2006, p. 170.
(23) Dresselhaus, M. S.; Dresselhaus, G. *Annual review of Material Sciences*. **1995**, *25*, 487-523.
(24) S., N. K.; Geim, A. K.; Morozov, S. V.; Jiang, D.; Zhang, Y.; Dubonos, S. V.; Grigorieva, I. . V.; Firsov, A. A. *Science*. **2004**, *306*, 666-669.
(25) Strano, M. S.; Dyke, C. a; Usrey, M. L.; Barone, P. W.; Allen, M. J.; Shan, H.; Kittrell, C.; Hauge, R. H.; Tour, J. M.; Smalley, R. E. *Science (New York, N.Y.)*. **2003**, *301*, 1519-22.
(26) Anantram, M. P.; Léonard, F. *Reports on Progress in Physics*. **2006**, *69*, 507-561.
(27) Odom, T. W.; Huang, J.-L.; Kim, P.; Lieber, C. M. *The Journal of Physical Chemistry B*. **2000**, *104*, 2794-2809.
(28) Dresselhaus, M.; Dresselhaus, G.; Saito, R.; Jorio, a *Physics Reports*. **2005**, *409*, 47-99.
(29) Chen, P.; Wu, X.; Sun, X.; Lin, J.; Ji, W.; Tan, K. *Physical Review Letters*. **1999**, *82*, 2548-2551.
(30) Pennington, G.; Goldsman, N. *Physical Review B*. **2003**, *68*, 1-11.
(31) Bonard, J.; Salvetat, J.; Stöckli, T.; Forro, L.; Châtelain, A. *Applied Physics A: Materials Science & Processing*. **1999**, *254*, 245-254.
(32) Harrison, A. W. *Electronic structure and properties of solids: The physiscs of the chemiacl bond*; 1980; pp. 90-92.
(33) Charlier, J.; Zhu, P. C. E. J.; Ferrari, A. C. *Topics in applied physics*. **2008**, *111*, 673-709.
(34) Wallace, P. R. *Physical Review Letters*. **1947**, *71*, 622-235.
(35) Goodrich, A. E. **1893**, 1-2, Patent.
(36) Berger, C.; Song, Z.; Li, T.; Li, X.; Ogbazghi, A. Y.; Feng, R.; Dai, Z.; Marchenkov, A. N.; Conrad, E. H.; First, P. N.; Heer, W. A. D. *Journal of Physical Chemistry B*. **2004**, *108*, 19912-19916.
(37) Geim, A. K.; Novoselov, K. S. *Nature*. **2007**, *6*, 183-191.

(38) Avouris, P.; Chen, Z.; Perebeinos, V. *Nature nanotechnology*. **2007**, *2*, 605-615.
(39) Novoselov, K. S.; Geim, a K.; Morozov, S. V.; Jiang, D.; Katsnelson, M. I.; Grigorieva, I. V.; Dubonos, S. V.; Firsov, a a *Nature*. **2005**, *438*, 197-200.
(40) Berger, C.; Song, Z.; Li, X.; Wu, X.; Brown, N.; Naud, C.; Mayou, D.; Li, T.; Hass, J.; Marchenkov, A. N.; Conrad, E. H.; First, P. N.; Heer, W. a de *Science (New York, N.Y.)*. **2006**, *312*, 1191-6.
(41) Bolotin, K.; Sikes, K.; Jiang, Z.; Klima, M.; Fudenberg, G.; Hone, J.; Kim, P.; Stormer, H. *Solid State Communications*. **2008**, *146*, 351-355.
(42) Morozov, S.; Novoselov, K. S.; Katsnelson, M.; Schedin, F.; Elias, D.; Jaszczak, J.; Geim, A. *Physical Review Letters*. **2008**, *100*, 11-14.
(43) Du, X.; Skachko, I.; Barker, A.; Andrei, E. Y. *Nature nanotechnology*. **2008**, *3*, 491-5.
(44) Castro, E.; Ochoa, H.; Katsnelson, M.; Gorbachev, R.; Elias, D.; Novoselov, K. S.; Geim, A.; Guinea, F. *Physical Review Letters*. **2010**, *105*, 16-18.
(45) Moser, J.; Barreiro, A.; Bachtold, A. *International Materials Reviews*. 3-6.
(46) Balandin, A. a; Ghosh, S.; Bao, W.; Calizo, I.; Teweldebrhan, D.; Miao, F.; Lau, C. N. *Nano letters*. **2008**, *8*, 902-7.
(47) Hároz, E. H.; Rice, W. D.; Lu, B. Y.; Ghosh, S.; Hauge, R. H.; Weisman, R. B.; Doorn, S. K.; Kono, J. *ACS nano*. **2010**, *4*, 1955-62.
(48) Nair, R. R.; Blake, P.; Grigorenko, A. N.; Novoselov, K. S.; Booth, T. J.; Stauber, T.; Peres, N. M. R.; Geim, A. K. *Science*. **2008**, *320*, 2008.
(49) Lee, C.; Wei, X.; Kysar, J. W.; Hone, J. *Science (New York, N.Y.)*. **2008**, *321*, 385-8.
(50) Booth, T. J.; Blake, P.; Nair, R. R.; Jiang, D.; Hill, E. W.; Bangert, U.; Bleloch, A.; Gass, M.; Novoselov, K. S.; Katsnelson, M. I.; Geim, a K. *Nano letters*. **2008**, *8*, 2442-6.
(51) Piscanec, S.; Lazzeri, M.; Robertson, J.; Ferrari, A.; Mauri, F. *Physical Review B*. **2007**, *75*, 1-22.
(52) Charlier, J.-C.; Roche, S. *Reviews of Modern Physics*. **2007**, *79*, 677-732.
(53) Bonaccorso, F. Universita degli studi di Messina, 2006.
(54) Reich, S.; Thomsen, C.; Maultzsch, J. *Carbon nanotube: basic concepts and physical properties*; Willey, 2004.
(55) Mintmire, J. W.; Dunlap, B. I.; White, C. T. *Physical Review Letters*. **1992**, *68*, 631-634.
(56) Warren, T.; Escalona, G.; Schweon, S. J. *Physical Review Letters*. **1992**, *68*, 1579-1582.
(57) Ducastelle, F.; Blase, J. M.; Charlier, J.-C.; Petitjean, P. *Understanding Carbon Nanotubes: From Basics to Applications*; Loiseau, A.; Launois, P.; Petitjean, P., Eds.; 2006; p. 199.
(58) Charlier, J.-C.; Roche, S. *Reviews of Modern Physics*. **2007**, *79*, 677-732.
(59) Louie, S. G. *Carbon nanotubes*; Dresselhaus, M. S.; Dresselhaus, G.; Avouris, P., Eds.; Springer.; Berlin, 2001; p. 113.
(60) Bachilo, S. M.; Strano, M. S.; Kittrell, C.; Hauge, R. H.; Smalley, R. E.; Weisman, R. B. *Science (New York, N.Y.)*. **2002**, *298*, 2361-6.
(61) Popov, V. *Materials Science and Engineering: R: Reports*. **2004**, *43*, 61-102.
(62) Saito, R.; Fujita, M.; Dresselhaus, G.; Dresselhaus, M. S. *Applied Physics Letters*. **1992**, *60*, 2204.
(63) Ludophk, B.; Ruitenbeekk, J. M. V. *Nature*. **1998**, *394*, 154-157.
(64) White, C. T.; Mintmire, J. W. *Nature*. **1998**, *394*, 29-30.
(65) Kane, C.; Mele, E. *Physical Review Letters*. **2003**, *90*, 1-4.
(66) Venema, L. C.; Wildo, J. W. G.; Dekker, C. *Nature*. **1998**, *584*, 1996-1999.
(67) Odom, T. W.; Huang, J.-lin *Nature*. **1998**, *391*, 1997-1999.
(68) Jorio, a.; Souza Filho, a.; Dresselhaus, G.; Dresselhaus, M.; Saito, R.; Hafner, J.; Lieber, C.; Matinaga, F.; Dantas, M.; Pimenta, M. *Physical Review B*. **2001**, *63*, 4-7.
(69) O'Connell, M. J.; Bachilo, S. M.; Huffman, C. B.; Moore, V. C.; Strano, M. S.; Haroz, E. H.; Rialon, K. L.; Boul, P. J.; Noon, W. H.; Kittrell, C.; Ma, J.; Hauge, R. H.; Weisman, R. B.; Smalley, R. E. *Science (New York, N.Y.)*. **2002**, *297*, 593-6.
(70) Lambin, P. *Comptes Rendus Physique*. **2003**, *4*, 1009-1019.
(71) Kataura, H.; Kumazawa, Y.; Maniwa, Y.; Umezu, I.; Suzuki, S.; Ohtsuka, Y.; Achiba, Y. *Synthetic Metals*. **1999**, *103*, 2555-2558.
(72) Ajiki, A.; Ando, T. *2Physica B: Condensed Matter*. **1994**, *201*, 349-352.
(73) Dresselhaus, M. S.; Eklund, P. C. *Advances in Physics*. **2000**, *49*, 705-814.
(74) Benedict, L. X.; Louise, S. G.; Cohen, M. L. *Physical Review B*. **1995**, *52*, 8541-8549.

(75) Rozhin, A. G.; Sakakibara, Y.; Kataura, H.; Matsuzaki, S.; Ishida, K.; Achiba, Y.; Tokumoto, M. *Chemical Physics Letters*. **2005**, *405*, 288-293.
(76) Ichida, M.; Mizuno, S.; Kataura, H.; Achiba, Y.; Nakamura, a. *Applied Physics A: Materials Science & Processing*. **2004**, *78*, 1117-1120.
(77) Kim, Y.; Minami, N.; Zhu, W.; Kazaoui, S.; Azumi, R.; Matsumoto, M. *Japanese Journal of Applied Physics*. **2003**, *42*, 7629-7634.
(78) Moore, V. C.; Strano, M. S.; Haroz, E. H.; Hauge, R. H.; Smalley, R. E.; Schmidt, J.; Talmon, Y. *Nano Letters*. **2003**, *3*, 1379-1382.
(79) Weisman, R. B.; Bachilo, S. M. *Nano Letters*. **2003**, *3*, 1235-1238.
(80) Jorio, a.; Fantini, C.; Pimenta, M.; Capaz, R.; Samsonidze, G.; Dresselhaus, G.; Dresselhaus, M.; Jiang, J.; Kobayashi, N.; Grüneis, a.; Saito, R. *Physical Review B*. **2005**, *71*, 1-11.
(81) Popov, V.; Henrard, L. *Physical Review B*. **2004**, *70*, 1-12.
(82) O'Connell, M. J.; Bachilo, S. M.; Huffman, C. B.; Moore, V. C.; Strano, M. S.; Haroz, E. H.; Rialon, K. L.; Boul, P. J.; Noon, W. H.; Kittrell, C.; Ma, J.; Hauge, R. H.; Weisman, R. B.; Smalley, R. E. *Science (New York, N.Y.)*. **2002**, *297*, 593-6.
(83) Jorio, A.; Dresselhaus, M. S.; Dresselhaus, G. *Carbon nanotubes: Advanced Topics in the synthesis, Structure, Properties and Applications*; Jorio, A.; Dresselhaus, M. S.; Dresselhaus, G., Eds.; Springer: Berlin, 2008.
(84) Bachilo, S. M.; Strano, M. S.; Kittrell, C.; Hauge, R. H.; Smalley, R. E.; Weisman, R. B. *Science (New York, N.Y.)*. **2002**, *298*, 2361-6.
(85) Hasan, T.; Tan, P. H.; Bonaccorso, F.; Rozhin, A. G.; Scardaci, V.; Milne, W. I.; Ferrari, A. C. *Journal of Physical Chemistry C*. **2008**, *112*, 20227-20232.
(86) Hasan, T.; Scardaci, V.; Tan, P.; Rozhin, A. G.; Milne, W. I.; Ferrari, A. C. **2007**, 12594-12602.
(87) Maultzsch, J.; Telg, H.; Reich, S.; Thomsen, C. *Physical Review B*. **2005**, *72*, 1-16.
(88) Fantini, C.; Jorio, a.; Souza, M.; Strano, M.; Dresselhaus, M.; Pimenta, M. *Physical Review Letters*. **2004**, *93*, 1-4.
(89) Tan, P. H.; Rozhin, A. G.; Hasan, T.; Hu, P.; Scardaci, V.; Milne, W. I.; Ferrari, A. C. *Quantum*. **2007**, *137402*, 1-4.
(90) Tan, P. H.; Hasan, T.; Bonaccorso, F.; Scardaci, V.; Rozhin, A. G. *Physica E*. **2008**, *40*, 2352-2359.
(91) Rao, A. M.; Richter, E.; Bandow, S.; Chase, B.; Eklund, P. C.; Williams, K. A.; Fang, S.; Subbaswamy, K. R.; Menon, M.; Thess, A.; Smalley, R. E.; Dresselhaus, G.; Dresselhaus, M. S. *Science*. **1997**, *275*, 187-191.
(92) Strano, M. S.; Doorn, S. K.; Haroz, E. H.; Kittrell, C.; Hauge, R. H.; Smalley, R. E. *Nano Letters*. **2003**, *3*, 1091-1096.
(93) Resasco, D. E.; Alvarez, W. E.; Pompeo, F.; Balzano, L.; Herrera, J. E.; Kitiyanan, B.; Borgna, A. *Journal of Nanoparticle Research*. **2002**, 131-136.
(94) Pimenta, M.; Marucci, a.; Empedocles, S.; Bawendi, M.; Hanlon, E.; Rao, a.; Eklund, P.; Smalley, R.; Dresselhaus, G.; Dresselhaus, M. *Physical Review B*. **1998**, *58*, R16016-R16019.
(95) Niyogi, S.; Densmore, C. G.; Doorn, S. K. *Journal of the American Chemical Society*. **2009**, *131*, 1144-53.
(96) Bachilo, S. M.; Balzano, L.; Herrera, J. E.; Pompeo, F.; Resasco, D. E.; Weisman, R. B. *Journal of the American Chemical Society*. **2003**, 11186-11187.
(97) Bruesch, P. *Phonons: theory and experiments I, lattice dynamics and models of interatomic forces*; Springer: Berlin, Heidelberg, New York, 1982.
(98) Yu, P.; Cardona, M. *Fundametals of semiconductors*; Springer: Berlin, Heidelberg, New York, 2005.
(99) Ferrari, A. C.; Robertson, J. *Raman spectroscopy in carbons: from nanotube to diamond*; Royal society Publishing: London, 2004.
(100) O'Connell, M.; Sivaram, S.; Doorn, S. *Physical Review B*. **2004**, *69*, 1-15.
(101) Lagerwall, J.; Scalia, G.; Haluska, M.; Dettlaff-Weglikowska, U.; Roth, S.; Giesselmann, F. *Advanced Materials*. **2007**, *19*, 359-364.
(102) Dresselhaus, M. S.; Dresselhaus, G.; Hofmann, M. *Vibrational Spectroscopy*. **2007**, *45*, 71-81.
(103) Henrard, L.; Hernández, E.; Bernier, P.; Rubio, A. *Physical Review B*. **1999**, *60*, R8521-R8524.
(104) Zólyomi, V.; Kürti, J. *Physical Review B*. **2004**, *70*, 1-8.
(105) Telg, H.; Maultzsch, J.; Reich, S.; Hennrich, F.; Thomsen, C. *Physical Review Letters*. **2004**, *93*, 1-4.

(106) Piscanec, S.; Lazzeri, M.; Mauri, F.; Ferrari, a.; Robertson, J. *Physical Review Letters.* **2004**, *93*, 1-4.
(107) Ferrari, A. C.; Robertson, J. *Physical Review B.* **2000**, *61*, 95-107.
(108) Ferrari, a.; Robertson, J. *Physical Review B.* **2001**, *64*, 1-13.
(109) Thomsen, C.; Reich, S. *Physical review letters*. **2000**, *85*, 5214-7.
(110) Grüneis, a.; Saito, R.; Kimura, T.; Cançado, L.; Pimenta, M.; Jorio, a.; Souza Filho, a.; Dresselhaus, G.; Dresselhaus, M. *Physical Review B.* **2002**, *65*, 1-7.
(111) Cançado, L.; Pimenta, M.; Saito, R.; Jorio, a.; Ladeira, L.; Grueneis, a.; Souza-Filho, a.; Dresselhaus, G.; Dresselhaus, M. *Physical Review B.* **2002**, *66*, 1-5.
(112) Jorio, a.; Souza Filho, a.; Dresselhaus, G.; Dresselhaus, M.; Swan, a.; Ünlü, M.; Goldberg, B.; Pimenta, M.; Hafner, J.; Lieber, C.; Saito, R. *Physical Review B.* **2002**, *65*, 23-27.
(113) Tan, P.; An, L.; Liu, L.; Guo, Z.; Czerw, R.; Carroll, D.; Ajayan, P.; Zhang, N.; Guo, H. *Physical Review B.* **2002**, *66*, 1-8.
(114) Khon, W. *Physical Review Letters*. **1959**, *2*, 393-394.
(115) Kasuya, a.; Sasaki, Y.; Saito, Y.; Tohji, K.; Nishina, Y. *Physical Review Letters*. **1997**, *78*, 4434-4437.
(116) Alvarez, L.; Righi, A.; Guillard, T.; Anglaret, E.; Laplaze, D.; Sauvajol, J.-louis *Chemical Physics Letters*. **2000**, 186-190.
(117) Rao, A. M.; Eklund, P. C.; Bandow, S.; Thess, A. *Nature.* **1997**, *191*, 257-259.
(118) Jorio, a.; Fantini, C.; Dantas, M.; Pimenta, M.; Souza Filho, a.; Samsonidze, G.; Brar, V.; Dresselhaus, G.; Dresselhaus, M.; Swan, a.; Ünlü, M.; Goldberg, B.; Saito, R. *Physical Review B.* **2002**, *66*, 1-8.
(119) Arnold, M. S.; Green, A. a; Hulvat, J. F.; Stupp, S. I.; Hersam, M. C. *Nature nanotechnology*. **2006**, *1*, 60-5.
(120) Hofstein, S. R.; Heiman, F. P. *Proceedings of the IEEE*. **1963**, *52*, 1190-1194.
(121) Avouris, P. *Nature Nanotechnology*. **2007**, *1*, 529-530.
(122) Avouris, P. *Chemical Physics*. **2002**, *281*, 429-445.
(123) Babi, B.; Iqbal, M.; Schnenberger, C. *Nanotechnology*. **2003**, *14*, 327-331.
(124) Weitz, R. T.; Zschieschang, U.; Forment-Aliaga, A.; Kälblein, D.; Burghard, M.; Kern, K.; Klauk, H. *Nano letters.* **2009**, *9*, 1335-40.
(125) Tans, S. J.; Verschueren, A. R. M.; Dekker, C. *Nature*. **1998**, *672*, 669-672.
(126) Martel, R.; Schmidt, T.; Shea, H. R.; Hertel, T.; Avouris, P. *Applied Physics Letters*. **1998**, *73*, 2447.
(127) Bachtold, a; Hadley, P.; Nakanishi, T.; Dekker, C. *Science (New York, N.Y.)*. **2001**, *294*, 1317-20.
(128) Wind, S. J.; Appenzeller, J.; Martel, R.; Derycke, V.; Avouris, P. *Applied Physics Letters*. **2002**, *80*, 3817.
(129) Wong, H.-S. P. *IBM Journal of Research and Development*. **2002**, *46*, 133-168.
(130) Lu, Y.; Bangsaruntip, S.; Wang, X.; Zhang, L.; Nishi, Y.; Dai, H. *Journal of the American Chemical Society*. **2006**, *128*, 3518-9.
(131) Chen, Z. *IEEE Electron Device Letters*. **2008**, *6*, 699-185.
(132) Franklin, A. D.; Sayer, R. a.; Sands, T. D.; Fisher, T. S.; Janes, D. B. *Journal of Vacuum Science & Technology B: Microelectronics and Nanometer Structures*. **2009**, *27*, 821.
(133) Cho, K. H.; Yeo, K. H.; Yeoh, Y. Y.; Suk, S. D.; Li, M.; Lee, J. M.; Kim, M.-S.; Kim, D.-W.; Park, D.; Hong, B. H.; Jung, Y. C.; Hwang, S. W. *Applied Physics Letters*. **2008**, *92*, 052102.
(134) Dag, S.; Gülseren, O.; Ciraci, S.; Yildirim, T. *Applied Physics Letters*. **2003**, *83*, 3180.
(135) Song, Y.; Kang, S. J. *Journal of Vacuum Science & Technology B: Microelectronics and Nanometer Structures*. **2011**, *29*, 011011.
(136) Ishii, H.; Kobayashi, N.; Hirose, K. *Journal of Physics: Conference Series*. **2008**, *100*, 052062.
(137) Ebbesen, T. W. *Journal of phisics and chemistry of Solids1*. **1996**, *57*, 951-955.
(138) Treacy, M. M. J.; Shreeve-keyer, J. L.; Haushalter, R. C. *Advanced Materials*. **1996**, *8*, 155-157.
(139) Heinze, S.; Tersoff, J.; Martel, R.; Derycke, V.; Appenzeller, J.; Avouris, P. *Physical Review Letters*. **2002**, *89*, 2-5.
(140) Appenzeller, J.; Knoch, J.; Martel, R.; Derycke, V.; Wind, S.; Avouris, P. *Digest. International Electron Devices Meeting,*. 285-288.
(141) Strus, M. C.; Chiaramonti, A. N.; Kim, Y. L.; Jung, Y. J.; Keller, R. R. *Nanotechnology*. **2011**, *22*, 265713.

(142) Strus, M. C.; Keller, R. R.; Barbosa, N. In *IEEE Nano 2011, Portland, Oregon*; 2011.
(143) Chen, C.; Liu, L.; Lu, Y.; Kong, E.; Zhang, Y.; Sheng, X.; Ding, H. *Carbon*. **2007**, *45*, 436-442.
(144) Nosho, Y.; Ohno, Y.; Kishimoto, S.; Mizutani, T. *Applied Physics Letters*. **2005**, *86*, 073105.
(145) Perello, D. J.; Chulim; Chae, S. J.; Lee, I.; Kim, M. J.; Lee, Y. H.; Yun, M. *ACS nano*. **2010**, *4*, 3103-8.
(146) Nosho, Y.; Ohno, Y.; Kishimoto, S.; Mizutani, T. *Nanotechnology*. **2006**, *17*, 3412-5.
(147) Mann, D.; Javey, A.; Kong, J.; Wang, Q.; Dai, H. *Nano Letters*. **2003**, *3*, 1541-1544.
(148) Xian, X.; Yan, K.; Zhou, W.; Jiao, L.; Wu, Z.; Liu, Z. *Nanotechnology*. **2009**, *20*, 505204.
(149) Chang-Jian, S.-K.; Ho, J.-R.; John Cheng, J.-W. *Microelectronic Engineering*. **2010**, *87*, 1973-1977.
(150) Chen, J.; Klinke, C.; Afzali, A.; Chan, K.; Avouris, P. *IEEE International Electron Devices Meeting 2004.* **2004**, 695-698.
(151) Klinke, C.; Afkali, a.; Avouris, P. *Conference Digest [Late News Papers volume included]Device Research Conference, 2004. 62nd DRC.* **2003**, *10606*, 137-138.
(152) Javey, A.; Tu, R.; Farmer, D. B.; Guo, J.; Gordon, R. G.; Dai, H. *Nano letters*. **2005**, *5*, 345-8.
(153) Klinke, C.; Chen, J.; Afzali, A.; Avouris, P. *Nano letters*. **2005**, *5*, 555-8.
(154) Wind, S. J.; Appenzeller, J.; Martel, R.; Derycke, V.; Avouris, P. *Applied Physics Letters*. **2002**, *80*, 3817.
(155) Javey, A.; Guo, J.; Farmer, D. B.; Wang, Q.; Wang, D.; Gordon, R. G.; Lundstrom, M.; Dai, H. *Nano Letters*. **2004**, *4*, 447-450.
(156) Auvray, S.; Derycke, V.; Goffman, M.; Filoramo, A.; Jost, O.; Bourgoin, J.-P. *Nano letters*. **2005**, *5*, 451-5.
(157) Chen, J.; Freitag, M.; Klinke, C.; Afzali, A.; Tsang, J.; Avouris, P.; Watson, I. B. M. T. J. *Nanotechnology*. **2005**, 5-8.
(158) Appenzeller, J.; Avouris, P. *IEEE Electron Device Letters*. **2005**, *26*, 823-825.
(159) Yang, M. H.; Teo, K. B. K.; Milne, W. I.; Hasko, D. G. *Applied Physics Letters*. **2005**, *87*, 253116.
(160) Klinke, C.; Hannon, J. B.; Afzali, A.; Avouris, P. *Nano letters*. **2006**, *6*, 906-910.
(161) Taeger, S.; Sickert, D.; Atanasov, P.; Eckstein, G.; Mertig, M. *Physica Status Solidi (B)*. **2006**, *243*, 3355-3358.
(162) Weitz, R. T.; Zschieschang, U.; Effenberger, F.; Klauk, H.; Burghard, M.; Kern, K. *Nano letters*. **2007**, *7*, 22-7.
(163) Inami, N.; Mohamed, M. A.; Shikoh, E.; Fujiwara, A. *Applied Physics Letters*. **2008**, *92*, 243115.
(164) Rinkiö, M.; Johansson, A.; Paraoanu, G. S.; Törmä, P. *Nano letters*. **2009**, *9*, 643-7.
(165) Goh, R. G. S.; Bell, J. M.; Motta, N.; Ho, P. K.-H.; Waclawik, E. R. *Superlattices and Microstructures*. **2009**, *46*, 347-356.
(166) Zavodchikova, M. Y.; Kulmala, T.; Nasibulin, A. G.; Ermolov, V.; Franssila, S.; Grigoras, K.; Kauppinen, E. I. *Nanotechnology*. **2009**, *20*, 085201.
(167) Helbling, T.; Hierold, C.; Roman, C.; Durrer, L.; Mattmann, M.; Bright, V. M. *Nanotechnology*. **2009**, *20*, 434010.
(168) Wang, Z.; Ding, L.; Pei, T.; Zhang, Z.; Wang, S.; Yu, T.; Ye, X.; Peng, F.; Li, Y.; Peng, L.-M. *Nano letters*. **2010**, *10*, 3648-3655.
(169) Franklin, A. D.; Chen, Z. *Nature nanotechnology*. **2010**, *5*, 858-62.
(170) Wang, Z.; Xu, H.; Zhang, Z.; Wang, S.; Ding, L.; Zeng, Q.; Yang, L.; Pei, T.; Liang, X.; Gao, M.; Peng, L.-M. *Nano letters*. **2010**, *10*, 2024-30.
(171) Franklin, A. D.; Luisier, M.; Han, S.-J.; Tulevski, G.; Breslin, C. M.; Gignac, L.; Lundstrom, M. S.; Haensch, W. *Nano letters*. **2012**, *12*, 758-62.
(172) Lewenstein, J. C.; Burgin, T. P.; Ribayrol, A.; Nagahara, L. A.; Tsui, R. K.; Technologique, E.; Aubin, S. *Nano Letters*. **2002**, *2*, 443-446.
(173) Ladd, J.; Boozer, C.; Yu, Q.; Chen, S.; Homola, J.; Jiang, S. *Langmuir□: the ACS journal of surfaces and colloids*. **2004**, *20*, 8090-5.
(174) Saccà, B.; Niemeyer, C. M. *Chemical Society reviews*. **2011**.
(175) Niemeyer, C. M.; Adler, M.; Gao, S.; Chi, L. *Bioconjugate chemistry*. **2001**, *12*, 364-71.
(176) Keren, K.; Krueger, M.; Gilad, R.; Ben-Yoseph, G.; Sivan, U.; Braun, E. *Science (New York, N.Y.)*. **2002**, *297*, 72-5.
(177) Braun, E.; Eichen, Y.; Sivan, U.; Ben-Yoseph, G. *Nature*. **1998**, *391*, 775-8.

(178) Keren, K.; Soen, Y.; Yoseph, G.; Gilad, R.; Braun, E.; Sivan, U.; Talmon, Y. *Physical Review Letters*. **2002**, *89*, 3-6.
(179) Keren, K.; Berman, R. S.; Buchstab, E.; Sivan, U.; Braun, E. *Science (New York, N.Y.)*. **2003**, *302*, 1380-2.
(180) Gothelf, K. V.; LaBean, T. H. *Organic & biomolecular chemistry*. **2005**, *3*, 4023-37.
(181) Dwyer, C.; Johri, V.; Cheung, M.; Patwardhan, J.; Lebeck, A.; Sorin, D. *Nanotechnology*. **2004**, *15*, 1240-1245.
(182) Mao, V.; Dwyer, C.; Chakrabarty, K. In *2008 IEEE International Test Conference*; Ieee, 2008; pp. 1-10.
(183) Dwyer, C.; Johri, V.; Cheung, M.; Patwardhan, J.; Lebeck, A.; Sorin, D. *Nanotechnology*. **2004**, *15*, 1240-1245.
(184) Rothemund, P. W. K. *Nature*. **2006**, *440*, 297-302.
(185) Maune, H. T.; Han, S.-P.; Barish, R. D.; Bockrath, M.; Iii, W. a G.; Rothemund, P. W. K.; Winfree, E. *Nature nanotechnology*. **2010**, *5*, 61-6.
(186) Eskelinen, A.-P.; Kuzyk, A.; Kaltiaisenaho, T. K.; Timmermans, M. Y.; Nasibulin, A. G.; Kauppinen, E. I.; Törmä, P. *Small*. **2011**, *7*, 746-750.
(187) Keren, K.; Braun, E. *Chemical Engineering & Technology*. **2004**, *27*, 447-452.
(188) Colinge, J. P. In *FinFETs and Other Multi-Gate Transistors (Integrated Circuits and Systems)*; 2008; pp. 14-15.
(189) Lemay, S. G.; Janssens, A. M.; Hout, P. van den; Mooij, M.; Bronikowski, M. J.; Willis, P. A.; Smalley, R. E.; Kouwenhoven, L. E.; Dekker, C. *Nature*. **2001**, *412*, 617-620.
(190) Marayuma, S. *3*, www.photon.t.u-tokyo.ac.jp.
(191) Jorio, A.; Pimenta, M. A.; Souza Filho, A.; Saito, R.; Dresselhaus, G.; Dresselhaus, M. S. *New Journal of Physics*. **2003**, *139*, 1-17.
(192) Graham, a. P.; Duesberg, G. S.; Hoenlein, W.; Kreupl, F.; Liebau, M.; Martin, R.; Rajasekharan, B.; Pamler, W.; Seidel, R.; Steinhoegl, W.; Unger, E. *Applied Physics A*. **2005**, *80*, 1141-1151.

# Chapter 2

## Synthesis and purification of carbon nanostructures.

### 2.1 Introduction.

The first report on carbon nanotubes (NTs) is dated back in 1952 by a Russian group (1). However, only in 1991 NTs were fully characterized by Iijima(2). He clearly imaged multi-wall carbon nanotubes (MWNTs) using a high resolution transmission electron microscope. The first experimental observation of single wall nanotubes was reported in 1993 contemporarily by Iijima (3) and an IBM group (4). In these reports the properties of the unidimensional carbon nanomaterials were discussed. In 1997 Tans et al (5) demonstrates the quantum wire transport in nanotubes, this means that electrons will experience quantum confinement in the transversal direction. One year later the same group published (6) the first report on the field effect properties of an individual semiconductor SWNT. In the same year, White and Todorov (7), demonstrated ballistic electron transport in carbon nanotubes for a length longer than 10 microns. The experimental evidence of ballistic transport in semiconducting SWNTs using a field effect transistor (FET) configuration was performed by Dai's group in 2003 (8). Since then a large number of publications covered the physical and chemical properties of

SWNTs. The reports demonstrated, at least theoretically (9–15) or in proof of principle devices (10, 15–24) , the superior performance of SWNTs devices compared with Silicon ones. An enormous effort has been made by the scientific community in order to put these properties in commercial applications, especially after the prediction of the International Technology Roadmap for Semiconductors (ITRS) that in 2020 the first commercial electronic devices based on carbon could be available in the market (11, 23, 25–29).

However, to date we have to face the reality that is far away from this prediction. The synthesis of SWNT produces a mixture of amorphous carbon, metallic nanoparticles and a wide diameter range of nanotubes with different chiralities. Until now there is not a method to synthesize nanotubes with just one diameter or single chirality, some research groups are challenging this issue. As was explained in chapter 1, the electronic behaviour of nanotubes is directly related to their chirality. Of course, in FET devices a unique electronic behaviour is requested, this is why a single chirality is necessary.

In this chapter I will be discuss the nanotubes growth processes, other than post-processing purification and sorting strategies. A short introduction and discussion on the graphite exfoliation in view of electronic devices integration will be presented as well.

## 2.2 Synthesis processes

Different techniques have been developed to produce SWNTs in large quantities such as arc discharge, laser ablation, high-pressure carbon monoxide (HiPco), chemical vapour deposition (CVD) and CO disproportionate (CoMoCAT). All these techniques produce samples with a different level of purity, length, diameter and chirality distributions. Moreover, the majority of the as produced samples (raw materials) have catalytic particles. To date, the production of high purity chirality controlled SWNTs sample remain a challenge.

### 2.2.1 Arc discharge

The nanotubes characterized by Iijima in 1991 were produced by the arc discharge method in the attempt to produce fullerenes. He applied 100 amperes through a couple of graphite electrodes in an ultra-high vacuum (UHV) chamber. After the discharge he observed carbon soot deposited on the electrodes. This process has been modified and improved over the years reaching a yield of~ 30% in weight. This process reported by Iijima in 1991 produces a mixture of MWNTs and SWNTs (30), with lengths that can exceed 50µm (2). Nowadays it is possible to produce just SWNTs or MWNTs with this technique. Moreover, this process yields nanotubes with a low degree of structural defects. The rate of semiconducting–metallic nanotubes is approximately 2:1 (31)

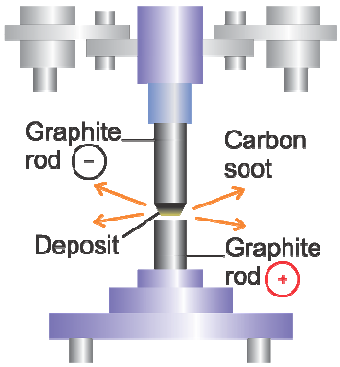


**Figure 2.1.** Schematic representation of arc discharge chamber

A commercial quantity of carbon nanotubes was produced by NEC's Fundamental Research Laboratory in 1992 (32). In the process, the carbon sublimates over the negative electrode due to the high-discharge temperatures. The electrodes are approximately 1 mm far apart. Normally the discharge is performed in UHV or in inert atmosphere. The disadvantages of this method are the low yield and the large quantities of impurities.

### 2.2.2 Laser ablation

This method was developed by researchers at Rice University in 1995 (33). The technique consists in a pulsed laser vaporizing a graphite target in a high-temperature reactor (1200 ºC); the process is performed in an inert atmosphere. The carbon condenses over the cooled collector producing a continuous growth of nanotubes.

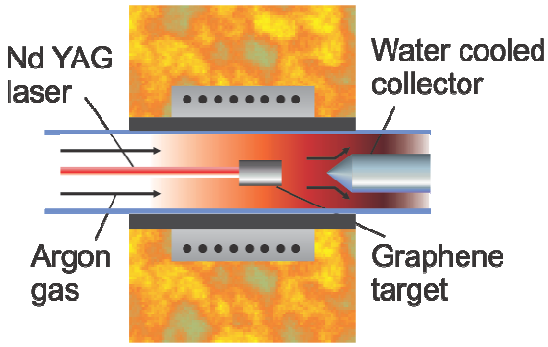


**Figure 2.2** Schematic diagram of a laser ablation oven

Using a mixture of cobalt and nickel catalyst particles the reaction produces a high yield of SWNTs (34–36). Instead if graphite is used as catalyst MWNTs are formed.

With this technique, it is possible to get a narrower diameter distribution with respect to the arc discharge method. The disadvantage of this technique relies in the low yield and the large amounts of impurities produced during the growth.

### 2.2.3 Chemical vapour deposition (CVD)

This method has been used to produce various types of carbon materials for more than 20 years. In 1993 Yacaman et al (37) reported the successful synthesis of nanotubes by this technique.

CVD nanotube synthesis is carried out by introducing a carbon source in gas phase and using an energy source, such as plasma or a heated coil, in order to transfer energy to carbon molecules and break it, producing reactive carbon atoms. The carbon sources used are gases such as methane, carbon monoxide and acetylene. A substrate is used with a layer of metal particles that act as catalyst for the nanotube growth. Most commonly used particles are nickel, cobalt, iron or a combination of them.

The initial growth step involves absorption, decomposition of hydrocarbon molecules on a catalyst particle, and diffusion of carbon atoms into the catalyst bulk from a supersaturated catalyst surface (38–40). The nanotube diameter is dependent on the metal nanoparticle size. The appropriate metal catalyst can preferentially grow SWNTs rather than MWNTs (41). The temperatures for the synthesis of nanotubes by CVD are generally within the 650-900 $^{o}$C range. Typical production yield is approximately 30%.

In the last decade, different techniques for the carbon nanotubes synthesis with CVD have been developed, such as plasma enhanced CVD, thermal chemical CVD, alcohol catalytic CVD, vapour phase growth, aero gel-supported CVD and laser-assisted CVD.

In particular nanotubes grown by CVD have been used to obtain nanotube devices containing isolated SWNTs at controlled locations. Controllable location of nanotubes over a substrate is the main advantage of other techniques. Additionally the cheap cost makes this technique the most used for nanotubes synthesis to date.

There are two processes widely used for massive production of nanotubes: CoMoCat and HiPco. SWNT are grown by CO disproportion (decomposition into C and $CO_2$) at 700-950ºC in a flow of pure CO at a total pressure ranging from 1 to 10 atm.

Several transition metal catalysts have been shown to be active for generation of carbon nanotubes (42, 43) The CoMoCAT method (see fig.1.12) is based on the use of Cobalt and Molybdenum as catalyst, containing 6 wt % total metals (44) A Co:Mo molar ratio of 1:2, exhibited the highest selectivity towards the production of SWNT. This catalyst is prepared by incipient wetness impregnation of aqueous solutions of Cobalt Nitrate and Ammonium Heptamolybdate, followed by drying in an oven at 80°C and calcination in flowing air at 500°C. For the production of nanotubes, 100–500 mg of calcined catalyst was placed in a horizontal quartz tubular reactor, heated in $H_2$ up to 500°C, and then in He to 700°C. Subsequently, CO was introduced at this temperature and at a flow rate of 100 $cm^3$/min for the production of nanotubes.

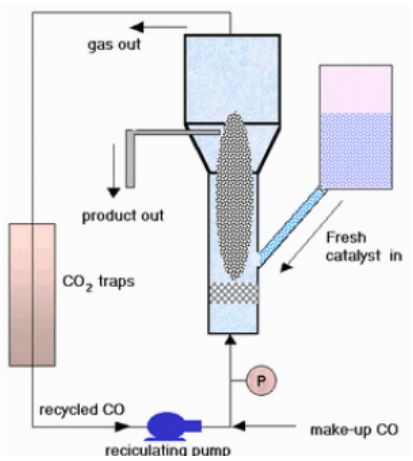


**Figure 12:** Experimental setup for the production of SWNTs by CoMoCat process (46).

The balance between Co and Mo is the most critical parameter for the performance of the process. The catalyst is effective when both metals are simultaneously present on a silica support with a low Co: Mo ratio. Indeed, not all Co–Mo formulations are equally effective in producing SWNT. For example, Mo sample does not produce SWNT at 700°C, but only amorphous carbon. The term ‘amorphous carbon’ implies carbonaceous deposits, which are not in the form of ordered nanotubes or graphite. On the other hand,

Co alone is not selective for the production of SWNT, and generates mainly graphitic carbon and MWNT (44). When Mo was added to Co, the selectivity towards SWNT greatly increased, which indicates that some sort of synergism between Co and Mo makes the combination of the two metals effective. With a Co:Mo molar ratio of 2:1 a significant fraction of MWNT is produced, as opposed to the catalyst with a molar ratio of 1:2, which mainly produce SWNT (44) .

Two different forms of Co can be present in a catalyst, the selective Co species (interacting with Mo) and the unselective one (non-interacting). The Co-Mo interaction inhibits the Co sintering that typically occurs at the high temperatures required for the formation of carbon nanotubes. When large Co particles are present less desirable forms of carbon (MWNT, fibres, and graphite) are produced. By contrast, when the Co clusters are small enough (i.e. <2 nm) only SWNT are grown.

Reference (45) Reported that the diameter of SWNTs obtained by CO disproportion over Co-Mo catalysts supported on silica gel can be varied by changing the operation temperature. As the temperature is increased, the average SWNTs diameter increases. The average diameter of a SWNTs produced at 750 °C was 0.9 nm, while it increase up to about 1.5 nm when the synthesis was conducted at 950° C (46) The same authors in ref. (47) have shown a full description of the structure and chemical state of a series of Co-W/SiO2 catalysts used for the production of SWNT by CO disproportion at 750-950 °C. The results are compared to those obtained with Co-Mo catalyst. It has been found that, similar to the Co-Mo system, the selectivity of the Co-W catalysts toward SWNT strongly depends on the stabilization of Co species in a non-metallic state before exposure to CO. This stabilization is a consequence of the interaction of Co with tungsten oxide (45).

The high pressure CO process (HiPco) is a technique for catalytic production of SWNTs in a continuous-flow gas phase using CO as the carbon feedstock and $Fe(CO)_5$ as the iron-containing catalyst precursor. SWNTs are produced by flowing CO, mixed with a small amount of $Fe(CO)_5$ through a heated reactor. Size and diameter distribution of the nanotubes can roughly be selected by controlling the pressure of CO, see figure 2.4. This process is promising for bulk production of carbon nanotubes. A hard disadvantage of

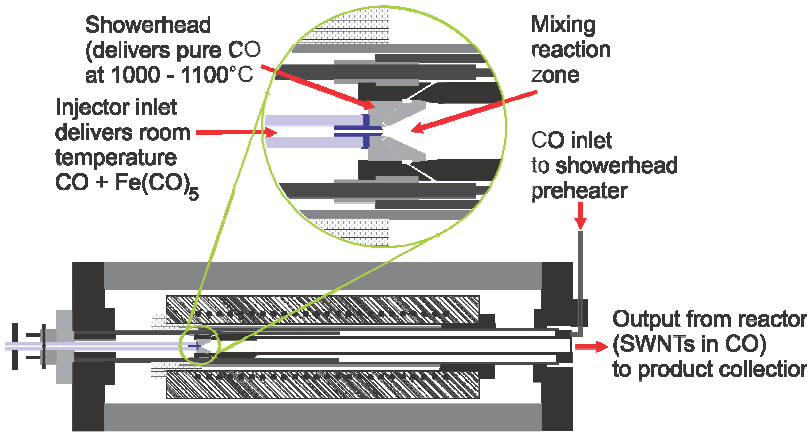


**Figure 2.4.** HiPco reactor, with the mixing/reaction zone enlarged, Modified from (147)

this technique is the elevated amount of undesired carbon structures and high levels of metallic impurities. The average diameter of nanotubes produced by this technique is 1.1 nm approximately. Commercial available, HiPco nanotubes are one of the most used in research labs today.

All synthesis processes give a wide range of nanotube diameters, including metallic and semiconducting. If it is desirable to explore the physical properties of nanotubes in electronics it is mandatory to have nanotube with exactly the same electronic behaviour. This means, a sample composed of a single chirality. In the same way, the impurities, like metallic particles or amorphous carbon, results of the production processes, need to be removed trough a purification process.

## 2.3 Purification of single-walled carbon nanotubes.

There are an extensive number of publications related with purification process of carbon nanotubes for the removal of metallic nanoparticles and amorphous carbon that are residual of the synthesis process. In the following I will list some of them explored to date. The most commonly used purification strategy of SWNTs makes use of nitric acid 2 to 3M stirring them under reflux to prevent lost by evaporation (48–51) (Reflux is a distillation technique involving the condensation of vapours and the return of this condensate to the system from which it originated. It is used in industrial and laboratory distillations). Other purification techniques rely in the use of a mixture of Nitric and Sulphuric acid (52) or using a Piranha solution. The latter is known to be a strong oxidative agent and hydroxylate hard surfaces and is used in carbon nanotubes to cut, disperse and purify them (53–56). Nevertheless, although these processes manage to remove metallic catalytic particles and amorphous carbon, some particles encapsulated by graphitic shells, prevents the acid to dissolves the particle within it. A treatment using gas phase exfoliation can break this graphitic shell, exposing and dissolving the metal content (57). In the same context, microwave assisted method has been used to break these graphitic shells and further hydrochloric acid can easily wash out the metal content, reaching a residual metal weight of ~ 1.5% (58–61). Thermal and acid treatments have also been studied (62). These processes burn the amorphous carbon and impurities exposing the residual metallic particles to hydrochloric acid that dissolve them. With these strategies it is possible to achieve a metal content less than 1%. However, the majority of the purification processes introduce structural defects on the nanotube walls, adding oxygen groups or removing carbon atoms. The addition of oxygen atoms disrupts the electron structure changing the physical properties and thus, sacrificing the ballistic electron transport, a very appreciable property for electronic applications.

A viable strategy to avoid defect formation on the nanotubes sidewalls relies in the use of organic functionalization. The latter makes the nanotubes dispersible in organic solvents, while on the other hand, the metallic impurities precipitate, making easier to remove them from solution. An annealing process remove the functional groups bonded to the

CNT, recovering its pristine electronic properties(63). Non-destructive or non-covalent purifications have also been reported making use of a surfactant to accomplish a homogeneous nanotubes dispersion in a non-polar solvent. It is then possible to filter and extract catalytic metal particles and amorphous carbon (64). Size exclusion chromatography that relies in a multistep process using a stationary phase with defined pore sizes is another purification procedure used for nanotubes. Size exclusion chromatography is a powerful tool for the separation of large molecules, e.g. biological macromolecules or virus particles, this technique have been used to purify nanotubes achieving purity of 90% (65).

I performed several purification procedures with the goal to obtain high amount of purified material in a shorter time with respect to the procedure reported in literature today.

#### 2.1.3.1 Piranha treatment

The first purification procedure that I carried out is the **Piranha treatment**. In short, 20 mg of raw HiPco nanotubes were dispersed in 200 ml of piranha solution, consisting in 160 ml of Sulphuric acid and 40 ml of hydrogen peroxide. The solution was produced in ice bath and hard stirring. Subsequently, the SWNTs were slowly added to this solution. Immediately, the obtained dark dispersion was treated in a sonic bath for 2 hours. To interrupt the CNTs oxidation reaction 2 L of distilled water was added to the initial dispersion and filtrated through a 0.1 µm Millipore filter, the filtered material was collected and washed several times with distilled water, and finally with pure ethanol. The filter was let dry under vacuum overnight. To know the metal content in the sample, I carried out thermo gravimetric analysis (TGA) in oxygen atmosphere. To analyze possible physical changes and the degree of purity of the obtained nanotubes, I used transmission electron microscopy (TEM). A qualitatively analysis of the presence of surface-defect was performed by Raman spectroscopy.

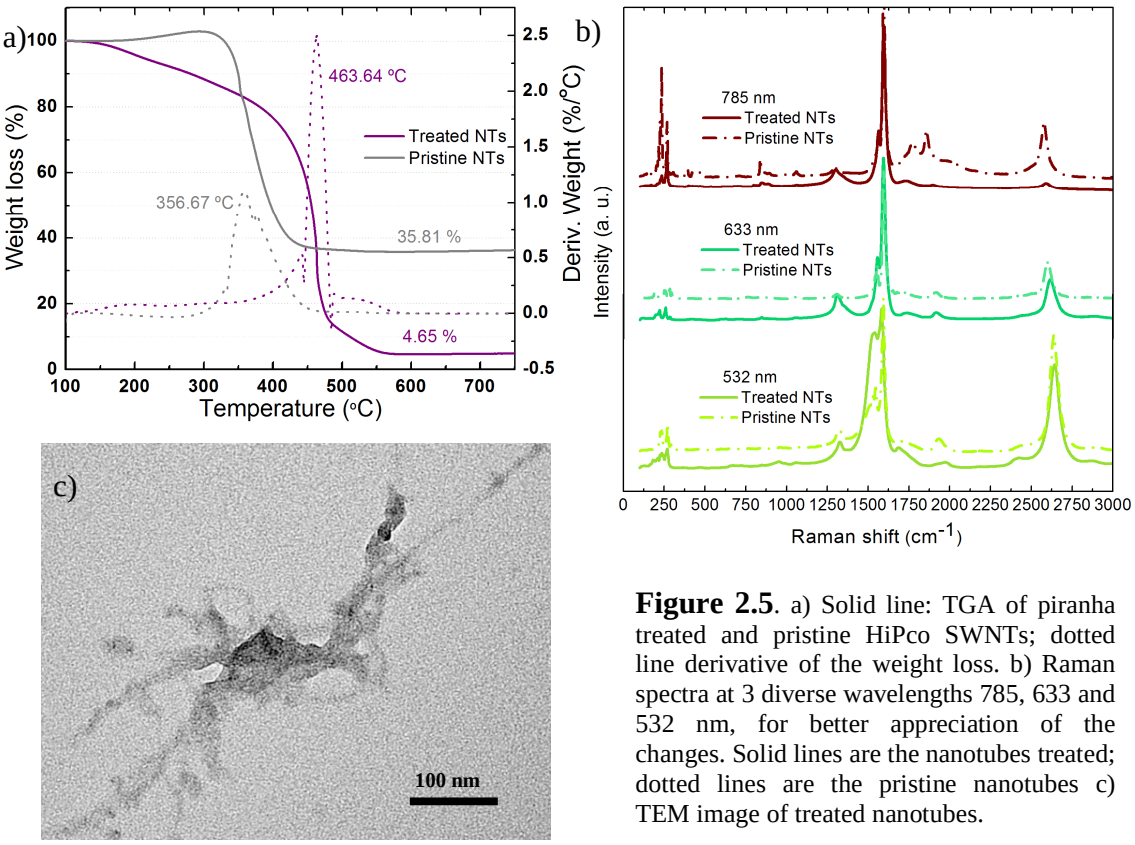


**Figure 2.5**. a) Solid line: TGA of piranha treated and pristine HiPco SWNTs; dotted line derivative of the weight loss. b) Raman spectra at 3 diverse wavelengths 785, 633 and 532 nm, for better appreciation of the changes. Solid lines are the nanotubes treated; dotted lines are the pristine nanotubes c) TEM image of treated nanotubes.

The TGA analysis reported in figure 2.5 shows the weight loss versus temperature curves of as-produced SWNTs, in grey, and the oxidized and purified SWNTs using piranha in violet. At temperature above 600 °C it is considered that CNTs have been burned, remaining just catalytic metal impurities. If it is compared the residual material of pristine and treated NTs samples the piranha treatment removed successfully the 87 % of metal content. Moreover, the derivative of weight loss with respect to temperature, shown as dotted curves in the TGA image; specify the temperature where the weight loss rate changes faster. The removal of metallic catalytic particles has the advantage of increasing the thermal stability of pristine SWNTs, which decomposes at 356 °C . In average, the treated nanotubes are almost 100 °C more stable than pristine sample. Now, it is possible to define a yield with the next equation, in order to qualify the metal removal and the material lost through the process:

$$Y_{\%} = \frac{w_{Tf}}{w_{Ti}}\left(1 - \frac{res_f}{ref_i}\right)$$

Where $w_{Tf}$ is the final total weight measured from the filtered and dried oxidized SWNTs, $w_{Ti}$ is the weight of pristine SWNTs before the treatment, $res_f$ is the residual material of the sample before the treatment, and $res_i$ is the residual material of the pristine nanotubes. The resulting yield of this process is 15.6 %.

Other important factor to consider is the creation of defects on the NTs walls produced by the purification treatment. It is expected to have an increase in defective hybridized carbon atoms ($sp^3$) over the nanotube walls, produced by the oxidation treatment. It is possible to qualify the change or increase of defects on the nanotubes by measuring the D-band in the Raman spectra.

Raman analysis shows the spectra using 785, 633 and 532 nm excitation wavelengths of pristine and treated nanotubes. It is seen a small increase of the D-band in the Raman spectrum of the treated SWNTs with respect to the pristine one, demonstrating that the piranha treatment do not induce considerable damage on the NT walls. The TEM image shows bundled nanotubes, while the presence of metallic catalytic particles was low.

### 2.3.2 Nitric acid treatment

To compare different purification methodologies I investigated other protocol widely used in literature: **Nitric acid** consists in mixing 250 ml of $HNO_3$ 2.6 M and 100 mg of pristine HiPco SWNTs. This blackish dispersion is hard stirred under reflux at 125 ºC for 48 hours. The oxidation reaction was stopped adding 500 ml of pure distilled water. The obtained diluted dispersion is then filtered through a 100 nm pore size filter. The latter is washed several times with distilled water until a neutral pH is reached. Finally the filtered material is washed with 200 ml of ethanol and let to dry under vacuum overnight.

The TGA, in figure 2.6, shows a low amount of residual material that is composed by metallic particles. The residual material is approximately 3 % of the total weight; this lower amount of metals and impurities (amorphous carbon) makes the tubes more stable at high temperatures. At the same time, the destruction of shorter tubes by the acid treatment renders the sample more stable. Indeed, smaller tubes will be air-oxidized faster than longer and bundled tubes. How it is shown in figure 2.6 a, the bigger mass loss occurs at 582 ºC. This treatment is more aggressive than piranha solution. Raman spectra clearly show a notable increase of the D-band (~1260 $cm^{-1}$). This is associated with the presence of a large number of defects with respect to the spectra measured for the sample purified via the piranha process. The second characteristic is the broadening of the G-band (1585 $cm^{-1}$) a consequence of the changes in the diameter distribution (46, 66). There are also differences between the as-produced and the purified samples in the RBM

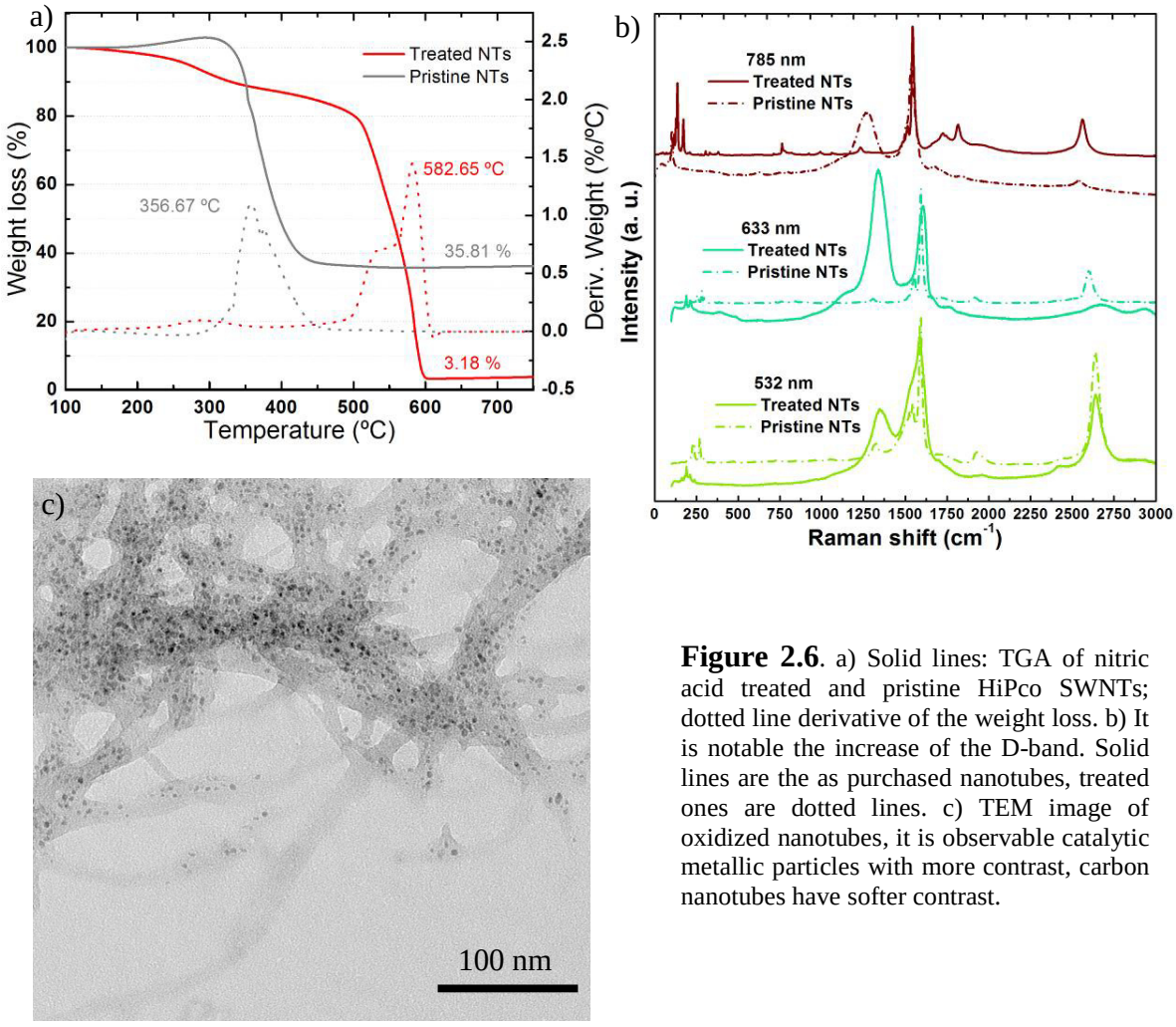


**Figure 2.6**. a) Solid lines: TGA of nitric acid treated and pristine HiPco SWNTs; dotted line derivative of the weight loss. b) It is notable the increase of the D-band. Solid lines are the as purchased nanotubes, treated ones are dotted lines. c) TEM image of oxidized nanotubes, it is observable catalytic metallic particles with more contrast, carbon nanotubes have softer contrast.

zone. The TEM analysis shows a considerable quantity of metallic particles, the image is a zone where the presence of particles was particularly high. The yield on this treatment was 45.8 %.

### 2.3.3 Sulphuric and Nitric acid treatment

Another procedure widely used for the purification of as-produced nanotubes relies in the use of a mixture of strong acids: **Sulphuric and nitric acids.** Briefly, 100 mg of pristine HiPco SWNTs are dispersed in $H_2SO_4$:$HNO_3$ [3:1] solution, the acid solution is prepared in ice, hard stirring and adding drop wise nitric acid in the sulphuric one. When the solution is at room temperature the nanotubes are added. The reaction is ultrasonicated under reflux. Due to the strong oxidation process, the reaction is performed for 12 hours. Afterwards the reaction is quenched using 1 L of distilled water, filtered and washed with DI water until neutral pH is reached. Finally the sample is washed with 50 ml of ethanol, rinsed and let it dry in vacuum overnight.

Despite the strong oxidation reaction the metallic removal was less efficient than that obtained with the previous procedures. This is observed in the TGA curves reported in figure 2.7. The residual material is approximately 20 % of total weight. This is another example where the removal of particles plays a key role in the stability when the temperature increases. The removal of short nanotubes plays a more important role. Here the higher degree of decompositions was done at 587 ºC. This temperature is higher than in previous procedures. From the analysis of the Raman spectra it is possible to determine a light increase in defects. This could mean a removal of amorphous carbon, but, it is appreciable as well the disappearing of RBM and $G^-$ peaks; this could indicate the destruction of some chiralities. The presence of metallic particles was high, TEM image show large bundles of nanotubes with a considerable presence of particles. The yield of this reaction was 8.41 %.

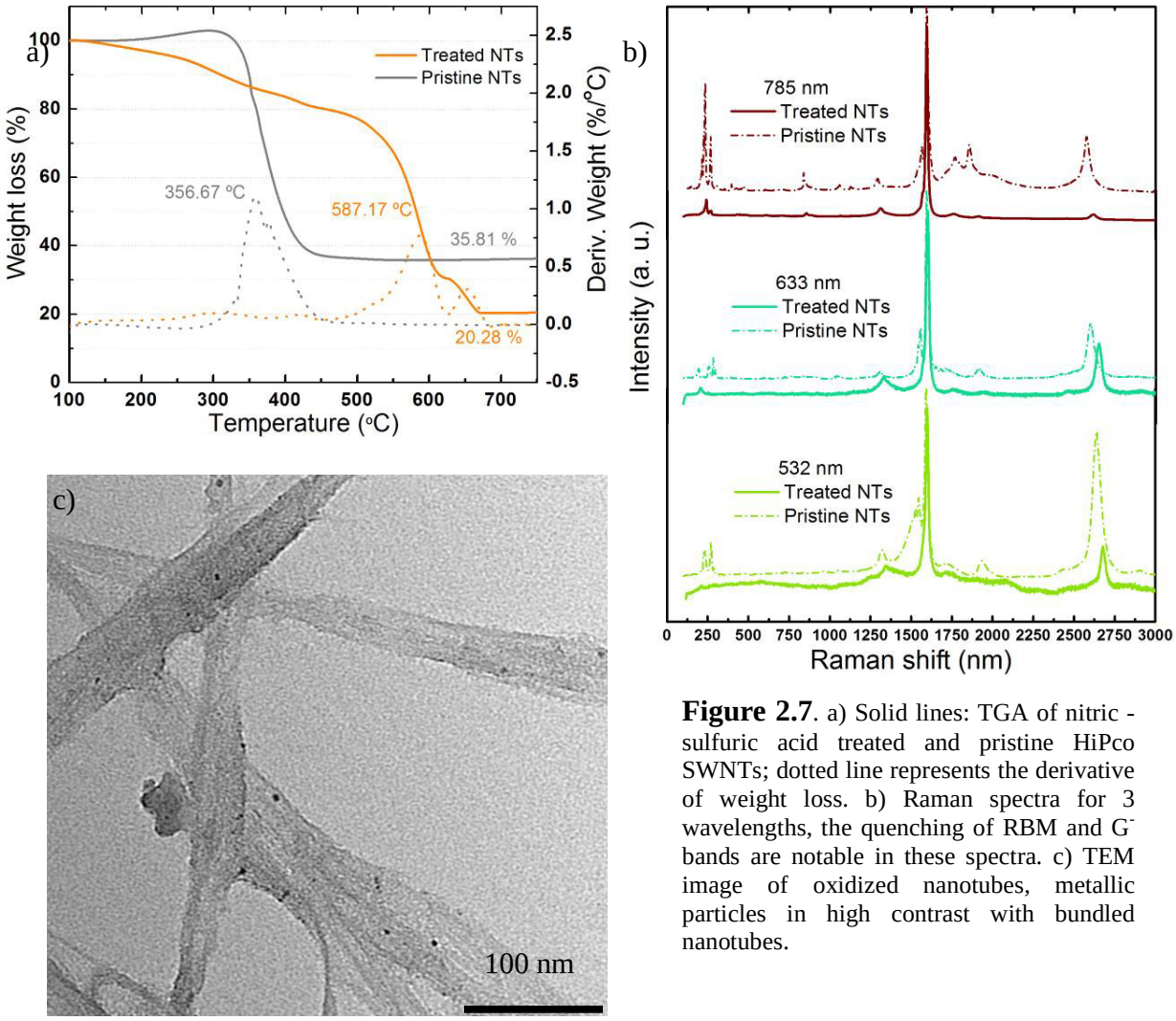


**Figure 2.7**. a) Solid lines: TGA of nitric - sulfuric acid treated and pristine HiPco SWNTs; dotted line represents the derivative of weight loss. b) Raman spectra for 3 wavelengths, the quenching of RBM and $G^-$ bands are notable in these spectra. c) TEM image of oxidized nanotubes, metallic particles in high contrast with bundled nanotubes.

### 2.3.4 Air-acid oxidation treatment

The last purification and metal removal procedure is a combination of air oxidation and acid treatments. The driven reason to do this purification is that some metallic particles are enclosed by carbon shells. The latter prevents the acid contact with the metallic particles and their solubilisation. The air oxidation breaks these carbon shells exposing the metal content to acid (67). The procedure is summarized in the following. 250 mg of HiPco SWNTs are dispersed with acetone and then filtered using a 0.1 µm pore size filter Millipore. The filtered material (buckypaper) is let to dry for a couple of hours. This is done to facilitate the handling. The "buckypaper" is placed in a ceramic boat and heated at 250 ºC for 1 hr, at a constant air flow. The product is dispersed in 250 ml of HCl

solution 2M, using a sonic bath for 4 hr. The dispersion is filtered and washed with 250 ml of distilled water and let dry at 100 ºC. The filtered material is heated at 450 ºC for 45 minutes, using a continuous air flow. The collected material is dispersed in 200 ml of nitric acid 2.6 M, using a sonic bath, to have a homogeneous dispersion, and then stirred for 24 hours at 125 ºC under reflux. The reaction was quenched using 1 L of DI water. The obtained dispersion was filtered using a 100 nm pore size Millipore filter, washed several times with DI water until get a neutral pH Afterward 50 ml of pure ethanol was added. Finally the sample was dried overnight under vacuum.

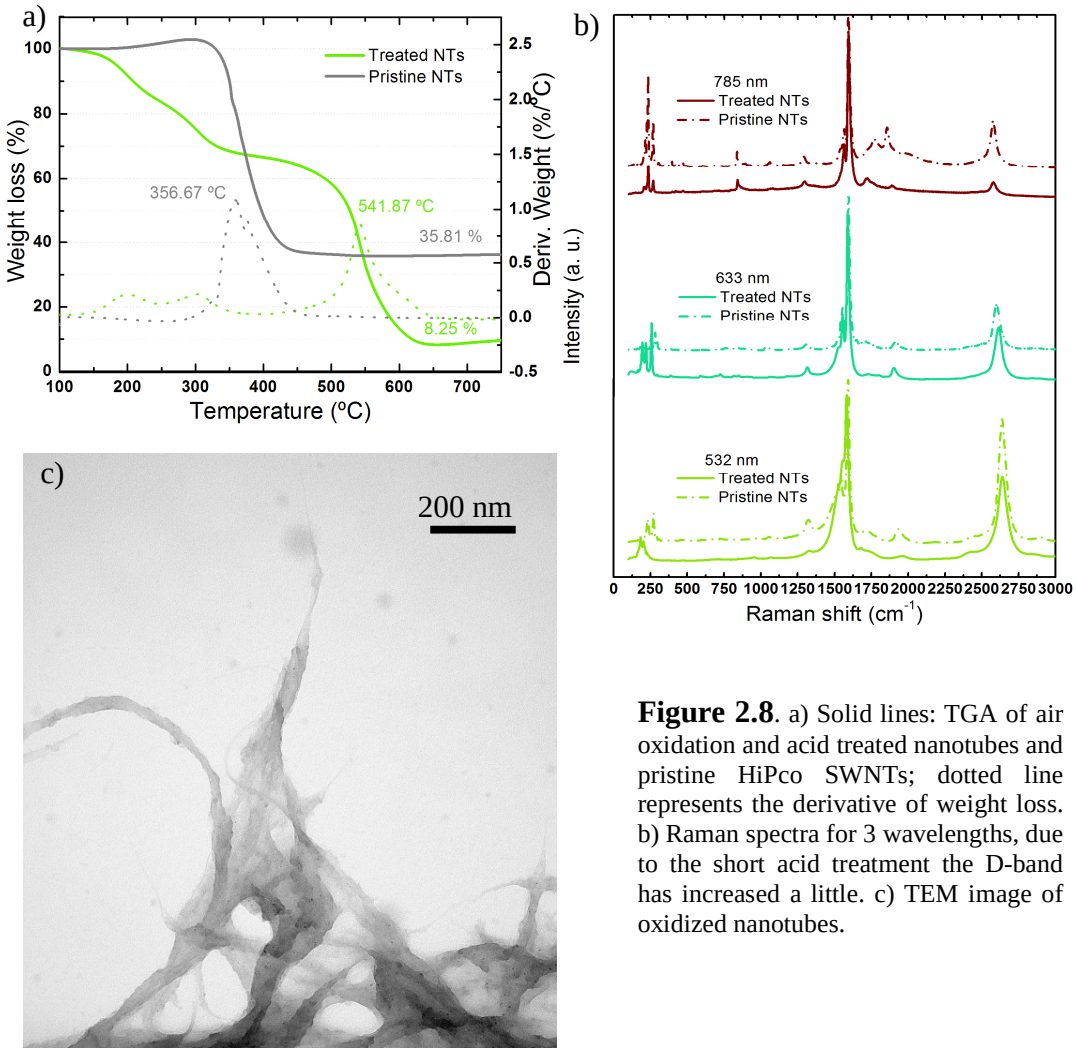


**Figure 2.8**. a) Solid lines: TGA of air oxidation and acid treated nanotubes and pristine HiPco SWNTs; dotted line represents the derivative of weight loss. b) Raman spectra for 3 wavelengths, due to the short acid treatment the D-band has increased a little. c) TEM image of oxidized nanotubes.

TGA analysis shows an elevated concentration of residual material (metallic particles), and a maximum stability at the temperature of 540 ºC. It can be observed two hips at 200 and 300 ºC. These might be due to the presence of very short tubes, or graphitic particles. I used longer reaction times for nitric acid oxidation trying to decrease the metal content, but the total yield was reduced considerably. Raman spectra show a little increase in the D-band with respect to the pristine tubes. TEM image shows a quite clean sample of nanotubes, considering that 9 % in weight are metals. Considering these results and the time of reaction under acid conditions I can say that this process is quite reliable, the short reaction times prevents the destruction of tubes, and apparently, the oxidation at 450 ºC helps to get very stable nanotubes removing metallic impurities. However this is not a drawback free process. Indeed, longer the process higher the material loss. I estimated a final yield of 13.0 % with this procedure.

**Table 2.1** Treatment result resume.

| Process | Procedure time (Hrs) | Residual Content (%) | Maximum weight loss (ºC) | D/G band ratio | Yield (%) |
|---|---|---|---|---|---|
| Pristine SWNTs | - | 35.8 | 356 | 0.0153 | - |
| Piranha | 85 | 4.25 | 463 | 0.1888 | 15.6 |
| $HNO_3$ | 102 | 3.18 | 582 | 0.5149 | 45.8 |
| $H_2SO_4 – HNO_3$ | 148 | 20.28 | 587 | 0.1889 | 8.4 |
| Air – acid oxidation | 132 | 8.25 | 541 | 0.0589 | 13 |

Thus, from a comparison of these 4 procedures, analyzing the yield, total time and metallic content, the nitric acid procedure is the more adequate for our proposes. The table 2.1 summarizes the obtained results. The procedure able to removes the higher fraction of metal particles and producing a higher yield is the one involving nitric acid. In the other procedures the yield was always too low and the metals presence remains high. Another important parameter that needs to be considered is the creation of defects. In this regards, the nitric acid process produces the higher amount of defects, while all others show less quantity of defects.

I have performed several studies on the purification of the HiPco nanotubes using nitric acid varying the reaction time. The metal composition and level of defects were studied by TEM, TGA, Infra-red (IR) and Raman spectroscopy. In figure 2.9 the TGA curves show that the metal removal is not effective if the tubes are let oxidize for longer time. In contrast it is notable that derivative of the weight loss curves are integrated by two peaks the first peak is between 350 to 450 ºC, and presumably related to the level of oxidation of some nanotubes. Nitric acid treatment binds oxygen groups at the open tips and defects, such as Stone Wales and carbon atom vacancies (68). Longer is the oxidation process higher is the number of functional groups attached at the sidewalls. This process occurs when the nanotubes are oxidized for more than 48 hours. The TGA curves after 72 hours of oxidation show that the sample is more stable with respect to samples oxidized for shorter times. This can be explained by the removal of short and heavy oxidized nanotubes. Nanotubes IR spectra is a non-quantitative characterization technique. The graph in figure 2.8 b) shows the presence of some groups with infrared resonant frequencies. There are three IR active peaks, the first one at 1739 $cm^{-1}$, representative of C=O bonds. This peak is barely present in the pristine sample, but increase for oxidized samples At 1581 $cm^{-1}$ we have a peak representative of C=C, which resulted invariant upon oxidation. The third peak is found at 1200 $cm^{-1}$ and it is related with the C-O-C bonds. In the oxidized sample the presence of this peak is increased. In addition IR bands for pristine HiPco nanotubes are less intense because the strong $\pi$-$\pi$ attractions among the nanotubes walls that promotes the aggregation in large bundles. This quenches the resonance frequency. Raman curves, figure 2.8 c), are taken using a wavelength of 633 nm. They show an increase of the D-band (~1305 $cm^{-1}$), practically inexistent on the pristine sample. After the oxidation treatment the $sp^3$ hybridized carbon atoms increases considerably. In the same context the broadening of $G^-$ and $G^+$ it is notable. Tubes after the oxidation treatment have a G band blue-shifted by 10 to 20 $cm^{-1}$ that is associated to the negative charge of oxygen atoms bonded to nanotube walls (69). Moreover, the shift increases with the oxidation time. In the magnification on the left of figure 2.9 (c) is appreciable the apparent selective destruction by diameter, besides the decrease in intensity with the reaction time for some diameters. According with Kataura plot (70–72) the destroyed chiralities are (7, 5) (283.3 $cm^{-1}$); (9, 2) (387 $cm^{-1}$); (8, 3) (395 $cm^{-1}$), the

possible chiralities for nanotubes below 200 $cm^{-1}$ are a lot, with diameters larger than 1.7 nm. The remaining chiralities correspond to (13, 1), (10, 3), (11, 1), (7, 6) (8, 4), from 220 $cm^{-1}$ to 262 $cm^{-1}$.

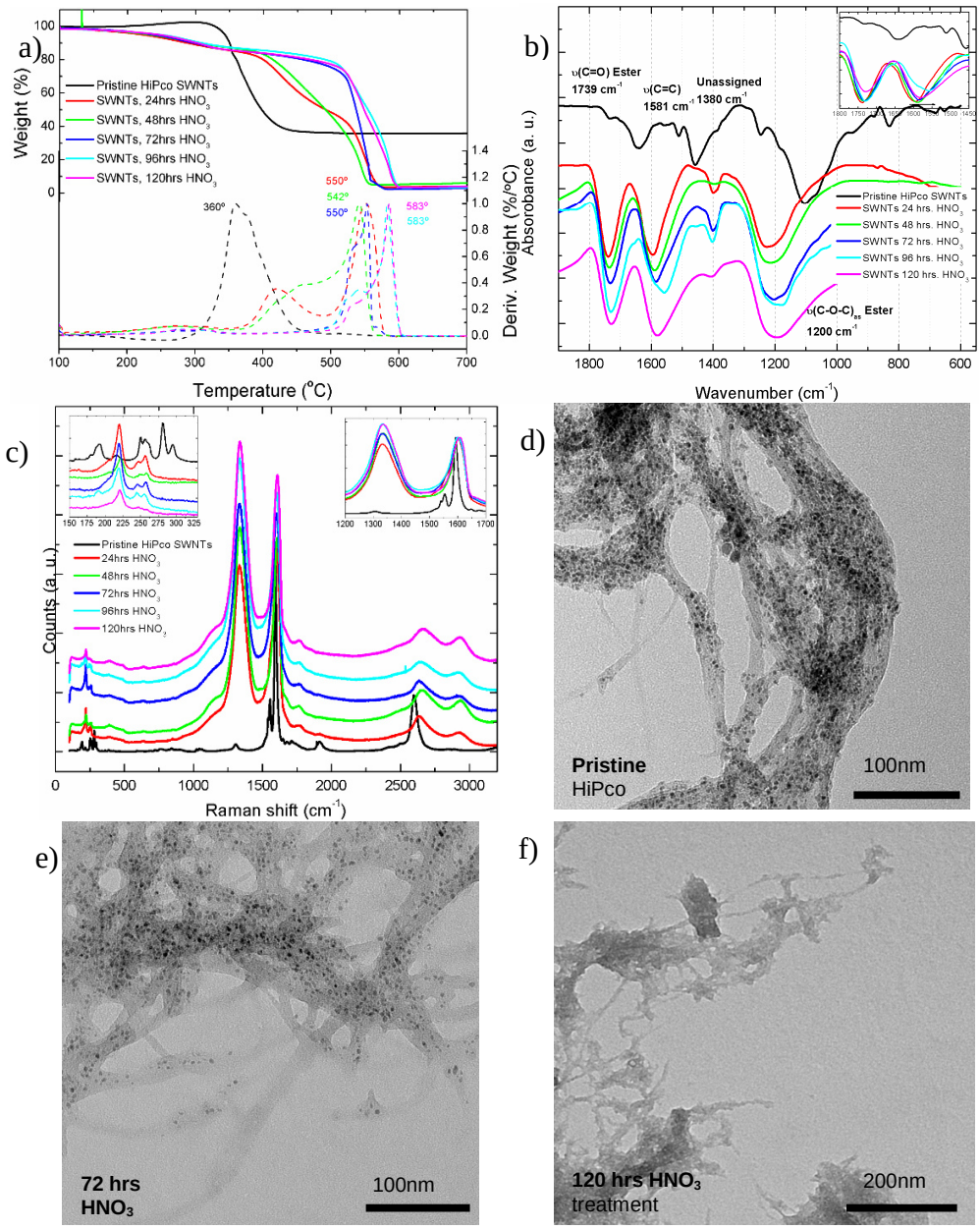


**Figure 2.9.** Analysis of HiPco oxidized nanotubes by nitric acid. a) TGA curves of pristine and 24 to 120 hours of reaction, the upper curves are the percentage weight loss and below the derivative, showing the temperatures where the maximum weight loss is performed. b) IR spectra, it is appreciable the apparition of oxygen –carbon peaks, in the inbox is shown the shift of the corresponding C=C band. c) Raman spectra using 633nm wavelength excitation. d), e) and f) are TEM images of pristine and 72 and 120 hours of treatment, still Fe nanoparticles are present.

Despite the strong acid attack, small amounts of iron particles remains in the sample, TEM images, figure 2.8 d) to f), are selected pictures from such irremovable particles, showing higher contrast due to their heavier atomic weight, which are encapsulated by graphitic shells, avoiding the acid contact, as TGA indicates, the metal content could not be reduced below the 3 % limit.

The table 2.2 enlists some characteristics of treated materials. For our propose the oxidation process for 3 days is best, it eliminates short nanotubes reducing heterogeneity and have a low metal content.

**Table 2.2.** Resume of TGA characterization.

| Treatment time | Maximum weight lost ( °C) | Residual material (%) | D/G band ratio | G-band shift ($cm^{-1}$) | Yield |
|---|---|---|---|---|---|
| Pristine | 360 | 34.0 | 0.036 | - | - |
| 24 hrs | 550 | 3.6 | 0.9147 | 7.31 | 79.0 |
| 48 hrs | 542 | 4.4 | 1.0536 | 12.6 | 67.5 |
| 72 hrs | 550 | 2.3 | 1.0495 | 7.5 | 58.6 |
| 96 hrs | 583 | 3.0 | 1.1708 | 8.21 | 63.3 |
| 120 hrs | 583 | 3.3 | 1.1771 | 15.25 | 67.5 |

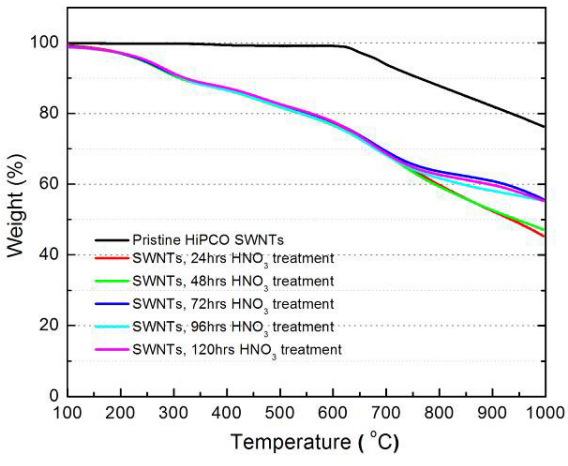


**Figure 2.10**. Nanotubes TGA curves under nitrogen atmosphere.

The defects over the nanotube wall are not desirable for electronic applications It is widely used an annealing process at high temperatures to remove the majority of defects, according whit TGA measurements, figure 2.10, in an inert atmosphere, or in atmosphere lacking of oxygen, the nanotubes demonstrate a great stability at high temperatures.

The annealing process was performed under argon atmosphere at 1000ºC for 1

hour. 5 mg of oxidized tubes were put in a ceramic boat and the air was purged out. The furnace tube was filled with argon and purged trice, finally the furnace tube was filled with argon. The heating ramp was set to increase 10 ºC per minute until 100 ºC, to remove all possible water, avoiding a non-desired oxidation, after 30 min, the ramp continue until arrive at 1000 ºC.

The figure 2.11 shows the TGA, IR, Raman and TEM characterization for this treatment.

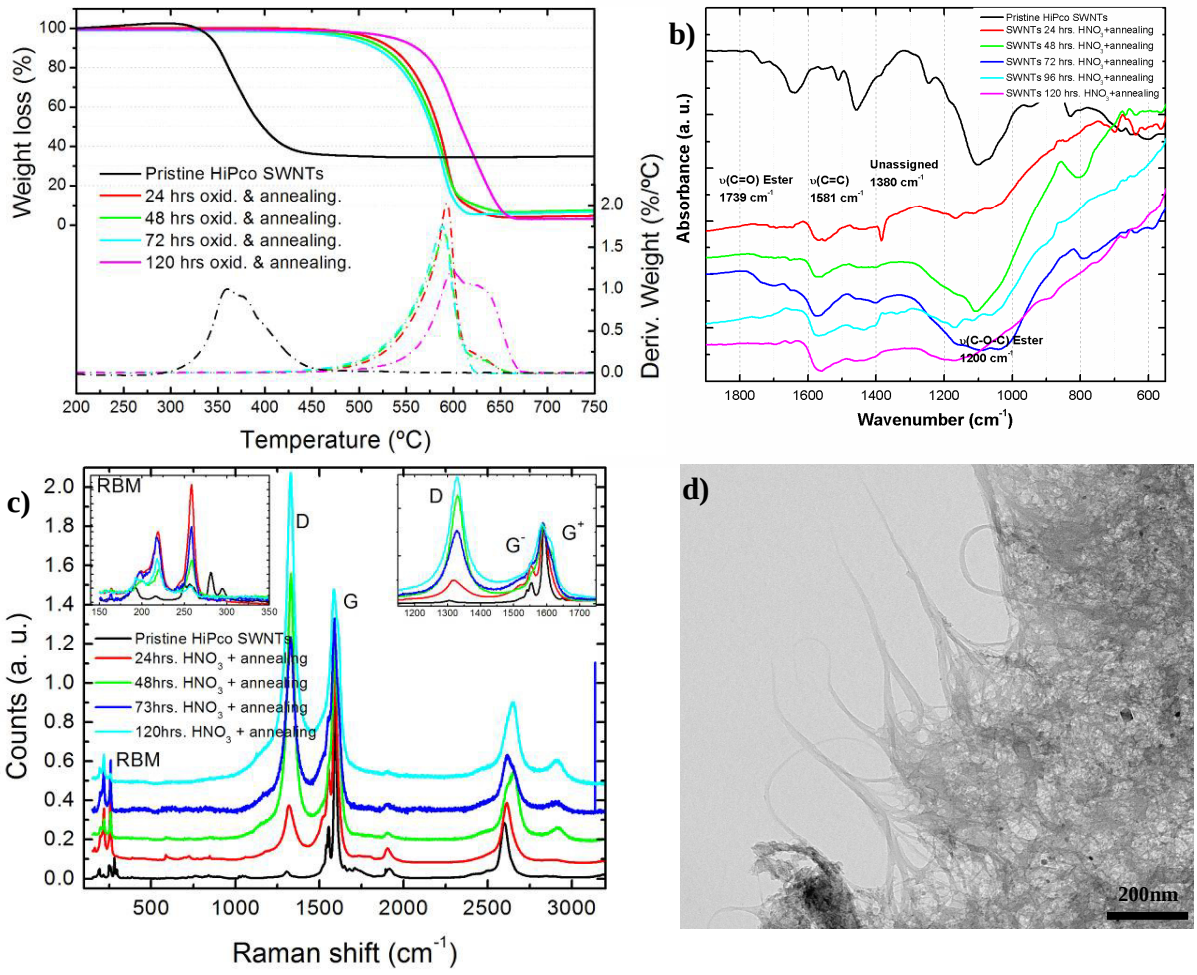


**Figure 2.11**. Analysis of annealed HiPco oxidized nanotubes. a) TGA curves of re-crystallized and pristine samples, the upper curves are the percentage weight loss and below the derivative. b) IR spectra, of the same samples as a). c) Raman spectra using 633nm wavelength excitation. d) TEM images of annealed sample of 120 hours of oxidation treatment. For the sample treated for 96 hours there are some characterization missing because the product was not enough.

In the TGA curves (fig 2.11 (a)), in average, all the analyzed samples tend to decompose at the same temperature. However, there are considerable increases in stability of almost 250 ºC, if are compared with pristine sample; the remaining metals content oscillate between 4 and 10 %. The IR spectrum shows the total removal of C=O peak, the C=C is shifted above 1600 $cm^{-1}$. The original curves were not recovered. The bundling is higher in annealed samples; the removal of amorphous carbon and re-crystallization of defects promotes the $\pi$ - $\pi$ interaction among tubes. The dispersion cannot be achieved successfully to reproduce the original IR spectra. Raman spectra show the evolution of defect removal. If the tubes are long time oxidized, the quantity of defects increase as well. Other interesting feature is the shifting of the G-band to its original position; this indicates the removal of oxygen atoms from the nanotube surface besides, the annealing induced an increase in intensity of RBM modes. TEM images show a randomly oriented aggregation of nanotubes, the purity is remarkable, but in spite of this, some metallic particles are still present. It is important to mention that annealed samples were difficult to handle, they were not fluffy but densely aggregated, similar to a small hard rock.

### 2.4Sorting by electronic behaviour

Each SWNT chirality behaves different and can be considered as a distinct molecule with a unique structure. Currently available SWNT synthesis methods yield nanotubes with uncontrolled diameter, chirality and, consequently, optical properties. Such heterogeneity is, from one hand, an impediment for the large scale realization of many SWNT-based devices such as field effect transistors and interconnects for nanometre scale integrated circuits (73). The enrichment of particular electronic types or chiralities of SWNTs is critical both from a theoretical point of view and for the optimization of their applications.

An effective sorting strategy should in principle be non-destructive, scalable, affordable, compatible with wide range of nanotube diameters and lengths and iteratively repeatable.

It has been found in a typical SWNT HiPco sample a mixture of approximately 50 different chiralities (51), in which it is estimated that two thirds of the total nanotubes has a semiconductor characteristic. The heterogeneity of as-produced SWNTs (70, 74) together with their natural formation of bundles due to strong van der Waals forces between them is the biggest impediment in the commercial realization of many SWNT based applications (43, 75). Post production enrichment of nanotubes is a challenging task owing to the tendency of nanotubes to aggregate into bundles and also due to their poor solubility. The solution to the latter problem is somewhat related to the former, as wet chemistry enables easier manipulation of the SWNTs. To date, successful dispersion of SWNTs in various solvents with or without the aid of dispersants has been demonstrated (76–78). When in dispersions, SWNTs resemble large biomolecules. Greater understanding of the dispersion mechanism, especially in aqueous environments, is crucial for the separation of SWNTs. This is because, well established techniques for the separation of biological molecules, *e.g.* conventional and density gradient ultracentrifugation (79–81), electrophoresis (82–84) and variations of chromatography (85) are the prime candidates for successful SWNT sorting

Separation of SWNTs in a liquid environment usually follows the strategy of ‘amplifying’ their subtle differences in chemical reactivity by covalent (86–89) and non-covalent functionalization (90, 91). Such differences arise from their electronic types or chiralities (72, 92). After the first step of functionalization, the SWNTs can be sorted by chromatographic (65, 91) or electrophoretic (93, 94) separation techniques and by conventional or density gradient ultracentrifugation (72, 95, 96). The choice of the separation methods depends on the type (*e.g.* difference in surface charge, length and buoyant density) of SWNT functionalization.

### 2.4.1 Selective destruction

The first attempt to separate metallic and semiconductor nanotubes was the selectively destruction of one type of SWNTs. Just to mention some interesting examples of selective attack: Miyata et al reported a chiral dependent combustion (97), they stated that high chiral angle and small diameter nanotubes decompose more rapidly; Qiu et al reported the purification via microwave radiation and high corrosive solution that destroys just metallic tubes (98). Miyata and collaborators presented a controversial report suggesting that semiconducting tubes are more reactive when are treated with $H_2O_2$ (99). Huang et al. published a direct burning *in situ* a Raman spectrometer using a wavelength of 524 nm and adjusting the power at 20 mW they demonstrate that m-SWNT burns, instead semiconducting tubes remains unaltered (100). For electronic applications, an IBM group made a FET-like device, where it is possible to use an unsorted sample of nanotubes, or even bundled nanotubes and electrically burn the undesired material. The device consist in a simple couple of electrodes, in which trough them a high electron current flows, the metallic tubes are burned, in the same way that a copper wire is burned in short-circuit, meanwhile semiconducting tubes remain unaltered. (101). Li *et al.* in 2004 fabricated wide source/drain electrodes on top of individual SWNTs grown on $SiO_2$/Si substrate. The gate voltage was held at 10 V to deplete the semiconducting nanotubes. It was seen that an increase in bias led to the preferential failing of metallic SWNTs (102)

I tried to destroy metallic nanotubes tubes using nitronium ions, this procedure theoretically takes advantage of the available density of states at the Fermi level, inducing a bigger reactivity than semiconducting ones, in this context the semiconducting tubes, in principle, will not be affected by the process, and after annealing they can be directly used in electronic applications (103). Nitronium ions are obtained in 100 ml TMS/chloroform [1:1 by weight] solution with 50 mM of nitronium hexafluoroantimonate $NO_2SbF_6$.

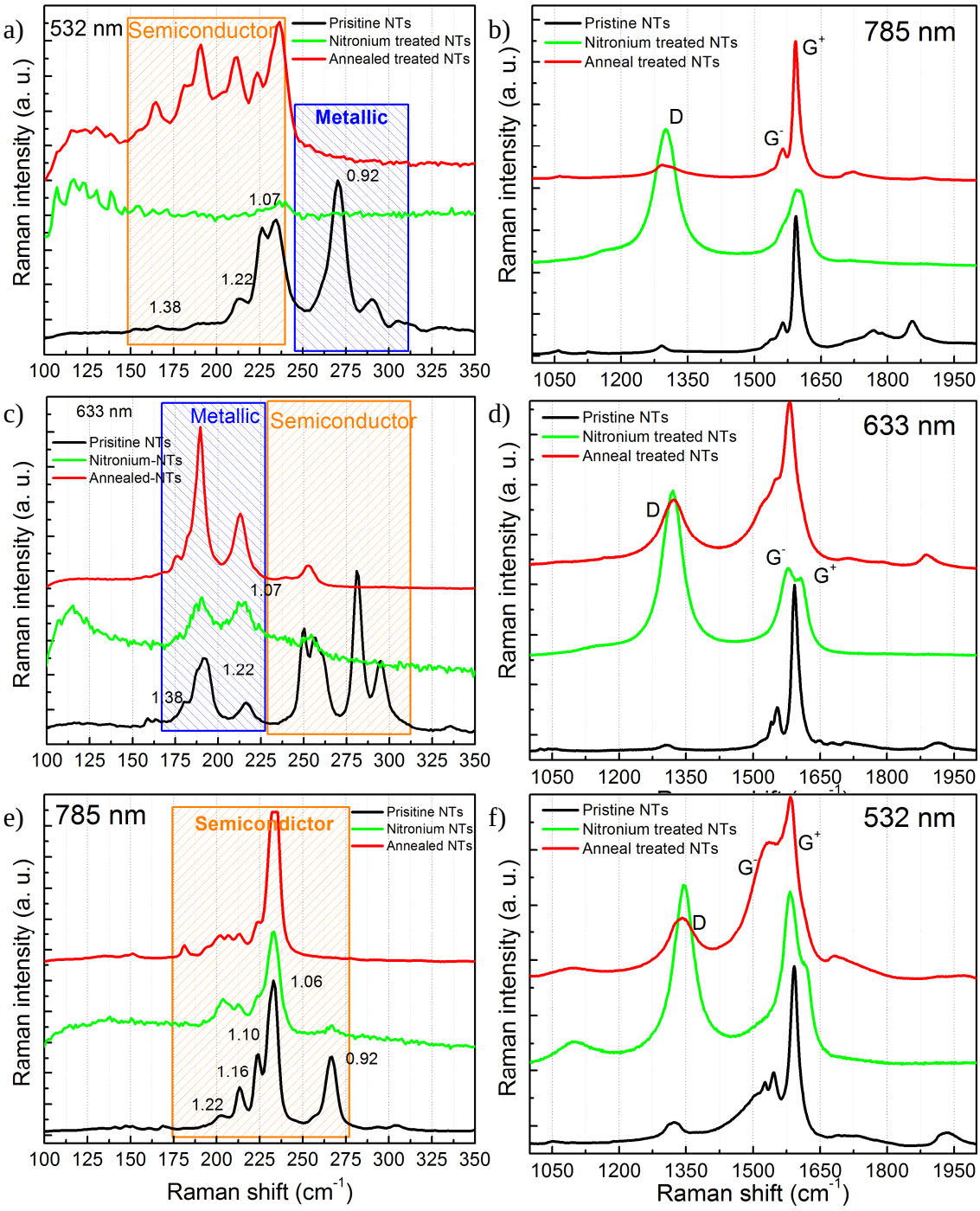


**Figure 2.12.** Raman spectra of nitronium process for metallic nanotubes removal. Using 3 diverse wavelengths 785, 633 and 532 nm.

I followed the same procedure published by An et al (103), shortly described, 10 mg of HiPco SWNTs are dispersed in the TMS/chloroform:$NO_2SbF_6$ solution described above, the dispersion was let it react for 24 hours in a sonic bath and nitrogen bubbling. Afterwards the sample was filtered trough a 0.1 µm Millipore filter, the filtered material was washed with large quantities of water and 100 ml of pure ethanol. The sample was dried under vacuum at 100 ºC. Finally the nanotubes are annealed at 1000 ºC for 30 min under an inert atmosphere.

The Raman spectra in the figure 2.12 show interesting results, first, in the RBM region some peaks disappear after the nitronium ions treatment. Notably, only nanotubes with diameters smaller than 0.97 nm disappear. On the other hand, all other nanotubes with larger diameters are reduced in intensity, due to the defects produced by the ions, green lines in a), c) and d). In fact the creation of $sp^3$ bonds or defects on the nanotube walls are clearly seen in the increased D-band intensity, green lines in b), d) and e).

The annealing process recovers and increases the RBM peaks, at least 3 times with respect to pristine sample. In 2.12 d,) excitation wavelength of 532 nm, apparently the selective metallic tubes removal is a success, but in figures a) and c), 633 and 785 nm respectively, it is clear that just small diameter tubes are removed, not the metallic ones. In the same context, the D-band is not reduced due to treatment, indicating that defects are still present, the original optical and electric properties are not recovered entirely.

The obtained results driven me to consider a change in the separation strategy, and look for a non-damaging process. Defective or functionalized tubes are not ideal for electronic and optical applications and the annealing process do not re-crystallize totally oxidized tubes. Thus a process that separate nanotubes without the drawback of damaging is desired.

### 2.4.2 Sorting of SWNTs by covalent and non-covalent functionalization

Covalent functionalization of SWNTs involves attachment of different reactive chemical groups on the SWNT sidewalls or end caps, (104, 105) disrupting the extended $\pi$-network on SWNT sidewalls, but compromising their optical properties. Therefore, covalent functionalization is used only to selectively remove a particular type of SWNTs. For example, diazonium salts is water soluble and form a covalent aryl bond by extracting electrons from nanotubes thereby demonstrating highly chemoselective reactions with metallic SWNTs (m-SWNTs) (87, 106), which can be subsequently separated by free solution electrophoresis (83). Covalent functionalization by optical means, based on the electronic properties of SWNTs, has been demonstrated. This includes selective osmylation of m- SWNTs by ultraviolet light exposure (107) and enhanced oxidative degradation of s- SWNTs through excitation of light. In this instance, selective degradation is possible by tuning the excitation wavelength corresponding to the band-gap of a particular SWNT species (108).

Non-covalent exohedral functionalization may be used in SWNT separation (92). Selective interaction of porphyrin with s-SWNTs is employed to separate them from m-SWNTs (109). Chiral diporphyrin molecules selectively adsorb on SWNT sidewalls with particular chiral angles; a useful trait for SWNT chirality enrichment (110). Selective wrapping of polymer or surfactant molecules may be used for separation purposes. For example, fluorine based polymers in toluene selectively disperses SWNTs of a narrow diameter range (~1.02-1.06 nm) by non-covalent interaction (111, 112). Polyvinylpyrrolidone (PVP) molecules exhibit diameter selective (~1nm) wrapping of SWNTs as well (76). Non-covalent dispersion of SWNTs in oligo-acene adducts (*e.g.* $C_{26}H_{17}NO$) in organic solvents can be used to separate SWNTs by diameter (90). In this case, the polymers act as ‘molecular tweezers’ and selectively bind SWNT sidewalls by $\pi$-stacking, depending on the dimension and angle between the ‘anchor’ part of the molecules (90).

A non-covalent and selective nanotube discrimination process is a gel based separation published in 2009 by Kataura's group (113). I perform the same experiment. Briefly the process consist in disperse 2 mg of HiPco SWNTs in 10ml of distilled water with 2 % in weight of SDS, ultrasonicated for four hours using a sonic tip at a duty cycle of 50 %. During the ultrasonication the sample is immersed in ice to avoid heating. Finally the sample is ultracentrifuged at 12000 RPM (16100 g) for 24 hours to remove thick bundles and impurities. The supernatant is collected and the precipitate is discarded. A gel was prepared from the SWNT dispersion by mixing and gelling the dispersion with liquid agarose gel. In a typical preparation, 0.8% of agarose melted in ×2 TB buffer (100 mM tris(hydroxymethyl) aminomethane and 97 mM boric acid at pH 8.2) by heating in a microwave oven was mixed with an equal amount of the SWCNT dispersion. The mixture was then let stand at room temperature to induce gelation. 0.4 mL of the SWCT-gel was ultracentrifuged for 3 h at 12000 rpm. The resulting sample is a gel-nanotube precipitation and a dark dispersion. According with the results in literature the semiconducting part is attached at the gel and metallic ones remain in dispersion. Raman and UV-Vis spectroscopy was used to characterize the enrichment of the samples.

Figure 2.13 shows the Raman spectra of the processed samples; the solid lines correspond to the pristine sample, the dashed lines is the spectrum of agar gel without nanotubes, while the dash-dotted line represents the spectrum of the nanotubes attached to the gel, supposed to be semiconducting nanotubes, and finally the dotted line correspond to the sample where nanotubes were not attached to the gel, the supposed metallic ones. Raman spectra were taken using 3 different wavelengths. As it can be observed in the RBM region, there is not appreciable diameter selectivity. Absorption spectra can give also information on the selective separation. Figure 2.14 is the absorption of the attached and detached nanotubes from the agar gel, in the same way there are not differences among spectra. I have tested this procedure for 3 times with similar results, I consider this an original idea, but diameter selectivity was not achieved.

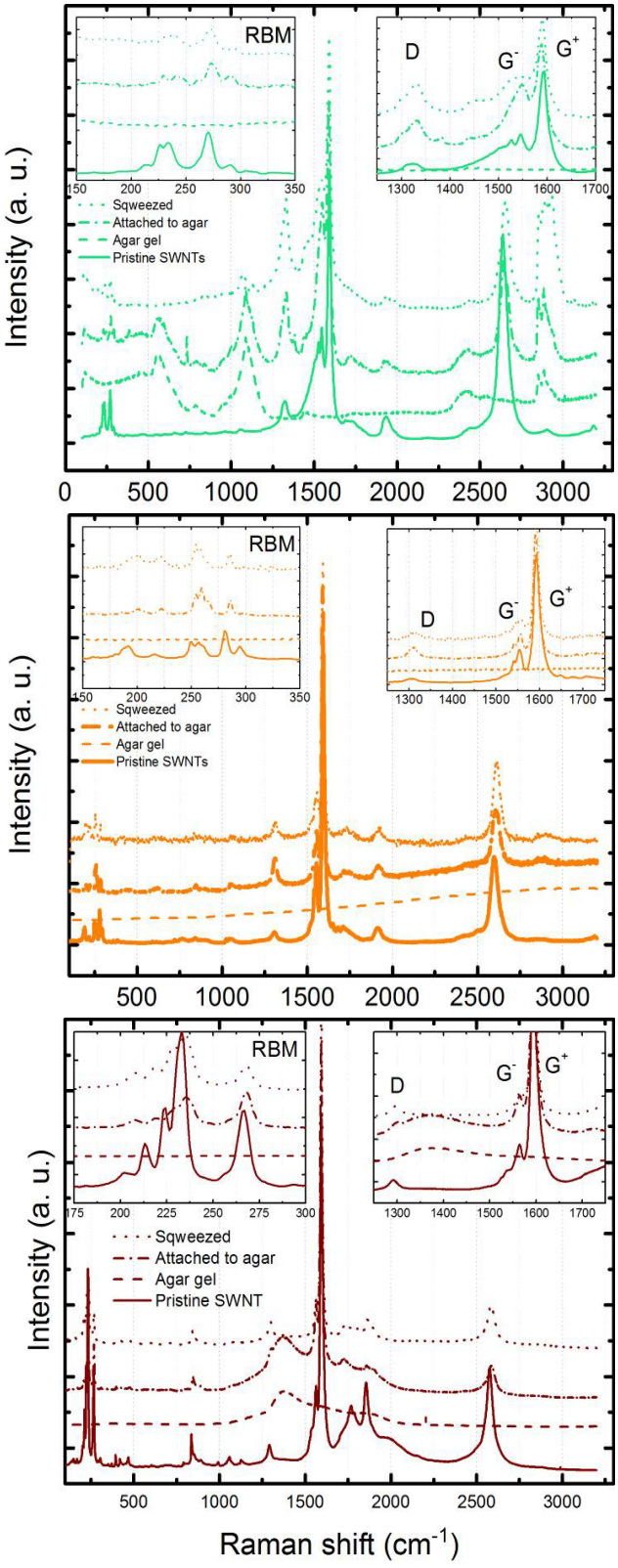


**Figure 2.13**. Raman spectra of agar separation of SWNTs, at different wavelengts, a) 514 nm; b) 633 nm and c) 785 nm. The in-squares shows an amplification of the RBM and the D, and G bands.

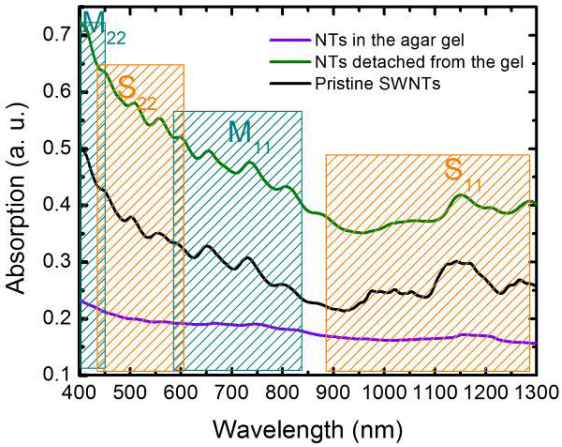


**Figure 2.14.** Absorption spectra of SWNTs in agar gel, for selective separation.

Another interesting case of study is the work done by Kataura's group (114). They have developed a effective protocol for chirality separation, scalable, economic, without damaging the tubes and produced in relatively short time. They used a gel in which semiconducting or metallic nanotubes have more affinity to the gel, remaining attached to it, while the counterpart is not attached and can be washed away. Following this procedure they built a selective mesh or filter. In the first approach they used agar gel as selective filter and reported a successful separation of nanotubes according with electronic properties (115, 116). However, the quality of separation was not high, the nanotube desorption of the agar gel was a challenge. In a successive work they solved the problem using a surfactant elution. In this way the surfactant attaches to nanotube surface desorbing from the agar gel (117, 118). They perfection the process until achieve an awesome purity of single chirality suspension of nanotubes (94 % for (7,6) chirality; 93 % for (6,5); 89 % for (7,3), (8,6) and (7,5) (119–121).

### 2.1.4.3 Density gradient ultracentrifugation

Another technique widely used for the separation of nanotubes is density gradient ultracentrifugation (DGU). It has recently emerged as a very promising tool to prepare such samples (72, 92, 95, 96, 122, 123). DGU is a well-known technique to purify macromolecules and biological materials (79–81, 124–127). It is one of the most suitable techniques for obtaining high-purity SWNTs of a single-electronic type. This approach exploits differences in the buoyant densities (mass per volume) among SWNTs of different structures; The buoyant density of SWNTs in aqueous solution does not only depend on density of the carbon nanotubes itself, but also on the surface functionalization and the filling and hydration of the surfactant-coating (72, 96), For DGU to be successful,

the buoyant density of a SWNT must be directly related to its physical and electronic structure (72, 95, 96, 122). The SWNT separation then is induced by ultracentrifugation through to the spatial redistribution of the nanotubes along the ultracentrifuge tube according to their buoyant density. In response to the resulting centripetal force, particles sediment toward their respective buoyant densities and spatially separate in the gradient (96). Surfactants with different chemical structure adsorb in a different way on the SWNTs due to different polarizability of metallic and semiconducting tubes (128). This results in different buoyant density, which enables the separation by electronic type. In this context, Bonaccorso and co-workers reported the first sorting of SWNTs according to the electronic behaviour (72). Other materials instead of surfactants had been selectively attached to different nanotube chiralities, *e. i.* bromine attaches better to metallic tubes and render a higher density to this type of tubes, in a density medium the bromine-nanotube composite precipitates and semiconducting tubes remain in solution (129); DNA can exploit the $\pi$ interactions of aromatic nucleotides to attach to the sidewalls of nanotube, rendering a good dispersion of individual SWNTs (130–132).

The procedure to sort SWNTs by DGU can be described as follows (76, 96). Optiprep, i.e. 60% w/v iodixanol ($C_{35}H_{44}I_6N_6O_5$) solution in water, ($\rho$=1.32 g·cm$^{-3}$) is used for the preparation of the density gradient medium (76, 96). By suitably diluting Optiprep in additional DI water, the density profile of the medium inside the ultracentrifuge tube can be shaped according to the specific need. Linear gradients are used to separate materials with buoyant density differences as little as ~ 0.01 g·cm$^{-3}$ (79). For this reason, linear gradients are very effective in SWNT sorting, as the difference in densities amongst different SWNTs diameters are in the order of ~ 0.01 g·cm$^{-3}$. The gradients are created directly in the centrifuge tubes by first overlapping discrete layers of gradually increasing densities of Optiprep solution and then letting the layers diffuse into each other thus forming the final linear density gradient (76, 96). Slanting of 90° the centrifuge tube speeds up, of several hours (~ 10) the self-diffusion process without compromising the linearity of the gradient (95). The gradient density and slope are both key parameters for SWNT sorting (76, 96). The gradient must be shaped in order to minimize the distance that the SWNTs have to travel before reaching their isopycnic point i.e. where the density

matches that of the surrounding medium (76, 96). Note that, during ultracentrifugation, the density profile redistributes as the density gradient medium responds to the centrifugal force, resulting in a steeper gradient over time (79).This press the SWNTs in a narrow layer. To overcome this disadvantage, it is important to form a density gradient, dense enough, thus the isopycnic point of the SWNTs of interest is positioned in a linear region as possible.

In the SWNT separation by diameter, the density of the medium is varied between ρ~ 1.03 g.cm$^{-3}$ at the top (5% w/v of iodixanol ) to ρ~ 1.21 g.cm$^{-3}$ (45% w/v iodixanol) at the bottom of the gradient (46, 76). In particular a 5-45% gradient is more stable than a 15-20 % gradient because it prevents vertical mixing between different gradient layers in the ultracentrifuge tube. A larger density gradient along the tube length also facilitates the extraction process. The dispersion and sorting process is illustrated in Fig. 2.14. Effect of separation of SWNTs in solution is visible by the appearance of bands of different colours. The spectral position of the second excitonic transition $eh_{22}$ in the visible range in fact determines their absorption properties in the visible range and hence, their colours. The appearance of different colours after DGU also gives an indication of the effectiveness of separation.

The procedure briefly explained is as follows, Dispersion and individualization of SWNTs in aqueous solutions are carried out adding 2 mg SWNTs to 10mL of de-ionized (DI) $H_2O$ with 2 w/v% surfactant. The SWNTs are dispersed by 120 min. ultrasonic treatment (Branson Sonifier 250) in an ice bath in order to prevent heating effect, figure 2.15 (a). The resultant dispersions are ultracentrifuged at 40kRPM (~ 150000 *g*) for 2hr in a

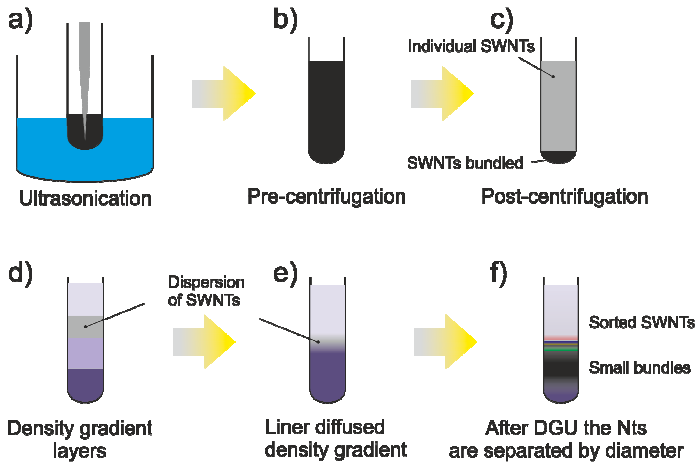


**Figure 2.15.** Representation of the Density Gradient Ultracentrifugation process. Modified from (72)

MLS 50 swinging bucket rotor in a Beckman-coulter ultracentrifuge (Optima MAX 80) (b). Insoluble materials and large bundles are removed by 30-minute ultracentrifugation treatment at 40kRPM. The top 60% is decanted for the DGU, figure 2.15 (c). The density gradient is formed layering four layers with decreasing Optiprep concentration in 2% w/v surfactant in an ultraclear ultracentrifuge tube (dimensions 13×51 mm, capacity 5.0 ml, Beckman Coulter). A layer of 0.5ml 100% Optiprep (density, $\rho$=1.32g/cm$^3$) with 2% w/v surfactant, SC:SDS [4:1] is used at the bottom of the tube as the stopping layer in order to raise the gradient in the centrifuge tube. Then 1.2 ml 50% Optiprep ($\rho$~1.18g/cm$^3$) with 2% w/v of surfactant, SC:SDS [4:1], is placed over the stopping layer. On the top of this second layer, 0.8ml SWNTs solution (density adjusted to 1.12 g/cm$^3$ by addition of Optiprep100% with 2% w/v surfactant, SC:SDS [4:1]) is placed. The ultracentrifuge tube is then filled with two more layers of Optiprep with different concentrations; 0.75 ml Optiprep 25% ($\rho$~1.09 g/cm$^3$) with 2% w/v of surfactant, SC:SDS [4:1] and ~1 ml DI water with 2% w/v surfactant, SC:SDS [4:1], respectively. This created a series of step gradients in the tube, figure 2.15 (d). The ultracentrifuge vial is capped and tilted horizontally for 2 hours in order to speed up the diffusion of the different layers, producing a linear gradient (e). SWNT sorting is carried out via ultracentrifugation in a MLS 50 swinging bucket rotor in a Beckman-coulter ultracentrifuge (Optima MAX 80) at 41 kRPM for 12 hours at 15°C (f). After DGU, the sorted SWNTs are removed from the ultracentrifuge tubes, layer by layer, using a syringe pump to extract small aliquots of sorted nanotubes. Fluorinert FC-40 ($\rho$~1.85 g/cm$^3$ Sigma-Aldrich) is used as a high density chase medium.

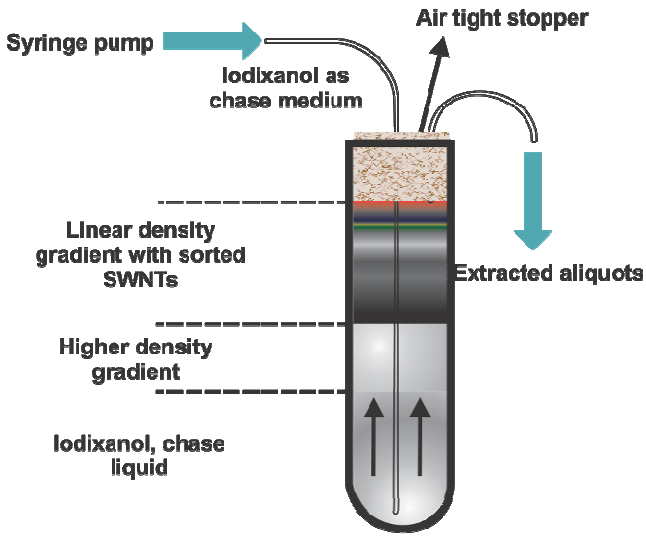


**Figure 2.16.** Schematic description of upward displacement fractionation. 150 µL of Fluorinert is injected to extract the same volume of the sorted tubes. taken form (72)

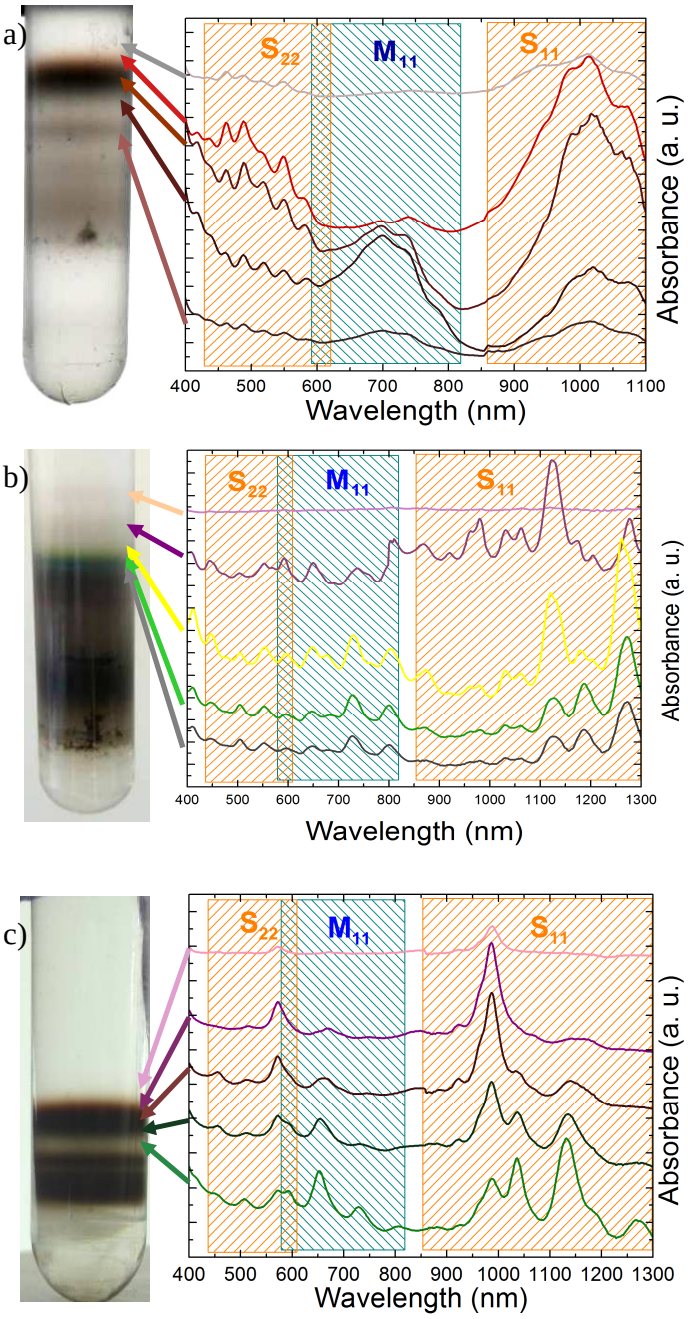


**Figure 2.17.** On the left, images of centrifuge tubes after DGU process; on the right absorption spectra for different layers. a) Arc discharge, b) HiPco and c) CoMoCat

After DGU, the sorted SWNTs are removed from the ultracentrifuge tubes, layer by layer (76, 96). This is a widely used process in life sciences by which certain quantities of a mixture are extracted to a large number of aliquots whose composition varies according to the original mixture (133). For SWNT separation, I use a syringe pump as upward displacement fractionator to extract small aliquots of sorted nanotubes (72, 96). Fluorinert FC-40 ($\rho$~1.85 g/cm$^3$ Sigma-Aldrich) is used as a high density chase medium (DCM). The extraction process is schematically presented in Fig. 2.16. First, the distance between the top level of the solution in the ultracentrifuge tube and the uppermost enriched band is measured and the corresponding volume calculated. This volume is then extracted and discarded by injecting the same volume of

Fluorinert at the bottom of the centrifuge tube. Once the bands enriched with separated SWNTs are at the top, ~70μL of Fluorinert are injected to extract the same volume of enriched SWNTs.

Absorption spectrum is taken to each fraction. Identical fractions are mixed together. In this way it is possible to assign measurements to each peak (134). In this context the capital letter S will denote semiconducting and M metallic in the absorption spectrum images.

Different synthesis processes produce diverse diameter distribution, HiPco nanotubes has the larger diameter distribution (135) if is compared with CoMoCat SWNTs where the distribution is much lower (136). The image 2.17 shows the absorption spectra of, arc discharge (a) (Carbon solutions, Inc. AP-SWNTs), HiPco (b) and CoMoCat (c). The pictures on the left are the centrifuge tubes after DGU process. In the case of arc discharge it is used a surfactant mixture SC:SDS [4:1] to promote a semiconductor enriched sorting, indeed, it is appreciable the total absence of metallic characteristic peaks in the absorption spectrum, gray and red spectra, but in denser extractions the metallic presence is more obvious, the peaks in the $M$ transitions are increased, but there is a remnant of semiconducting nanotubes. For HiPco nanotubes the absorption feature is totally different. The diameter richness of this source of nanotubes can be observed in the colour variety of the centrifuge tube. Each coloured band corresponds to different diameter and/or chirality. In the absorption spectrum, there is not a tendency of preferential sorting.

Chirality enrichment of tubes with the same diameter is done by first separating s- from m-tubes and then repeating diameter separation on the fractions of interest. This allows, for example, to selectively enrich (6,5) with respect to (7,4) and (6,6). This is a two step procedure, involving a first DGU process in a cosurfactant mixture, for m/s separation, followed by a second step, where SC is used to separate tubes with different diameter. For the first step 2 mg of CoMoCAT tubes are dispersed in 10 mL of DI water with 2% w/v SC. Dispersion and individualization proceed as described previously. The dispersion

is then diluted into 2% w/v cosurfactant solution (SC-SDS) to achieve 1.6% w/v SC and 0.4% w/v SDS. Then, a linear density gradient and ultracentrifugation processes are prepared as explained in the previous section.

The DGU of CoMoCat shows a very clean spectrum of a single chirality nanotube (6, 5) in the upper layer, while going in deeper layers the presence of other chiralities contaminate the spectra. In CoMoCat tubes the reached purity is higher but the nanotubes per volume are much lower.

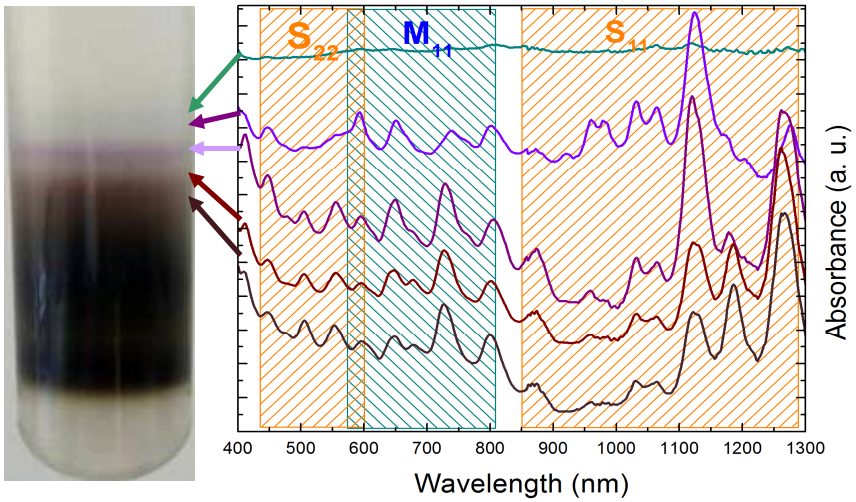


**Figure 2.18.** DGU image of purified HiPco SWNTs. On the right is shown the absorption spectra.

The image 2.18 shows the DGU of HiPco nanotubes purified by nitric-sulphuric acid. It was expected to have a similar behaviour than pristine HiPco SWNT of the figure 2.17 b), instead of yellow and greenish bands I obtain a more purple coloured tube.

Arc discharge nanotubes was used for this work because the concentration of tubes in was high enough, and the single electronic behaviour is achieved relatively simple, in contrast HiPco nanotubes makes a harder work to isolate a single electric. Additionally, in arc discharge it is possible to separate a metallic enriched portion of tubes following the same protocol that is used for an enriched semiconducting sample.

The process to obtain a m-SWNTs sample is similar to the separation of s-SWNTs, briefly explained, the individualization and dispersion using SC is carried out as in previous experiments. The density gradient is formed layering four layers with decreasing Optiprep concentration in 2% w/v surfactant in an ultraclear ultracentrifuge tube (dimensions 13×51 mm, capacity 5.0 ml, Beckman Coulter). A layer of 0.5ml 100% Optiprep with 2% w/v surfactant, SC:SDS [1:4], is used at the bottom of the tube as the stopping layer in order to raise the gradient in the centrifuge tube. Then 1.2 ml 50% Optiprep (ρ~1.18g/cm$^3$) with 2% w/v, SC:SDS [1:4], of surfactant is placed over the stopping layer. On the top of this second layer, 0.8ml SWNTs solution (density adjusted to 1.12 g/cm$^3$ by addition of Optiprep100% with 2% w/v surfactant) is placed. The ultracentrifuge tube is then filled with two more layers of Optiprep with different concentrations; 0.75 ml Optiprep 25% (ρ~1.09 g/cm$^3$) with 2% w/v of surfactant and ~1 ml DI water with 2% w/v surfactant, respectively. This created a series of step gradients in the tube, figure 2.15. Diffusion, ultracentrifugation, and extraction are carried out as before.

The figure 2.19 is illustrated a DGU with metallic enrichment, it is observable the colour change of the upper layer, from orange (figure 2.17 a) to blue (figure 2.19), corresponding with the portions of semiconducting and metallic respectively.

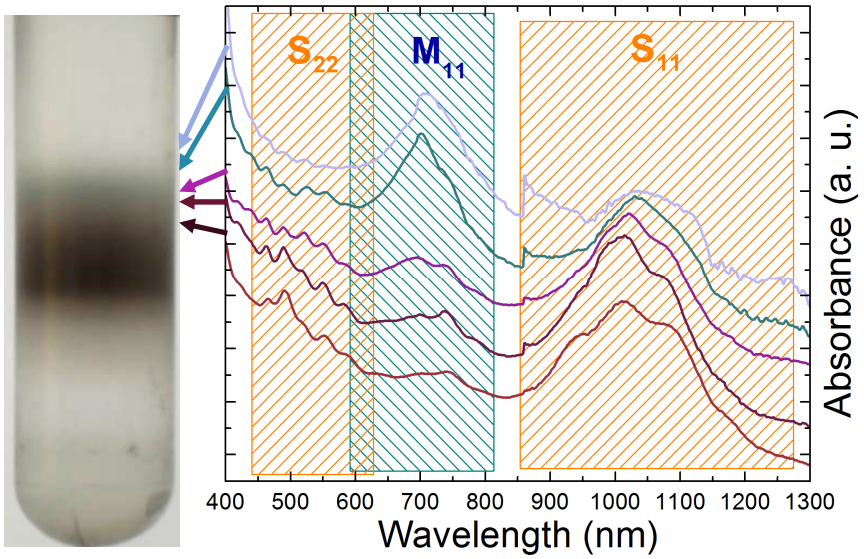


**Figure 2.19.** DGU image of metallic enriched sample arc discharge SWNTs, using a SC:SDS [4:1].

For a higher enrichment of m- or s-SWNTs additional DGU runs can be done to increase the purity, always keeping constant the proportion of surfactants. It is necessary to take the purest parts of the 1st run and re-adjust the density gradient of the nanotube layer. In figure 2.20 is depicted the absorption spectra after a 2nd DGU of arc discharge nanotubes, it is observable the selectivity of the separation process from the absorption spectra. However the nanotube concentration decreases considerably with respect to the first run.

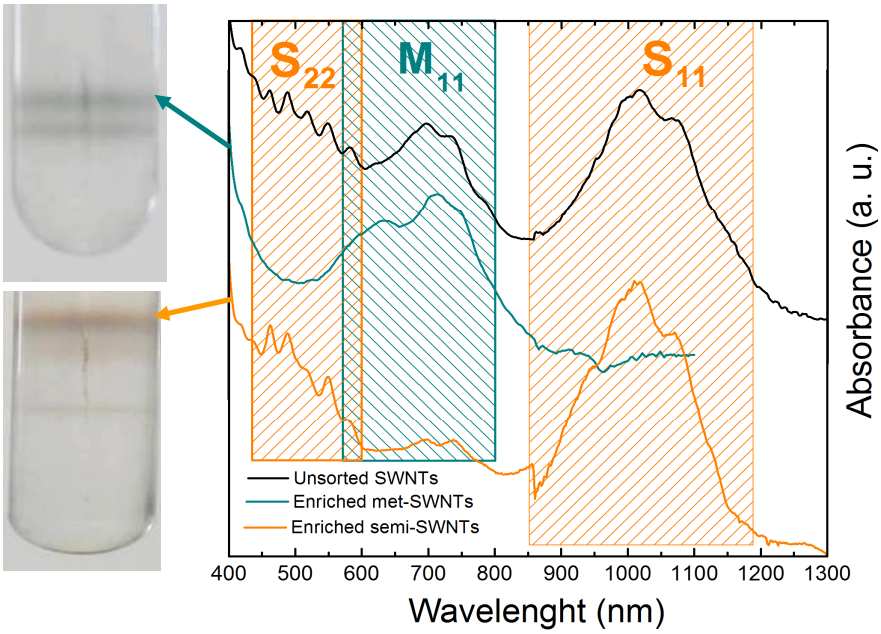


**Figure 2.20** Extra-purified (2nd run) samples of semiconducting and metallic portions.

To deal with the low concentration problem a different procedure was proposed. The figure 2.21 a) and b) shows a classical density gradient tube before and after DGU respectively, the arrows in b) indicate the layer densities. The general idea to increase the yield per DGU run is to reduce the gradient limits, as is depicted in the figure c). The new densities limits in the ultracentrifuge tube are determined by the measured densities, as reported in figure 2.21 b) and indicated as red and green dashed boxes, these values are used to calibrate the density of the top, and bottom layers respectively, in the new density gradient, figure 2.21 (c). Figure 2.21 d) shows a picture of a centrifuge tube after DGU with the new gradient, it is observed a larger band separation as it was expected. Even

more, it was possible to increase the yield two fold; this means that it is feasible to get 3 ml or even more of SWNTs of a single electronic property in one DGU run.

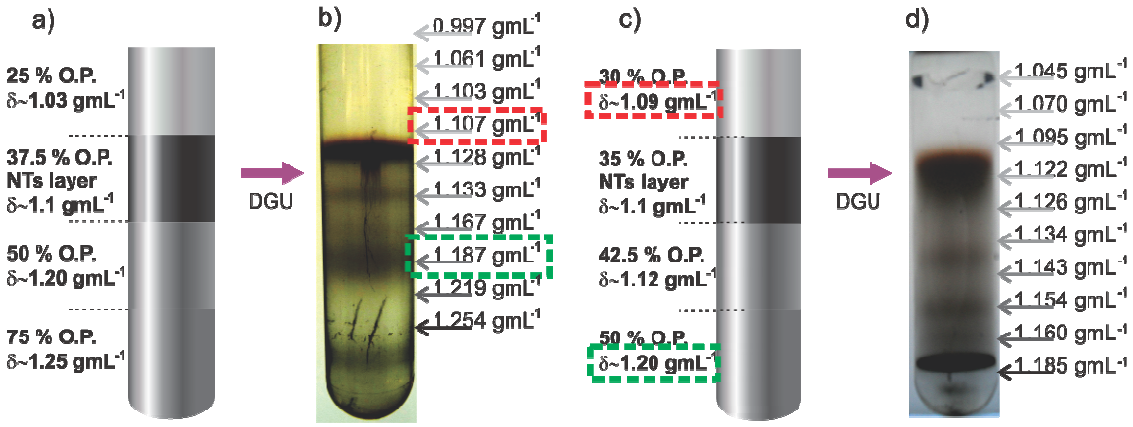


**Figure 2.21.** Schematic procedure to enhance the yield for sorted nanotubes by DGU. a) representation of the centrifuge tube prior diffusion, each of the four densities layer are indicated, after DGU, the density was measured for each extraction, b), the sorting of the nanotubes were found between 1.107 and 1.187 $gmL^{-1}$, these values were used to design a new gradient, c). After DGU the separation among layer was higher, d), achieving the sorting in a larger volume.

For further experiments it is necessary to have a light oxidation of the tubes in order to get functional groups attached at the nanotube-ends without causing structural damages on the nanotube walls. So, a fast oxidation was performed using nitric and sulphuric acid s mixtures for 1 and 3 hours. Raman spectroscopy was performed monitoring the D-band to ensure that the nanotube walls were not destroyed. In figure 2.22 the continuous line represents the pristine sample, dashed line the arc discharge SWNTs with one hour of oxidation process, finally the dash-dotted line is the spectra of the sample treated for 3 hours. It can be observed that there were not defects added to the nanotube walls, this means no $sp^3$ hybridized carbon atoms were added. Moreover the $G^+$ band presents a smooth decrease in intensity with respect to pristine sample while the attenuation is more consistent in the $G^-$ band at 457 nm. RBM did not suffer changes.

The DGU procedure of soft oxidized nanotubes had no difference with the pristine nanotubes and it was possible to use the same procedure of gradient limit to increase the

yield. Finally the image 2.23 is a picture that shows the enriched metallic and semiconducting fractions.

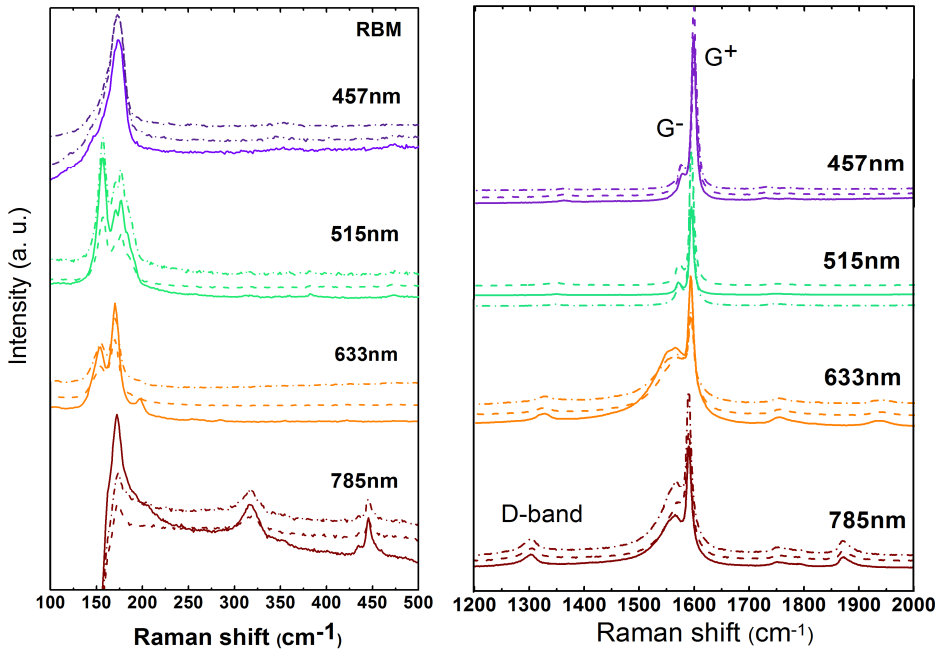


**Figure 2.22.** Raman spectra at 4 different wavelengths. Solid line: Pristine SWNTs; dashed line: oxidation treatment for 1 hour and dash-dotted line: sample treated for 3 hours. On the left, RBM it is appreciable the narrow diameter distribution of arc discharge tubes (P2-SWNT) and the intensity reduction when the sample is treated for longer period. On the right D, G- and G+ bands.

**Figure 2.23.** Enriched metallic and semiconducting samples.

### 2.5 Graphite exfoliation: graphene.

In the last years graphene had inspired a lot of scientist all around the world due to its promising properties, high conduction levels, and a very wide absorptions spectrum. In the same context graphene is the thinnest known material making it ideal for some electric and optical applications.

Graphene can be obtained peeling off a piece of graphite by means of adhesive tape(137). It has been optimized to produce SLG of up to millimetres in size, and with high structural and electronic quality. Although this is the method of choice for fundamental research, with most key results on individual SLG being obtained on such flakes, it has disadvantages in terms of yield and throughput, and is impractical for large-scale applications.(138). The thin flakes attached to the tape are transferred on $SiO_2$ substrates. Whit this procedure chemical modification is avoided, resulting in graphene with a very clean surface out of defects and impurities.

In figure 2.24 are appreciable the contrasts between different graphene thicknesses.

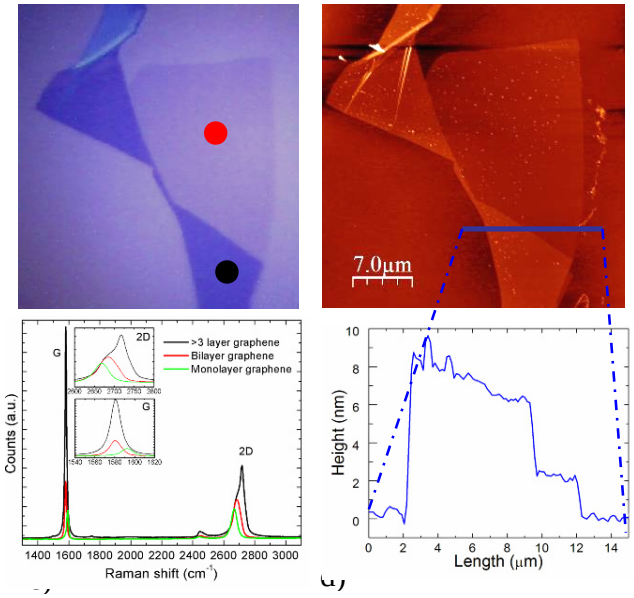


**Figure 2.24. a)** Optical microscope image of bilayer and multilayer graphen flake. **b)** Atomic force microscopy image, in tapping mode. **c)** Raman spectra of mono, bi and multilayer, line red and black in the spectrum correspond to red and black points in a). **d)** outline of the solid blue line over b), the height of the thinnest part of the graphene flake is of 2nm, corresponding to a bilayer graphene, in concordance with the Raman spectra.

Novoselov *et al.* introduced a manual cleaving process of graphite, frequently called "mechanical exfoliation", to obtain SLG and few layer graphene (FLG) (137, 139). This process makes use of adhesive tape to pull graphene films off a graphite crystal. When observed through an optical microscope, SLG and FLG add to the

optical path compared to the bare substrate. If a proper $SiO_2$ thickness is chosen, the resultant visible contrast is sufficient to identify the number of layers (140–143).In the visible range, $SiO_2$ films of ~90 nm and ~300 nm maximise contrast, hence are widely used as substrates. This pragmatic, low-cost method has enabled researchers to conduct a wide variety of fundamental physics and engineering experiments, even though it cannot be considered a process suitable for industrial exploitation (even though approaches for large scale mechanical exfoliation have been proposed). An example of typical exfoliated flake, with a varying number of layers, on an oxidized silicon wafer is shown in Fig. 2.24 a. These layers have a slightly different colour in the optical microscope.

This is one big disadvantage of mechanical exfoliation: it is not possible to get a perfect graphene monolayer, the samples are produced in a mixture of graphite and graphene, not always monolayer. Atomic force microscopy (AFM) and Raman spectroscopy are powerful techniques which allow us to elucidate the quantity of layers(144)(140), image b) shows an AFM image of the same sample, it is possible to have a transversal view, in this case is indicated with a blue line, the transversal cross section is depicted in the figure d), the height of the thinnest zone is approximately 1.8 nm, much more thick than single layer graphene (< 1 nm), with this measure it is possible to assume that this is not a monolayer. A more accurate approach can be given by the 2D Raman peak, (145, 146). The red and black dots represent the measure zone for Raman spectra that can be seen in c), there are two characteristics in this spectra, the shift of the G-band and the shape itself of the 2D band. Figure 2.25 shows the dependence of the 2D band on the number of layers (146). While one layer graphene exhibits a single very intense Lorentzian peak, fitting the bi-layer 2D-band requires four Lorentzians, which are related to the four possible double resonance scattering processes, rather than to one possible process for single layer, resulting from the splitting of the $\pi$ electronic structure of graphene when a second layer is added. With an increase in the number of layers, the number of double resonance scattering processes increases, and eventually the line shape converges to graphite, where only two peaks are observed (146).

The image 2.26 a) shows a graphene flake and some graphene monolayers. To corroborate the monolayer presence a mapping-Raman spectroscopy is used, this process consists in taking Raman spectra of the whole sample, mapping dot by dot (at a distance of ~250 nm a new spectra is taken) and using the proper software (WiRE 3.3, Renishaw) it is possible to deconvolute the spectra and, relate the peak distribution with the layer number (2D band) or the functionalization degree (D-band). Thus this characterization can give information about the level of functionalization or defects, and even more, I am able to know the location where the defects are located in the graphene flake.

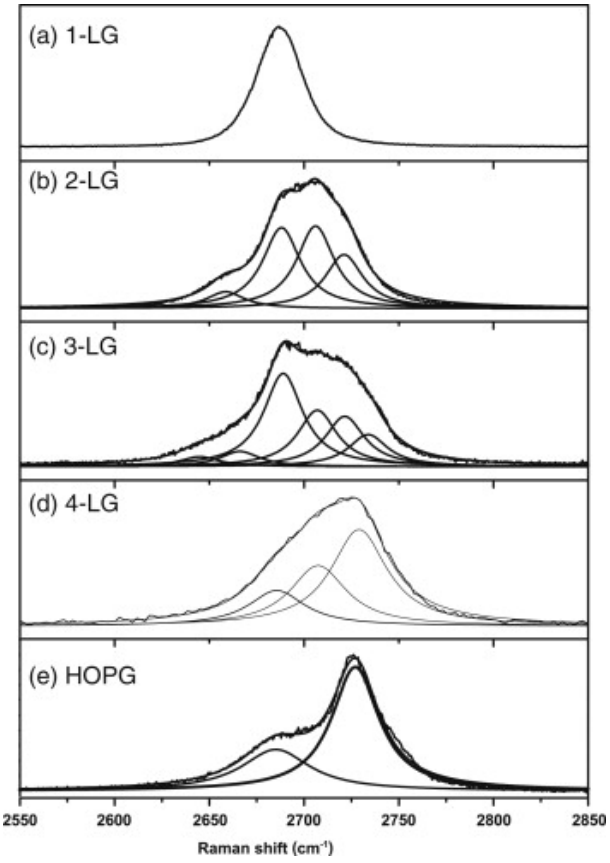


**Figure 2.25.** The measured 2D Raman band with 514 nm laser wavelength for (a) monolayer, (b) bi-layer, (c) 3-layer, (d) 4-layer graphene, (e) High oriented pyrolytic graphite (HOPG) and (f) turbostratic graphite. The splitting of the 2D Raman band opens up in going from mono- to three-layer graphene and then closes up in going from 4-LG to HOPG. Taken from (146)

In this context, making the deconvolution of the D-band I obtained the image 2.26 (b). An intense blue means high level of defects, dark blue or black means absence of defects, or a crystalline surface. As was expected the edges are highly enlighten, meaning high level of defects; in contrast, the graphene surface lacks completely of the $sp^3$ carbon atoms showing a blackish surface.

The mapping colours red and green correspond to the deconvolution of the 2D band, to analyse the number of graphene layers, the deconvolution is compared with the spectra

shown in figure 2.25. in the case of multi- layer, the correspondence was calibrated with the peak position at 2726 $cm^{-1}$ (140, 146), and for the monolayer the correspondence was calibrated at 2680 $cm^{-1}$ according with the characteristic intense Lorenzian peak (140, 146) of single layer and taking in mind the absence of any other Lorenzian, the more accurate the fitting the more the colour intensity.

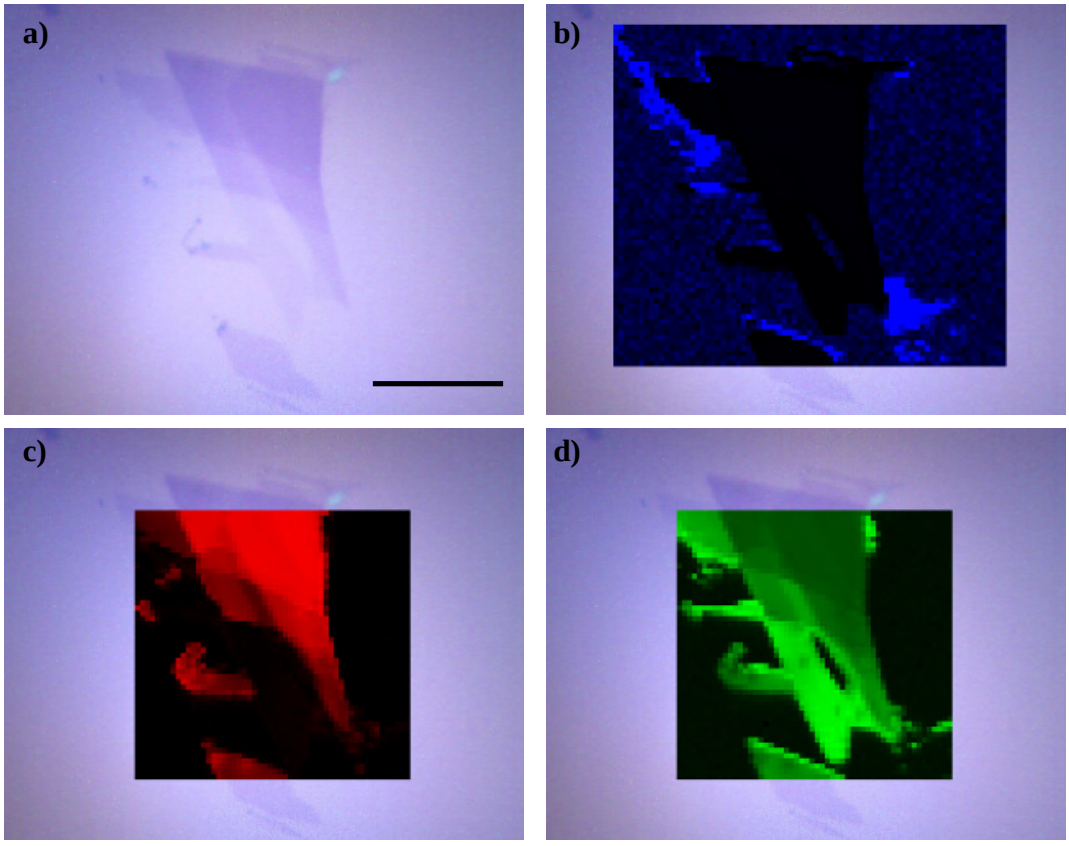


**Figure 2.26.** Optic photograph (a) and Raman mapping of exfoliated graphene. (b - d) Scale bar corresponds to 10µm.

## 2.6 Conclusions

In this chapter I outlined the procedure that I developed for the elimination of impurities and reduction of metallic particles in as-produced SWNTs. Amongst diverse purification procedures, Nitric acid treatment demonstrate to be the most effective one. Indeed, after the purification process, the metal content was below 5 % of total weight, and shows the highest yield. Unfortunately the re-crystallization of the walls was defective, and reduces even more the final quantity of product. There must be a compromise between content of metallic particles and defects level. Indeed, both are counterproductive for electronic devices.

I succeed in the separation of SWNTs by electronic type. The sorting of nanotubes by electronic behaviour gave better results using non covalent methods like DGU. Unfortunately DGU has a very low yield; in contrast the purity of the final material is optimum. I was able to separate both semiconducting and metallic tubes. Additionally I was able to increase the yield, using a different density gradient. In the same way, the sorting of softly oxidized nanotubes were successfully achieved, opening new possibilities for chemistry of nanotubes with single electronic behaviour.

Additionally, graphene was exfoliated in a simple and economic way, the presence of defects and impurities were avoided. I was able to isolate and characterize single layer graphene. This method is a rapid procedure that allows proving essential physical and chemical concepts; the main drawback is that it is not possible to scale up to an industrial production. Graphene is an interesting material in which proof concepts are easier than in carbon nanotubes due to its simpler geometry.

## 2.7 References


(1) Radushkevich, L. V.; Lukyanovich, V. M. *Soviet Journal of Physical Chemistry*. **1952**, 88-99.
(2) Iijima, S. *Nature*. **1991**, *354*, 56-58.
(3) Iijima, S. *Nature*. **1993**, *363*, 603-605.
(4) Bethune, D. S.; Klang, C. H.; Vries, M. S. de; Gorman, G.; Savoy, R.; Vazquez, J.; Beyers, R. *Nature*. **1993**, *363*, 605-607.
(5) Tans, S. J.; Devoret, M. H.; Dai, H.; Thess, A.; Smalley, R. E.; Geerlings, L. J.; Dekker, C. *Nature*. **1997**, *386*, 474-477.
(6) Tans, S. J.; Verschueren, A. R. M.; Dekker, C. *Nature*. **1998**, *672*, 669-672.
(7) White, C. T.; Todorov, T. N. *Nature*. **1998**, *393*, 240-242.
(8) Mann, D.; Javey, A.; Kong, J.; Wang, Q.; Dai, H. *Nano Letters*. **2003**, *3*, 1541-1544.
(9) Martel, R.; Misewich, J.; Tsang, J. C.; Avouris, P. In *Device research confernce, 2004.*; 2004; pp. 198-201.
(10) Javey, A.; Guo, J.; Wang, Q.; Lundstrom, M.; Dai, H. *Nature*. **2003**, *424*, 654-7.
(11) Wong, H.-S. P. *IBM Journal of Research and Development*. **2002**, *46*, 133-168.
(12) Liao, A. D. University of Illinois, 2007.
(13) Wind, S. J.; Appenzeller, J.; Martel, R.; Derycke, V.; Avouris, P. *Applied Physics Letters*. **2002**, *80*, 3817.
(14) Appenzeller, J.; Frank, D. J. *Applied Physics Letters*. **2004**, *84*, 1771.
(15) Javey, A.; Kim, H.; Brink, M.; Wang, Q.; Ural, A.; Guo, J.; McIntyre, P.; McEuen, P.; Lundstrom, M.; Dai, H. *Nature materials*. **2002**, *1*, 241-6.
(16) Martel, R.; Derycke, V.; Appenzeller, J.; Wind, S.; Avouris, P. *Proceedings 2002 Design Automation Conference (IEEE Cat. No.02CH37324)*. 94-98.
(17) Martel, R.; Derycke, V.; Appenzeller, J.; Wind, S.; Avouris, P. *Ieee Spectrum*. **2002**, *10*, 94-98.
(18) Avouris, P. *Accounts of chemical research*. **2002**, *35*, 1026-34.
(19) Rutherglen, C.; Jain, D.; Burke, P. *Nature nanotechnology*. **2009**, *4*, 811-9.
(20) Martel, R.; Wong, H.-sum P.; Chan, K.; Avouris, P. *IEEE International Electron Devices Meeting 2001*. **2001**, *1*, 159-162.
(21) Avouris, P. *Physica B: Condensed Matter*. **2002**, *323*, 6-14.
(22) Alvi, P. A.; Lal, K. M.; Siddiqui, M. J.; Naqvi, A. H. *Indian Journal of Pure & Applied Physics*. **2005**, *43*, 899-904.
(23) Introduction, I. *Engineering Sciences*. **2006**, 99-103.
(24) Goh, R. G. S.; Bell, J. M.; Motta, N.; Ho, P. K.-H.; Waclawik, E. R. *Superlattices and Microstructures*. **2009**, *46*, 347-356.
(25) Wang, Z.; Xu, H.; Zhang, Z.; Wang, S.; Ding, L.; Zeng, Q.; Yang, L.; Pei, T.; Liang, X.; Gao, M.; Peng, L.-M. *Nano letters*. **2010**, *10*, 2024-30.
(26) Srivastava, N.; Banerjee, K. *Proceedings of the 21st International VLSI Multilevel Interconnect Conference (VMIC)*. **2004**, 393-398.
(27) Schwierz, F. *Nature Nanotechnology*. **2010**.
(28) Gnani, E.; Reggiani, S.; Rudan, M.; Baccarani, G. *Solid state devices conference*. **2006**, 170-173.
(29) Strus, M. C.; Chiaramonti, A. N.; Kim, Y. L.; Jung, Y. J.; Keller, R. R. *Nanotechnology*. **2011**, *22*, 265713.
(30) Ando, Y.; Zhao, X. *Carbon*. **2006**, 123-137.
(31) Lu, F.; Meziani, M. J.; Cao, L.; Sun, Y.-P. *Langmuir*. **2011**, *27*, 4339-50.
(32) W., E. T.; Ajayan, P. M. *Nature*. **1992**, *358*, 220-221.
(33) Guo, T.; Nikolaev, P.; Rinzler, A. G.; Tombnek, D.; Colbert, D. T.; Smalley, R. E. *Journal of Physical Chemistry*. **1995**, *99*, 10694-10697.
(34) Rafique, M.; Iqbal, J. *Journal of Encapsulation and Adsorption Sciences*. **2011**, *2011*, 29-34.
(35) Puretzky, A.; Schittenhelm, H.; Fan, X.; Lance, M.; Allard, L.; Geohegan, D. *Physical Review B*. **2002**, *65*, 1-9.
(36) Kataura, H.; Kumazawa, Y.; Maniwa, Y.; Ohtsuka, Y.; Sen, R.; Suzuki, S. *Physical Review B*. **2000**, *38*, 1691-1697.
(37) Yacamán, M. J.; Yoshida, M. M.; Rendón, L.; Santiesteban, J. G. *Applied Physics Letters*. **1993**, *62*, 657-659.

(38) Ermakova, M.; Ermkov, D.; Chuvilin, A.; Kuvshinov, G. *Carbon*. **2001**, *201*, 183-197.
(39) Cassell, A. M.; Raymakers, J. A.; Kong, J.; Dai, H. **1999**, 6484-6492.
(40) Huang, S.; Woodson, M.; Smalley, R.; Liu, J. *Nano*. **2004**.
(41) Sinnott, S. B.; Andrews, R. *Chemical Physics Letters*. **1999**, 25-30.
(42) Brotons, V.; Coq, B.; Planeix, J. M. *Journal of molecular catalysis A:Chemical1*. **1997**, *116*, 397-403.
(43) Thess, A.; Lee, R.; Nikolaev, P.; Dai, H.; Petit, P.; Xu, C.; Lee, Y. H.; Kim, S. G.; Rinzler, A. G.; Colbert, D. T.; Scuseria, G. E.; Tománek, D.; Fischer, J. E.; Smalley, R. E. *Science*. **1996**, *273*, 483-487.
(44) Kitiyanan, B.; Alvarez, W. E.; Harwell, J. H.; Resasco, D. E. *Chemical Physics Letters*. **2000**, 497-503.
(45) Herrera, J. E.; Balzano, L.; Pompeo, F.; Resasco, D. E. *Journal of Nanoscience and Nanotechnology*. **2003**, *3*, 133-138.
(46) Bonaccorso, F. Universita degli studi di Messina, 2006.
(47) Herrera, E.; Resasco, D. E. *Journal of Physical Chemistry B.* **2003**, *107*, 3738-3746.
(48) Rinzler, A. G.; Liu, J.; Dai, H.; Nikolaev, P.; Huffman, C. B.; Rodr, F. J. *Physics*. **1998**, *37*, 29-37.
(49) Hu, H.; Zhao, B.; Itkis, M. E.; Haddon, R. C. *The Journal of Physical Chemistry B.* **2003**, *107*, 13838-13842.
(50) Holzinger, M.; Hirsch, A.; Bernier, P.; Duesberg, G. S.; Burghard, M. *Physics*. **2000**, *602*, 599-602.
(51) Chiang, I. W.; Brinson, B. E.; Smalley, R. E.; Margrave, J. L.; Hauge, R. H. *The Journal of Physical Chemistry B.* **2001**, *105*, 1157-1161.
(52) Liu, J. *Science*. **1998**, *280*, 1253-1256.
(53) Wang, Y.; Gao, L.; Sun, J.; Liu, Y.; Zheng, S.; Kajiura, H.; Li, Y.; Noda, K. *Chemical Physics Letters*. **2006**, *432*, 205-208.
(54) Ziegler, K. J.; Schmidt, D. J.; Rauwald, U.; Shah, K. N.; Flor, E. L.; Hauge, R. H.; Smalley, R. E. *Nano letters*. **2005**, *5*, 2355-9.
(55) Ziegler, K. J.; Gu, Z.; Peng, H.; Flor, E. L.; Hauge, R. H.; Smalley, R. E. *Journal of the American Chemical Society*. **2005**, *127*, 1541-7.
(56) Zhang, J.; Zou, H.; Qing, Q.; Yang, Y.; Li, Q.; Liu, Z.; Guo, X.; Du, Z. *The Journal of Physical Chemistry B.* **2003**, *107*, 3712-3718.
(57) Xu, Y.-Q.; Peng, H.; Hauge, R. H.; Smalley, R. E. *Nano letters*. **2005**, *5*, 163-8.
(58) Vázquez, E.; Georgakilas, V.; Prato, M. *Chemical communications (Cambridge, England)*. **2002**, 2308-9.
(59) Whitsitt, E. A.; Moore, V. C.; Smalley, R. E.; Barron, A. R. *Journal of Materials Chemistry*. **2005**, *15*, 4678.
(60) Gomathi, A.; Vivekchand, S. R. C.; Govindaraj, A.; Rao, C. N. R. *Advanced Materials*. **2005**, *17*, 2757-2761.
(61) Vivekchand, S. R. C.; Jayakanth, R.; Govindaraj, a; Rao, C. N. R. *Small (Weinheim an der Bergstrasse, Germany)*. **2005**, *1*, 920-3.
(62) Moon, J.-M.; An, K. H.; Lee, Y. H.; Park, Y. S.; Bae, D. J.; Park, G.-S. *The Journal of Physical Chemistry B.* **2001**, *105*, 5677-5681.
(63) Georgakilas, V.; Voulgaris, D.; Vázquez, E.; Prato, M.; Guldi, D. M.; Kukovecz, A.; Kuzmany, H. *Journal of the American Chemical Society*. **2002**, *124*, 14318-9.
(64) Bandow, S.; Rao, a. M.; Williams, K. a.; Thess, a.; Smalley, R. E.; Eklund, P. C. *The Journal of Physical Chemistry B.* **1997**, *101*, 8839-8842.
(65) Duesberg, G. S.; Burghard, M.; Muster, J.; Philipp, G.; Roth, S. *Chemical communications (Cambridge, England)*. **1998**, 435-436.
(66) Charlier, J.; Zhu, P. C. E. J.; Ferrari, A. C. *Topics in applied physics*. **2008**, *111*, 673-709.
(67) Huang, H.; Maruyama, R.; Noda, K.; Kajiura, H.; Kadono, K. *The journal of physical chemistry. B.* **2006**, *110*, 7316-20.
(68) Balasubramanian, K.; Burghard, M. *Small (Weinheim an der Bergstrasse, Germany)*. **2005**, *1*, 180-92.
(69) Wang, Y.; Ni, Z.; Yu, T.; Shen, Z. X.; Wang, H.; Wu, Y.; Chen, W.; Thye, A.; Wee, S. *Journal of Physical Chemistry C*. **2008**, *112*, 10637-10640.
(70) Weisman, R. B.; Bachilo, S. M. *Nano Letters*. **2003**, *3*, 1235-1238.
(71) Marayuma, S. *3*, www.photon.t.u-tokyo.ac.jp.

(72) Bonaccorso, F.; Hasan, T.; Tan, P. H.; Sciascia, C.; Privitera, G.; Marco, G. D.; Gucciardi, P. G.; Ferrari, A. C. *Journal of Physical Chemistry C*. **2010**, 88-90.
(73) Baughman, R. H.; Zakhidov, A. a; Heer, W. a de *Science (New York, N.Y.)*. **2002**, *297*, 787-92.
(74) Kataura, H.; Kumazawa, Y.; Maniwa, Y.; Umezu, I.; Suzuki, S.; Ohtsuka, Y.; Achiba, Y. *Synthetic Metals*. **1999**, *103*, 2555-2558.
(75) Girifalco, L. A.; Hodak, M.; Lee, R. S. *Physical Review B*. **2000**, *62*, 13104.
(76) Hasan, T.; Tan, P. H.; Bonaccorso, F.; Rozhin, A. G.; Scardaci, V.; Milne, W. I.; Ferrari, A. C. *Journal of Physical Chemistry C*. **2008**, *112*, 20227-20232.
(77) O'Connell, M. J.; Bachilo, S. M.; Huffman, C. B.; Moore, V. C.; Strano, M. S.; Haroz, E. H.; Rialon, K. L.; Boul, P. J.; Noon, W. H.; Kittrell, C.; Ma, J.; Hauge, R. H.; Weisman, R. B.; Smalley, R. E. *Science (New York, N.Y.)*. **2002**, *297*, 593-6.
(78) Moore, V. C.; Strano, M. S.; Haroz, E. H.; Hauge, R. H.; Smalley, R. E.; Schmidt, J.; Talmon, Y. *Nano Letters*. **2003**, *3*, 1379-1382.
(79) Brakke, M. K. *Arch. Biochem.* **1953**, *45*, 275.
(80) Svedberg, T.; Pedersen, K. O. *The Ultracentrifuge*. **1940**.
(81) Brakke, M. K.; Daly, J. M. *Science*. **1965**, *148*, 387.
(82) Westermeir, R. *Electrophoresis in practice.*; Weinheim, Ed.; 2005th ed.; wiley-VCH, 2005.
(83) Kim, W. J.; Usrey, M. L.; Strano, M. S. *Chemistry of Materials*. **2007**, *19*, 1571.
(84) Landers, J. P. *Handbook of capillary and microchip electrophoresis and associated microtechniques*; Landers, J. P., Ed.; CRC Press: Boca Raton, Fl., 2008.
(85) Ahuja, S.; O'Keefe, D. O. *Handbook of bioseparation*; Ahuja, S., Ed.; Academic Press: San Diego, Ca., 2000.
(86) Strano, M. S.; Dyke, C. a; Usrey, M. L.; Barone, P. W.; Allen, M. J.; Shan, H.; Kittrell, C.; Hauge, R. H.; Tour, J. M.; Smalley, R. E. *Science (New York, N.Y.)*. **2003**, *301*, 1519-22.
(87) Strano, M. S. *Journal of the American Chemical Society*. **2003**, *125*, 16148-53.
(88) Toyoda, S.; Yamaguchi, Y.; Hiwatashi, M.; Tomonari, Y.; Murakami, H.; Nakashima, N. *Chemical asian journal*. **2007**, *2*, 145.
(89) Kim, S. N.; Luo, Z.; Papadimitrakopoulos, F. *Nano letters*. **2005**, *5*, 2500.
(90) Tromp, R. M.; Afzali, a; Freitag, M.; Mitzi, D. B.; Chen, Z. *Nano letters*. **2008**, *8*, 469-72.
(91) Zheng, M.; Jagota, A.; Strano, M. S.; Santos, A. P.; Barone, P.; Chou, S. G.; Diner, B. a; Dresselhaus, M. S.; McLean, R. S.; Onoa, G. B.; Samsonidze, G. G.; Semke, E. D.; Usrey, M.; Walls, D. J. *Science (New York, N.Y.)*. **2003**, *302*, 1545-8.
(92) Hersam, M. C. *Nature nanotechnology*. **2008**, *3*, 387-94.
(93) Heller, D. a; Mayrhofer, R. M.; Baik, S.; Grinkova, Y. V.; Usrey, M. L.; Strano, M. S. *Journal of the American Chemical Society*. **2004**, *126*, 14567-73.
(94) Krupke, R.; Hennrich, F.; Löhneysen, H. V.; Kappes, M. M. *Science (New York, N.Y.)*. **2003**, *301*, 344-7.
(95) Arnold, M. S.; Stupp, S. I.; Hersam, M. C. *Nano letters*. **2005**, *5*, 713-8.
(96) Arnold, M. S.; Green, A. a; Hulvat, J. F.; Stupp, S. I.; Hersam, M. C. *Nature nanotechnology*. **2006**, *1*, 60-5.
(97) Miyata, Y.; Kawai, T.; Miyamoto, Y.; Yanagi, K.; Maniwa, Y.; Kataura, H. *Journal of Physical Chemistry C*. **2007**, *111*, 9671-9677.
(98) Qiu, H.; Maeda, Y.; Akasaka, T. *Journal of the American Chemical Society*. **2009**, *131*, 16529-33.
(99) Miyata, Y.; Maniwa, Y.; Kataura, H. *The journal of physical chemistry. B*. **2006**, *110*, 25-9.
(100) Huang, H.; Maruyama, R.; Noda, K.; Kajiura, H.; Kadono, K. *The journal of physical chemistry. B*. **2006**, *110*, 7316-20.
(101) Collins, P. G.; Arnold, M. S.; Avouris, P. *Science (New York, N.Y.)*. **2001**, *292*, 706-9.
(102) Li, Y.; Mann, D.; Kim, W.; Ural, A.; Hung, A.; Javey, A.; Cao, J.; Wang, D.; Yenilmenz, E.; Wang, Q.; Gibbons, J. E.; Nishi, Y.; Dai, H. *Nano letters*. **2004**, 317.
(103) An, K. H.; Park, J. S.; Yang, C.-M.; Jeong, S. Y.; Lim, S. C.; Kang, C.; Son, J.-H.; Jeong, M. S.; Lee, Y. H. *Journal of the American Chemical Society*. **2005**, *127*, 5196-203.
(104) Banerjee, S.; Hemraj-Benny, T.; Wong, S. S. *Advanced Materials*. **2005**, *17*, 17-29.
(105) Hirsch, A. *Chem. Int. Ed.* **2002**, *41*, 1853.
(106) Strano, M. S.; Dyke, C. a; Usrey, M. L.; Barone, P. W.; Allen, M. J.; Shan, H.; Kittrell, C.; Hauge, R. H.; Tour, J. M.; Smalley, R. E. *Science (New York, N.Y.)*. **2003**, *301*, 1519-22.
(107) Banerjee, S.; Wong, S. S. *Journal of the American Chemical Society*. **2004**, *126*, 2073-81.

(108) Yudasaka, M.; Zhang, M.; Iijima, S. *Chemical Physics Letters*. **2003**, *374*, 132-136.
(109) Lin, Y.; Taylor, S.; Li, H.; Fernando, K. a. S.; Qu, L.; Wang, W.; Gu, L.; Zhou, B.; Sun, Y.-P. *Journal of Materials Chemistry*. **2004**, *14*, 527.
(110) Peng, X.; Komatsu, N.; Bhattacharya, S.; Shimawaki, T.; Aonuma, S.; Kimura, T.; Osuka, A. *Nature nanotechnology*. **2007**, *2*, 361-5.
(111) Nish, A.; Hwang, J.-Y.; Doig, J.; Nicholas, R. J. *Nature nanotechnology*. **2007**, *2*, 640-6.
(112) Chen, F. M.; Wang, B.; Chen, Y.; Li, J. *Nano letters*. **2007**, *7*, 3013.
(113) Tanaka, T.; Jin, H.; Miyata, Y.; Fujii, S.; Suga, H.; Naitoh, Y.; Minari, T.; Miyadera, T.; Tsukagoshi, K.; Kataura, H. *Nano Letters*. **2009**, *2*, 2-5.
(114) Liu, H.; Nishide, D.; Tanaka, T.; Kataura, H. *Nature Communications*. **2011**, *2*, 309.
(115) Tanaka, T.; Urabe, Y.; Nishide, D.; Kataura, H. *Applied Physics Express*. **2009**, *2*, 125002.
(116) Tanaka, T.; Jin, H.; Miyata, Y.; Fujii, S.; Nishide, D.; Kataura, H. *Physica Status Solidi (B)*. **2009**, *246*, 2490-2493.
(117) Liu, H.; Tanaka, T.; Feng, Y.; Kataura, H. *Physica Status Solidi (B)*. **2010**, *247*, 2649-2652.
(118) Tanaka, T.; Urabe, Y.; Nishide, D.; Liu, H.; Asano, S.; Nishiyama, S.; Kataura, H. *Physica Status Solidi (B)*. **2010**, *247*, 2867-2870.
(119) Liu, H.; Tanaka, T.; Kataura, H. *Physica Status Solidi (B)*. **2011**, *248*, 2524-2527.
(120) Tanaka, T.; Liu, H.; Fujii, S.; Kataura, H. *physica status solidi (RRL) - Rapid Research Letters*. **2011**, *5*, 301-306.
(121) Feng, Y.; Miyata, Y.; Matsuishi, K.; Kataura, H. *The Journal of Physical Chemistry C*. **2011**, *115*, 1752-1756.
(122) Sato, Y.; Yanagi, K.; Miyata, Y.; Suenaga, K.; Kataura, H.; Iijima, S. *Nano letters*. **2008**, *8*, 3151-4.
(123) Arnold, K.; Hennrich, F.; Krupke, R.; Lebedkin, S.; Kappes, M. M. *Physica Status Solidi (B)*. **2006**, *243*, 3073-3076.
(124) Graham, J. M. *Biological centrifugation*; BIOS scientific Publisher Limited: Oxford, 2001.
(125) Freifelder, D. J. *Molecular Biology*. **1970**, *54*, 567.
(126) Newel, J. O.; Schachman, H. K. *Biophys. Chem.* **1960**, *37*, 183.
(127) Creeth, J. H.; Pain, R. H. *Prog. Biophys, Mol. Biol.* **1967**, *17*, 217.
(128) Kozinsky, B.; Marzari, N. *Physical Review Letters*. **2006**, *96*, 4.
(129) Chen, Z.; Du, X.; Du, M.-H.; Rancken, C. D.; Cheng, H.-P.; Rinzler, A. G. *Nano Letters*. **2003**, *3*, 1245-1249.
(130) Tu, X.; Manohar, S.; Jagota, A.; Zheng, M. *Nature*. **2009**, *460*, 250-3.
(131) Zheng, M.; Jagota, A.; Semke, E. D.; Diner, B. a; McLean, R. S.; Lustig, S. R.; Richardson, R. E.; Tassi, N. G. *Nature materials*. **2003**, *2*, 338-42.
(132) Zheng, M.; Jagota, A.; Strano, M. S.; Santos, A. P.; Barone, P.; Chou, S. G.; Diner, B. a; Dresselhaus, M. S.; McLean, R. S.; Onoa, G. B.; Samsonidze, G. G.; Semke, E. D.; Usrey, M.; Walls, D. J. *Science (New York, N.Y.)*. **2003**, *302*, 1545-8.
(133) Stillemark, P.; Boren, J.; Andersson, M.; Larsson, T.; Rustaeus, S.; Karlsson, K. A.; Olofsson, S. O. *J. Biol. Chem.* **2000**, *275*, 10506.
(134) Saito, T.; Ohmori, S.; Shukla, B.; Yumura, M.; Iijima, S. *Applied Physics Express*. **2009**, *2*, 095006.
(135) Maruyama, S.; Miyauchi, Y.; Murakami, Y. *New Journal of Physics*. **2003**, *149*.
(136) Bachilo, S. M.; Balzano, L.; Herrera, J. E.; Pompeo, F.; Resasco, D. E.; Weisman, R. B. *Journal of the American Chemical Society*. **2003**, 11186-11187.
(137) Novoselov, K. S.; Jiang, D.; Schedin, F.; Booth, T. J.; Khotkevich, V. V.; Morozov, S. V.; Geim, A. K. *Proceedings of the National Academy of Sciences of the United States of America2*. **2005**, *102*, 10451-10453.
(138) Novoselov, K. S. *Science*. **2010**, *666*.
(139) Novoselov, K. S.; Geim, a K.; Morozov, S. V.; Jiang, D.; Zhang, Y.; Dubonos, S. V.; Grigorieva, I. V.; Firsov, a a *Science (New York, N.Y.)*. **2004**, *306*, 666-9.
(140) Casiraghi, C.; Hartschuh, A.; Lidorikis, E.; Qian, H.; Harutyunyan, A. R.; Gokus, T.; Novoselov, K. S.; Ferrari, A. C. *2Nano Letters*. **2007**, *7*, 2711-2717.
(141) Blake, P.; Castro Neto, A. H.; Novoselov, K. S.; Jiang, D.; Yang, R.; Booth, T. J.; Geim, A. K. *Applied Physics Letters2*. **2007**, *91*, 63124.
(142) Abergel, D. S. L.; A., R.; Fal'ko, V. I. *Applied Physics Letters*. **2007**, *91*, 63125.

(143) Ni, Z. H.; Wang, H. M.; Kasim, J.; Fan, H. M.; Yu, T.; Wu, Y. H.; Feng, Y. P.; X., S. Z. *Nano Letters*. **2007**, *7*, 2758-2763.
(144) Ferrari, a.; Robertson, J. *Physical Review B.* **2001**, *64*, 1-13.
(145) Dresselhaus, M. S.; Jorio, A.; Hofmann, M.; Dresselhaus, G. *Nano letters*. **2010**, *10*, 751-758.
(146) Malard, L. M.; Pimenta, M. a.; Dresselhaus, G.; Dresselhaus, M. S. *Physics Reports*. **2009**, *473*, 51-87.
(147) Bronikowski, M. J.; Willis, P. a.; Colbert, D. T.; Smith, K. a.; Smalley, R. E. *Journal of Vacuum Science & Technology A: Vacuum, Surfaces, and Films*. **2001**, *19*, 1800.

# Chapter 3

# Synthesis of gate dielectric.

## 3.1 Introduction

Field effect transistors (FETs) consist of three main parts: a **channel**, two **electrodes** and a **gate**. The gate is located between the electrodes and controls the electron flow through the channel (Figure 3.1) Metal electrodes, namely source and drain, are deposited on a high doped silicon substrate (1–3). Between the electrode, and above the channel, is located a thin insulator layer of silicon dioxide or hafnium oxide (1–6). This thin layer prevents uncontrolled electrons jumping from channel to gate. The insulator layer is a very important part of device, thus one can consider it as “transistor’s soul”. In the last decades, the FET dimensions have been reduced drastically, the first transistors in a microchip had a channel length of 10 µm

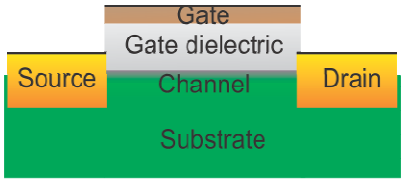


**Figure 3.1**. Schematic representation of silicon based Metal-Oxide–Semiconductor Field-Effect-Transistor (MOSFET) deposited over a silicon substrate

(Intel® 4004 processor, 1971); nowadays the channel length in actual microchips is 32 nm (Intel® Core i3/i5/i7, 2006). This reduction is size introduce some operational problems: the voltage applied must be reduced as well, the threshold voltage has to be reduced as well, as the threshold voltage is reduced the transistor cannot be turned off completely, additionally leakage currents emerge between source and drain electrodes and between channel and gate (7, 8). To continue with electronic device improvement the study of new materials to overcome these problems is mandatory. As was discussed in chapter 1, single-walled carbon nanotubes (SWNTs) has been proposed as a very probable substitute for silicon devices and in the last 12 years, individual SWNTs have been widely used to construct carbon nanotube field effect transistors (CNT-FETs).(9–27). This chapter aim toward innovative synthesis of the insulating layer, which relies on deposition of silica molecules on the surface carbon nanotubes. I pretend to use this insulating coating as dielectric gate, in a CNT-FET, imitating a gate all-around configuration, but constructed using a bottom-up synthesis.

In CNTFET the gate configuration and diverse materials have been the subject of intense studies (10–14, 28–30). The most general configuration consists of silicon-doped substrate as back-gate, in which thermally-grown layer of $SiO_2$ plays role of dielectric gate. Deposition of electrodes requires techniques as microlithography, electron beam lithography or metal evaporation, among others. Finally, above/below the electrodes are located CNT. (11, 12, 31, 32). Other configurations and dielectric materials have also been proposed, for instant bottom-gate tungsten (33), top gate $SiO_2$ (13), bottom gate $Al_2O_3$ (34), top gate $HfO_2$ (35) or $ZrO_2$ (36), among others. These works considerably improved performance of CNT-FET. It is noteworthy to emphasize that all these dielectric materials require using energy-demanding techniques as atomic layer deposition (ALD) or chemical vapour deposition (CVD). Nevertheless, few groups have explored a concept of self-assembly to produce dielectric gate. Self-assembly process relies on using building blocks (e.g. molecules) that spontaneously organize into extended structures (2 or 3D). More properly the study of self-assembled organic-based dielectrics (37) or organic-inorganic bilayers (38) based CNT-FETs have been studied superficially. In this context Weitz et al. studied CNT-FETs using a organic-inorganic

self-assembled monolayer (SAM) (39), obtaining remarkable results. Robert et al. used the same procedure to get a double back-gate transistor using a SAM (40), a similar work was published by Cui et al. (41). It is important to note that the first step in these reports is the functionalization of the substrate, with or without the nanotube placed on it. This is important for us because differs totally from our approach, in which I functionalize the nanotube instead of the substrate. A closer approach to our objective is the nanotube functionalization with organic molecules and using ALD to attach the dielectric layer, Lu et al. used DNA and $HfO_2$ as dielectric (42), Klinke et al. used functionalized nanotubes to link it with $Al_2O_3$ dielectric (43), Borghetti and collaborators functionalized the tube and used a polymer as dielectric (44). There are few reports that exploited functionality of organic chemistry in order to construct or attach a dielectric material on nanotubes (45, 46). There is plenty of room in this subject.

Even more, carbon nanotubes have the most convenient shape for ultimate gate design: a Gate-all around structure. It has been demonstrated that a gate-all around (GAA) configuration in silicon nanowire FET's confers a better trigger control (16–18, 47, 48). Theoretical reports agreed that all-around devices are better in terms of gate electrostatic control (49–53), where this configuration is compared with back and top gate transistors. Some experimental reports demonstrated better performance of CNT-FETs when using a GAA structure. Avouris et al. have used ALD to coat an individual nanotubes with a bilayer of tungsten nitride and $Al_2O_3$ (54). Franklin et al. used a dielectric/metal deposition to surround vertically aligned nanotubes in a predefined template (9). Franklin et al. reported a comparison between a back-gate CNT-FET and a GAA CNT-FET. Figure 3.2 illustrates the variation of screening length from the two device configurations as a function of (1) nanotube diameter ($d_{body}$), (2) gate dielectric thickness ($d_{ox}$), (3) dielectric constant of the gate dielectric material ($\varepsilon_{ox}$), and (4) dielectric constant of the channel material ($\varepsilon_{body}$). The plots show advantages of a GAA configuration, which allows shortening channel length by nearly one order of magnitude than back-gate geometry, while still avoiding short-channel effects (9). In terms of the choice of channel material, the term $\varepsilon_{body}$ plays a minor role while $d_{body}$ strongly affects the screening length for aggressively scaled devices (9). This is an inherent influence of the small $d_{body}$ of

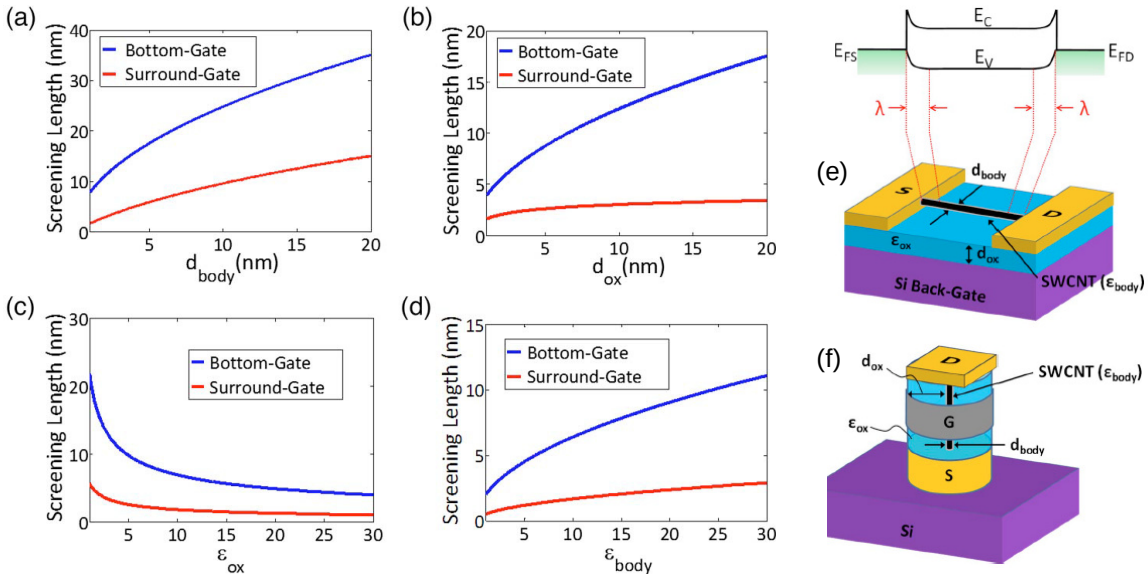


**Figure 3.2.** Plots of the screening length vs (a) channel body thickness (i.e., nanowire or nanotube diameter), (b) gate oxide thickness, (c) gate oxide dielectric constant, and (d) body dielectric constant. (e) Schematic band diagram of a hypothetical CNTFET illustrating the screening length ($\lambda$) in the channel. CNTFET with back-gate configuration and (C) a GAA configuration. Taken from (9)

SWNTs, in contrast to semiconductor nanowires which have diameters typically between 10–100 nm. Another important observation from figure 3.2 is that the oxide thickness has a less significant impact on $\lambda$ in the GAA geometry than in the back-gate configuration. In addition, the benefit to $\lambda$ of using high-$\kappa$ dielectrics in the GAA configuration diminishes as $\varepsilon_{ox}$ rises above approximately 10 (9).

These results demonstrate the superior characteristics of the GAA configuration, making it the ultimate gate configuration for the most aggressive scaling down device. Despite these advantageous characteristics, the GAA configuration have not been further explored because the difficulties on the construction.

Trying to overcome this drawback I proposed to use a **bottom-up synthesis** and growth the dielectric material over the nanotube walls. In this context, several groups have reported the successful coating of carbon nanotubes with different materials, just to mention some. MWNTs have been coated with a thin tin oxide film and was reported for

gas sensing (55–57); MWNTs coated with manganese dioxide for energy storage (58); barium strontium oxide coating of MWNTs for field emitters (59), ZnO coating of SWNTs for piezoelectric applications (60), iron oxide coated MWNTs for arsenic removal for drinking water (61), I can include germanium oxide (62) titanium oxide and $Al_2O_3$ (63–65), and cadmium sulphide or cadmium selenide (46) coatings of MWNTs all of them. More challenging coating of SWNTs with above-mentioned materials is due to thin body, and chemical reactivity of the walls.

The most studied material for nanotubes coating is silica or silicon dioxide ($SiO_2$). Kim and collaborators (45) coated oxidized nanotubes using 2-aminomethyl-3-aminopropyl trimethoxy silane as a linker between nanotubes and the silica layer. Grzelczak et al. achieved compacted silica coating and wormlike hollow structure (66); Lee et al. studied the possibility of coating as-produced and oxidized nanotubes (67), with negative results for pristine tubes;. Colorado and Barron used sodium dodecyl benzene sulfonate (SDBS) to individualize and disperse pristine nanotubes and as silicon source used sodium silicate, achieving coating of small bundles and rugs (68). Following the same approach, Whitsitt et al. (69, 70) have successfully coated individual nanotubes using a liquid phase deposition by means of dodecyl trimethyl ammonium bromide (DTAB) as a surfactant and fluorosilic acid as silicon source. This method required a calibration process of surfactant and silicon source.

### 3.2 Sol-Gel chemistry

Sol-Gel process is able to produce different inorganic networks from silicon monomer precursors. Sol-Gel is a technique able to form glasses from inorganic gels, avoiding the use of high temperature or melting processes (71). Through this process, homogeneous inorganic oxide materials with desirable properties of hardness, optical transparency, chemical durability, tailored porosity, and thermal resistance, can be produced at room temperatures, as opposed to the much higher melting temperatures required in the production of conventional inorganic glasses (71–73). I intend to make use of this process for dielectric, but there are many applications including synthesis of films, optical

coating, reinforcement fibers, fillers, superconductors, windows insulators, catalysis, among others.

The Sol-Gel process involves the development of inorganic networks through the formation of a colloidal suspension (sol) and gelation to form a network in a continuous liquid phase (gel) (74, 75). The precursors for synthesizing these colloids consist of a metal or metalloid element surrounded by various reactive ligands. Metal alkoxides are most used because they react readily with water. The most widely used metal alkoxides are the alkoxysilanes, such as tetramethoxysilane (TMOS) and tetraethyl orthosilane (TEOS)

Two reactions are generally used to describe the sol-gel process: hydrolysis and alcohol or water condensation. This general reaction scheme can be seen in figure 3.3. However, the characteristics and properties of a particular sol-gel inorganic network are related to a number of factors that affect the rate of hydrolysis and condensation reactions, such as, pH, temperature and time of reaction, reagent concentrations, catalyst nature and concentration, H2O/Si molar ratio, aging temperature and time, and drying. (71, 76, 77), where the most important factors are pH, nature and concentration of catalysts, H2O/Si molar ratio and temperature. In this way, by controlling these factors, it is possible to vary the structure and properties of the Sol-Gel-derived inorganic network over wide ranges (77)

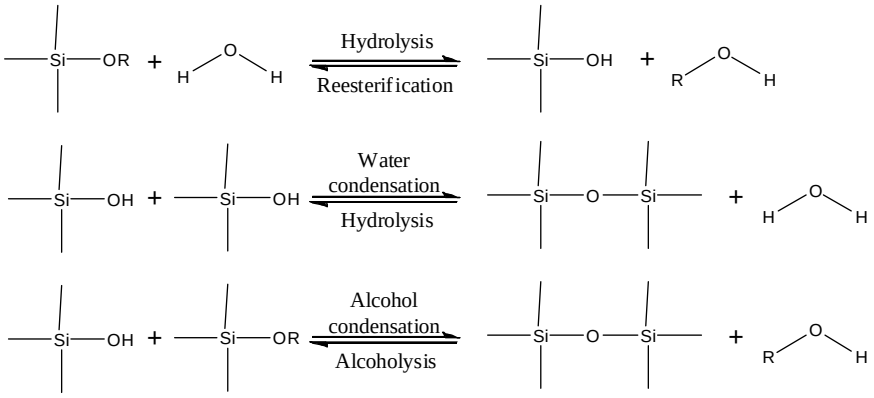


**Figure 3.3**. General scheme of hydrolysis and condensation reactions. The hydrolysis reaction, through the addition of water, replaces OR groups with OH groups. Subsequent condensation reactions involving the Si-OH groups produce Si-O-Si bonds plus the by-products

Commonly, the condensation process begins before hydrolysis is complete. To force the complete hydrolysis before condensation begins it is possible to adjust some conditions like pH and Silicon-water molar ratio (73). Once the colloidal suspension particles aggregate a gel is formed. Drying the residual solvent the network shrinks, anyway, it is important to mention that the addition of solvent may promotes the esterification and de-polymerization according with the reverse equations in the figure 3.3.

Even if hydrolysis can be done without addition of a catalyst, it is faster and complete when they are employed. Mineral acids, like hydrochloric acid, or ammonia are most generally used, however, other catalysts are acetic acid, KOH, amines, KF, and HF (71). Additionally, it has been observed that the rate and extent of the hydrolysis reaction is most influenced by the strength and concentration of the acid or base catalyst, strong acids behave similarly, whereas weaker acids require longer reaction times to achieve the same extent of reaction (78).

Aelion et al. shown that under basic conditions the reaction is more affected by the nature of the solvent (78).

An increased value of water/Silicon molar ratio is expected to promote the hydrolysis reaction. Aelion et al. found the acid-catalyzed hydrolysis of TEOS to be first-order in water concentration; however, they observed an apparent zero-order dependence of the water concentration under basic conditions (78). However, the effect of the increased value of water/Silicon molar ratio is the acceleration of the hydrolysis reaction. Additionally, higher values of water/Silicon molar ratio cause more complete hydrolysis of monomers before significant condensation occurs. Generally, with under-stoichiometric additions of water, the alcohol producing-condensation mechanism is favored (79)

Although increased values of water/Silicon molar ratio generally promote hydrolysis, when this ratio is increased while maintaining a constant solvent: silicate ratio, the silicate concentration is reduced. This causes a reduction of hydrolysis and condensation rates, resulting in longer gel times. This effect is clearer in figure 3.4 which shows gel times for acid-catalyzed TEOS systems as a function of water/Silicon molar ratio and the initial alcohol: TEOS molar ratio (79, 80).

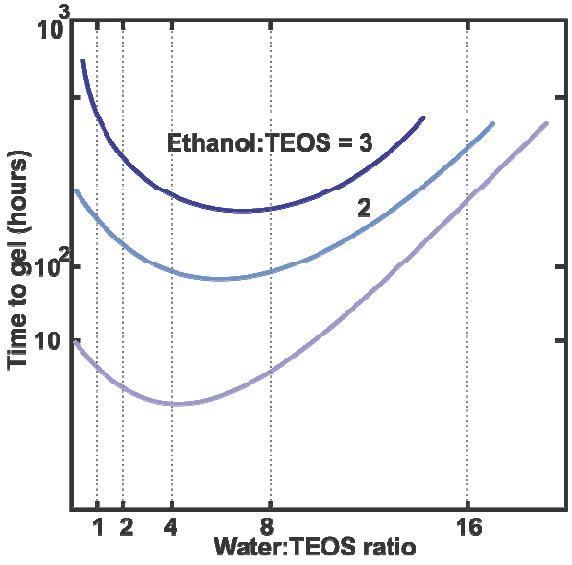


**Figure 3.4.** Time to gel vs. water/TEOS ratio for 3 ratios of EtOH to TEOS. Taken from (79)

In polymerizations below pH 2, the condensation rates are proportional to the [H+] concentration. Because the solubility of silica is quite low below pH 2, formation and aggregation of primary silica particles occur together and ripening (i.e., growth of a network) contributes little to growth after particles exceed 2nm in diameter, see figure 3.5. Thus, developing gel networks are composed of exceedingly small primary particles (71, 80).

It is generally agreed that between pH 2 and pH 6 condensation rates are proportional to [-OH] concentrations. Condensation preferentially occurs between more highly condensed species and those less highly condensed and somewhat neutral. Further growth occurs by addition of lower molecular weight species to more

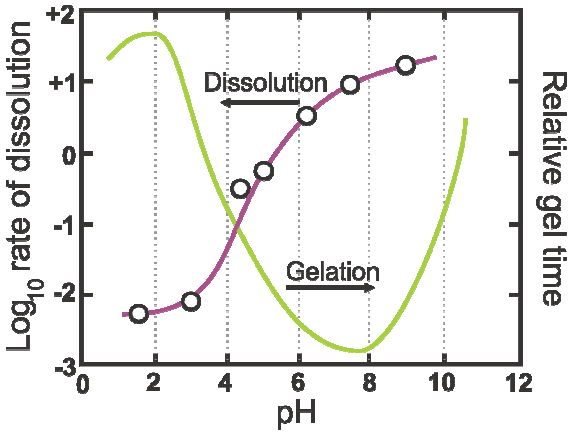


**Figure 3.5.** Dissolution rate and relative gel time as a function of pH. Taken from (71)

highly condensed species and aggregation of the condensed species to form chains and networks. The solubility of silica in this pH range is again low and particle growth stops when the particles reach 2-4 nm in diameter (73, 80).

Above pH 7, polymerization happen the same as in the pH 2 to pH 6 range. However, in this pH range, condensed species are ionized and therefore, mutually repulsive. Growth occurs primarily through the addition of monomers to the more highly condensed particles rather then by particle aggregation. Due to the greater solubility of silica and the greater size dependence of solubility above pH 7, particles grow in size and decrease in number as highly soluble small particles dissolve and re-precipitate on larger, less soluble particles. Growth stops when the difference in solubility between the smallest and largest particles becomes indistinguishable (80).

### 3.2.1 $SiO_X$ coating of SWNTs

There were performed progressive steps in the coating procedure learning and modifying the protocol until a desired coating was achieved. Some of these attempts are described in this sub-chapter.

#### 3.2.1.1 Covalently linked $SiO_X$ layer to SWNTs

As first approach I coated oxidized SWNTs. The oxidation process creates carboxylic acid groups on the nanotube surface (81–88), these carboxylic groups act as anchor points for silanol moieties, through amidation if 3-aminopropyltriethoxysilane (APTES) is used or esterification if TEOS is used. Once the silicon moiety is attached to nanotube surface, the pH of the solution can be reduced to 2 or 3 to promote silica growth. This silanol groups attached to the CNT act as seed points for silica polymerization.

The silica growth over the nanotube condenses and colloids free silanol molecules with the seed molecule, if the pH value is maintained low (~2) spherical silica particles are grown all over the tube, instead if the pH value is increased slowly to 8 the silica condensations growth in the nanotube direction (71, 73, 80). At this point if the

concentration of monomers is still high the coated nanotube starts to coalesce whit other large silica structures without stop until the depletion of free silanol molecules. Thus to achieve a good silica coating, special attention should be focused on silicon molar ratios and pH indices. Figure 3.6 show the expected reaction for coating oxidized nanotubes.

The experimental part is briefly explained, APTES and TEOS were used as silicon sources. HiPco SWNTs where cleaned for 48 hours, using $HNO_3$ as explained in section 2.1.3.4. 0.1 mg of oxidized nanotubes was dispersed in 20 ml of Ethanol:water (EtOH:$H_2O$) [4:1] using a sonic tip for 2 hours in ice bath to avoid evaporation. The pH was set to 8 by means of $NH_4OH$ 0.5 M. 100 µL of APTES were added to the nanotube solution and dispersed in ultrasonic bath. The suspension was centrifuged at 1800 *g* to precipitate the coated nanotubes and wash out the un-attached APTES molecules. The

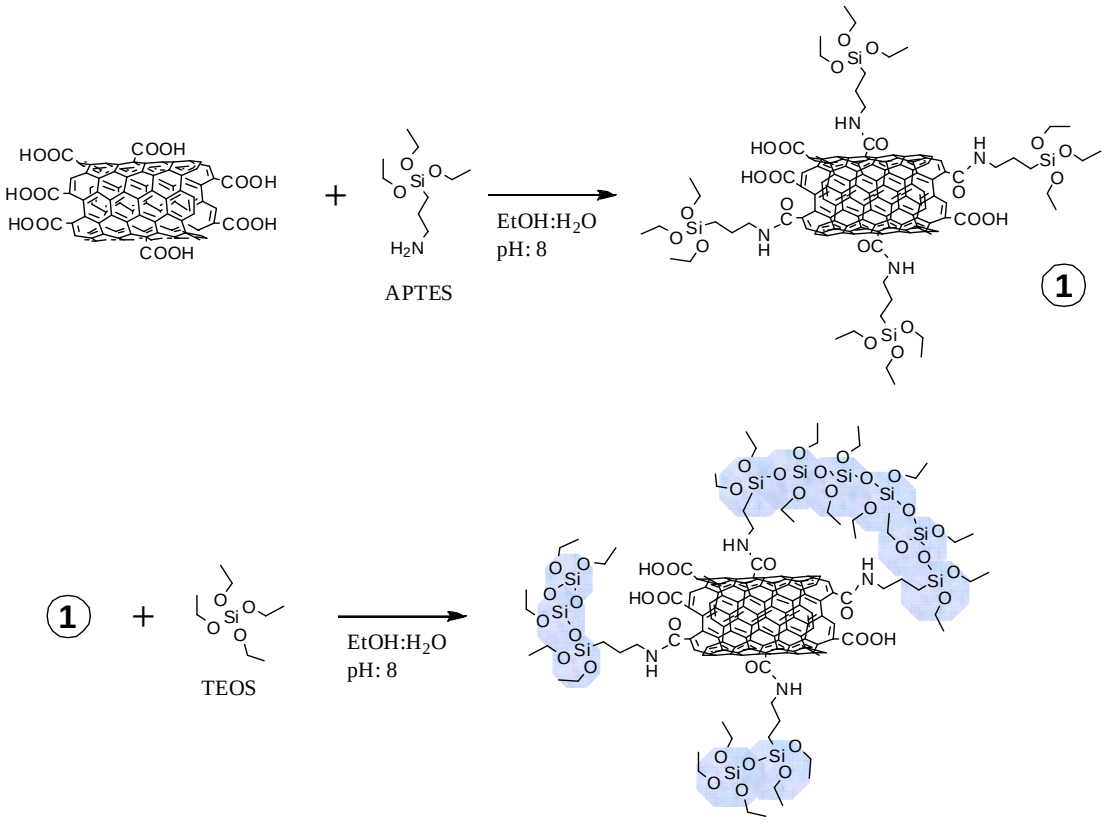


**Figure 3.6** Reaction scheme of coating process for oxidized SWNTs.

precipitate was collected and resuspended in 20 ml of fresh EtOH:$H_2O$ [4:1] using ultrasonic bath. 100 µL of TEOS was dispersed in 5 ml of EtOH:$H_2O$ [4:1] solution, which where added drop wise to nanotube dispersion, always monitoring the pH equal to 8. Finally the solution was filtered avoiding getting dry. The sample was washed several times to remove excess of free monomers, and re-suspended in 5 mL of fresh EtOH.

TEM was performed to observe the morphology of the coating. It is appreciable the presence of silica particles, after the filtering they coalesce making thick bundles or mats together with nanotubes. Despite this, tubular silica shapes are observed, covering completely the nanotube walls, even more, when higher magnifications are analysed it is possible to see a thin and wrinkled surface. Naked nanotubes were not observed.

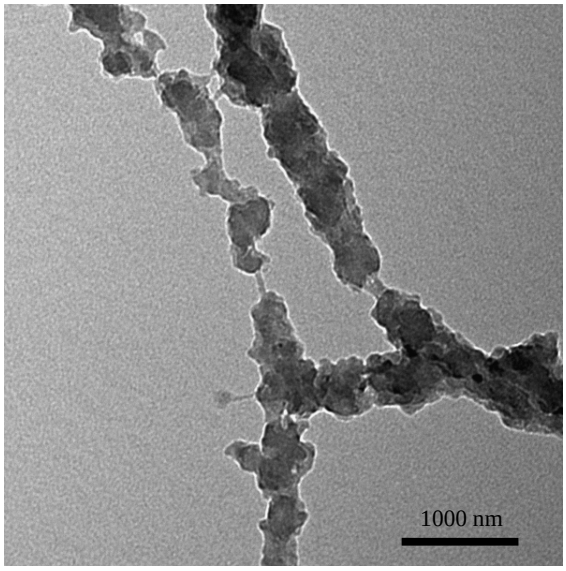


Despite the success and relative easy synthesis, the nanotubes are oxidized and defective, this means that are not ideal for electronic applications. It has been reported that an annealing process can re-crystallize the nanotube surfaces (89–91), but, according with our results the defect removal is not total, as was discussed in the previous chapter. Knowing this, I looked for a new methodology to coat the nanotubes without adding defects.

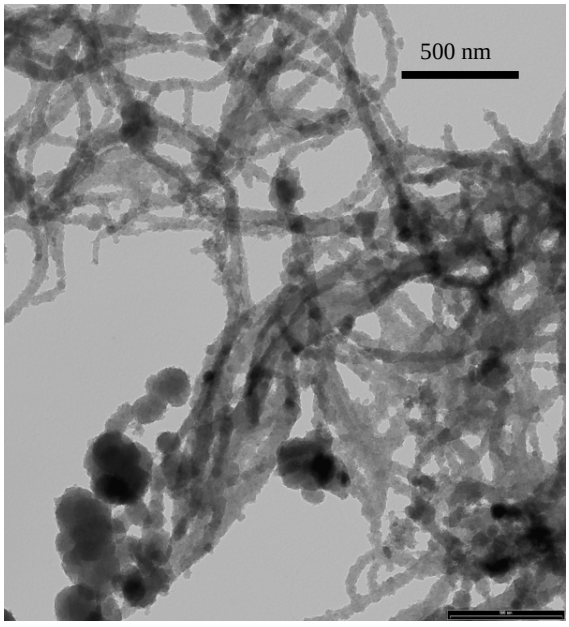


**Figure 3.7.** TEM images of oxidized SWNTs coated with $SiO_X$

The annealing process was performed in a

horizontal oven (thermocouple carbolite® tube furnace (PCT)), at 1000 ºC for 30 minutes, in an inert atmosphere. This process was performed to remove $sp^3$ hybridized carbon atoms and recover the crystalline structure of SWNTs. During the annealing some material was lost, and the removal of $sp^3$ hybridized carbon atoms was not total, may be due to the formation of silicon carbides, as explains Tsetseris et al (92).

#### 3.2.1.2 Non-covalent $SiO_X$ coating of SWNT

The pyrene-nanotube system was selected due to its strong □˜□ interactions (93, 94). It is possible to use attach APTES to the carboxylic tail of Pyrene butyric acid (PBA). Taking advantage of these two characteristics it was possible to link the nanotube surface to a silicon moiety, which can be used as anchor point for further silica growth.

Using an ultrsonicsonic tip was possible to attach PBA molecules to nanotube walls. The procedure is as follows; the PBA was dispersed in 5 ml of Chloroform ($CHCl_3$) in a concentration of 10mM, 2 mg of ultra purified HiPco SWNTs (Carbon Nanotechnologies Incorporated®) were added to 10 ml of DI water. The PBA solution was added to the water nanotube mixture, and the bi-phase solution ultrasonicated for 4 hours in ice bath. The sonic tip evaporates the $CHCl_3$, remaining in aqueous dispersion SWNTs and PBA. The absence of the non-polar solvent, and the hydrophobicity of SWNTs and PBA, produces a re-arrange of PBA over the nanotube surface, in such way that the hydrophilic tale (Butyric acid) of PBA is in contact with water, surrounding the nanotube, as can be seen in figure 3.9 (a).

Fluorescence spectroscopy was performed to corroborate the PBA attachment, figure 3.9 (a) shows the emission response to an excitation wavelength of 242 nm, a red shifting of approximately 6 nm is observed demonstrating the coupling of the system, additionally TGA analysis were performed, as can be observed in figure 3.9 (b) the decomposition curve of purified nanotubes is illustrated in black; PBA-SWNTs curve, in green and just for comparison pyrene acetic acid (PAA) -SWNTs in blue. It is appreciable the decomposition of the PBA molecule at 400 ºC.

For TGA and fluorescence spectroscopy the samples were washed several times to remove the un-attached molecules, despite this, the pyrene moieties remain attached to nanotube walls. In TGA figure 3.9 (b) different weight losses according with the alkyl chain length of PBA and PAA are observed. The in-square shows the decomposition under nitrogen atmosphere of PBA-SWNTs and pristine SWNTs, it is notable the weight differences between curves at ~750 º, this weight difference corresponds to the weight of PBA attached to SWNTs. According with these measurements, pyrene chain can be removed increasing the temperature at 400°C under oxygen atmosphere.

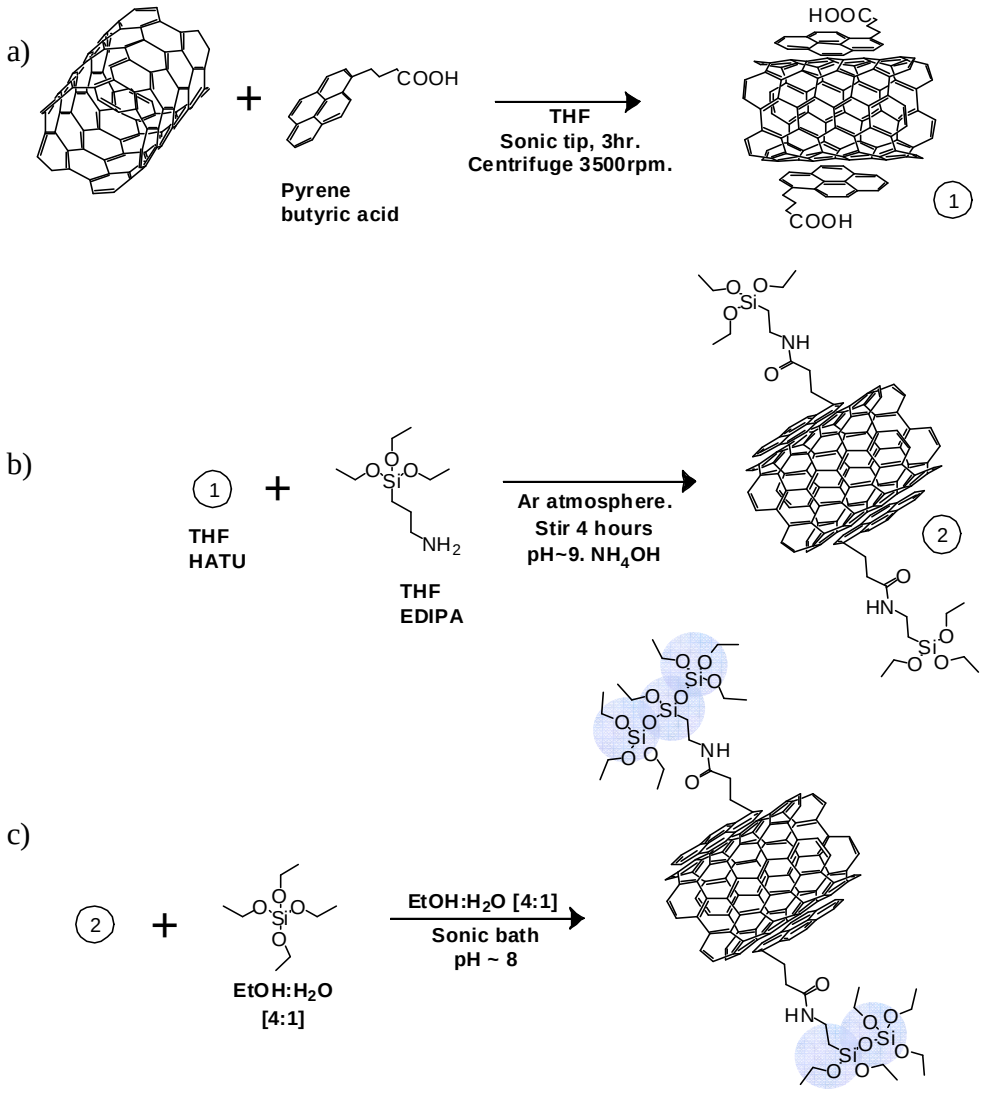


**Figure 3.8**. Non covalent coating of carbon nanotubes, in three steps:1. Attaching pyrenebutyric acid to the surface of NT; 2. Covalent attachment of APTES; and 3. Polymerization of $SiO_x$ adding TEOS.

Once the complex PBA-SWNT is completed, it is possible to follow with coating process, figure 3.8 shows the coating reactions. To accomplish the nucleophilic substitution O-(7-Azabenzotriazol-1-yl)-*N*, *N*, *N'*, *N'*-tetramethyluronium hexafluorophosphate (HATU) and *N*, *N*-Diisopropylathylamine (EDIPA) where used as coupling agents.

2 mg of product (1) of figure 3.8 are dispersed in 20 ml of dry THF solution of HATU (2 mg); additionally 75 µL of APTES are dispersed in 5 ml of dry THF with EDIPA (1.5 mg). APTES concentration was adjusted to represent >2 equivalents of PBA (10 % weight of PBA-SWNT according to TGA). The nanotube dispersion and APTES solution are mixed together and hardly stirred for 4 hours under inert atmospheres and the pH value is adjusted to ~9 using ammonium hydroxide ($NH_4OH$).

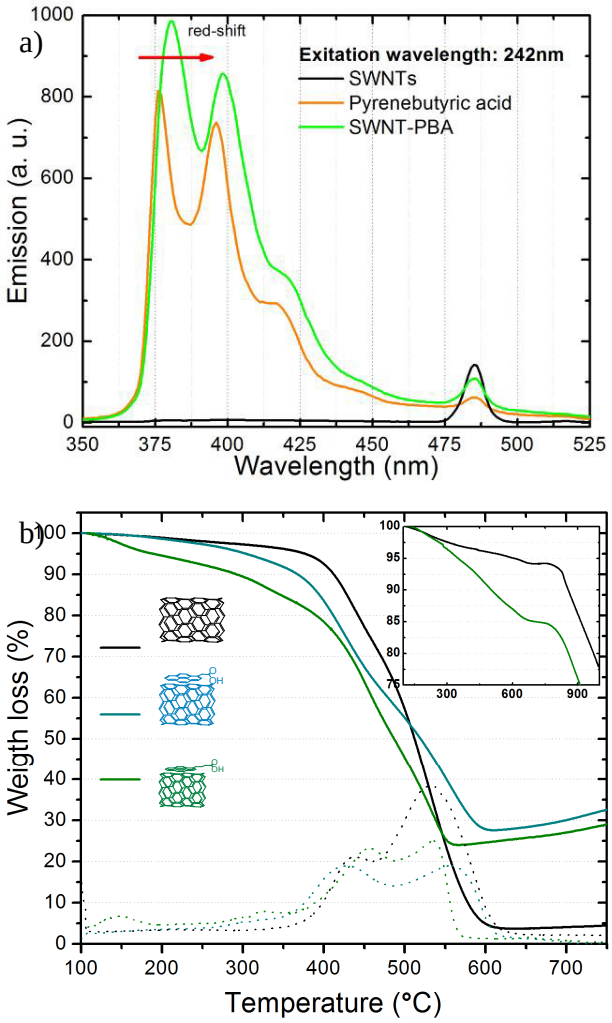


**Figure 3.9.** a) Fluorescence emission of PBA, HiPco SWNT & PBA-SWNT complex, taken at 242 nm exitation wavelength. b) TGA curves of SWNT (black), and SWNT -Pyrene acetic acid (blue) & PBA-SWNTs, dotted lines are derivative of the weight loss, in-square of the samples in nitrogen atmosphere

The suspension was centrifuged (16 000 *g* for 4 hours), the supernatant discarded and precipitate dispersed in 20 ml of EtOH:$H_2O$ [4:1] solution. Consecutively, 100 µL of TEOS dissolved in 5 mL of EtOH:$H_2O$ [4:1] were added drop wise, (fig. 3.8 (c)). The solution was sporadically sonicated to avoid aggregation.

Finally the product was filtered, through 100 µm Millipore filter, avoiding to dry the sample. The filtered product is washed with 20 ml of EtOH: $H_2O$ [4:1] at pH 9. Finally the sample was resuspended in fresh EtOH. TEM images were taken to corroborate the coating. The images show a poor coating of SWNTs; it is observed mainly thick bundles of SWNT, some of them coated with silica. Figure 3.10.

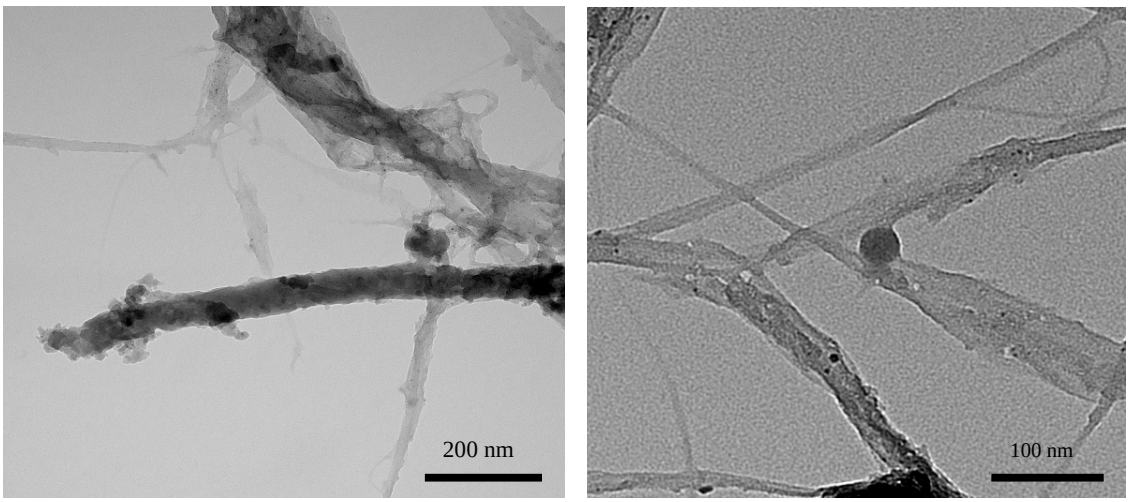


**Figure 3.10.** TEM images of attempt of coating SWNTs using a non.covalent approach with APTES-PBA-SWNTs.

I change some variables, trying to optimise this result, ultrasonication times were modified; different solvent were tested as well. The result was not improved.

Changing a bit the focus of the problem, I thought that synthesising first the Pyrene-Silanol molecule, and then attaching it to SWNT it could be possible to achieve the coating. So, I synthesize the molecule shown in figure 3.11 and tested the coating as in the previous experiment. Again the result was a partial coating of bundled SWNTs.

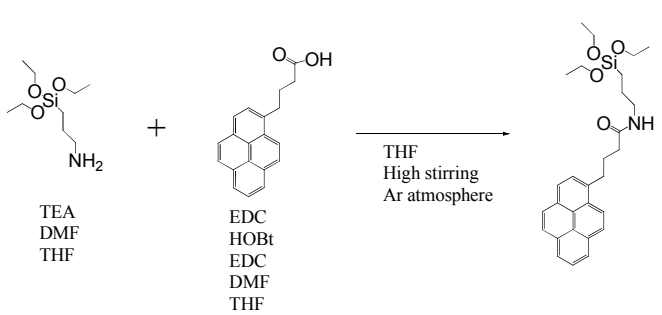


**Figure 3.11.** Schematic reaction for the synthesis of aromatic-silane moiety.

Apparently the ultrasonication of pyrene and nanotubes is not enough to break and disperse the bundles.

I moved to a different approach in order to get a better dispersability and still avoid the damaging of nanotubes. The use of a surfactant is a good option as Barron et al. have done. I have tested anionic, cationic and neutral surfactants to disperse the tubes and use the surfactant it self as nucleation point for silica growth. The idea is to take advantage of the hydrophobic part of the surfactant, attracting it to the hydrophobic nanotube surface, in this way the surfactant hydrophilic tale can be used to attach a silicon molecule. The surfactant should have the following characteristics:

1. Compatible with the inert surface of the nanotube, an aromatic head or long alkyl chain should be ideal,
2. Able to render individual nanotubes or small bundles dispersible in EtOH- $H_2O$ solution,
3. Stable at diverse pH values, to prevent the detachment while the silica is growing,
4. Additionally, it should be able to attach a silicon oxide moiety, an amine, hydroxyl or carboxyl group at the end of hydrophilic tale is ideal.

Therefore, I examinee the performance of 6 different surfactants for coat individual HiPco nanotubes, four linear chain surfactant are considered, in which 2 are anionic (SDS and SDBS), 2 are cationic (Cetyl trimethylammonium bromide (CTAB) and dodecyl trimethyl ammonium bromide (DTAB)), additionally a non-ionic copolymer (Triton x-100) and a bile salt (SC) are tested. All chemical structures are schematized in the table 3.1.

The surfactants are prepared in an EtOH solution (EtOH: $H_2O$ [4:1]) to disperse SWNTs and then proceed with the coating. 0.5 mg of HiPco SWNTs are dispersed in 100 of ml EtOH: $H_2O$ solution [4:1] with 2 mg of surfactant. The solution was dispersed using a sonic tip, with a duty cycle 50 % for 3 hours. Afterwards, large bundles and indispersible material are precipitated and discarded via ultracentrifugation at 11 200 *g* for 2 hours, the

supernatant are individual and small bundles of SWNTs covered with surfactant, figure 3.12 (a). The supernatant is collected and used for silica growth.

**Table 3.1.** Synthesis of coating using a variety of surfactants.

| Surfactant | Characteristics | TEM |
|---|---|---|
| SDBS | Sodium Dodecylbenzenesulfonate<br>M.W.: 348.48 g/mol<br>Type: anionic<br>Structure:<br> 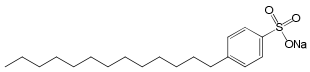 | 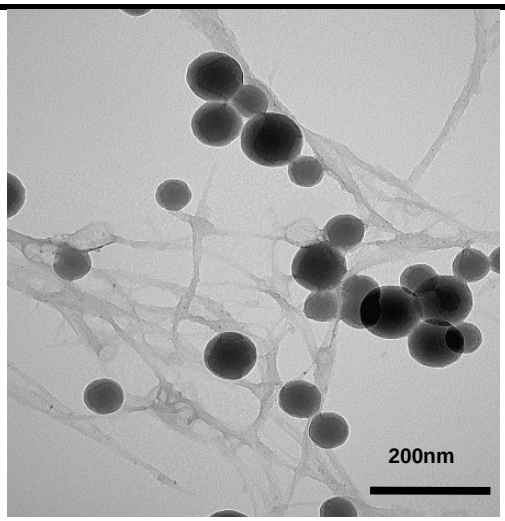 |
| SDS | Sodium dodecyl sulphate<br>M.W.: 288.38 g/mol<br>Type: anionic<br>Structure:<br> 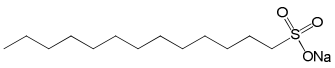 | 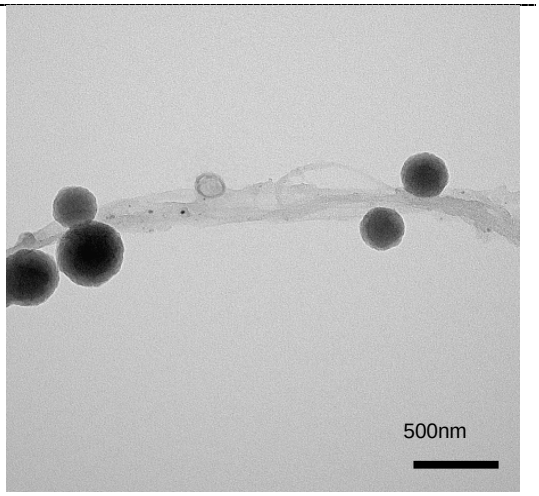 |

DTAB

Dodecyltrimethylammoium bromide

M.W.: 308.3 g/mol

Type: cationic

Structure:

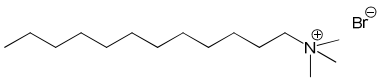


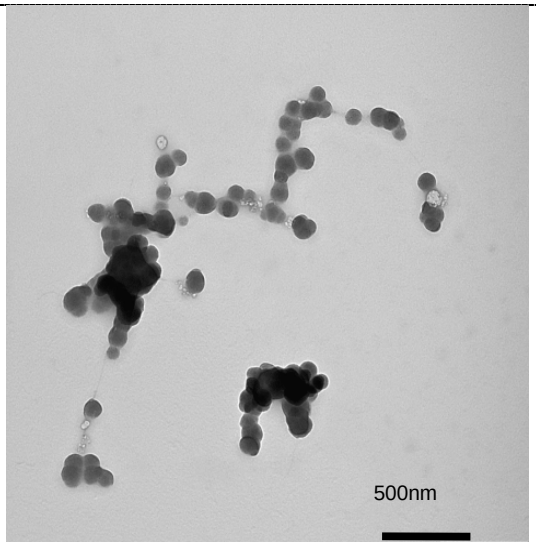


CTAB

Cetyl trimethylammonium bromide

M.W.: 364.45 g/mol

Type: cationic

Structure:

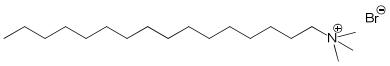


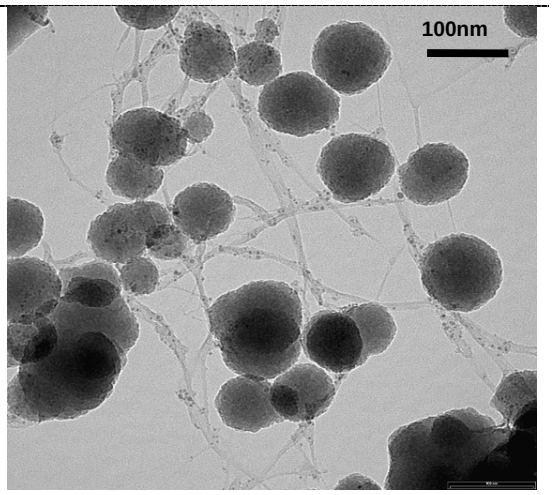


Triton x-100

M.W.: 625 g/mol (average)

Type: anionic

Structure:

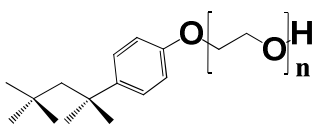


n = 9-10

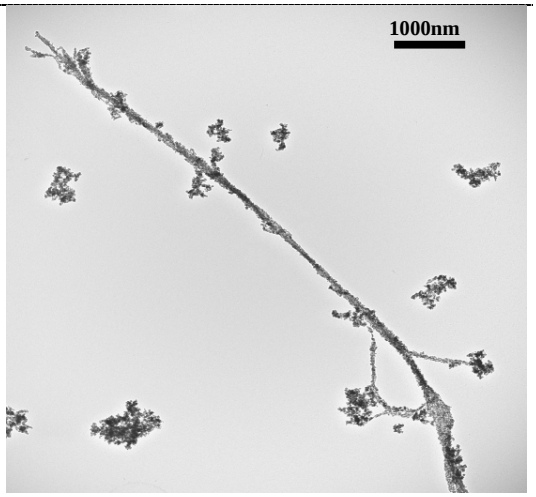

Sodium Cholate

M.W.:430.55 g/mol

Type: anionic

Structure:

SC

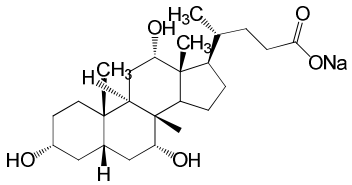


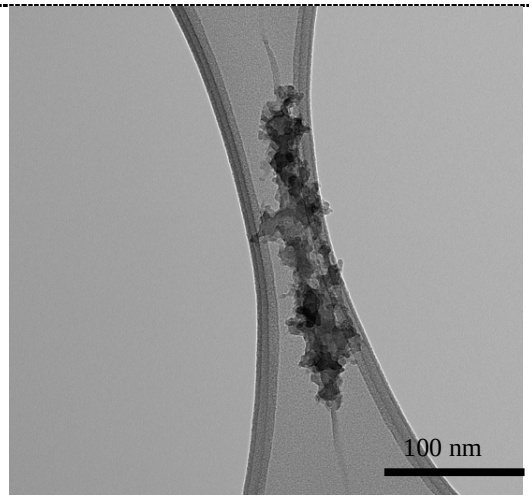


5 ml TEOS solution is prepared, consisting in 4ml EtOH, 1 ml water and 0.1 ml TEOS, fig. 3.12 (b).The centrifuged suspension of covered SWNTs is ultrasonicated; the pH is adjusted to ~2 with diluted HCl. Then TEOS solution is added drop wise, at the same time the pH is increased slowly whit diluted $NH_4OH$ until pH 8 – 9. The solution is let it react for 12 hours. Sporadical sonication is done to avoid aggregation, fig. 3.12 (c). Finally the nanotubes are filtered preventing to get dry, and are resuspended in fresh EtOH. Table 3.1 summarizes the surfactants used, their characteristics, and TEM images for each process.

The best coating was achieved using Triton x-100 and SC. Additional experiments demonstrate that varying slightly the concentration of TEOS it is possible to tune the $SiO_X$ thickness. The figure 3.13 (e) shows how the thickness is controlled adjusting the molar concentration of TEOS, while the EtOH: $H_2O$ ratio remains unchanged.

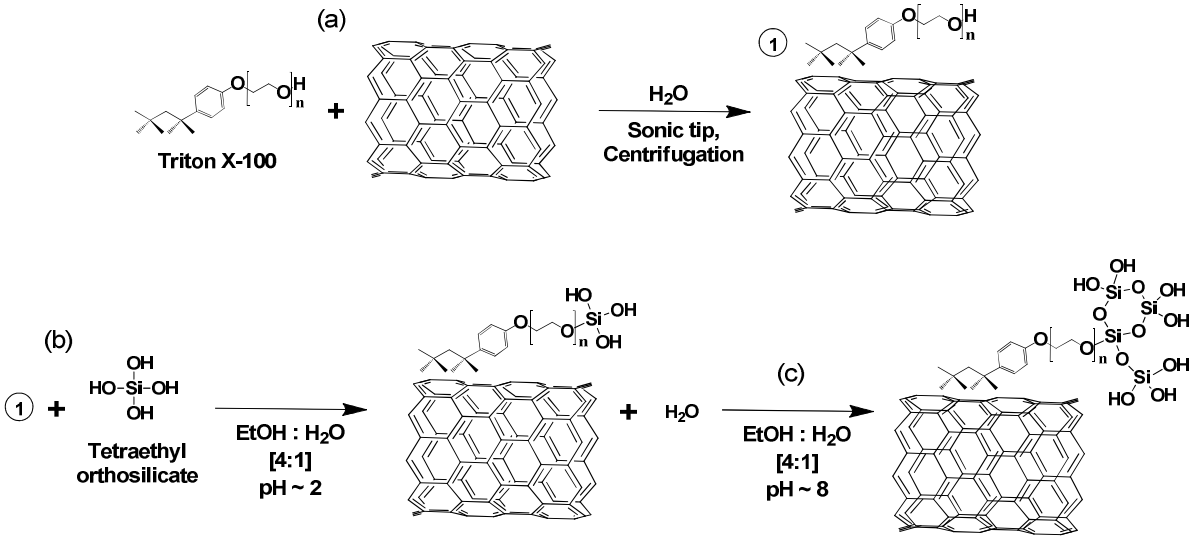


**Figure 3.12.** Coating process of SWNTs using Triton x-100.

Additionally, TEM images illustrate the coating dimensions (fig. 3.13 (a), (b) and (d)). If TEOS concentration is increased even more, the formation of silica spheres are promoted, moreover, the coalescence between coated tubes is increased considerably (c).

In order to have continuity in the fabrication process of the transistor, it is necessary to take advantage of the conditions given in the previous step, the sorting by electronic behaviour or single chirality, done by DGU. As it was explained in the previous chapter, DGU process is performed in the presence of 3 substances, SDS, SC & the density medium. The semiconducting enriched sample was performed using a surfactant mixture of SC: SDS [4:1], this mixture is favourable for the surfactant-silica coating. Instead, metallic enriched sample was obtained with SC: SDS [1:4], a non favourable condition in our coating procedure due to higher presence of SDS, as can be seen in the table 3.1. Figure 3.14 shows the coating process using the nanotubes coated immediately after DGU. The excess of surfactants and the presence of iodixanol promote the formation of silica spheres, which grow consuming the TEOS molecules in solution. To avoid this, it is necessary a centrifugation in pure EtOH (18 000 *g*), and resuspension in fresh EtOH: water solution using a sonic tip, this step removes the excess of surfactants but it is

promoted the formatrion of small bundles. The silica growth is performed as explained lines above.

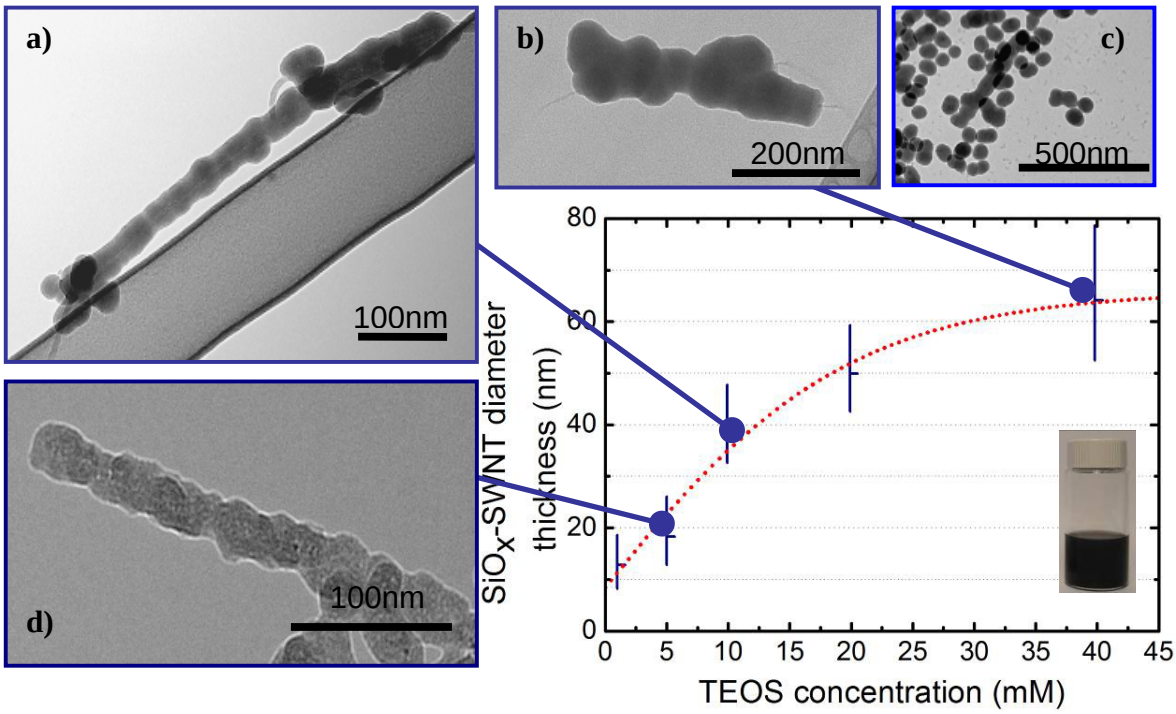


**Figure 3.13.** (a-d) TEM images with diverse $SiO_X$ coating diameters just changing the TEOS concentration, (e) curve traced taking measurements on TEM images. The vial is a sample of nanotubes coated with silica.

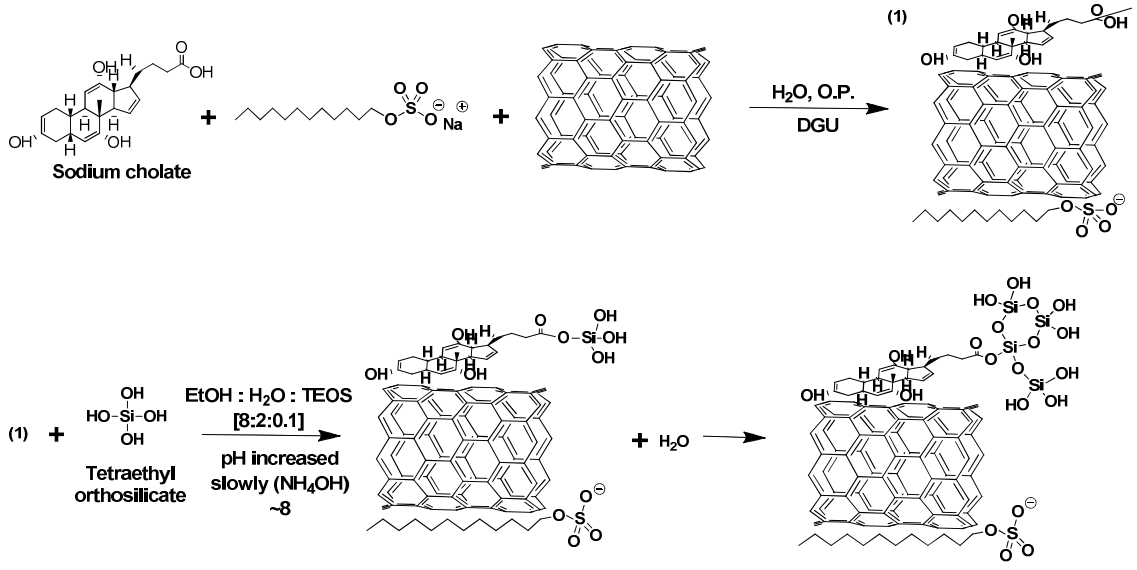


**Figure 3.14**. Non covalent attachment of silica coating over nanotubes surface, of sorted nanotubes by DGU, in a surfactant mixture of SC:SDS [4:1].

### 3.2.1.3 Measuring the dielectric quality

The dielectric quality can be measured as a function of leakage current. Leakage is a phenomenon in semiconductor physics where electrons or holes are able to cross through an insulator, this phenomenon increases exponentially as the thickness of the insulator decreases. In transistors the leakage current produce an increase in power consumption, if this current rises enough the transistor may be destroyed. Leakage current is one of the main factors that limit the progressive shrinking and improvement in the microprocessors.

Ideally to test the dielectric properties for the $SiO_X$ coating it is necessary an individual coated nanotube placed on a highly doped silicon substrate, and a thin $SiO_2$ layer thermally growth on the surface of the substrate, metallic electrodes are deposited over the nanotube naked tips via electron beam lithography, and finally the gate electrode, located in between the previous electrodes and over the coated nanotube. For time reasons I use a general approach in order to have a more general view of the sample.

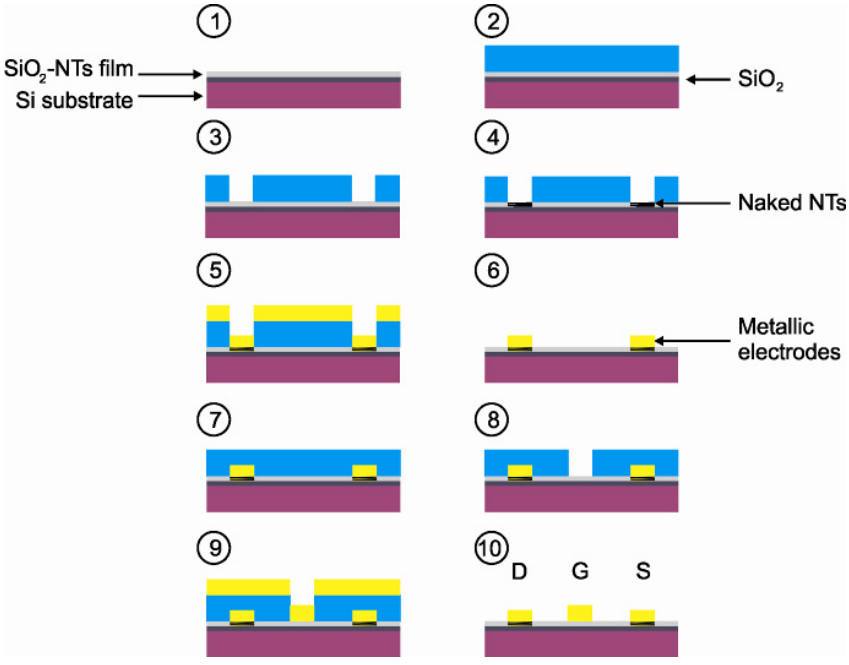


**Figure 3.15.** Schematic representation of the process, step by step, to construct a "like" thin film transistor, using semiconducting SWNTs coated with $SiO_X$

100 ml of $SiO_X$-NTs solution were drop casted over the $SiO_2$ substrate, as is illustrated in the figure 3.15 (1). The blue layer in (2) is a thin film of Poly(methyl methacrylate) (PMMA) spin coated over the $SiO_X$-NTs film. This polymer can be modified with UV light or high energy electrons, so, it is possible to selectively remove small areas of polymer with extraordinary precision. In this context, the electrodes zones are defined burning the PMMA using electron beam lithography, the burned PMMA is removed with isopropyl alcohol (IPA): $H_2O$ [4:1]. This removal lets exposed small zones of $SiO_X$-NTs (3); step (4) shows the removal of silica from nanotubes using hydrofluoric acid. The electrodes are deposited via metal evaporation (5). PMMA is removed washing the substrate with pure IPA (6). For the gate electrode deposition the sample is again coated with PMMA (7) and the new strip is drawn between the previous deposited electrodes, once again PMMA is burned and removed using IPA:$H_2O$ solution (8), and finally the metal is deposited again (9), the metal and PMMA excess is removed together with PMMA with pure IPA. The final structure is a complete field effect transistor, using coated semiconducting SWNTs as channel (10).

I developed different electrode patterns in order to determine the quality of the silica coating, through the measurement of the leakage current.

Unfortunately the deposited $SiO_X$-NT layer was not able to contact 2 electrodes. Trying use the same approach the concentration of the deposited layer was increased 10 times hoping to contact at least one device, the result was again the same: no devices contacted among electrodes. It is necessary to change the methodology fabrication of the device.

### 3.3 Growth of $SiO_X$ thin film over graphene for electronic applications

For a top-gate graphene transistor, the fabrication process is large and tricky; this is due to the difficulties to locate and deposit electrodes, then deposit the dielectric material, and finally deposit more electrodes to finish the device, the precision must be very accurately, and mistakes occurs often (95–101).

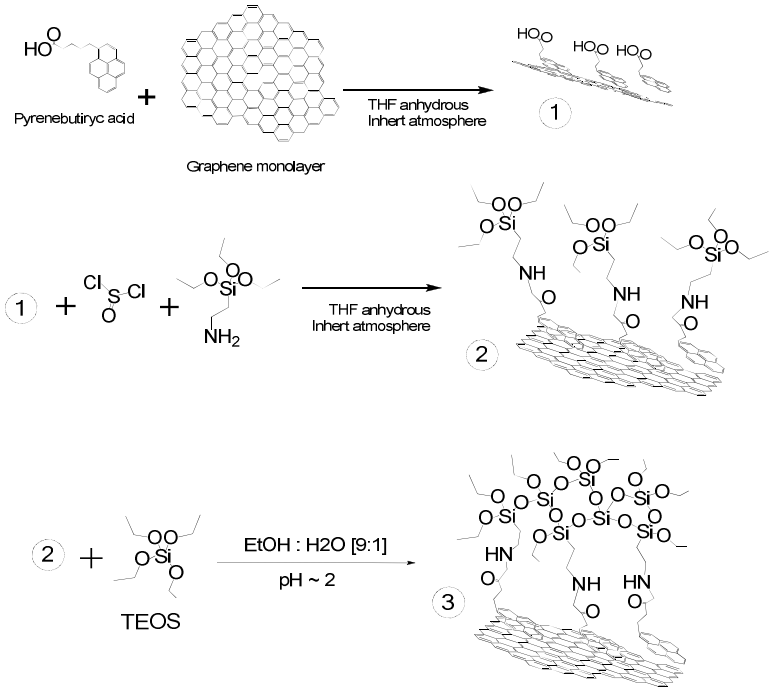


**Image 3.16** $SiO_X$ thin film growth over graphene flakes, using a non-covalent procedure.

Our proposal is to chemically growth (using a bottom-up approach) the electrodes, and/or dielectric material, in order to reduce the fabrication steps and consuming time. Using this approach the fabrication process might be much easier and, possibly, commercial applications could start to be visualized seriously.

My approach is as follows, to use PBA to take advantage of $\pi - \pi$ stacking. The carboxylic acid group of the PBA will act as anchor point for APTES, and promote the $SiO_X$ growth on graphene surface, as is explained in the figure 3.16. In theory the silica will growth selectively over the graphene or graphite. This silica layer is the dielectric gate. The dielectric must prevent tunnelling through the metallic gate electrode and the semiconducting channel, in this case, the graphene monolayer. For this reason the layer must lack of cracks and holes.

Different pH values were tested to study the quality of the thin film. Figure 3.17 show morphological differences among silica thin films at diverse pH values using bright and dark field microscopy.

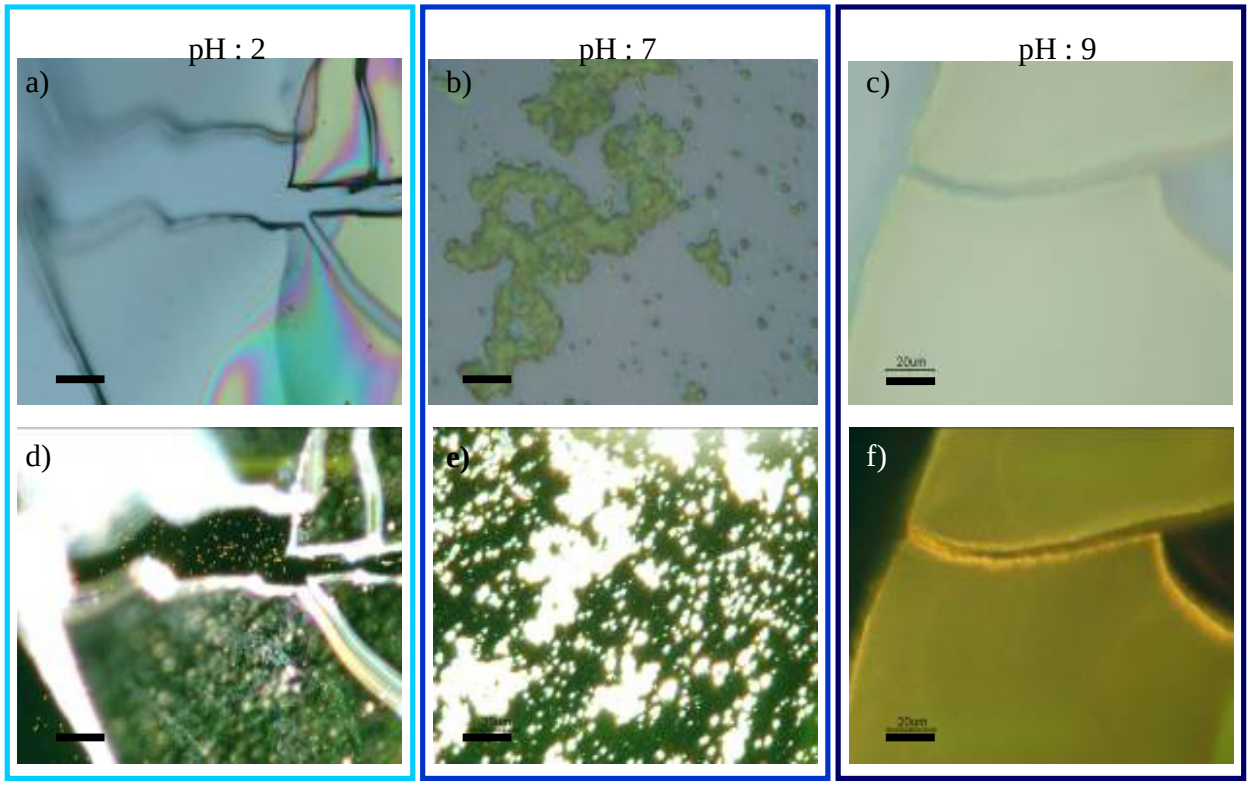


**Figure 3.17**. Optical microscope dark and bright filed images for silica synthesized by sol-gel processes at different regimens, growth over $SiO_X$ substrate. All scale bars represents 20µm.

When a low pH is used the layer becomes homogeneous as can be seen in the bright field picture (a), some particles can be seen on the surface of the silica layer in the dark field (d), probably this dots are holes in the film. When the pH is increased to neutral value the silica takes spherical shape, useless for our purposes (b) and (e). Increasing the pH at 9, porous films are formed (c), in dark field is appreciable the scattered light all over the film, the scattering is produced by small holes (f), making it, as well, useless for our applications.

The fabrication process for the graphene-silica device is schematized in figure 3.18. Briefly, the graphene exfoliation was explained in the section 2.2.Once a monolayer

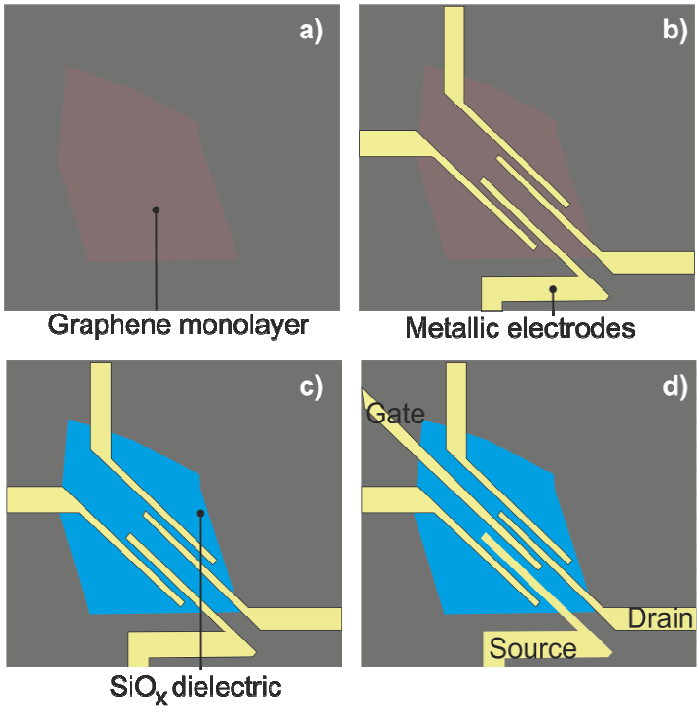


**Figure 3.18.** Schematic representation of device construction, step by step. a) monolayer graphene over Si substrate; b) deposition of metal electrodes, c) synthesis of dielectric material, and finally, d) deposition of gate metallic electrode.

graphene is localized on the substrate (a), four electrodes are deposited over the graphene (b), to take 4 probe measurements. The deposition of electrodes is performed in the same way as for nanotubes. The dielectric material is growth following the figure 3.16. The graphene-on-substrate (GoS) is immersed in a solution 10 mL dry THF with PBA 10mM, the GoS is let it un repose for 20 min, then the THF is replaced with 10 mL of fresh THF, this step is repeated 3 times. The final washing at THF is added 100 µL of APTES and 100 µL of thionil chloride ($SOCl_2$). This reaction catalyzes the amidation (fig. 3.17 (2)). Again, the THF-APTES-$SOCl_2$ solution is replaced by dry THF, to remove the excess of reagents; this washing process is repeated twice, two final washes are done with EtOH: $H_2O$ solution [9:1]. The pH is adjusted to 2 using HCl 0.1M. Finally, 100 µL of TEOS of is added to complete the crystallization (fig. 3.17 (3)). The GoS is let it react over night. Then the GoS is washed with EtOH: $H_2O$ [9:1] and let it dry. The coating should be seen as in figure 3.18 (c).

At last, metal gate electrode is deposited (d) in the same way using PMMA and e-beam lithography, fig. 3.18 (d).

The figure 3.19 shows the first two of those steps experimentally. To monitor any change in doping or damages on the graphene sheet Raman analysis were done.

Figure 3.19 (a) graphene monolayer is identified by optical microscope, and metal electrodes are deposited over the graphene flake (b).

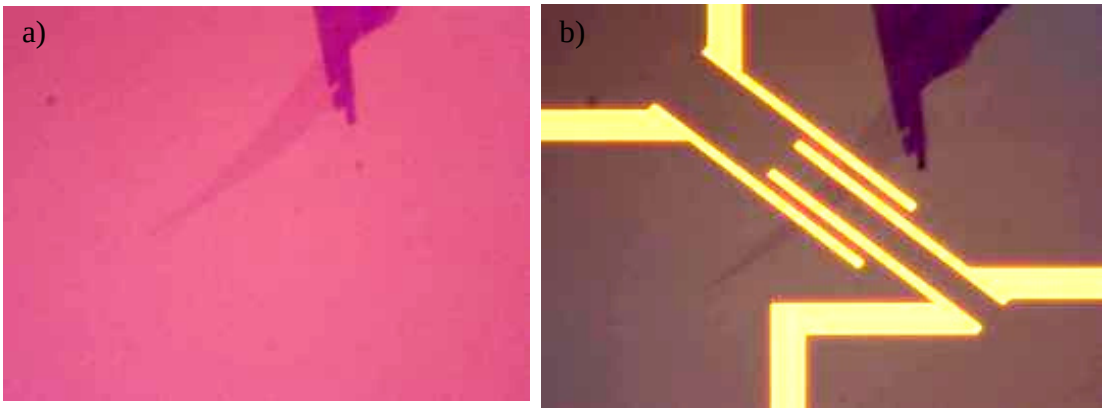


**Figure 3.20.** Optic microscope images of single layer graphene (a), and deposited electrodes over graphene (b). Scale bar is 100µm.

Four-point probes method is an impedance measuring technique that uses separate pairs of current and voltage electrodes to make more accurate the measurements compared with two points measurement. Four-probe analysis is traditionally used to measure sheet resistance of thin films. The advantage four-probe measurement over two probe is the separation of current and voltage electrodes eliminates the impedance contribution of the wiring and contact resistances.

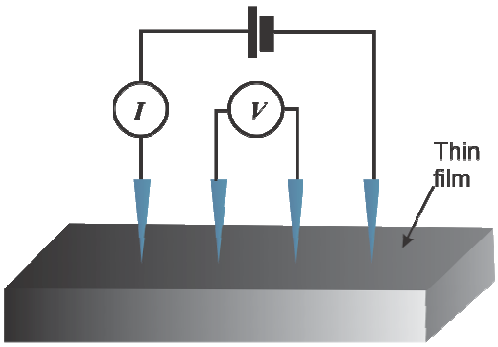


**Figure 3.20.** Schematic diagram of test circuit for measuring thin film sample with a four-probe method

When a four-probe connection is used, a current is applied through a pair of “force” connections (a couple of wires that supply the electron current). These generate a voltage drop across the impedance to be measured according to Ohm's law $V = RI$. This current causes a voltage drop through the force wires themselves. To prevent the measurement of

such voltage drop, a pair of "sense" connections (voltage leads) are located directly adjoining to the target impedance, a schematic diagram of this arrange can be seen in figure 3.20. The accuracy of the technique comes from the fact that almost no current flows in the sense wires, so the voltage drop *V=RI* is extremely low.

The sheet resistance of graphene was 400Ω·□ in average, this measurement was taken on 5 devices. The green slashed line in the figure 3.21 is the measurement of the sheet resistance. The continuous blue line is the FET behaviour of the graphene monolayer, using as gate the silicon substrate. It is notorious the low *on*/*off* current ratio (~6) characteristic of graphene devices (99, 102–108). The turn *on* current at forward bias occurs at 45 volts with a potential between source and drain of 10 mV.

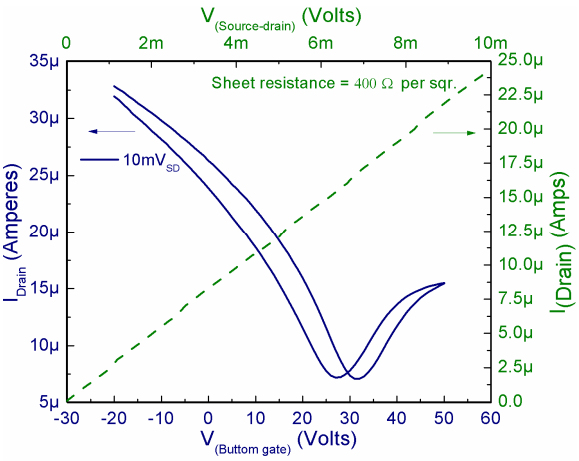


**Figure 3.21.** Four probe measurement of graphene device, in green. In blue is the voltage vs current curves, using the substrate as back-gate configuration.

In the figure 3.22 (a) is appreciable the $SiO_X$ coating, shows that silica is attached on the substrate as well; this is because PBA has a hydrophilic part that is attracted to the $SiO_2$ substrate surface. On the image (a) the graphene layer cannot be observed due to light diffraction produced by the coating.

Raman spectra, fig. 3.22 (b), of each steps show absence of D-band, this means that the metal deposition and synthesis procedures do not alter the graphene structure; in the same context, G-band is slightly shifted when electrodes are deposited, due to charge transfer of metal electrodes (109).

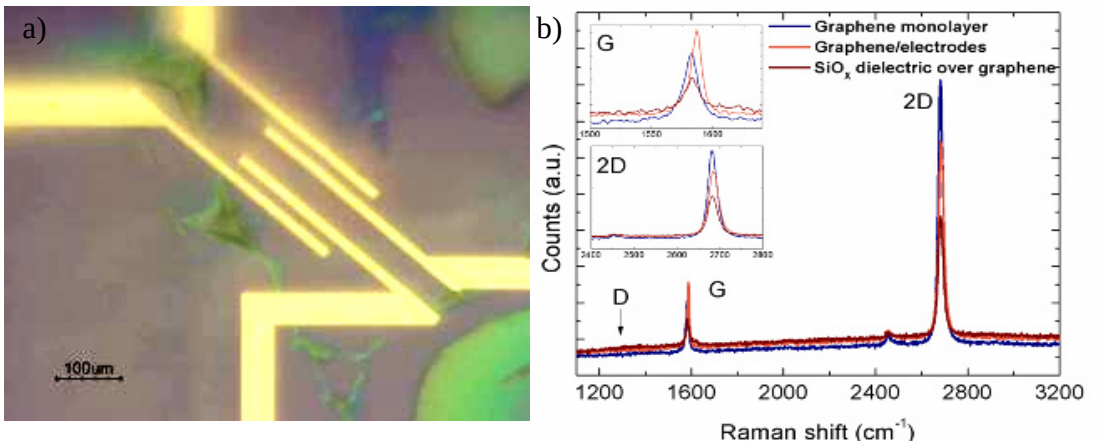


**Figure 3.22**.Optic microscope image of silica grown over the graphene device (a). Raman spectra made on each step, metal deposition and dielectric growth (b).

Three devices were constructed successfully, to these devices the silica layer is growth over graphene. This process broke one device, removing the graphene from bellow the electrodes. Additionally the electrodes were damaged, preventing the correct operation of the device. So, it was possible just to measure the leakage current, unfortunately it was not possible to demonstrate the FET behaviour.

Figure 3.23 show an image of the deposited electrode over the silica layer. The leakage current was measured applying a voltage between one electrode and the gate electrode, the voltage was increased in steps of 0.2 mV from 0 to 10mV, the leakage current at maximum voltage was of 100 fA.

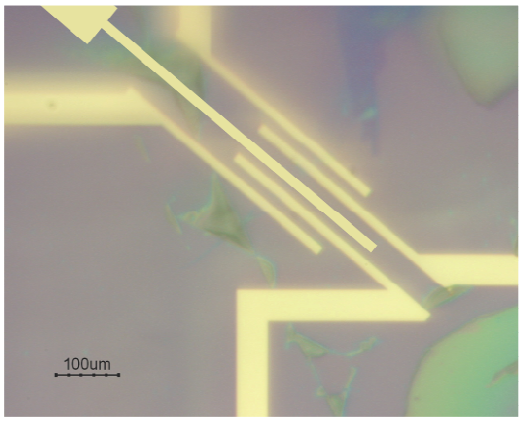


**Figure 3.23.** Optic microscopy of gate electrode deposited over silica growth by Sol-Gel.

### 3.3 Conclusions

The coating was successfully achieved, using both, oxidized and pristine SWNTs. As was expected the coating of oxidized nanotubes was relatively. The coating of pristine SWNTs using a pyrene moiety to growth silica was not achieved, even if I tried diverse procedures; if a surfactant is used instead of pyrene, it is possible to have individual or small bundles of SWNTs, even more, SC and Triton x-100 demonstrate to be good anchor point of silica seed. The carboxyl and hydroxyl groups in the surfactant tales, acts as linkers, were the hydrolysis o esterification process proceeds with ethyl groups of TEOS. The surfactant attached to nanotube walls seems to be stable at pH variations.

To our knowledge, this is the first attempt to use sol-gel process to coat CNTs for electronic applications directly. Unfortunately the device could not be fabricated; I believe that the building procedure was not the adequate, continuous work is currently being carried out to improve the device fabrication. Despite of this, further work must be done to understand better and modify the silica growing on coated nanotubes if it is desirable to use them as transistor channel and the coating as dielectric material.

In the same way, this is the first attempt trying to build, via sol-gel, a graphene device. The coating was achieved successful, a thin and homogeneous film was created with out leakage, this is a encourageable result because I have demonstrate that it is feasible to synthesise a gate dielectric, without defects, using bottom-up procedures. Additional work must be focused to improve and render less aggressive the graphene coating in order to do not damage the deposited metallic electrodes.

Additional studies can be done in the research of better dielectric materials, like hafnium oxide or aluminium oxide.

## 3.4 References


(1) Grove, A. S. *Physics and Technology of Semiconductor devices*; John Wiley and Sons, International edition, 1971.
(2) Brews, J. R.; Nicollian, E. H.; Sze, S. M. *IEEE Electron Device Letters*. **1980**, *1*, 2-4.
(3) Sze, S. M.; Ng, K. K. *Physics of semiconductor Devices*; 3rd ed.; Jhon Wiley & Sons: Hoboken, New Jersey, 2006.
(4) Chau, R.; Member, S.; Datta, S.; Doczy, M.; Doyle, B.; Kavalieros, J.; Metz, M. *IEEE Electron Device Letters*. **2004**, *25*, 408-410.
(5) Kang, L.; Lee, B. H.; Member, S.; Qi, W.-jie; Member, S.; Jeon, Y.; Member, S.; Nieh, R.; Member, S.; Gopalan, S.; Onishi, K.; Lee, J. C. *IEEE Electron Device Letters*. **2000**, *21*, 181-183.
(6) Campbell, S. A.; He, B.; Smith, R.; Ma, T.; Hoilien, N.; Taylor, C.; Gladfelter, W. L. *MRS proceedings*. **1999**, *606*, 23-33.
(7) Yeo, K.-S.; Roy, K. *Low-Voltage, Low-powe VLSI Subsystems*; McGraw Hill Professional: New York, 2005.
(8) Vasileska-Kafedzika; Stephen, G. *No TitleComputational sciences*; First Ed.; Morgan & Claypool Publishers, 2006.
(9) Franklin, A. D.; Sayer, R. a.; Sands, T. D.; Fisher, T. S.; Janes, D. B. *Journal of Vacuum Science & Technology B: Microelectronics and Nanometer Structures*. **2009**, *27*, 821.
(10) Bachtold, a; Hadley, P.; Nakanishi, T.; Dekker, C. *Science (New York, N.Y.)*. **2001**, *294*, 1317-20.
(11) Tans, S. J.; Verschueren, A. R. M.; Dekker, C. *Nature*. **1998**, *672*, 669-672.
(12) Martel, R.; Schmidt, T.; Shea, H. R.; Hertel, T.; Avouris, P. *Applied Physics Letters*. **1998**, *73*, 2447.
(13) Wind, S. J.; Appenzeller, J.; Martel, R.; Derycke, V.; Avouris, P. *Applied Physics Letters*. **2002**, *80*, 3817.
(14) Wong, H.-S. P. *IBM Journal of Research and Development*. **2002**, *46*, 133-168.
(15) Lu, Y.; Bangsaruntip, S.; Wang, X.; Zhang, L.; Nishi, Y.; Dai, H. *Journal of the American Chemical Society*. **2006**, *128*, 3518-9.
(16) Colinge, J. P.; Gao, M. H.; Romano-Rodriguez, A.; Maes, H.; Claeys, C. *IEDM Technical Digest. IEEE International Electron Devices Meeting, 1990*. **1990**, 595-598.
(17) Cho, K. H.; Yeo, K. H.; Yeoh, Y. Y.; Suk, S. D.; Li, M.; Lee, J. M.; Kim, M.-S.; Kim, D.-W.; Park, D.; Hong, B. H.; Jung, Y. C.; Hwang, S. W. *Applied Physics Letters*. **2008**, *92*, 052102.
(18) Liang, G. *IEEE Conference on electron devices and solid state circuits*. **2007**, 129-132.
(19) Franklin, A. D.; Luisier, M.; Han, S.-J.; Tulevski, G.; Breslin, C. M.; Gignac, L.; Lundstrom, M. S.; Haensch, W. *Nano letters*. **2012**, *12*, 758-62.
(20) Avouris, P. *Physica B: Condensed Matter*. **2002**, *323*, 6-14.
(21) Avouris, P. *Nature Photonics*. **2008**, *73*, 235427-350.
(22) Avouris, P. *Accounts of Chemical Research*. **2002**, *35*, 1026-1034.
(23) Avouris, P. *Proceedings of the IEEE*. **2003**, *2*, 1043-1784.
(24) Alvi, P. A.; Lal, K. M.; Siddiqui, M. J.; Naqvi, A. H. *Indian Journal of Pure & Applied Physics*. **2005**, *43*, 899-904.
(25) Alam, K.; Lake, R. *Applied Physics Letters*. **2005**, *87*, 073104.
(26) Avouris, P.; Chen, Z.; Perebeinos, V. *Nature nanotechnology*. **2007**, *2*, 605-615.
(27) Boudenot, J. *Comptes Rendus Physique*. **2008**, *9*, 41-52.
(28) Graham, a. P.; Duesberg, G. S.; Hoenlein, W.; Kreupl, F.; Liebau, M.; Martin, R.; Rajasekharan, B.; Pamler, W.; Seidel, R.; Steinhoegl, W.; Unger, E. *Applied Physics A*. **2005**, *80*, 1141-1151.
(29) Babi, B.; Iqbal, M.; Schnenberger, C. *Nanotechnology*. **2003**, *14*, 327-331.
(30) Weitz, R. T.; Zschieschang, U.; Forment-Aliaga, A.; Kälblein, D.; Burghard, M.; Kern, K.; Klauk, H. *Nano letters*. **2009**, *9*, 1335-40.
(31) Zhou, C.; Kong, J.; Dai, H. *Applied Physics Letters*. **2000**, *76*, 1597-1599.
(32) Liu, X.; Han, S.; Zhou, C. *Nano letters*. **2006**, *6*, 34-9.
(33) Javey, A.; Wang, Q.; Ural, A.; Li, Y.; Dai, H. *Nano Letters*. **2002**, *2*, 929-932.
(34) Bachtold, a; Hadley, P.; Nakanishi, T.; Dekker, C. *Science (New York, N.Y.)*. **2001**, *294*, 1317-20.
(35) Javey, A.; Guo, J.; Farmer, D. B.; Wang, Q.; Wang, D.; Gordon, R. G.; Lundstrom, M.; Dai, H. *Nano Letters*. **2004**, *4*, 447-450.

(36) Javey, A.; Kim, H.; Brink, M.; Wang, Q.; Ural, A.; Guo, J.; McIntyre, P.; McEuen, P.; Lundstrom, M.; Dai, H. *Nature materials*. **2002**, *1*, 241-6.
(37) Hur, S.-H.; Yoon, M.-H.; Gaur, A.; Shim, M.; Facchetti, A.; Marks, T. J.; Rogers, J. a *Journal of the American Chemical Society*. **2005**, *127*, 13808-9.
(38) Cao, Q.; Xia, M.-G.; Shim, M.; Rogers, J. a. *Advanced Functional Materials*. **2006**, *16*, 2355-2362.
(39) Weitz, R. T.; Zschieschang, U.; Effenberger, F.; Klauk, H.; Burghard, M.; Kern, K. *Nano letters*. **2007**, *7*, 22-7.
(40) Robert, G.; Derycke, V.; Goffman, M. F.; Lenfant, S.; Vuillaume, D.; Bourgoin, J.-P. *Applied Physics Letters*. **2008**, *93*, 143117.
(41) Cui, T.; Liang, G. *Applied Physics Letters*. **2005**, *86*, 064102.
(42) Lu, Y.; Bangsaruntip, S.; Wang, X.; Zhang, L.; Nishi, Y.; Dai, H. *Journal of the American Chemical Society*. **2006**, *128*, 3518-9.
(43) Klinke, C.; Hannon, J. B.; Afzali, A.; Avouris, P. *Nano letters*. **2006**, *6*, 906-10.
(44) Borghetti, J.; Derycke, V.; Lenfant, S.; Chenevier, P.; Goffman, M.; Vuillaume, D.; Bourgoin, J.-philippe *Advanced Materials*. **2006**, *18*, 1535-1540.
(45) Kim, M.; Hong, J.; Lee, J.; Hong, C. K.; Shim, S. E. *Journal of colloid and interface science*. **2008**, *322*, 321-6.
(46) Loscutova, R.; Barron, A. R. *Journal of Materials Chemistry*. **2005**, *15*, 4346.
(47) Vulliet, N.; Bernard, E.; Cherns, P.; Damlencourt, J.; Vizioz, C.; Colonna, J. P. *ECS Trans*. **2009**, *25*, 471.
(48) Gnani, E.; Reggiani, S.; Rudan, M.; Baccarani, G. *Solid state devices conference*. **2006**, 170-173.
(49) Clifford, J. P.; John, D. L.; Castro, L. C.; Pulfrey, D. L. *IEEE Transactions On Nanotechnology*. **2004**, *3*, 281-286.
(50) Clifford, J. P.; John, D. L.; Member, S.; Pulfrey, D. L. *IEEE Transactions on Nanotechnology*. **2003**, *2*, 181.185.
(51) D'Honinvthun, H. C.; Galdin-Retailleau, S.; Bournel, A.; Dollfus, P.; Bourgoin, J. P. *Comptes Rendus Physique*. **2008**, *9*, 335-342.
(52) Neophytou, N.; Guo, J.; Lundstrom, M. *Electr. & Comput. Eng*. **2004**, 176-175.
(53) Guo, J.; Goasguen, S.; Lundstrom, M.; Datta, S. *Applied Physics Letters*. **2002**, *81*, 1486.
(54) Chen, Z. *IEEE Electron Device Letters*. **2008**, *6*, 699-185.
(55) Liang, Y. X.; Chen, Y. J.; Wang, T. H. *Applied Physics Letters*. **2004**, *85*, 666.
(56) Fang, H.-tao; Sun, X.; Qian, L.-hua; Wang, D.-wei; Li, F.; Chu, Y.; Wang, F.-ping; Cheng, H.-ming *Journal of Physical Chemistry C*. **2008**, *112*, 5790-5794.
(57) Han, W.-Q.; Zettl, a. *Nano Letters*. **2003**, *3*, 681-683.
(58) Ma, S.-B.; Nam, K.-W.; Yoon, W.-S.; Yang, X.-Q.; Ahn, K.-Y.; Oh, K.-H.; Kim, K.-B. *Journal of Power Sources*. **2008**, *178*, 483-489.
(59) Jin, F.; Liu, Y.; Day, C. M. *Applied Physics Letters*. **2007**, *90*, 143114.
(60) Lin, C.-C.; Chu, B. T. T.; Tobias, G.; Sahakalkan, S.; Roth, S.; Green, M. L. H.; Chen, S.-Y. *Nanotechnology*. **2009**, *20*, 105703.
(61) Ntim, S. A.; Mitra, S. *Journal of chemical and engineering data*. **2011**, *56*, 2077-2083.
(62) Pumera, M.; Iwai, H.; Miyahara, Y. *Nanotechnology*. **2009**, *20*, 425606.
(63) Gomathi, A.; Vivekchand, S. R. C.; Govindaraj, A.; Rao, C. N. R. *Advanced Materials*. **2005**, *17*, 2757-2761.
(64) Bi, S.; Su, X.; Hou, G.; Gu, G.; Xiao, Z. *Physica B: Condensed Matter*. **2010**, *405*, 3312-3315.
(65) Fu, L.; Liu, Y. Q.; Liu, Z. M.; Han, B. X.; Cao, L. C.; Wei, D. C.; Yu, G.; Zhu, D. B. *Advanced Materials*. **2006**, *18*, 181-185.
(66) Grzelczak, M.; Correa-Duarte, M. a; Liz-Marzán, L. M. *Small (Weinheim an der Bergstrasse, Germany)*. **2006**, *2*, 1174-7.
(67) Lee, K. G.; Wi, R.; Imran, M.; Park, T. J.; Lee, J.; Lee, S. Y.; Kim, D. H. *ACS nano*. **2010**, *4*, 3933-42.
(68) Colorado, R.; Barron, A. R. *Chemistry of Materials*. **2004**, *16*, 2691-2693.
(69) Whitsitt, E. A.; Moore, V. C.; Smalley, R. E.; Barron, A. R. *Journal of Materials Chemistry*. **2005**, *15*, 4678.
(70) Whitsitt, E. A.; Barron, A. R. *Nano Letters*. **2003**, *3*, 775-778.
(71) Brinker, C. J.; Scherer, G. w. *Sol-Gel science: The physics and chemistry of Sol-Gel processing*; Academic Press, Inc.: New York, 1990.

(72) Brinker, C. J.; Schunk, P. R. *Journal of Non-Crystalline Solids*. **1992**, *148*, 424-436.
(73) Keefer, K. D. In *Silicon based polymer sciences*; 1989; pp. 221-240.
(74) Tsionsky, M.; Lev, O. *Analytica chimica*. **1995**, *67*, 2409-2414.
(75) Bergna, H. E. In *In the colloidal Chemistry of Silica, advances in Chemistry*; Bergna, H. E., Ed.; American Chemical Society: Washington DC, 1994; Vol. 234.
(76) Prassas, M.; Hench, L. L. *Ultrastructure Processing of Ceramics, Glasses, and Composites*; Hench, L. L.; Ulrich, D. R., Eds.; Jhon Wiley & Sons: New York, 1984; pp. 100-125.
(77) Brinker, C. J. *Journal of Non-Crystalline Solids*. **1988**, *100*, 31-50.
(78) Aelion, R.; Loebel, A.; Eirich, F. *Journal of the American Chemical Society*. **1950**, *72*, 5705-5712.
(79) Klein, L. C. *Annual review of Material Sciences*. **1985**, *15*, 227-248.
(80) Mauritz, K. A. *University of Southern Mississippi*.
(81) Niyogi, S.; Hamon, M. a.; Hu, H.; Zhao, B.; Bhowmik, P.; Sen, R.; Itkis, M. E.; Haddon, R. C. *Accounts of Chemical Research*. **2002**, *35*, 1105-1113.
(82) Marshall, M.; Popanita, S.; Shapter, J. *Carbon*. **2006**, *44*, 1137-1141.
(83) Treacy, M. M. J.; Shreeve-keyer, J. L.; Haushalter, R. C. *Advanced Materials*. **1996**, *8*, 155-157.
(84) Musso, S.; Porro, S.; Vinante, M.; Vanzetti, L.; Ploeger, R.; Giorcelli, M.; Possetti, B.; Trotta, F.; Pederzolli, C.; Tagliaferro, a *Diamond and Related Materials*. **2007**, *16*, 1183-1187.
(85) Banerjee, B. S.; Hemraj-benny, T.; Wong, S. S. *Covalent Surface Chemistry of Single-Walled Carbon Nanotubes*; 2005; pp. 17-29.
(86) Banerjee, S.; Hemraj-Benny, T.; Wong, S. S. *Advanced Materials*. **2005**, *17*, 17-29.
(87) Hirsch, A.; Vostrowsky, O.; Chemie, O.; Erlangen-nürnberg, U. *Anion Sensing*. **2005**, 193- 237.
(88) Bahr, J. L.; Tour, J. M. *Journal of Materials Chemistry*. **2002**, *12*, 1952-1958.
(89) Martinez, M. . T.; Callejas, M. A.; Benito, A. M.; Cochet, M.; Seeger, T.; A., A.; Schreiber, J.; Gordon, C.; Marhic, C.; Chuavet, O.; Fierro, J. L. G.; Maser, W. K. *Carbon*. **2003**, *41*, 2247-2256.
(90) Huang, W.; Wang, Y.; Luo, G.; Wei, F. *Carbon*. **2003**, *41*, 2585-2590.
(91) Mart, M. T. *Carbon*. **2003**, *691*.
(92) Tsetseris, L.; Pantelides, S. *Physical Review Letters*. **2006**, *97*, 1-4.
(93) Ehli, C.; Rahman, G. M. A.; Jux, N.; Balbinot, D.; Guldi, D. M.; Paolucci, F.; Marcaccio, M.; Paolucci, D.; Melle-Franco, M.; Zerbetto, F.; Campidelli, S.; Prato, M. *Journal of the American Chemical Society*. **2006**, *128*, 11222-31.
(94) Tasis, D.; Mikroyannidis, J.; Karoutsos, V.; Galiotis, C.; Papagelis, K. *Nanotechnology*. **2009**, *20*, 135606.
(95) Wang, X.; Zhi, L.; Müllen, K. *Nano letters*. **2008**, *8*, 323-7.
(96) Gilje, S.; Han, S.; Wang, M.; Wang, K. L.; Kaner, R. B. *Nano letters*. **2007**, *7*, 3394-8.
(97) Wu, Y. Q.; Ye, P. D.; Capano, M. a.; Xuan, Y.; Sui, Y.; Qi, M.; Cooper, J. a.; Shen, T.; Pandey, D.; Prakash, G.; Reifenberger, R. *Applied Physics Letters*. **2008**, *92*, 092102.
(98) Lin, Y.; Dimitrakopoulos, C.; Jenkins, K. A.; Farmer, D. B.; Chiu, H.; Grill, A.; Avouris, P. *Nano*. 100.
(99) Meric, I.; Han, M. Y.; Young, A. F.; Ozyilmaz, B.; Kim, P.; Shepard, K. L. *Nature nanotechnology*. **2008**, *3*, 654-9.
(100) Wang, Z.; Zhang, Z.; Xu, H.; Ding, L.; Wang, S.; Peng, L.-M. *Applied Physics Letters*. **2010**, *96*, 173104.
(101) Zhang, Y.; Tang, T.-T.; Girit, C.; Hao, Z.; Martin, M. C.; Zettl, A.; Crommie, M. F.; Shen, Y. R.; Wang, F. *Nature*. **2009**, *459*, 820-3.
(102) Li, S.-L.; Miyazaki, H.; Kumatani, A.; Kanda, A.; Tsukagoshi, K. *Nano letters*. **2010**.
(103) Lin, Y.-M.; Jenkins, K. a; Valdes-Garcia, A.; Small, J. P.; Farmer, D. B.; Avouris, P. *Nano letters*. **2009**, *9*, 422-6.
(104) Chen, J.-H.; Jang, C.; Xiao, S.; Ishigami, M.; Fuhrer, M. S. *Nature nanotechnology*. **2008**, *3*, 206-9.
(105) Schwierz, F. *Nature Nanotechnology*. **2010**.
(106) Sordan, R.; Traversi, F.; Russo, V. *Applied Physics Letters*. **2009**, *94*, 073305.
(107) Xia, F.; Farmer, D. B.; Lin, Y.-M.; Avouris, P. *Nano letters*. **2010**, *10*, 715-8.
(108) Sun, Z.; Yan, Z.; Yao, J.; Beitler, E.; Zhu, Y.; Tour, J. M. *Nature*. **2010**, *468*, 549-52.
(109) Echtermeyer, T. J.; Britnell, L.; Jasnos, P. K.; Lombardo, a.; Gorbachev, R. V.; Grigorenko, a. N.; Geim, a. K.; Ferrari, a. C.; Novoselov, K. S. *Nature Communications*. **2011**, *2*, 458.

# Chapter 4

# Improvement of the contact resistance between SWNT and electrodes

## 4.1 Metal electrodes.

s-SWNTs had been visualized as the most promising material for the next transistor's generation (1–13). In the same way, m-SWNTs could play an important role for device interconnections (14–16). Both applications have a close dependence in the electric contact between CNTs and metal electrodes. This junction has been widely studied theoretically demonstrating that the quality of the contact strongly depends on the metal type (17, 18), the nanotube chirality (19, 20), and how the nanotube is positioned in the electrode (21). Experimental works has been published as well; Seidel and collaborators had developed a multilayer structure for growing nanotubes *in situ* over electrodes (22), Song et al, achieved a contact resistance reduction depositing aluminium in the interface CNTs (film)-electrodes (23). Nosho et al. had investigated the response of CNT-FET with diverse metal contacts (24). Also, these studies has been applied to graphene devices (25, 26). These reports indicate that a low-resistance contact is a fundamental prerequisite for applications of CNT-based devices.

Despite the aforementioned results, the traditional way to fabricate a CNT-FET is depositing the nanotube on the top of metal electrodes (with work function ≥ 5 eV), driven by week van deer Walls bonds between electrodes and SWNTs (27, 28). For instance, Figure 4.1 shows a conventional CNT device where the nanotube is deposited over the metal electrodes (29). This "no ideal" preparation strategy produces a considerable barrier for electronic conduction, resulting in a high contact resistance between nanotube and electrodes (19). Even more, this way to place a nanotube on the top of electrodes prevents further applications since it is impossible to repeat in a reproducible way this process to fabricate commercial devices. Therefore, it is of fundamental importance to reduce the contact resistance to improve devices based on CNTs.

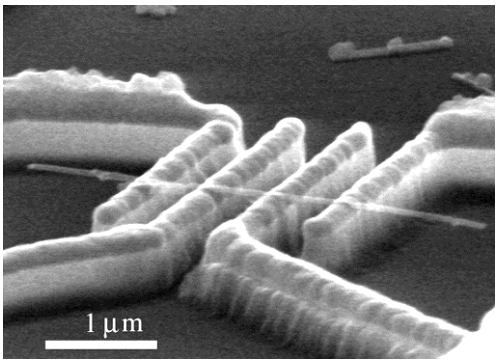


**Figure 4.1.** SEM image of a carbon nanotube lying across four metal electrodes, utilizing the traditional way to fabricate a nanotube CNT-FET. Taken from (29)

Much effort had been done to improve the contact between CNTs and metal electrodes. Many techniques to efficiently join nanotubes to metal electrodes had been proposed as for example, fusing the metal parts to obtain a carbide-metal junction (30–32) or exposing the electrodes to high energy beams (22). Nevertheless, all these protocols play with top-down techniques, using always procedures that prevent the miniaturization and assembly of large quantities of devices.

Following the strategy of fabrication of electronic devices using bottom-up techniques, few groups had attempted to attach metallic moieties to semiconductor nanostructures. Mokari et

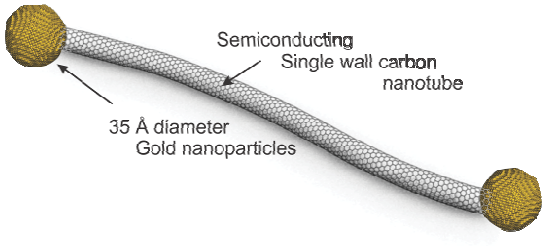


**Figure 4.2.** Schematic representation of the ideal structure AuNP/NT/AuNP.

al. have grown metallic particles at CdSe nanorods (33), Deng et al. have demonstrated theoretically that covalent linking molecules joining graphene and metal particles increases considerably the electric and mechanical performance (34). According with this study -COO- and -CON- functional groups as linking molecules are able to reduce the electric resistance 40 and 60 times respectively. Recently, Weizmann et al. reported the synthesis of amine monofunctionalized gold nanorods covalently attached just to the nanotube tips (35). The last two reports have inspired this thesis chapter and the work carried out on it. Figure 4.2 represents an ideal gold-nanotube configuration which represents as well the goal of this chapter.

### 4.1.1 Gold nanoparticles

Two different sizes of gold nanoparticles (Au-NPs): ~1.5 or ~14 nm in diameter were synthesized, using traditional methods (36–38) and inexpensive reactants.

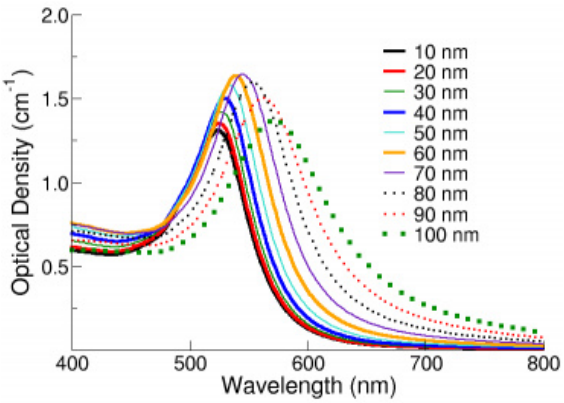


**Figure 4.3.** Spectra of 10 different sizes of gold nanoparticles. Taken from (43)

Gold nanoparticles absorb and scatter light with extraordinary efficiency (39–41). Their strong interaction with light occurs because the conduction electrons on the metal surface feel a collective oscillation when they are excited by light at specific wavelengths. This oscillation is known as a surface plasmon resonance (SPR) (42). Gold nanoparticle absorption properties can be tuned by controlling the particle size and shape (36–49). Thus the optical properties of gold nanoparticles are strongly dependent on the nanoparticle diameter. The spectra of gold nanoparticles with 10 different sizes, at identical mass concentrations (0.02 mg/mL), are shown in the figure 4.3. The small particles (10-20 nm) have peaks near 520 nm, while larger particles (~100nm) have peaks that broaden significantly and shift towards longer wavelengths.

Gold nanoparticles are synthesized in liquid-phase using 2 diverse procedures in order to have different sizes. The first one is the so called Turkevich method, (36) invented by himself and successfully modified by Frens (37, 38). This method produces spherical gold nanoparticles with an average diameter of 14 nm. The synthesis method is briefly summarized in the following. Chloroauric acid ($H[AuCl_4]$) 0.5 mM (500 ml) is boiled under fast stirring. At the same time 25 ml of sodium citrate 1 % solution is softly heated. When the Au solution starts to boil, the solution of sodium citrate is added abruptly, and a change of the colour from light-yellow to black and finally to a dark red coloration was observed. The final solution is then cooled to room temperature. Figure 4.4 (a) shows a TEM image of particles synthesized by the Turkevich method. The as-synthesized gold-nanoparticles have a spherical shape with average diameter of 14 nm. Figure 4.4 (b) shows the absorption spectra in yellow of the gold nanoparticles. The plasmon hip is closely related with the particle

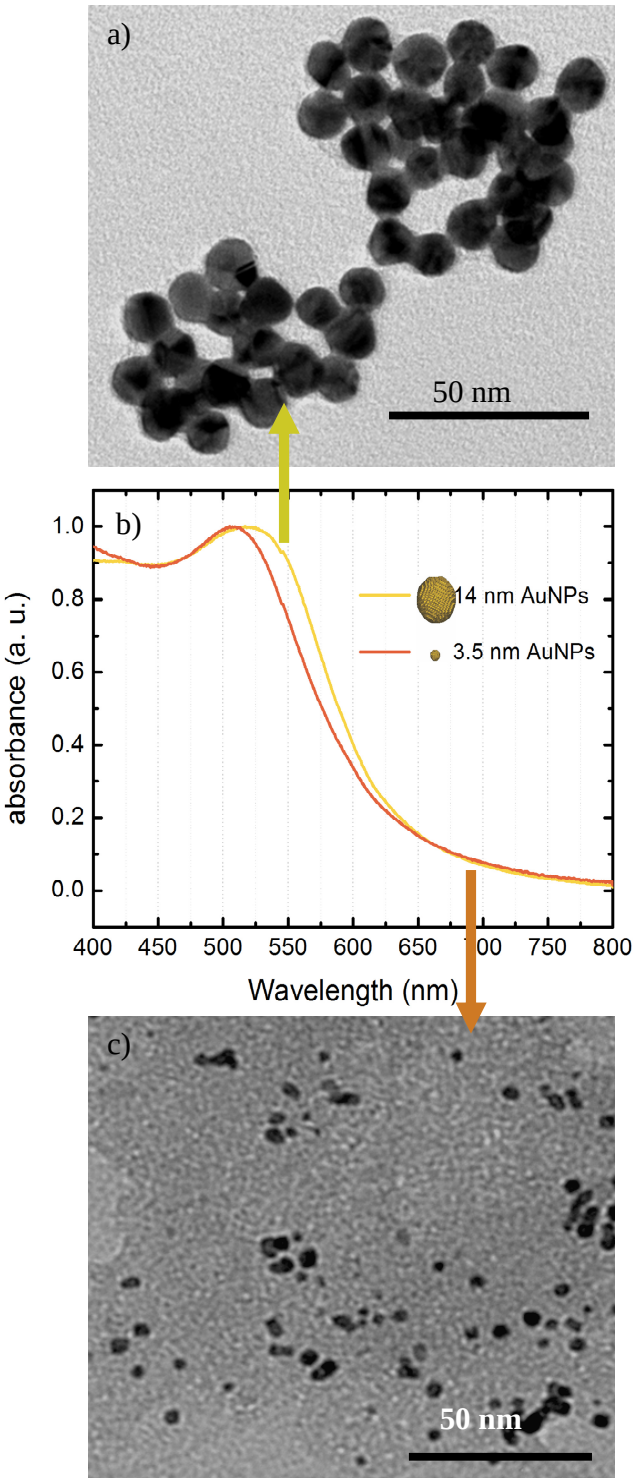


**Figure 4.4.** a). TEM image of ~ 14 nm AuNPs. b) Absorption spectra of 14 and 3 nm diameter AuNPs and c) TEM image of 3.5 nm AuNPs.

size (43–45, 47, 50, 51), and its shape and position with the aggregation degree, in this case it is an almost perfect Gaussian peak, representative of spherical particles (43–45, 47, 50, 51). The position of Plasmon can be shifted changing the solvent or attaching molecules to the particle surface (43–45, 47, 50–52)

In the second procedure the particles are formed due to gold reduction from $Au^{3+}$ to $Au^{0}$ using Sodium Borohydrate ($NaBH_4$) as reducing agent. This process was first proposed by Brust et al. (53). The modified process that I have used is summarized as follow:. first, 5 ml of a CTAB 15 mM and $AuCl_3$ 50 mM are stirred until a yellow colour and homogeneous solution is achieved. Then, 0.3 ml of $NaBH_4$ 20mM is added and stirred for 10 minutes. CTAB covers and stabilizes the particles, preventing further growth and aggregation, This method produce ~4 nm size diameter particles. Figure 4.4 (c) shows the TEM image of 3.5 nm gold nanoparticles, and its corresponding absorption spectra is shown in colour red in fig. 4.4 (b).

PVP. PEG, or a surfactant can be added to the colloidal solution to prevent particle aggregation and stabilize the suspension.

### 4..1.2 Au nanoparticle/nanotube/Au nanoparticle heterojunctions

As already explained in chapter 2, carbon nanotubes as produced are considered as inert chemically. Thus, it is necessary to treat the tubes in order to induce chemical reactivity (54–56). If the oxidation treatment time is reduced to a couple of hours it is possible to selectively oxidize the most reactive nanotube zones: the tips (57). The Nitric acid oxidation process was done as explained in the section 2.1.3.2. The oxidation process was performed for 3 hours. 2mg of oxid-SWNTs was dispersed in triton x-100 and PEG solution (both in concentration1 % w/v) and ultrasonicated using a sonic tip tuned at 30 % of maximum power (750 W) with a duty cycle of 50 %. The solution is ultracentrifuged at 16000 *g* (12 kRPM) for 24 hours. The supernatant of the obtained dispersion, SWNTs coated with a triton-PEG bilayer, is then collected while the precipitate material is discarded.

The surfactant coating prevents undesirable functionalization of SWNT sidewalls, letting free just the ends. This procedure, as discussed in chapter 2 is fundamental for the de-bundling of the nanotubes, and render a higher quantity of completed structures AuNP/NT/AuNP. The coating process is depicted schematically in the figure 4.5.

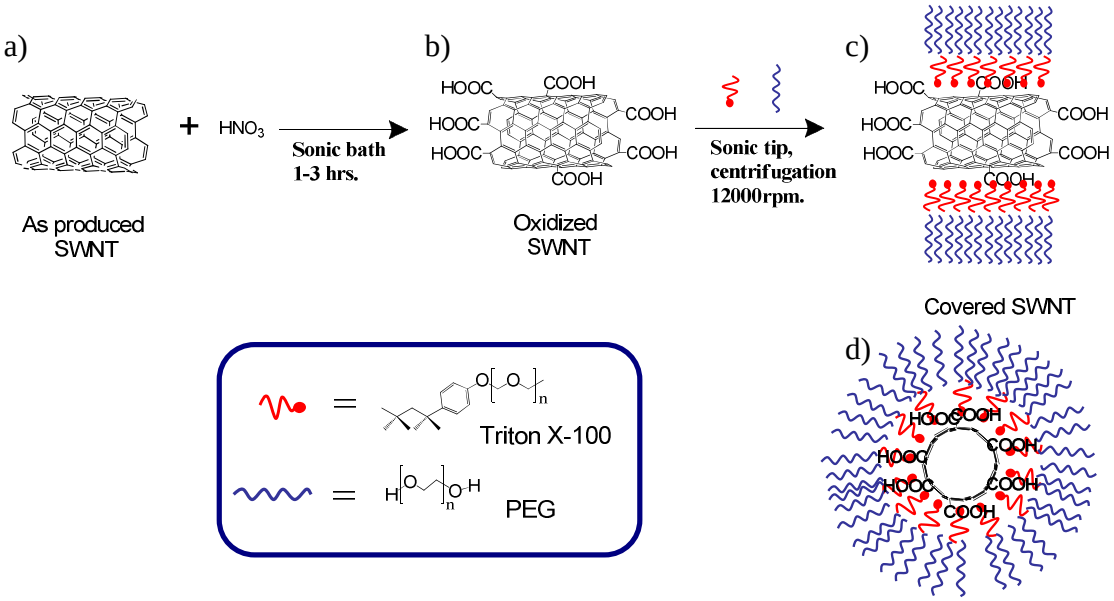


**Figure 4.5** Schematic representation of oxidation and covering of SWNTs, using Triton x-100 and PEG in order to blind the functional groups all over the nanotube walls, while those located in the tips are available. a) pristine material; b) nanotubes after soft oxidation, explained in chap 2; c) individual or small bundles of tubes covered wit a bi-layer triton-PEG; d) orthogonal view of (c).

The bonding between the AuNP and SWNT is designed with the aid of a "linking molecule". The linking molecule should be able to react covalently with the carboxylic groups situated on the nanotube ends, and provide a strong bond with nanoparticle surface. Additionally, the length of the linking molecule should be short enough to allow the electrons to flow through it (58–65).

#### 4.1.2.1 Cystamine as linking molecule

The first approach used in this thesis work relied in the exploitation of **Cystamine hydrochloride** as linker molecule, as shown in Figure 4.6. It is possible to bond one amine group of the cystamine to one carboxylic group in the nanotube tips, as illustrated in orange ellipse, letting the disulfide group available for coupling with AuNP surface, as is depicted as a blue circle in figure 4.6.

During the formation of the amide bond, 1-ethyl-3-(3-dimethylamino propyl) carbodiimide (EDC) and sulfo-N-Hydroxysuccinimide (s-NHS) were used as the coupling agents to increase the amidation yield.

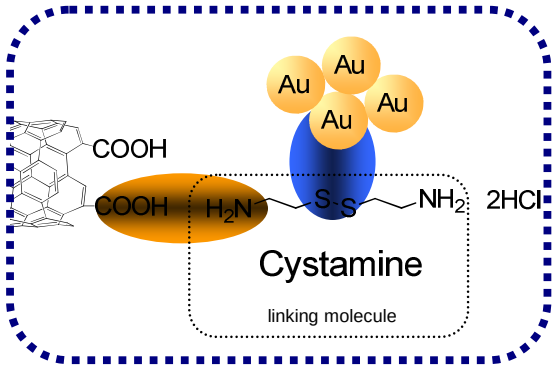


**Figure 4.6.** Schematic representation of the *linking molecule*, cystamine, and their possible coupling with the nanotube and AuNP

The linking process is carried out following the procedure detailed below and illustrated in the figure 4.7. First, 10 mL of Triton-PEG-SWNT dispersion is immersed in an icy sonic bath for 20 minutes, Afterward, 1mL of EDC (2mM) and 1 mL of s-NHS (5mM) are added to the nanotube dispersion. Then, 3 mL of a Cystamine dihydrochloride 10 mM are added and the obtained dispersion is ultrasonicated for 6 hours. Finally, the sample is ultracentrifuged at 16000 *g* until the nanotubes sediment into the bottom and eliminate the solution, then,the residue is re-dispersed in Triton x-100 & PEG solution (both 0.2 % w/v). This washing step is repeated 3 times to remove the excess, of EDC, s-NHS and Cystamine. At this point the SWNTs are functionalized by the ends with Cystamine, for clarity reasons the Cystamine functionalized SWNTs will be mention as Cys-SWNTs. The Cys-SWNT are resuspended in fresh Triton-PEG solution.

The final step of the linking process relies in the addition of AuNP to create the AuNP/NT/AuNP structure. A 0.1 % in weight of PEG solution is added to 10 mL 14 nm-AuNPs solution prepared previously, and the colloidal Au dispersion is stirred for 2 hours. Finaly, 5 mL of Cys-SWNTs suspension are added dropwise to the AuNP solution.

Finally, the dispersion is let it settle for 48 hours. During this period the nanotubes with AuNPs/NT/AuNTs precipitate. This is observable in the bottom of the flask as a darkish precipitate. Supernatant is discarded and the precipitate is re-dispersed in fresh PVP-Triton solution.

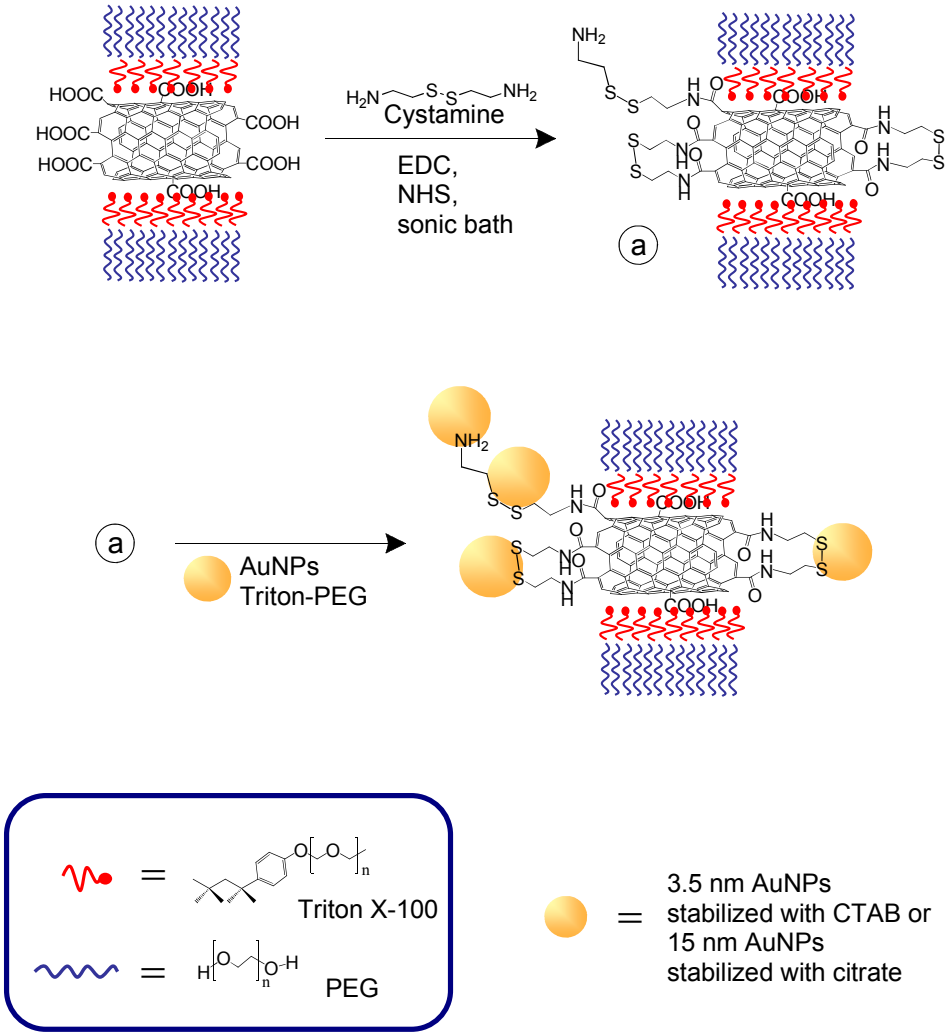


**Figure 4.7.** Synthesis of AuNP-NT-AuNP complex, using Cystamine as linking molecule.

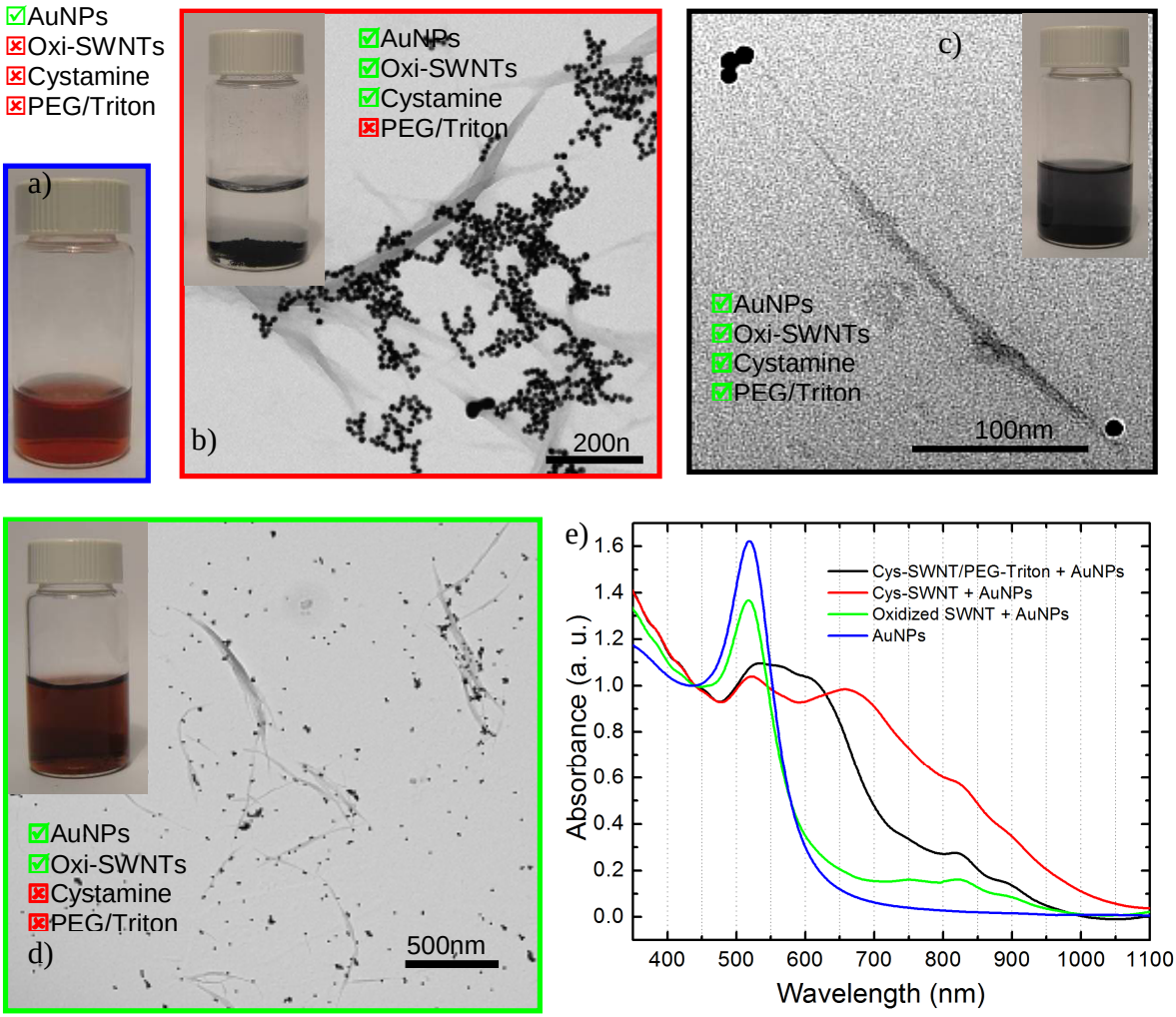


**Figure 4.8.** Photograph, TEM, and absorption spectra of AuNPs-nanotubes, in different conditions, each border colour TEM image have its respective absorption spectra and vial photograph, except for the sample AuNPs, TEM image is shown in figure 4.3. The red and green boxes indicate the absence or presence of surfactants, the linking molecule, or nanotubes.

Figure 4.8 shows clearly the importance to add Cystamine and PEG/Triton to the reaction. It is known that carboxylic groups can be attached to gold surfaces (66). The picture (a) is an image of as synthesized 14nm-AuNPs, its absorption spectrum corresponds with the blue line in (e). If the coupling reaction is performed without the aid of Cystamine and without the protecting bilayer Triton-PEG, the result is a non selective coupling between NTs and AuNPs, as in the image (d) shows a TEM picture where the resulting dispersion consists practically in a mixture of nanotubes and NPs. In the

absorption spectra graph is appreciable in green its corresponding curve, and it shows no difference with the AuNPs curve. A diminished intensity due to concentration is observed and the peaks due to the functionalized nanotubes are present as well. The respective vial picture is presented in (d). In contrast to the Cystamine attached to SWNTs without the protection of Triton-PEG (b), the particles are localized together with SWNTs (where, in any position), the tubes are more bundled, and the particles aggregated. This product precipitates, as can be observed in the vial of the figure (b). Additionally, the particles aggregation induces changes on its electronic distribution, and this can be monitored by absorption studies as the red line in (d), where the original plasmon signal is reduced and new peaks appear resembling larger metallic structures or aggregates (36–49). Finally, if the reaction is achieved with all the components, the result is the desired structure AuNP/NT/AuNP, as can be observed in the figure (c). The coloration change on the vial is a product of particle aggregation; in the absorption spectrum (black line) it is appreciable a red-shift of the plasmon band that may be produced by the small particle aggregates.

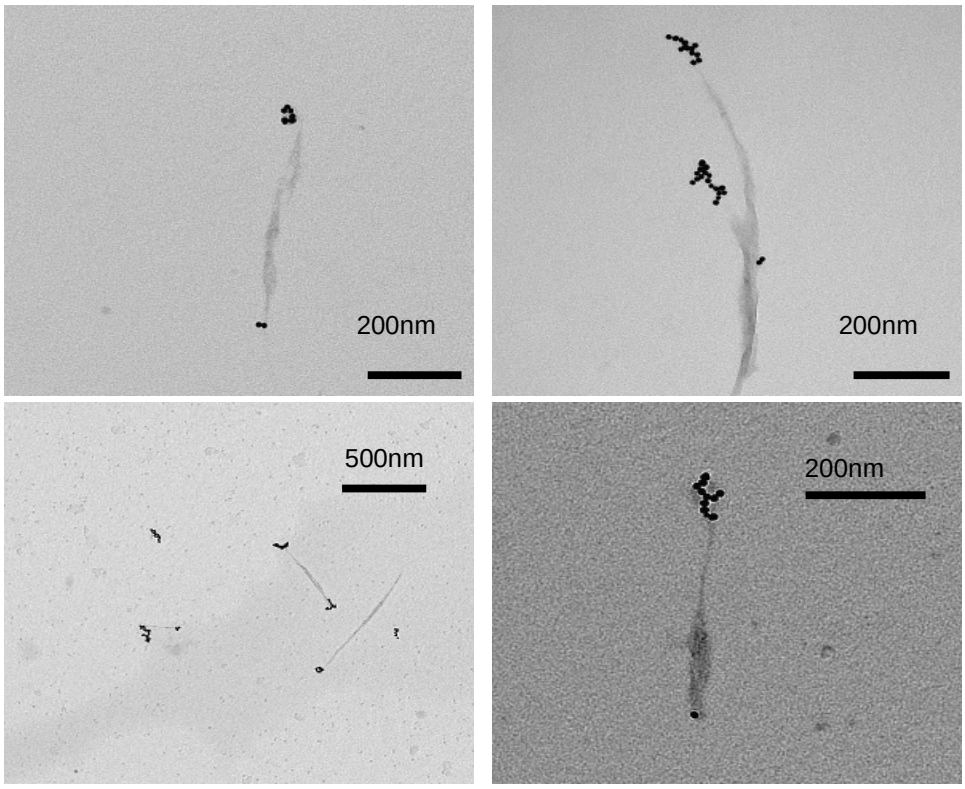


**Figure 4.8.** TEM images of some AuNP/CNT/AuNP structures. Particle size: 14 nm.

The achievement of the AuNP/NT/AuNP configuration was possible following the last strategy which is the last, specify. Unfortunately, the quantity of successful structures was low, even more, the particles aggregates preventing to use them for further row growth. Figure 4.8 shows some successfully linked AuNP/NT/AuNP structures. However, I have to point out that for a more detailed characterization it is necessary to increase the number of these structures.

### 4.1.2.2 Dipropylamine-dithiocarbamate as linking molecule

In my view, the yield of the AuNP/NT/AuNP structure can be improved if the contact angle between the linking molecule and the AuNP is increased. Figure 4.9 (a) represents the geometry of contact between the sulphur atoms and the AuNPs using Cystamine. Figure b) shows how it is believed that the yield should increase with improved contact geometry using other linking molecule with more accessible sulphurs. .The dotted blue lines indicate the possible area in which the particles approaches to the sulphur atoms. This cystamine configuration prevents reaching the particles easily. Thus, this geometry might not be the most adequate. I thus proposed to change the geometry disposing the sulphur atoms more accessible to AuNPs, as can be seen in Figure 4.9 (b).

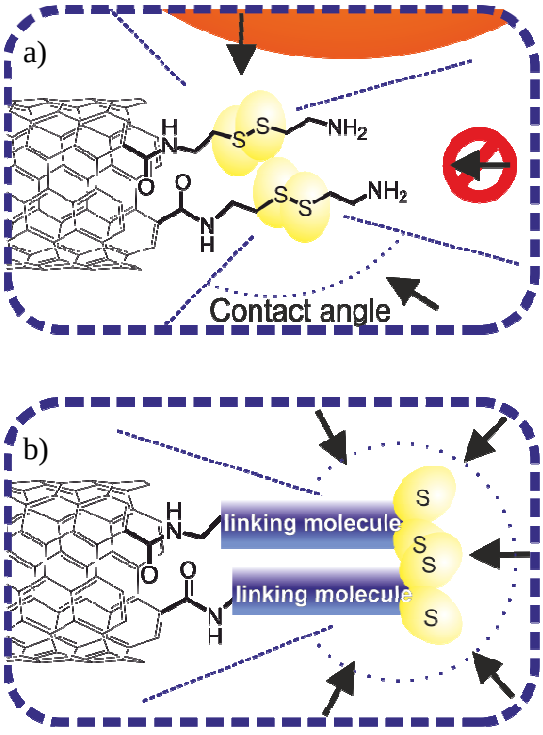


**Figure 4.9**. Representation of the possible reduced contact angle between AuNPs and cystamine a), proposed system with an increased contact angle should promote the AuNPs linking b).

As linking molecule I used 1, 3-propanediamine (PDA). Interestingly enough, with this molecule is possible to attach diverse reactive groups to each amine.

I used the procedure schematically depicted in Figure 4.10. Briefly, a 3 hours nanotube oxidation was performed as described in section 2.1.3.2, and as in the previous experiment, the nanotubes are dispersed and wrapped by triton x-100 to prevent the functionalization on the nanotube walls. Figure 4.10 (a).

PDA mono-protection was carried out dissolving 2 gr of di-tert-butyl dicarbamate (Boc) in 30 ml THF, and 3ml of PDA in 50 ml THF, these rates gives a molar ratio of 3:1 [PDA:Boc] to ensure that only one amine of PDA will react with one Boc, the no-reacted PDA can be easily eliminated by evaporation. The Boc-solution is added dropwise to a cold solution containing the PDA,. The solvent is evaporated and the solid was extracted with a solution of ethyl acetate-water three times. The water fraction is discarded because contains the residual PDA. The ethyl acetate phase is collected dryed with MgSO4. The monoBoc product (N-Boc-1,3-propanediamine, Boc-PDA) was purified by chromatography (ethylacetate:hexane) if necessary. This reaction is illustrated in the figure 4.10 (b).

The amidation process is carried out following the procedure detailed below and illustrated in the figure 4.10 (c). First, 10 mL of Triton-PEG-SWNT dispersion in water is immersed in an icy sonic bath for 20 minutes, afterward, 1mL of EDC 2mM is added to the nanotube dispersion to obtain reactive carboxylic groups. Then, 3 mg of Boc-PDA containing 1 mL of s-NHS 5mM are added to the previous solution and the obtained dispersion is ultrasonicated for 6 hours. Finally, the sample is ultracentrifuged at 16000 *g* until the nanotubes sediment, then the sample is re-dispersed in Triton x-100 & PEG solution (both 0.2 % w/v). This washing step is repeated 3 times to remove the excess of EDC, s-NHS and Boc-PDA. At this point the SWNTs are functionalized by the ends with Boc-PDA. The Boc-PDA-SWNT are resuspended in fresh Triton-PEG solution (both 0.2 % w/v).

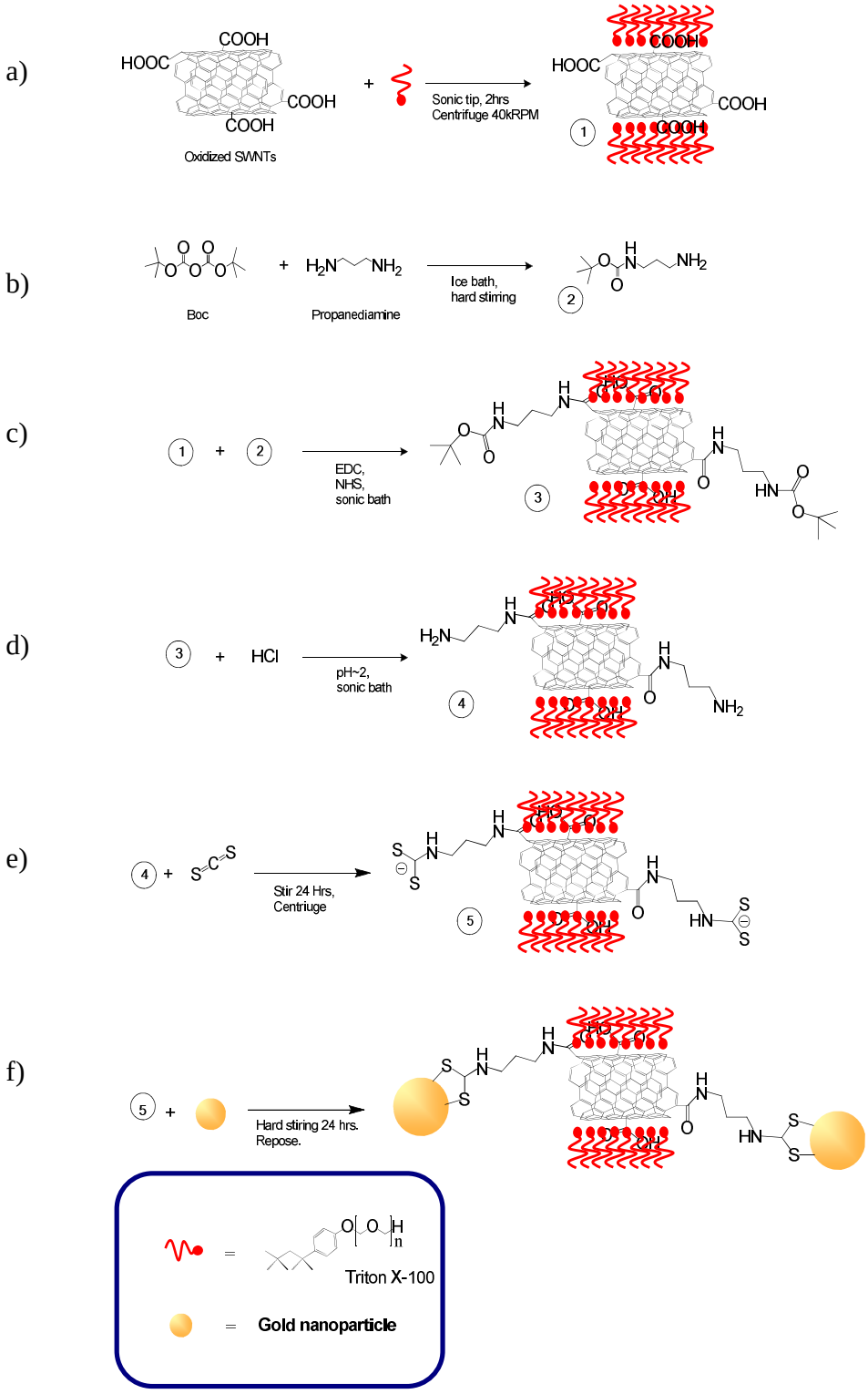


**Figure 4.10. S**ynthesis of AuNP/NT/AuNP complex, using propanediamine as an linkeing molecule.

Once Boc-PDA-SWNTs is obtained, the Boc-protected-amine can be deprotected using hydrochloric acid 2M, as is shown in fig. 4.10 (d). This procedure assures that the free amine moieties are located at the tube ends. Again the product is washed with water and resuspended in Triton-PEG using ultrasonic bath overnight.

Following the Almeida et al. procedure, (67) it is possible to link di-thiocarbamate to the amine group making an ideal connection to gold surfaces. In this way, dispersing the material in a solution of carbon disulfide ($CS_2$) it is possible to get free sulphur atoms at the end of the linking molecule, figure 4.10 (e). To the PDA-SWNTs solution is added 5 ml of CS2, and strongly stirred overnight. At this step the sulphur atoms are available to be linked with AuNP, with the desired geometry: sulphur at the tube ends (S-SWNT-S)

This solution (S-SWNT-S) is added dropwise to a stirring solution of AuNP, in order to obtain the desired structure AuNP/SWNT/AuNP. Finally, this solution is centrifuged at 8 000 *g*, the precipitate collected and resuspented in Triton-PEG aqueous solution, using ultrasonic bath overnight.

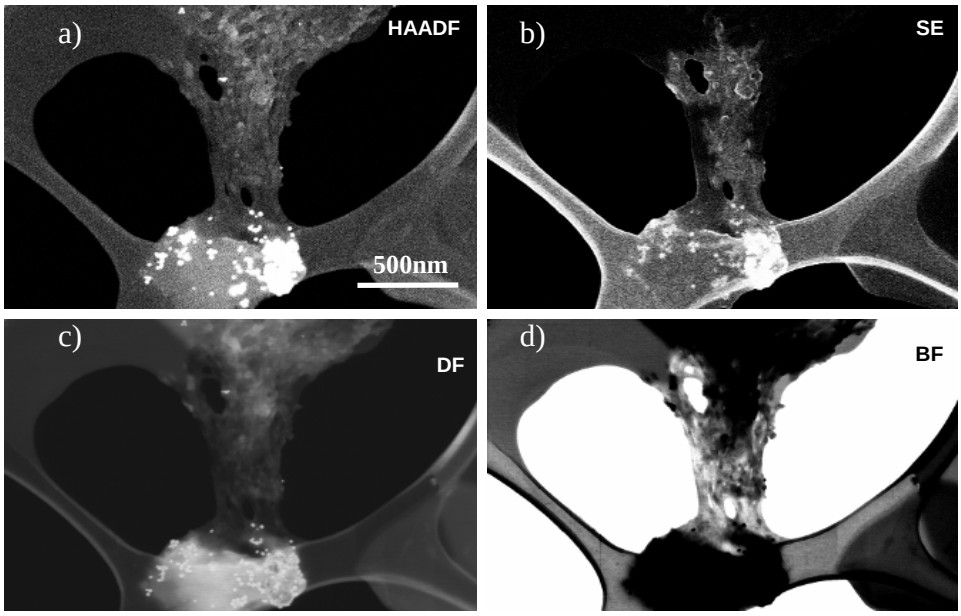


**Figure 4.11.** Different image techniques using scanning electron microscopy. a) high annular angle dark field, b) secondary electrons, c) Dark field and d) bright field.

Scanning-transmission electron microscopy (STEM) images show the gold nanoparticles attached to the ends of bundled nanotubes. Figure 4.11 shows diverse STEM characterization images. High angle annular dark field (HAADF) is used to locate the place of heavier atomic weight particles, see figure 4.11a). It is important to note that the particles are mainly located at the bundle ends (a). Figure 4.11 (b) is a secondary electrons (SE) image, where the surface of the sample is scanned, giving information on the constitutional content of the sample. Image (c) and (d) show the dark and bright field respectively. For the characterization of this sample emerges some differences with respect to the one produced by the Cys-SWNT approach. Indeed, the sample produced with DPA linked molecule gives a more amount of structures AuNP/CNT/AuNP, but in bundles. Even though, it was possible to perform an atomic force measurement of some individual structures. Figure 4.12 illustrates the AFM image collected in tapping mode. The image shows the presence of metallic particles with a height below the average (8 nm), and the tubular structure between the AuNPs, which has a height of ~1.2 nm. Even more, this procedure was able to avoid particle aggregation and increase the successful coupling, but nanotube aggregation was still present. TEM analysis is a better technique for the evaluation of the interaction nanoparticles-nanotubes ends. Figure 4.13 shows nanotube bundles in which some nanotube ends are decorated with metallic nanoparticles. This is a good example on how tightly the nanotubes are bundled. Additionally, some particles appears conveniently bonded to the tips. A representation of how the particles may be bonded is illustrated in the up-right figure.

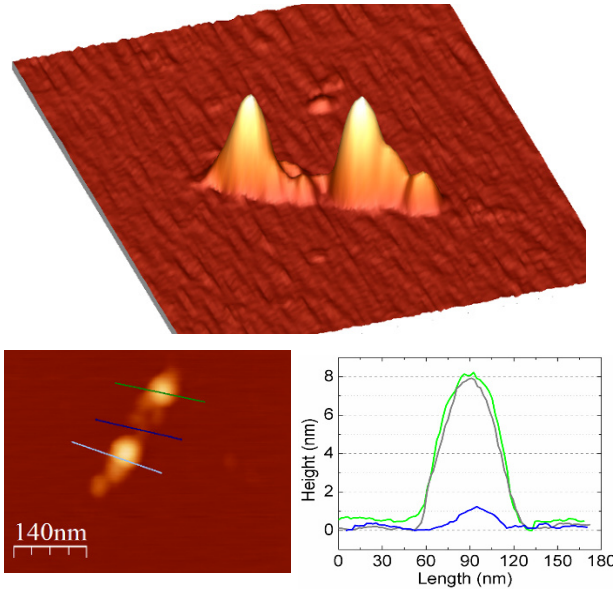


**Figure 4.12.** AFM in tapping mode image of AuNPs/CNT/AuNPs structure.

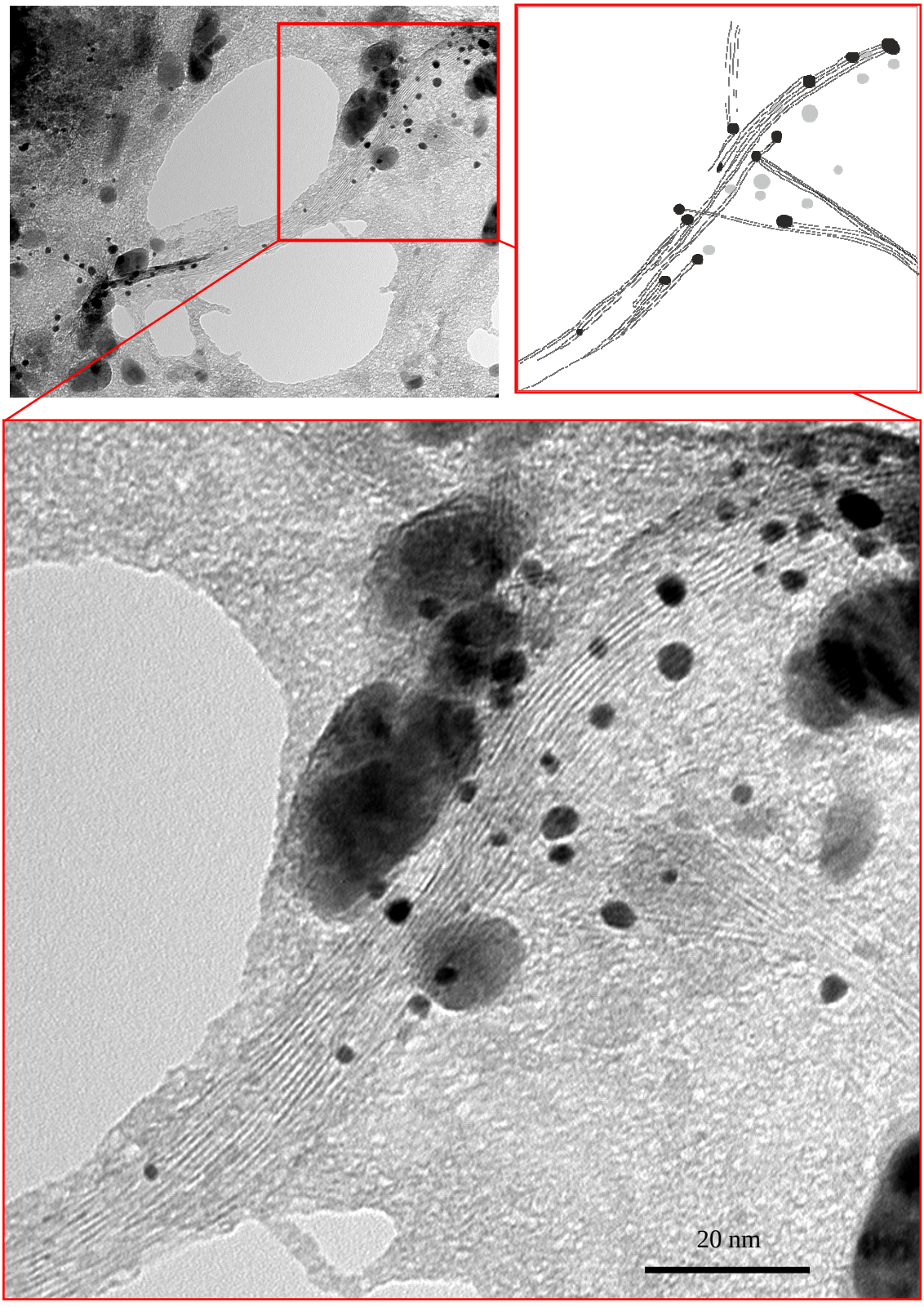


**Figure 4.13.** TEM image of AuNP bonded to CNT tips.

Also, the structure AuNP/CNT/AuNP was dispersible in aqueous solution, making possible to measure the absorption spectrum. In figure 4.14 are plotted the absorption spectra of bare AuNPs (blue line), of triton x-100 (slash-dotted brown line), triton-protected AuNPs (green dotted line), and the final complex AuNP/CNT/AuNP (red slashed line) The latter shows a red shift with respect to the spectrum of the bare gold nanoparticles. This is due to the charge transfer from metallic particle to nanotube (68, 69).

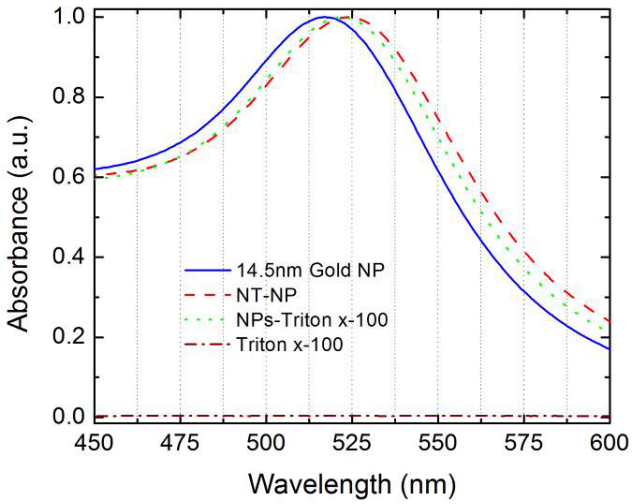


**Figure 4.14.** Absorption spectrum of AuNP/CNT/AuNP using propanediame $-CS_2$ as linking molecule.

The charge transfer from triton to nanoparticle is observed as a red shift of 5 nm, instead the shifting when the system is coupled is about 8 nm.

It is desirable to take measurements of the contact resistance between the SWNT and the AuNPs, the deposition of the electrodes over the complex is a difficult process. The particle diameter is ~15 nm, (when the bigger particle is used) this dimension is practically invisible to the electron beam apparatus. Thus, a very precise procedure must be performed in order to deposit metal electrodes and characterize the electron transport. Additionally, to get a precise measure of the contact resistance between nanoparticles and nanotube it is necessary to perform a 4 probe measurement. Thus, it is necessary to get four point contacts to gold attachment in an individual SWNT. Unfortunately, this is complicated, even more to deposit the metal electrodes with an extraordinary precision makes the challenge even more complex. Electric transport of this structure is still on development.

## 4.2 Conclusions

The coupling between carbon nanotubes and gold nanoparticles was successfully performed by using 2 different methodologies. The Cys-SWNT process produces more individual nanotubes, but unfortunately the coupling to AuNPs is very low. The S-SWNT-S procedure give a considerable number of AuNPs coupled to nanotubes. The synthesis of such complex structures is a promising step towards the controllable and specific functionalization of SWNT and its applications in photonic and electronic devices. The electron transport measurements are in progress, the structural shape of the device prevents the use of actual technologies to measure the contact resistance between nanotube and nanoparticle, so new methodologies and techniques must be developed to characterize such nano device.

To my knowledge this is the first report were gold nanoparticles are attached just to nanotube ends, using inexpensive bottom-up protocols.

Applications taking advantage of optical and electric properties of this structure are under study.

## 4.3 References


(1) Rogers, J. a; Someya, T.; Huang, Y. *Science (New York, N.Y.)*. **2010**, *327*, 1603-7.
(2) Alvi, P. A.; Lal, K. M.; Siddiqui, M. J.; Naqvi, A. H. *Indian Journal of Pure & Applied Physics*. **2005**, *43*, 899-904.
(3) Avouris, P. *Accounts of chemical research*. **2002**, *35*, 1026-34.
(4) Martel, R. *ACS nano*. **2008**, *2*, 2195-9.
(5) Appenzeller, J. *Microelectronic Engineering*. **2002**, *64*, 391-397.
(6) Avouris, P. *Accounts of Chemical Research*. **2002**, *35*, 1026-1034.
(7) McEuen, P. L.; Fuhrer, M. S. *IEEE Transactions On Nanotechnology*. **2002**, *1*, 78-85.
(8) Lu, W.; Lieber, C. M. *Nature*. **2007**, *6*, 841-850.
(9) Avouris, P. *Chemical Physics*. **2002**, *281*, 429-445.
(10) Terrones, M. *International Materials Reviews*. **2004**, *49*, 325-377.
(11) Liu, Z.; Jiao, L.; Yao, Y.; Xian, X.; Zhang, J. *Advanced materials (Deerfield Beach, Fla.)*. **2010**, 2285-2310.
(12) Baughman, R. H.; Zakhidov, A. a; Heer, W. a de *Science (New York, N.Y.)*. **2002**, *297*, 787-92.
(13) Wong, H.-S. P. *IBM Journal of Research and Development*. **2002**, *46*, 133-168.
(14) Naeemi, A.; Member, S.; Meindl, J. D.; Fellow, L. *IEEE Electron Device Letters*. **2005**, *26*, 544-546.
(15) Srivastava, N.; Banerjee, K. *Proceedings of the 21st International VLSI Multilevel Interconnect Conference (VMIC)*. **2004**, 393-398.
(16) Wang, M. S.; Wang, J. Y.; Chen, Q.; Peng, L.-M. *Advanced Functional Materials*. **2005**, *15*, 1825-1831.
(17) Maiti, A.; Ricca, A. *Chemical Physics Letters*. **2004**, *395*, 7-11.
(18) Dag, S.; Gülseren, O.; Ciraci, S.; Yildirim, T. *Applied Physics Letters*. **2003**, *83*, 3180.
(19) Tersoff, J. *Applied Physics Letters*. **1999**, *74*, 2122.
(20) Anantram, M. P.; Datta, S.; Xue, Y. *Physical Review B*. **2000**, *61*, 219-224.
(21) Leonard, F.; Tersoff, J. *Physical review letters*. **2000**, *84*, 4693-6.
(22) Seidel, R.; Liebau, M.; Duesberg, G. S.; Kreupl, F.; Unger, E.; Graham, A. P.; Hoenlein, W.; Pompe, W. *Nano Letters*. **2003**, *3*, 965-968.
(23) Song, Y.; Kang, S. J. *Journal of Vacuum Science & Technology B: Microelectronics and Nanometer Structures*. **2011**, *29*, 011011.
(24) Nosho, Y.; Ohno, Y.; Kishimoto, S.; Mizutani, T. *Nanotechnology*. **2006**, *17*, 3412-5.
(25) Giovannetti, G.; Khomyakov, P.; Brocks, G.; Karpan, V.; Brink, J. van den; Kelly, P. *Physical Review Letters*. **2008**, *101*, 4-7.
(26) Xia, F.; Perebeinos, V.; Lin, Y.-ming; Wu, Y.; Avouris, P. *Nature nanotechnology*. **2011**, *6*, 179-84.
(27) Tersoff, J. *Applied Physics Letters*. **1999**, *74*, 2122.
(28) Dag, S.; Gülseren, O.; Ciraci, S.; Yildirim, T. *Applied Physics Letters*. **2003**, *83*, 3180.
(29) Bachtold, A.; Henny, M.; Terrier, C.; Strunk, C.; Scho, C.; Forro, L. *Applied Physics Letters*. **1998**, *73*, 274-276.
(30) Avouris, P. *Proceedings of the IEEE*. **2003**, *2*, 1043-1784.
(31) Martel, R.; Wong, H.-sum P.; Chan, K.; Avouris, P. *IEEE International Electron Devices Meeting 2001*. **2001**, *1*, 159-162.
(32) Martel, R.; Derycke, V.; Lavoie, C.; Appenzeller, J.; Chan, K.; Tersoff, J.; Avouris, P. *Physical Review Letters*. **2001**, *87*, 17-20.
(33) Mokari, T.; Rothenberg, E.; Popov, I.; Costi, R.; Banin, U. *Science (New York, N.Y.)*. **2004**, *304*, 1787-90.
(34) Deng, W.-Q.; Matsuda, Y.; Goddard, W. a *Journal of the American Chemical Society*. **2007**, *129*, 9834-5.
(35) Weizmann, Y.; Lim, J.; Chenoweth, D. M.; Swager, T. M. *Nano letters*. **2010**, 0-3.
(36) Turkevich, J.; Stevenson, P. C.; Hillier, J. *Discussions of the Faraday Society*. **1951**, *11*, 55-75.
(37) Frens, G. *Colloidal and polymere science*. **1972**, *250*, 736-741.
(38) Frens, G. *Nature*. **1973**, *241*, 20-22.
(39) Link, S.; El-sayed, M. A. *Journal of Physical Chemistry B*. **1999**, *103*, 4212-4217.

(40) Turkevich, J.; Garton, G.; Stevenson, P. C. *Journal of colloidal science*. **1954**, *9*, 26-35.
(41) Turkevich, J. *Gold Bull.* **1995**, *18*, 125-131.
(42) Burdick, G. A. *Physical Review*. **1963**, *129*, 138-150.
(43) Young, J. K.; Lewinski, N. a; Langsner, R. J.; Kennedy, L. C.; Satyanarayan, A.; Nammalvar, V.; Lin, A. Y.; Drezek, R. a *Nanoscale research letters*. **2011**, *6*, 428.
(44) Ung, T.; Liz-Marzán, L. M.; Mulvaney, P. *Langmuir*. **1998**, *14*, 3740-3748.
(45) Sönnichsen, C.; Reinhard, B. M.; Liphardt, J.; Alivisatos, a P. *Nature biotechnology*. **2005**, *23*, 741-5.
(46) Au, L.; Lim, B.; Colletti, P.; Jun, Y.-S.; Xia, Y. *Chemistry, an Asian journal*. **2010**, *5*, 123-9.
(47) Leff, D. V.; Brandt, L.; Heath, J. R. *Society*. **1996**, *7463*, 4723-4730.
(48) Zijlstra, P.; Chon, J. W. M.; Gu, M. *Nature*. **2009**, *459*, 410-3.
(49) Milligan, W. O.; Morris, R. H. *Journal of the American Chemical Society*. **1964**, *86*, 3461-3467.
(50) Gerber, C. *Small (Weinheim an der Bergstrasse, Germany)*. **2008**.
(51) Liu, K.; Nie, Z.; Zhao, N.; Li, W.; Rubinstein, M.; Kumacheva, E. *Science*. **2010**, *329*, 197-200.
(52) Ghosh, S. K.; Pal, T. *Chemical Reviews*. **2007**, *107*, 4797-4862.
(53) Brust, M.; Walker, M.; Bethell, D.; Schiffrin, D. J.; Whyman, R. *Journal of chemical society, chemmical communicatioins*. **1994**, 801-802.
(54) Zhang, J.; Zou, H.; Qing, Q.; Yang, Y.; Li, Q.; Liu, Z.; Guo, X.; Du, Z. *The Journal of Physical Chemistry B*. **2003**, *107*, 3712-3718.
(55) Silva, A. M. Da; Junqueira, G. M. a.; Anconi, C. P. a.; Santos, H. F. Dos *The Journal of Physical Chemistry C*. **2009**, *113*, 10079-10084.
(56) Simmons, J. M.; Nichols, B. M.; Baker, S. E.; Marcus, M. S.; Castellini, O. M.; Lee, C.-S.; Hamers, R. J.; Eriksson, M. a *The journal of physical chemistry. B*. **2006**, *110*, 7113-8.
(57) Carroll, D.; Redlich, P.; Ajayan, P.; Charlier, J.; Blase, X.; Vita, a. De; Car, R. *Physical Review Letters*. **1997**, *78*, 2811-2814.
(58) Wold, D. J.; Frisbie, C. D. *Journal of the American Chemical Society*. **2001**, *123*, 5549-56.
(59) Nitzan, A.; Ratner, M. a *Science (New York, N.Y.)*. **2003**, *300*, 1384-9.
(60) Bumm, L. a.; Arnold, J. J.; Dunbar, T. D.; Allara, D. L.; Weiss, P. S. *The Journal of Physical Chemistry B*. **1999**, *103*, 8122-8127.
(61) Creager, S.; Yu, C. J.; Bamdad, C.; O'Connor, S.; MacLean, T.; Lam, E.; Chong, Y.; Oslen, G. T.; Luo, J.; Gozin, M.; Kayyem, J. F. *Journal of the American Chemical Society*. **1999**, *121*, 1059-1064.
(62) Shen, L.; Zeng, M.; Yang, S.-W.; Zhang, C.; Wang, X.; Feng, Y. *Journal of the American Chemical Society2*. **2010**, *132*, 11481-11486.
(63) Lang, N. D.; Avouris, P. *2Physical Review Letters*. **2000**, *84*, 385-361.
(64) Ke, S.-H.; Baranger, H. U.; Yang, W. *Physical Review B*. **2004**, *70*, 085410-085422.
(65) Tongay, S.; Senger, R. T.; Dag, S.; Ciraci, S. *Physical Review Letters*. **2004**, *93*, 136404136408.
(66) Paik, W.-kie; Han, S.; Shin, W.; Kim, Y. *Adsorption Journal Of The International Adsorption Society*. **2003**, 4211-4216.
(67) Almeida, I.; Cascalheira, A. C.; Viana, A. S. *Electrochimica Acta*. **2010**, *55*, 8686-8695.
(68) Wang, S.-C.; Chang, Y.-C.; Lien, der H.; Hsu, T.; Chang, C.-S. *Applied Physics Letters2*. **2010**, *97*, 133105.
(69) Ou, Y.-Y.; Huang, M. H. *The journal of physical chemistry. B*. **2006**, *110*, 2031-6.

# Chapter 5

*The 'bottom-up' paradigm is analogous to the way that biology so successfully works, may prove to be a solution to the technological challenges faced by the semiconductor industry, and could open up new strategies for increasing overall device density by allowing aggressive scaling in three dimensions. Charles Lieber, 2007.*

## Future work, assembling the device

### 5.1 Self-assembly

The term Self-assembly (SA) is used to describe process where the components are autonomous organized in structures or patterns without human intervention. SA processes are common throughout nature. They involve components from the molecular to the planetary scale and many different kinds of interactions (1).

SA can be classified in two main kinds, static and dynamic (1). The first one is referred to systems in equilibrium and do not dissipate energy, *e. g.* crystalline structures and lipid bilayers; the later is referred to systems in which the assembly occurs if the system is dissipating energy, the patterns formed by competition between reaction and diffusion in oscillating chemical reactions (1–4), *e. g.* the solar system and biological cells (1). The most studied SA is the static type.

In nanosciences, SA is emerging as an elegant bottom-up approach to fabricating nanostructured materials (1, 3, 5–10). Furthermore, by combining the easy and control of

self-assembly based on organic materials with the special electronic, magnetic or photonic properties of inorganic components, powerful new functionality can be achieved (10–21).

The importance of self-assembly lies on the fact that arranging nanosize materials by hand and/or scanning microscope tips is technologically impractical due to the unfeasible amount of time it would take. Therefore, SA approach manipulate the nanomaterial's properties by various treatments so that they can simply "dump" the particles in a treated area, whereby they automatically arrange themselves (1, 9–18, 22, 23). This ability is, in a sense, the basis of all nanotechnology.

In this way, one can have different functional structures performing selective chemical reactions (5, 6, 24–28). The importance of self-assembly in nanotechnology is further emphasized by the fact that the nanostructures are not compatible with the conventional methods in semiconductor processing, *e. g.*, if m-SWNTs are employed for electronic applications, we should be able to interconnect them so they can communicate to each other.

Specially, for electronic applications SA is widely used to create thin films or self assembled monolayers (SAM). SAM is an organized layer of amphiphilic molecules, in which one end of the molecule show a specific affinity for a substrate (29–33). It is possible to design organic SAM and use it as gate dielectric in transistors. In this context, diverse groups have reported a good performance of such devices, Schön and collaborators developed a SAM field-effect transistor (SAMFET) configuration, using 4, 4-biphenyldithiol as dielectric SAM (34); Halic et al, used a pentacene- (18-phenoxyoctadecyl)trichlorosilane SAM to construct a thin-film transistor (TFT) (35); reference (36) is a review of some examples of TFT using a SAM as dielectric material. Additionally, SAMFET had been designed using individual s-SWNTs as channel, improving the gate-source voltage, transconductance, hysteresis and subthreshold swing of prevoius SAMFETs without SWNTs (28, 37).

In this thesis I want to make emphasis to SA as the process to promote the addressing of a particular nanostructure into a precise position, and to support the necessary conditions for the operation of the device using weak forces, *e. i.* molecular recognition, ionic forces, hydrogen bonding, van der Waals forces, etc. Deoxyribonucleic acid (DNA) is a good option to achieve such SA.

### 5.2 Deoxyribonucleic acid (DNA)

Deoxyribonucleic acid (DNA) is a nucleic acid containing the genetic information used in the development and functioning of all known living organisms. Likewise, other DNA sequences have structural purposes, or are involved in regulating the use of this genetic information. Along with Ribonucleic acid (RNA) and proteins, DNA is one of the three major macromolecules that are essential for all known forms of life.

DNA is a long polymer made from repeating units called nucleotides(38) (39–41). As first discovered by James D. Watson and Francis Crick (38), the structure of DNA comprises two helical chains each coiled round the same axis, and each with a pitch of 34 Ångstroms and a radius of 10 Ångstroms (38).

In living organisms DNA does not usually exist as a single molecule, but instead as a pair of molecules that are held tightly together (38). These two long strands are arranged in a shape of a double helix. The nucleotide repeats contain both the segment of the backbone of the molecule, which holds the chain together, and a nucleobase, which interacts with the other DNA strand in the helix. A nucleobase linked to a sugar is called a nucleoside (39–41) and a base linked to a sugar and one or more phosphate groups is called a nucleotide (39–41).

The backbone of the DNA strand is made from alternating phosphate and sugar residues (42) The sugar in DNA is 2-deoxyribose, which is a pentose sugar. The sugars are joined together by phosphate groups that form phosphodiester bonds between the third and fifth carbon atoms of adjacent sugar rings. These asymmetric bonds mean a strand of DNA

has a direction. In a double helix the direction of the nucleotides in one strand is opposite to their direction in the other strand: the strands are antiparallel. The asymmetric ends of DNA strands are called the 5′ (five prime) and 3′ (three prime) ends, with the 5' end having a terminal phosphate group and the 3' end a terminal hydroxyl group, as is observed in the figure 5.1 (39–44).

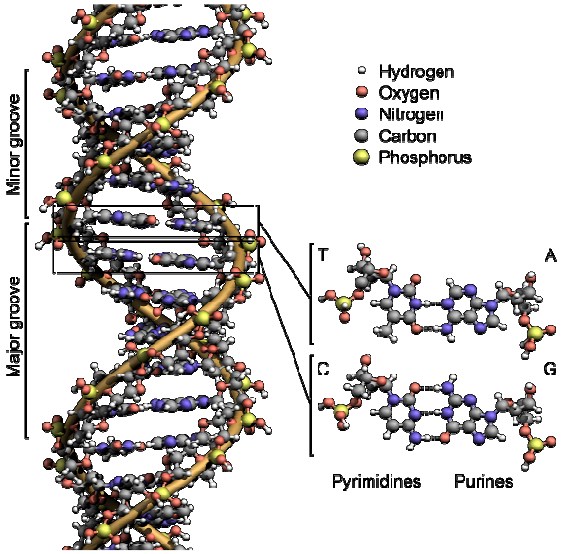


**Figure 5.1.** Structure of DNA forming its characteristic double helixm. All conforming atoms are represented as coloured spheres. Taken form (43)

The DNA double helix is stabilized primarily by hydrogen bonds between nucleotides and base-stacking interactions among the aromatic nucleobases (44). The four bases found in DNA are adenine (A), cytosine (C), guanine (G) and thymine (T). These four bases are attached to the sugar/phosphate to form the complete nucleotide, as is shown in the figure 5.1.

### 5.3 DNA in self assembly

To obtain a high impact in the construction of devices, exploiting SA approach, relays in the placement of nanostructures, nanotubes in this case, into an ordered and pre-defined pattern, location or sequence. In this context biomolecules are the most widely used agents to address the placement, specifically Biotin, Streptavidin and DNA. They had probed to be a good agents for SA, Lyonnais and co-workers selectively place a strepatavidin functionalized SWNT (strep-SWNT) over a pre-designed Y-shaped DNA pattern, resembling a FET geometry, figure 5.2 (45–47).

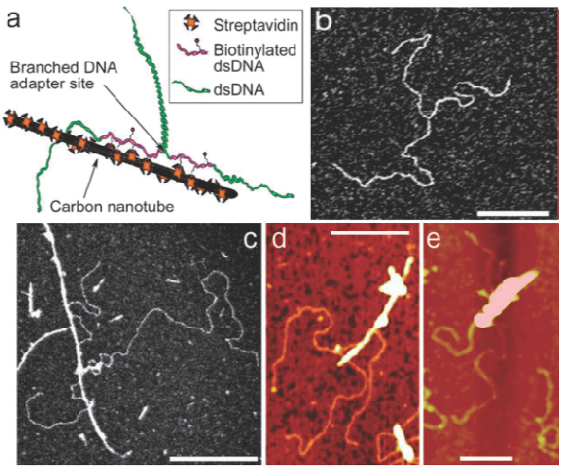


**Figure 5.2** DNA–SWNT conjugates. Schematic diagram of the complexes. (a). TEM image of the three-branched DNA structure. (b). TEM imaging (c) the DNA template with streptavidin and SWNTs. (d, e) AFM images. Scale bars: 250 nm. Modified from (45).

In addition to the assembly properties of DNA, Lee et al.(48) described a new form of DNA, metallized-DNA (M-DNA), in which the imino proton of the DNA base-pairs is replaced by a $Zn^{2+}$, $Ni^{2+}$, or $Co^{2+}$ ion. They show that M-DNA behaves like a molecular wire. In the same way, Braun and collaborators (49, 50) demonstrate the successful deposition of Silver and Gold. The deposition of Pd (51), Au (52), and Pt (53) on DNA have also been investigated as a potential approach for creating conductive nanowires. Monson et al. (54) described the construction of DNA-templated Cu nanowires successfully constructed DNA templated Ag nanowires by electroless deposition, producing nanowires ~100 nm thick and 15 µm long. Keren and Sivan (19, 50) recently reported protecting specific regions of DNA molecules from metal deposition by associating proteins along selected sections of the DNA. The ability to control metallization spatially provides an important technological advantage for the assembly of functional nanocircuits (13).

Keren and co-workers realized the possibility to use these properties to assembly a FET (21). They developed a scaffold for self-assemble the CNTFET using DNA and a homologous DNA complement Figure 5.3. They used the homologous recombinant of the double strand DNA (ds-DNA) functionalized with the protein RecA (i) and (ii), RecA act as anchor point for biotin, additionally they used Strep-SWNT localized at a desired address on a DNA scaffold using homologous recombination by the RecA protein (fig. (iii), finally the metalization of DNA, with the RecA doubling as a sequence-specific resist (iv), led to the formation of extended conductive wires that electrically contact the SWNT (v). The conduction through the SWNT was controlled by a voltage applied to the substrate supporting the structure.

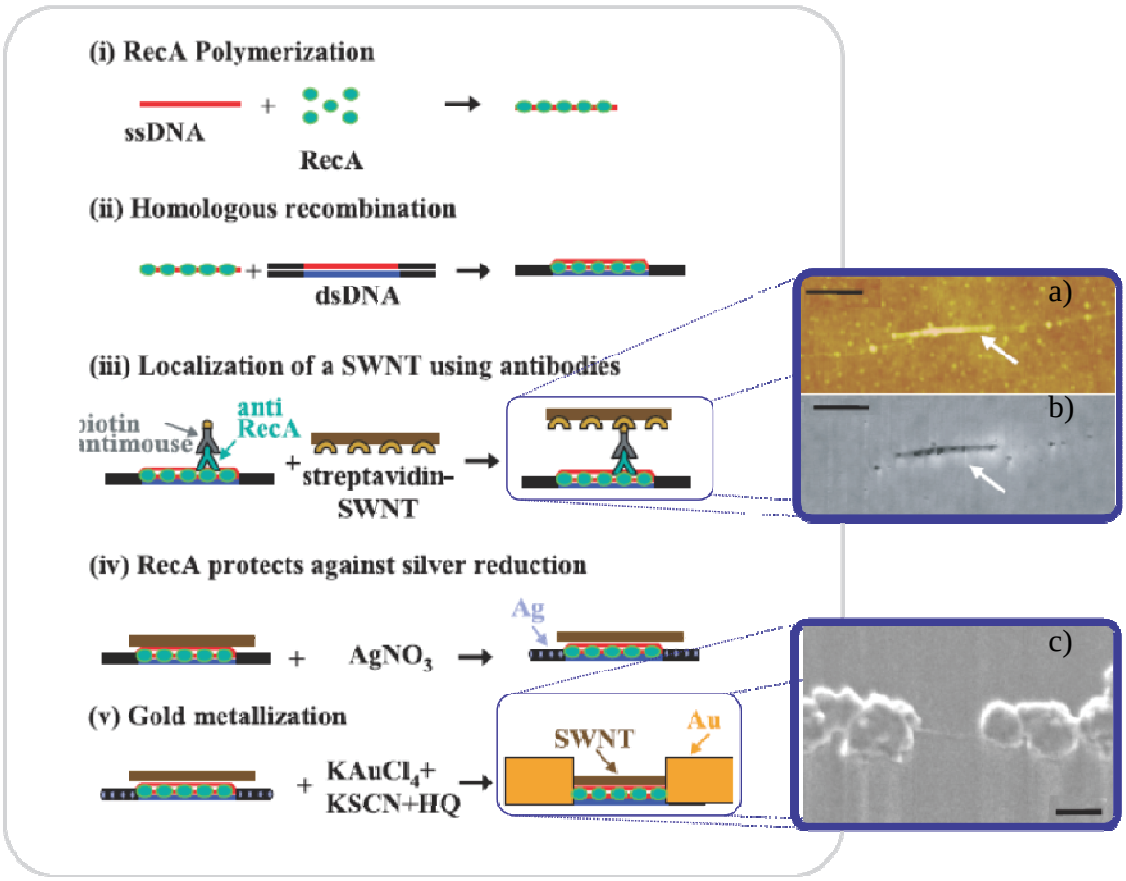


**Figure 5.3,** Self assembly of CNTFET using DNA as template. (a) AFM image of a streptavidin-coated SWNT (white arrow) bound to a 500-base-long nucleoprotein filament localized on a DNA scaffold molecule. (b) A scanning conductance image of the same region as in (a). The conductive SWNT (white arrow) yields a considerable signal whereas the insulating DNA is hardly resolved. Bar, 300 nm. (c) DNA-templated carbon nanotube FET and metallic wires contacting it. SEM images of SWNTs contacted by self-assembled DNAtemplated gold wires Bar, 100 nm. Modified from (21)

The device performance was not outstanding, but the proof of concept was demonstrated: it is possible to SA a full functional transistor. It is achievable to improve the gate shape using a GAA configuration, instead a back-gate (Chapter 3). Additionally, the electrode-nanotube contact was not the best, it is possible to improve it linking covalently SWNT and electrodes (chapter 4), additionally if Pd is used instead of gold the performance should increase considerably (chapter 4). Even more, today it is possible to use more complex configurations for DNA, to design totally the FET, including the gate. In this context DNA nanotechnology is playing a big role.

### 5.4 DNA-Origami (DNA Nanotechnology)

The concept to design and manufacture of artificial nucleic acid structures for technological uses was first introduced by Nadrian Seeman in 1981 (55, 56), where he visualized 3 dimensional (3D) DNA lattices able to support other molecules or structures. He believed that immobile nucleic acid junctions could be created by properly designing the strand sequences to remove symmetry in the assembled molecule, and that these immobile junctions could in principle be combined into rigid crystalline lattices, he published a theoretical study of such structures (55) and years later he demonstrated the synthesis of the a cube made of DNA (57), he and their collaborators succeed in the design and construction of a truncated octahedron (58). In 1998 he developed crystalline arrangement of 2D lattices (6). By 2004 Rothemund performed the next step, DNA origami, this technique enable to design and synthesize complex 2D shapes (59, 60), the desired shape is computationally drawn, the design is then fed into a computer program that calculates the placement of individual staple strands. Each staple binds to a specific region of the DNA template (he used a circular genomic DNA from the

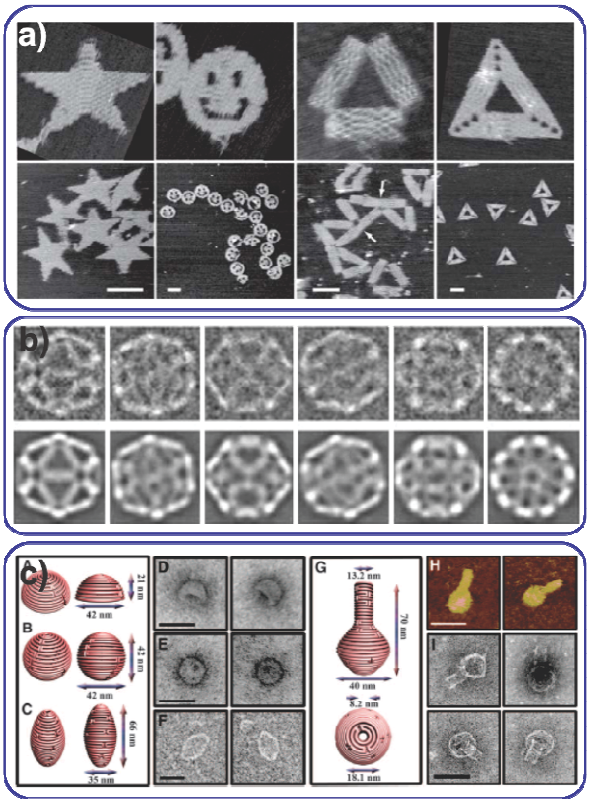


Figure 5.4, a) Rothmound DNA origami arrenged in 2D structures, scale bars 100 nm. b) Zhang 3D structures, Cryogenic transimission electron microscopy analysis of DNA icosahedron. Comparison of class average of particle images with similar views (Upper) and the corresponding computer- generatedmodelprojections (Lower). icosahedron diameter ~25 nm.. c) Han DNA nanostructures DNA nanostructures with complex 3D curvatures. (A) Schematic representation of the hemisphere. (B) sphere. (C) ellipsoid. (D)TEM of the hemisphere, (E) sphere and. (F) ellipsoid. (G) Schematic representation of the nanoflask. (H) AFM images. Scale bar is 75 nm. (I) TEM images of the nanoflask, TEM Scale bars are 50 nm. Taken from (60)(61)(63)

virus M13mp18 as scaffold or template), and thus due to base pairing recognition, the necessary sequences of all staple strands are known and displayed. The DNA is mixed, then heated and cooled. As the DNA cools, the various staples pull the long strand into the desired shape. Arranging the base-pairs in a DNA origami the final structure is more rigid, it enables the construction of 3D structures, in this context, Zhang and co-workers were able to design and synthesize DNA icosahedrons and truncated icosahedrons (61), Douglas et al, designed a different software, increasing the number of successful 2D and 3D structures synthesized (62) and making more friendly the programming, recently Han and collaborators reported the synthesis of 3D spherical shells, ellipsoidal shells, and a nanoflasks (63)

DNA origami opened the door to completely new applications, just to mention some, Voigt and collaborators performed single molecule reactions using a 2D origami template to address their reactants (16), Liu and co-workers demonstrated that it is possible to metalize DNA origami structures (64, 65), Numajiri et al, published the selective location and/or removal of proteins over a DNA origami ribbon (66), Stain and co-workers used

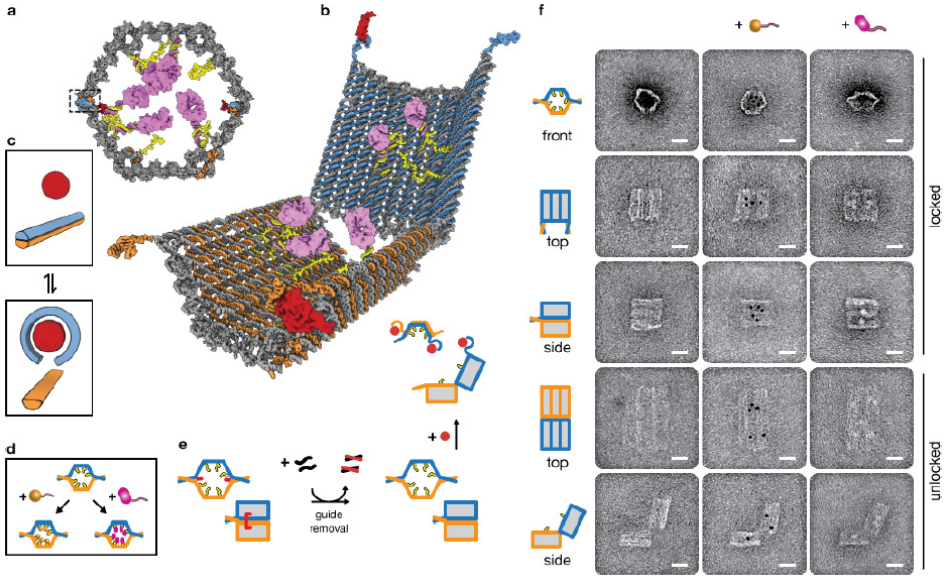


**Figure 5.5** Design and TEM analysis of an aptamer-gated DNA nanorobot. The device transitions from its closed state (a) to open (b) when aptamer-based locks are displaced by binding to an antigen key (c). Payloads such as gold nanoparticles and antibody fragments (d) can be loaded. Removable guide staples (e) aid in initial folding to high yield. Electron micrographs show the nanorobot with different payloads and conformations. Scale bars 20 nm. Taken from (68).

DNA origami to arrange fluorophores that transport excited-state energy from an input dye to an output dye (67). Recently Douglas and co-workers at Harvard University's Wyss Institute used DNA origami to build a "nanorobot", they used a clam-shape cage to holds anti-cancer drugs inside, these drugs are enclosed until a leukemia cell "un-locks" the cage, releasing the drug, attacking and killing the leukemia cell (68), see figure 5.5.

DNA origami also had played with CNTs, they had been used to selective cross a couple of SWNTs in a 2D DNA array (69, 70), Maune and collaborators used this × shape to interconnect s-SWNT and a m-SWNT in a FET configuration, the m-SWNT act as gate to trigger the device. Both reports agree that the successful coupling of nanotubes was low. Additionally, the large scale synthesis of origami arrays always presented defects. Until now, this technique is dominantly probabilistic; it is not possible to ensure the successful coupling of 100 % of the devices.

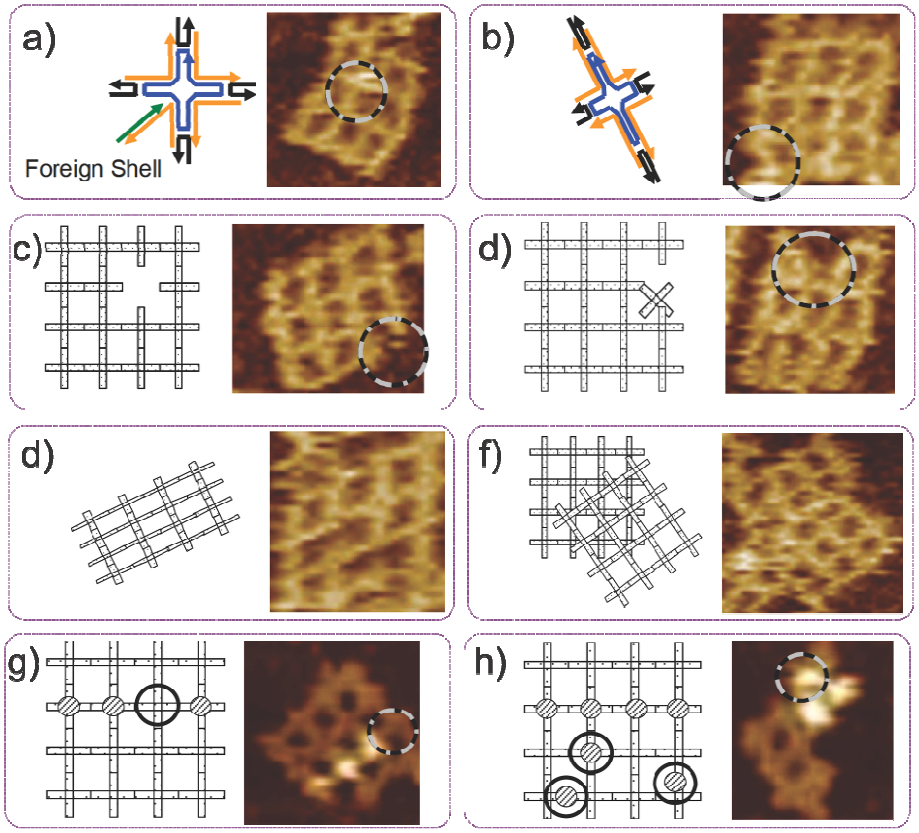


**Figure 5.5** Example images of AFM-observable defects at the tile and grid levels. (a) Mismatched or foreign tile defect, (b) tile distortion defect, (c) missing tile defect, (d) broken arm tile defect, (e) grid distortion defect, (f) grid aggregation defect, (g) missing functionalization site defect and (h) defect caused non specific functionalization. Modified from (71).

In 2008 International Test Conference realized in Santa Clara, California, Mao and co-workers from Duke University presented a complete analysis of structural defects reported of 2D DNA SA arrays (71). They classified defects as being either structural defects that can currently be observed, or anticipated defects that are expected to occur in future nanostructures. They had related these defects to circuit-level fault models and predicted their likely impact on the behaviour of logic gates. The image 5.5 show some defects analysed in Mao's report.

Despite of this, world wide research groups continue developing techniques to use DNA origami to apply it directly in electronic devices (18, 23, 45, 62, 67, 69, 71–77).

### 5.5 Perspectives: How to assemble our device…

Until now, I successful sorted individual **s-SWNT** and m-SWNTs, with the objective to use them in electronic applications, taking advantage of their physical properties. Additionally I have exploited the SWNT shape to growth **dielectric material** around it, using the small body of the SWNT to make the most aggressive shrinking of the device; I achieved this using Sol-Gel process, a bottom-up approach. Finally, I attached covalently **metallic moieties to SWNT ends**, expecting to improve the electric resist between SWNT and electrodes, once again, using a bottom-up approach. These results should be merged, in order to continue with the construction of the device, *i. e.* coating an individual s-SWNT with the dielectric material and attach covalently the metallic moieties to nanotube ends, as is exemplified in figure 5.6, and always using a bottom-up process. Once obtained this structure, the SA can proceed.

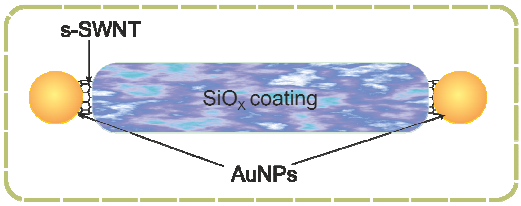


**Figure 5.6.** Schematic representation of the coated s-SWNT & AuNP/NT/AuNP structures merged.

To address the assembly biomolecules for self recognition may be used, like Streptavidin/ Avidin and Biotin, as had been used in previous reports for assembly of nanostructures

(5, 19, 27, 46, 66, 74, 78–81). In this context, Biotin can be attached to silica coating, by means of APTES, this procedure is widely used for protein immobilization on silica surfaces for biological tests (26, 82–86). Briefly explained, the silica surface is reactivated using hydrofluoric acid (HF) 0.1 mM, so, 5 mg of $SiO_X$-SWNT are dispersed in EtOH:$H_2O$ [9:1] solution, pH is adjusted to 2 adding HF solution under sporadic ultrasonication to avoid aggregation (fig. 5.6 (1)). Immediately, 5 mL (EtOH) of APTES 5 mM is added drop wise (fig. 5.6 (2)). Afterwards, 1 mL of Biotin (10 mM), 1 mL of EDC (2mM) and 1 mL of s-NHS (5 mM) water solutions are added. The solution is let it react for 2 hours, sporadic sonication is done to avoid aggregation. Finally, the dispersion is centrifuged at 2800 *g*, the supernatant is discarded. Precipitate is resuspended in fresh DI water, centrifugation and redispersion is repeated twice (fig. 5.6 (3)).

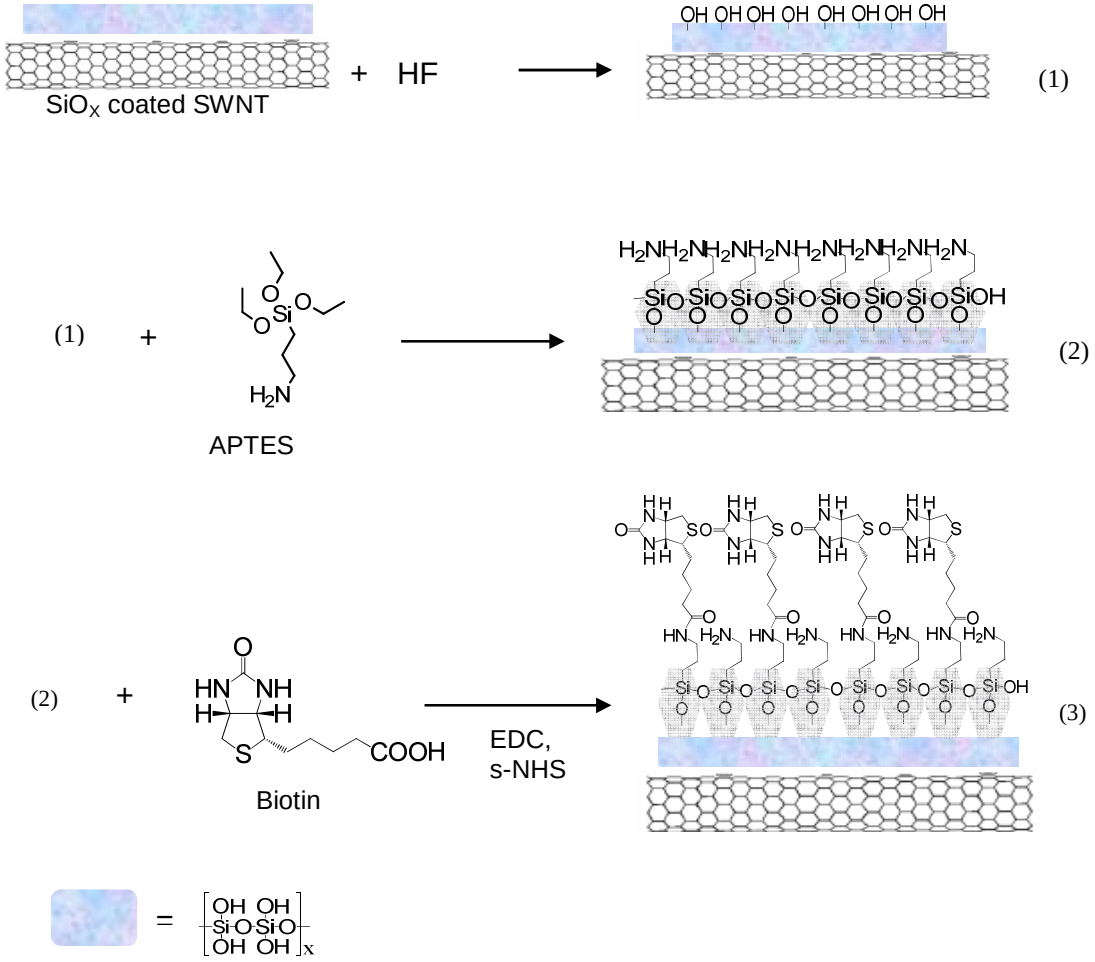


**Figure 5.7.** Schematic representation of Biotin attachment over nanotube silica coating

Once Biotin is attached to the nanotube structure, it can be placed over a Streptavidin or Avidin functionalized substrate, for a SA device, the substrate can be a DNA Origami. Some groups had reported the successfully functionalization of DNA with proteins like Streptavidin or Avidin, (6, 16, 18, 19, 22, 23, 46, 66, 74, 87–93).

The functionalization of the DNA prevents the metallic growth, in this way it is possible to selectively grow metal on the electrodes and gate zone, figure 2.7 exemplify the possible design for assembly.

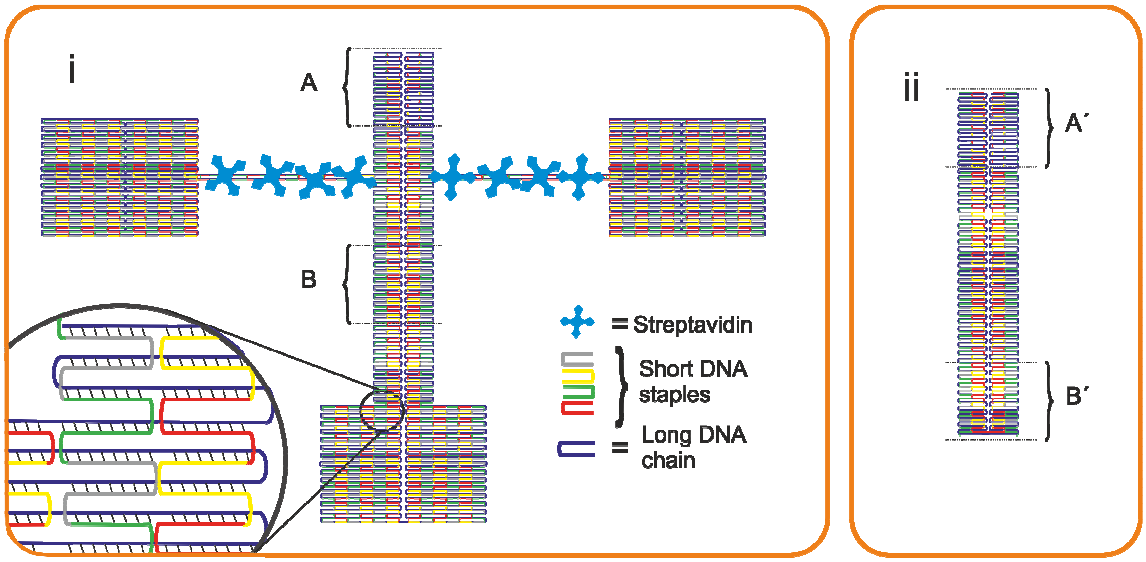


**Figure 5.8** Proposed DNA origami templates to ensemble the transistor. (i) Main scaffold functionalized with Streptavidin or Avidin, where is placed the structure functionalized with Biotin, the black circle shows an enlargement of the DNA folding. (ii) DNA scaffold for half top gate electrode.

The main DNA template is shown in (i), in which the blue crosses represent Streptavidin protein. The Strepatvidine decorating the DNA prevents the metal growth, in this way it is possible to selectively growth metal in the “naked” DNA(5, 13, 19, 51, 54, 90, 94, 95). Note that there is a path free of Streptavidin just in the middle, here will be grown the gate electrode. Additionally a second DNA template is designed (ii), the function of this ribbon-like origami, is to cover the top part of the dielectric gate, in such way to form surround the dielectric completely with metal. Both templates are designed with complementary connectors in the extremes (A complemented with A’, and B with B’),

this connectors will act as a singular Velcro tapes, in which A can be “glued” just to A’ and B can be glued just with B’.

In general the device assembling is shown in the figure 5.9, and should proceeds as follows, the Streptavidin-DNA structure from fig. 5.8 (i) is dispersed over a substrate (preferentially insulating) (5.9 (i)). The SWNT structure is located over the DNA template (ii). Streptavidine-Biotine interaction helps to locate the tube in the precise position over the DNA scaffold (iii). Afterwards, the second DNA structure (figure 5.8 (ii)) is dripped in the substrate, the ribbon-like structure covers the dielectric material, as is shown in fig. 5.9 (iv). The complementary connectors A-A’ and B-B’ are bonded together by self-recognition, covering by the top and bottom of the $SiO_X$-SWNT structure. These “Velcro-like” connectors could be complementary DNA strands.

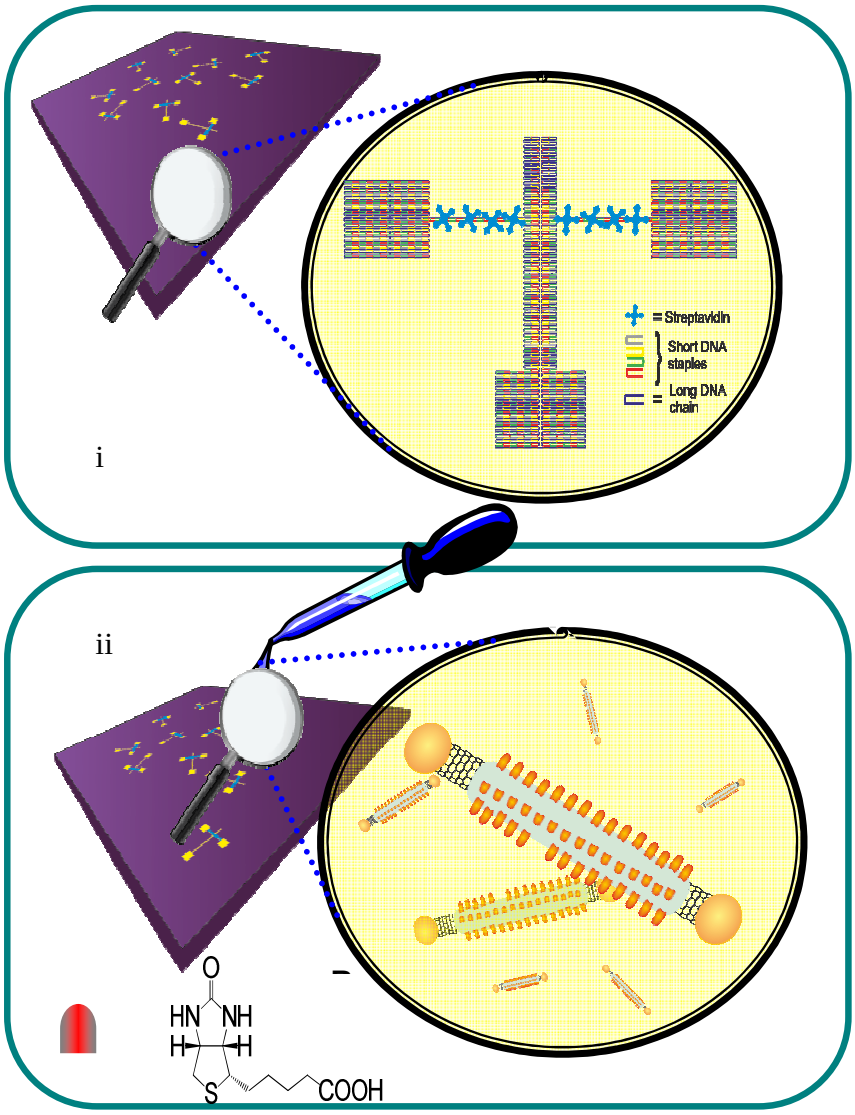


Finally the metallization and growth of particles over the DNA can be performed. The metallic particles grow coalescing and forming a continuous and conductive wires (v). The wires will act as electrodes or

connectors between devices.

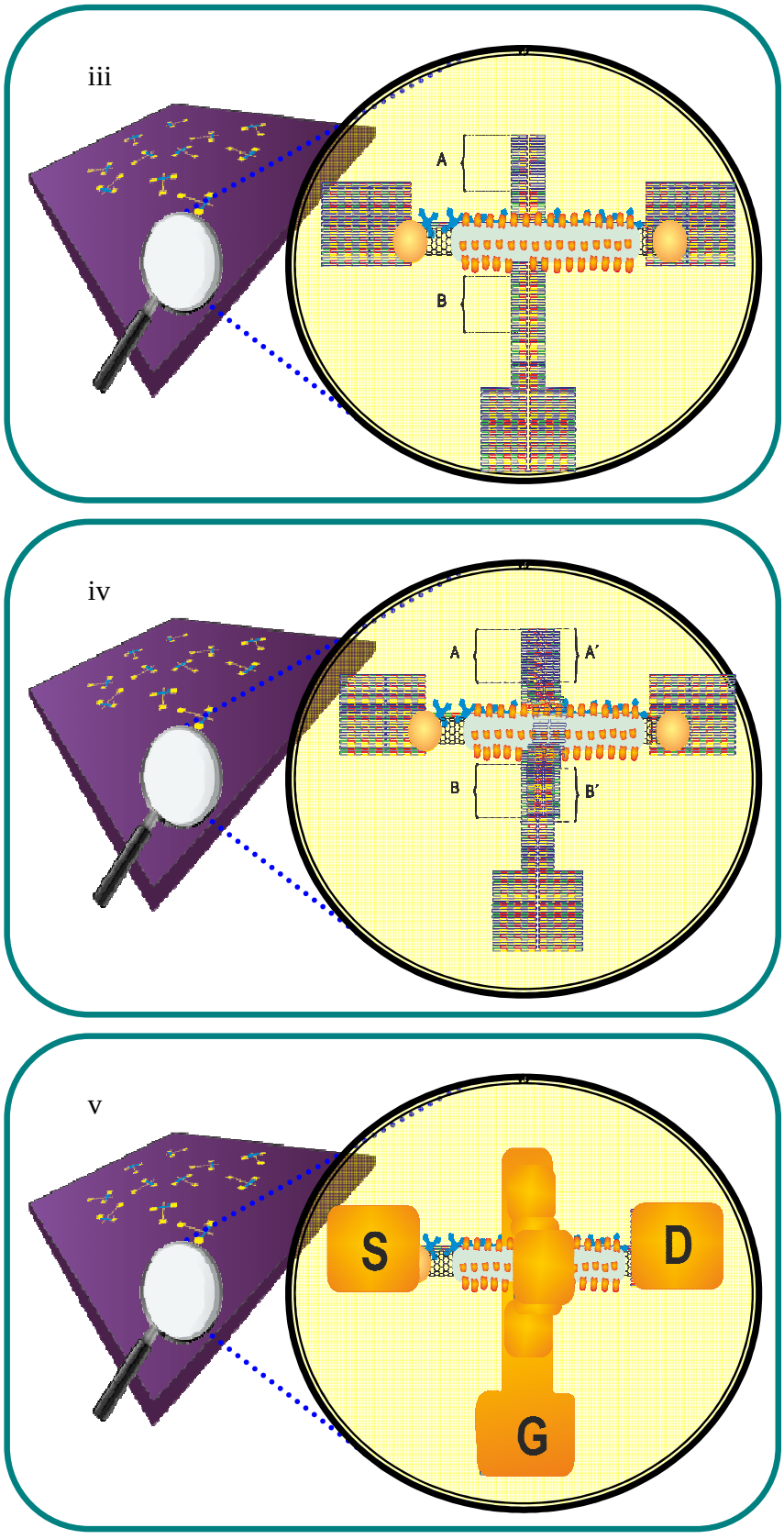


**Figure 5.9**. Schematic images of how could proceed the final assembly for the device. (i) DNA template over a insulating substrate. (ii) a drop of $SiO_X$-AuNP/NT/AuNP functionalized with Biotin over the DNA template. (iii) Streptavidin-Biotin addresses the structure over the DNA scaffold. (iv) The second DNA structure is added. This is placed over the SWNT structure and it is located by self recognition of A-A' and B-B' connectors. (v) Metal is grown over the not functionalized DNA, metal grows over and bellow the SWNT structure, together with the metal particles, and construct the connecting wires.

### 5.6 Conclusions

I propose a new methodology to construct nanodevices, using bottom-up procedures.

In this work I have developed the first steps for a new and probably better device compared with current Silicon transistors, these steps are: the selection of semiconducting material (semiconductor single walled carbon nanotube); the synthesis of dielectric gate and the develop of an optimal contact between nanotube and electrodes.

These methodologies are cheaper than the actual top-down procedures used to fabricate electronic devices.

All the process can be improved in:

- Semiconductor material. Increase the purity and quantity on the sorting of SWNT, may be using chromatography processes (96).
- Dielectric gate. The use of better dielectrics as $HfO_2$ (97, 98) or $Al_2O_3$ (99) could improve the device performance
- Ohmic contacts. The use of other metals, like palladium (100, 101), also helps to improve the device performance.
- Device dimensions: The SWNT length in this work is around 200-1000 nm, recently it has been demonstrated CNT-FETs with a channel length of 9 nm (102).

If the operation of this device is demonstrated, it could be possible to increase the complexity of DNA origami template in order to self-assemble logic devices.

## 5.7 References


(1) Whitesides, G. M.; Grzybowski, B. *Science (New York, N.Y.)*. **2002**, *295*, 2418-21.
(2) Hess, B. *Die Naturwissenschaften*. **2000**, *87*, 199-211.
(3) Lopes, W. A.; Jaeger, H. M. *Nature*. **2001**, *414*, 735-738.
(4) Hab-er, F.; Ges-ellschaft, D. M. P.-nck *Physical Review*. **1990**, *65*.
(5) Yan, H.; Park, S. H.; Finkelstein, G.; Reif, J. H.; LaBean, T. H. *Science (New York, N.Y.)*. **2003**, *301*, 1882-4.
(6) Winfree, E.; Liu, F.; Wenzler, L. a; Seeman, N. C. *Nature*. **1998**, *394*, 539-44.
(7) Black, C. T. *Science*. **2012**, *1131*.
(8) Boal, A. K.; Ilhan, F.; Derouchey, J. E.; Thurn-albrecht, T.; Russell, T. P.; Rotello, V. M. *Nature*. **2000**, *404*, 746-748.
(9) Philp, D.; Stoddart, J. F. *1Angewandte Chemie (International ed. in English)*. **1996**, *33*, 1159-1196.
(10) Drain, C. M. *Proceedings of the National Academy of Sciences of the United States of America*. **2002**, *99*, 5178-82.
(11) Wu, L.-Q.; Payne, G. F. *Trends in biotechnology*. **2004**, *22*, 593-9.
(12) Strle, J.; Vengust, D.; Mihailovic, D. *Nano letters*. **2009**, *9*, 1091-5.
(13) LaBean, T. H.; Li, H. *Nano Today*. **2007**, *2*, 26-35.
(14) Cao, Q.; Xia, M.-G.; Shim, M.; Rogers, J. A. *Advanced Functional Materials*. **2006**, *16*, 2355-2362.
(15) Tseng, R. J.; Tsai, C.; Ma, L.; Ouyang, J.; Ozkan, C. S.; Yang, Y. *Nature nanotechnology*. **2006**, *1*, 72-7.
(16) Voigt, N. V.; Tørring, T.; Rotaru, A.; Jacobsen, M. F.; Ravnsbaek, J. B.; Subramani, R.; Mamdouh, W.; Kjems, J.; Mokhir, A.; Besenbacher, F.; Gothelf, K. V. *Nature nanotechnology*. **2010**, *5*, 200-3.
(17) Lehn, J.-M. *Proceedings of the National Academy of Sciences of the United States of America*. **2002**, *99*, 4763-8.
(18) Saccà, B.; Niemeyer, C. M. *Chemical Society reviews*. **2011**.
(19) Keren, K.; Krueger, M.; Gilad, R.; Ben-Yoseph, G.; Sivan, U.; Braun, E. *Science (New York, N.Y.)*. **2002**, *297*, 72-5.
(20) Braun, E.; Eichen, Y.; Sivan, U.; Ben-Yoseph, G. *Nature*. **1998**, *391*, 775-8.
(21) Keren, K.; Berman, R. S.; Buchstab, E.; Sivan, U.; Braun, E. *Science (New York, N.Y.)*. **2003**, *302*, 1380-2.
(22) Tørring, T.; Voigt, N. V.; Nangreave, J.; Yan, H.; Gothelf, K. V. *Chemical Society reviews*. **2011**.
(23) Nangreave, J.; Han, D.; Liu, Y.; Yan, H. *Current opinion in chemical biology*. **2010**, *14*, 608-615.
(24) Llanes-Pallas, A.; Palma, C.-A.; Piot, L.; Belbakra, A.; Listorti, A.; Prato, M.; Samorì, P.; Armaroli, N.; Bonifazi, D. *Journal of the American Chemical Society*. **2009**, *131*, 509-20.
(25) Salant, A.; Amitay-Sadovsky, E.; Banin, U. *Journal of the American Chemical Society*. **2006**, *128*, 10006-7.
(26) Daniel, M.-C.; Astruc, D. *Chemical reviews*. **2004**, *104*, 293-346.
(27) Hazani, M.; Hennrich, F.; Kappes, M.; Naaman, R.; Peled, D.; Sidorov, V.; Shvarts, D. *Chemical Physics Letters*. **2004**, *391*, 389-392.
(28) Auvray, S.; Derycke, V.; Goffman, M.; Filoramo, A.; Jost, O.; Bourgoin, J.-P. *Nano letters*. **2005**, *5*, 451-5.
(29) Aviram, A. *Chemical Physics Letters*. **1974**, *29*, 277-283.
(30) Sigal, G. B.; Bamdad, C.; Barberis, a; Strominger, J.; Whitesides, G. M. *Analytical chemistry*. **1996**, *68*, 490-7.
(31) Zhou, C.; Deshpande, M. R.; Reed, M. A.; Tour, J. M. *American Institute of Physics*. **1997**, *71*, 611-613.
(32) Strong, L.; Whitesides, G. M. *Langmuir*. **1988**, *4*, 546-558.
(33) Möbius, D. *Berichte der Bunsengesellschaft für physikalische Chemie*. **1978**, *82*, 848-858.
(34) Schön, J. H.; Meng, H.; Bao, Z. *Nature*. **2001**, *413*, 713-6.
(35) Halik, M.; Klauk, H.; Zschieschang, U.; Maisch, S.; Effenberger, F.; Dehm, C.; Schu, M.; Brunnbauer, M.; Stellacci, F. *Nature*. **2004**, *431*, 963-966.
(36) DiBenedetto, S. a.; Facchetti, A.; Ratner, M. a.; Marks, T. J. *Advanced Materials*. **2009**, *21*, 1407-1433.

(37) Weitz, R. T.; Zschieschang, U.; Forment-Aliaga, A.; Ka, D.; Burghard, M.; Kern, K.; Klauk, H.; Kälblein, D. *Nano letters*. **2009**, *9*, 1335-40.
(38) Watson, J. M.; Crick, F. H. C. *Nature*. **1953**, *171*, 737-738.
(39) Neidle, S. *Principles of nucleic acid structure*; Elsevier: London, UK, 2007.
(40) Butler, J. M. *Forensic DNA Typing*; Elsevier: San Diego, Ca., 2001.
(41) Alberts, B.; Johnson, A.; Lewis, J.; Raff, M.; Roberts, K.; Walter, P. *Molecular Biology of the cell*; 4th ed.; Garland Science: New York, 2001.
(42) Schneider, B.; Neidle, S.; Berman, H. M. *Biopolymers*. **1998**, *42*, 113-124.
(43) Zapheris *www.wikipedia.org*. **2011**.
(44) Yakovchuk, P.; Protozanova, E.; Frank-Kamenetskii, D. F. *Nucleic acids research*. **2006**, *34*, 564-574.
(45) Lyonnais, S.; Chung, C.-L.; Goux-Capes, L.; Escudé, C.; Piétrement, O.; Baconnais, S.; Cam, E. Le; Bourgoin, J.-P.; Filoramo, A. *Chemical Communications*. **2009**, 683-5.
(46) Lyonnais, S.; Goux-Capes, L.; Escudé, C.; Cote, D.; Filoramo, A.; Bourgoin, J.-P. *Small (Weinheim an der Bergstrasse, Germany)*. **2008**, *4*, 442-6.
(47) Goux-capes, L.; Filoramo, A.; Cote, D.; Bourgoin, J.-philippe; Patillon, J.-nöel *American Institute of Physics*. **2004**, 17-25.
(48) Lee, J. S.; Latimer, L. J. P.; Reid, S. *Biochemistry and cell biology*. **1993**, *71*, 162-168.
(49) Braun, E.; Eichen, Y.; Sivan, U.; Ben-Yoseph, G. *Nature*. **1998**, *391*, 775-8.
(50) Keren, K.; Soen, Y.; Yoseph, G.; Gilad, R.; Braun, E.; Sivan, U.; Talmon, Y. *Physical Review Letters*. **2002**, *89*, 3-6.
(51) Richter, B. J.; Seidel, R.; Kirsch, R.; Mertig, M.; Pompe, W.; Plaschke, J.; Schackert, H. K. *Advanced Materials*. **2000**, 507-510.
(52) Patolsky, F.; Weizmann, Y.; Oleg, L.; Itamar, W. *Advanced Materials*. **2002**, *41*, 2323-2327.
(53) Ford, W. E.; Harnack, O.; Yasuda, a.; Wessels, J. M. *Advanced Materials*. **2001**, *13*, 1793-1797.
(54) Monson, C. F.; Woolley, A. T. *Nano letters*. **2003**, *3*, 359-363.
(55) Seeman, N. C. *Journal of theoretical Biology*. **1982**, *99*, 237-247.
(56) Seeman, N. C.; Rosenberg, J. M.; Rich, A. *Proceedings of the National Academy of Sciences of the United States of America*. **1976**, *73*, 804-8.
(57) Chen, J. H.; Seeman, N. C. *Nature*. **1991**, *350*, 631-3.
(58) Zhang, Y.; Seeman, N. C. *Journal of the American Chemical Society*. **1994**, *116*, 1661-1669.
(59) Rothemund, P. W. K.; Papadakis, N.; Winfree, E. *PLoS biology*. **2004**, *2*, e424.
(60) Rothemund, P. W. K. *Nature*. **2006**, *440*, 297-302.
(61) Zhang, C.; Su, M.; He, Y.; Zhao, X.; Fang, P.-an; Ribbe, A. E.; Jiang, W.; Mao, C. *Proceedings of the National Academy of Sciences of the United States of America*. **2008**, *105*, 10665-9.
(62) Douglas, S. M.; Dietz, H.; Liedl, T.; Högberg, B.; Graf, F.; Shih, W. M. *Nature*. **2009**, *459*, 414-8.
(63) Han, D.; Pal, S.; Nangreave, J.; Deng, Z.; Liu, Y.; Yan, H. *Science*. **2011**, *332*, 342-346.
(64) Liu, J.; Geng, Y.; Pound, E.; Gyawali, S.; Ashton, J. R.; Hickey, J.; Woolley, A. T.; Harb, J. N. *ACS nano*. **2011**, *5*, 2240-7.
(65) Schreiber, R.; Kempter, S.; Holler, S.; Schüller, V.; Schiffels, D.; Simmel, S. S.; Nickels, P. C.; Liedl, T. *Small*. **2011**, n/a-n/a.
(66) Numajiri, K.; Kimura, M.; Kuzuya, A.; Komiyama, M. *Chemical communications (Cambridge, England)*. **2010**, *46*, 5127-9.
(67) Stein, I. H.; Steinhauer, C.; Tinnefeld, P. *Journal of the American Chemical Society*. **2011**, *133*, 4193-5.
(68) Douglas, S. M.; Bochelet, I.; Church, G. M.; Bachelet, I. *Science (New York, N.Y.)*. **2012**, *335*, 831-834.
(69) Eskelinen, A.-P.; Kuzyk, A.; Kaltiaisenaho, T. K.; Timmermans, M. Y.; Nasibulin, A. G.; Kauppinen, E. I.; Törmä, P. *Small*. **2011**, *7*, 746-750.
(70) Maune, H. T.; Han, S.-P.; Barish, R. D.; Bockrath, M.; Iii, W. a G.; Rothemund, P. W. K.; Winfree, E. *Nature nanotechnology*. **2010**, *5*, 61-6.
(71) Mao, V.; Dwyer, C.; Chakrabarty, K. In *2008 IEEE International Test Conference*; Ieee, 2008; pp. 1-10.
(72) Lin, C.; Liu, Y.; Yan, H. *Biochemistry*. **2009**, *48*, 1663-74.
(73) Ding, B.; Wu, H.; Xu, W.; Zhao, Z.; Liu, Y.; Yu, H.; Yan, H. *Nano letters*. **2010**, 0-4.

(74) Michelotti, N.; Johnson-Buck, A.; Manzo, A. J.; Walter, N. G. *Wiley interdisciplinary reviews. Nanomedicine and nanobiotechnology*. **2011**, *4*.
(75) Tan, S. J.; Campolongo, M. J.; Luo, D.; Cheng, W. *Nature nanotechnology2*. **2011**, *6*, 268-276.
(76) Penzo, E.; Wang, R.; Palma, M.; Wind, S. J. *Journal of Vacuum Science & Technology B: Microelectronics and Nanometer Structures2*. **2011**, *29*, 205-210.
(77) Hu, S.; Cho, J.-H.; Gracias, D. H. *Three-Dimensional Nanoarchitectures, Building 3D Nanostructured Devices by Self Assembly*; Zhou, W.; Wang, Z. L., Eds.; Springer, 2011.
(78) Bianco, A.; Kostarelos, K.; Partidos, C. D.; Prato, M. *Chemical communications (Cambridge, England)*. **2005**, 571-7.
(79) Katz, E.; Willner, I. *Chemphyschem□: a European journal of chemical physics and physical chemistry*. **2004**, *5*, 1084-104.
(80) Eskelinen, A.-P.; Kuzyk, A.; Kaltiaisenaho, T. K.; Timmermans, M. Y.; Nasibulin, A. G.; Kauppinen, E. I.; Törmä, P. *Small (Weinheim an der Bergstrasse, Germany)*. **2011**, *7*, 746-50.
(81) Ladd, J.; Boozer, C.; Yu, Q.; Chen, S.; Homola, J.; Jiang, S. *Langmuir□: the ACS journal of surfaces and colloids*. **2004**, *20*, 8090-5.
(82) Palestino, G.; Agarwal, V.; Aulombard, R.; Pérez, E.; Gergely, C. *Langmuir□: the ACS journal of surfaces and colloids*. **2008**, *24*, 13765-71.
(83) Lee, S. C.; Keener, M. T.; Tokachichu, D. R.; Bhushan, B.; Barnes, P. D.; Cipriany, B. R.; Gao, M.; Brillson, L. J. *Journal of Vacuum Science & Technology B: Microelectronics and Nanometer Structures*. **2005**, *23*, 1856.
(84) Michalet, X.; Pinaud, F. F.; Bentolila, L. a; Tsay, J. M.; Doose, S.; Li, J. J.; Sundaresan, G.; Wu, a M.; Gambhir, S. S.; Weiss, S. *Science (New York, N.Y.)*. **2005**, *307*, 538-44.
(85) Yang, X.; Yuan, R.; Chai, Y.; Zhuo, Y.; Mao, L.; Yuan, S. *Biosensors & bioelectronics*. **2010**, *25*, 1851-5.
(86) Yakovleva, J.; Davidsson, R.; Lobanova, A.; Bengtsson, M.; Eremin, S.; Laurell, T.; Emnéus, J. *Analytical Chemistry*. **2002**, *74*, 2994-3004.
(87) Seeman, N. C.; Belcher, A. M. *Proceedings of the National Academy of Sciences of the United States of America*. **2002**, *99 Suppl 2*, 6451-5.
(88) Kane, R. S.; Stroock, A. D. *Biotechnology progress*. **2007**, *23*, 316-9.
(89) Puchner, E. M.; Kufer, S. K.; Strackharn, M.; Stahl, S. W.; Gaub, H. E. *Nano letters*. **2008**, *8*, 3692-5.
(90) Samano, E. C.; Pilo-Pais, M.; Goldberg, S.; Vogen, B. N.; Finkelstein, G.; LaBean, T. H. *Soft Matter*. **2011**, *7*, 3240.
(91) Seeman, N. C. *Annual review of biophysics and biomolecular structure*. **1998**, *27*, 225-48.
(92) Liu, Y.; Lin, C.; Li, H.; Yan, H. *Angewandte Chemie (International ed. in English)*. **2005**, *44*, 4333-8.
(93) Hegner, M.; Smith, S. B.; Bustamante, C. *Proceedings of the National Academy of Sciences of the United States of America*. **1999**, *96*, 10109-14.
(94) Keren, K.; Braun, E. *Chemical Engineering & Technology*. **2004**, *27*, 447-452.
(95) Gazit, E. *The FEBS journal*. **2007**, *274*, 317-22.
(96) Liu, H.; Nishide, D.; Tanaka, T.; Kataura, H. *Nature Communications*. **2011**, *2*, 309.
(97) Javey, A.; Kim, H.; Brink, M.; Wang, Q.; Ural, A.; Guo, J.; McIntyre, P.; McEuen, P.; Lundstrom, M.; Dai, H. *Nature materials*. **2002**, *1*, 241-6.
(98) Franklin, A. D.; Chen, Z. *Nature Nanotechnology*. **2010**, 1-8.
(99) Bachtold, a; Hadley, P.; Nakanishi, T.; Dekker, C. *Science (New York, N.Y.)*. **2001**, *294*, 1317-20.
(100) Javey, A.; Guo, J.; Wang, Q.; Lundstrom, M.; Dai, H. *Nature*. **2003**, *424*, 654-7.
(101) Avouris, P.; Chen, Z.; Perebeinos, V. *Nature nanotechnology*. **2007**, *2*, 605-615.
(102) Franklin, A. D.; Luisier, M.; Han, S.-J.; Tulevski, G.; Breslin, C. M.; Gignac, L.; Lundstrom, M. S.; Haensch, W. *Nano letters*. **2012**, *12*, 758-62.